Université de Toulouse

THÈSE

En vue de l'obtention du

DOCTORAT DE L'UNIVERSITÉ DE TOULOUSE

Délivré par :

Institut Supérieur de l'Aéronautique et de l'Espace (ISAE)

Présentée et soutenue par :
Haris Ahmad Bin ISRAR AHMAD
le vendredi 21 février 2014

Titre :
Etude expérimentale et numérique de l'écrasement de stratifiés composites à base de fibres de carbone

Experimental and numerical investigation of CFRP composite laminates under crushing

---

École doctorale et discipline ou spécialité :
ED MEGeP : Génie mécanique, mécanique des matériaux

Unité de recherche :
Institut Clément Ader

Directeur(s) de Thèse :

M. Jean-Jacques BARRAU (directeur de thèse)
M. Samuel RIVALLANT (co-directeur de thèse)

Jury :

M. Olivier ALLIX, Professeur, ENS Cachan Président
Mme Nadia BAHLOULI, Professeur, Université de Strasbourg Rapporteur
M. Laurent GORNET, Maître de Conférences, EC-Nantes Rapporteur
M. Jean-Jacques BARRAU, Professeur, Université Paul Sabatier Directeur de thèse
M. Samuel RIVALLANT, Ingénieur Chercheur, ISAE Co-directeur de thèse

Acknowledgement

This work is performed at Institut Clement Ader under group research « Matériaux et Structures Composites » and at Department of Mechanics of Structures and Materials at Institut Supérieur de l'Aéronautique et de l'Espace (ISAE) Toulouse. I would like to thank all those who have contributed directly or indirectly to the completion of this thesis.

First at all, I would like to express the deepest appreciation to my supervisors Prof. Jean-Jacques Barrau and Dr. Samuel Rivallant as they always believed in my abilities and provided whatever advice and resources necessary for me to accomplish my goals. They spent countless hours meeting with me to discuss various aspects of my research. This work would not have been possible without their interesting ideas, guidance and help.

It is an honor for me to have Prof. Olivier Allix as president of jury. I owe my deepest gratitude to Prof Nadia Bahlouli and Dr. Laurent Gornet for honoring me by evaluating this work.

A series of experiments conducted during this study would not have been possible without help from Mr. Marc Chevalier as he helped me learn the use of Hydraulic Instron Machine and Scanning Electron Microscope. I would like to thank all the Master AMA students who chose to do their internships related to this study and generated some valuable experimental results. Especially, Paolo, Nandan and Sudeep are thanked for their important contributions. Moreover, the guidance and ideas from Prof. Bouvet and Hakim to improve my works especially in the numerical model are really appreciated. I am also in debt to Kol. Khairol Amali, Syed Fairus and Norhashimah, for their helps and supports during the thesis writing.

A special thank goes to Ministry of Higher Education Malaysia for their financial support throughout my PhD study under Aerospace Scholarship Scheme.

Last but not least, this important milestone of my life would not have been possible without the precious support from my wife, Ain Zalikha, my little motivator, Hadif and my family members in Malaysia. Without their sacrifices and patience the ups and downs of life would have been more difficult.

Organisation du manuscrit

Ce rapport de thèse est principalement écrit en anglais.

Les règles en matière de langue de rédaction du mémoire de thèse imposent qu'une partie de ce rapport soit rédigé en français.

Ainsi, ce mémoire se divise en deux parties.

La première partie est une synthèse des travaux, rédigée en français.

La seconde partie constitue le corps du rapport dans sa forme plus classique, rédigée en anglais

Organization of the manuscript

This PhD thesis is mainly written in English.

The rules regarding the writing language for the thesis require that part of the report is written in French.

Thus, this thesis is divided into two parts.

The first part is a summary of the work, written in French.

The second part is the body of the report in its most classic form, written in English

Etude Expérimentale et Numérique de l'Ecrasement de Stratifiés Composites à Base de Fibres de Carbone

Synthèse des travaux en français

RESUME

L’un des défis de la simulation numérique de la résistance au crash des structures composites est de pouvoir prédire les endommagements, leur évolution au cours de l’écrasement et l'énergie absorbée, à partir d'un nombre limité de propriétés matériau. Le but de cette étude est d'améliorer la compréhension des mécanismes élémentaires impliqués dans l'écrasement de stratifiés de plis unidirectionnels à base de fibres de carbone et de développer un modèle numérique.

Des essais sont réalisés à différentes échelles (macro, micro), et conduisent à la définition d'une nouvelle propriété matériau, essentielle : la contrainte moyenne d'écrasement que peuvent soutenir les plis à 0° ou 90°, et la méthode de caractérisation associée. L’analyse des tests montre également que pour représenter correctement le comportement du matériau pendant le crash (évasement, fragmentation...), il est nécessaire de choisir un modèle à l’échelle méso.

Le modèle éléments finis développé repose sur cinq idées principales : 1-mailler chaque pli; 2-utiliser des éléments cohésifs pour représenter le délaminage et l’évasement des plis; 3-pouvoir représenter la rupture des plis en gros fragments; 4-représenter l'écrasement localisé des plis, à leurs extrémités, par l'introduction d'un concept de « free-face-crushing », associé à un critère spécifique basé sur la contrainte moyenne d'écrasement; 5-représenter les contacts entre plis, plis et socle, plis et débris.

Ce modèle phénoménologique est ensuite appliqué à la simulation du crash de plaques stratifiées. A partir des propriétés matérielles élémentaires du pli, il permet de prédire la force, les principaux mécanismes de rupture et la phénoménologie observée lors des expériences.

TABLE DES MATIERES

INTRODUCTION

Cette partie, rédigée en français, ne constitue qu'une synthèse des travaux réalisés. En particulier, toutes les figures ne sont pas présentées. Pour plus de détails, le lecteur est invité à consulter la seconde partie, rédigée en anglais.

Depuis les années 70, le composite remplace progressivement les matériaux métalliques dans les structures aéronautiques, grâce à sa rigidité et sa résistance spécifique élevées. Aujourd'hui, la part du composite dans la structure d'un avion dépasse 50%. Dans d'autres domaines, comme la formule 1, elle atteint 75%.

Cependant, l'utilisation du composite n'apporte pas que des avantages, notamment dans le domaine des chargements extrêmes, tels que le crash. En effet, pour des raisons évidentes de sécurité, les structures sont également dimensionnées au crash. En ce qui concerne les avions, il s'agit d'assurer la survie des passagers pour les cas d'atterrissage dur, lorsqu'il y a défaillance des atterrisseurs. Il s'agit donc pour la structure (ici essentiellement la partie inférieure du fuselage) d'absorber l'énergie du crash par déformation ou rupture progressive de certains éléments de la structure. Avec les matériaux métalliques, cette fonction se fait assez naturellement par la déformation de la partie inférieure du fuselage sous les effets combinés de pliage, flambage et plastification. A l'inverse, les structures composites ont un comportement plutôt fragile en général, et une conception spécifique est donc nécessaire pour assurer le rôle d'absorption d'énergie. Dans la plupart des cas, on intègre des éléments spécifiques tels que des absorbeurs de crash.

Il existe donc de nombreuses études expérimentales dans la littérature concernant le crash des composites, qui ont démontré la possibilité de concevoir des structures spécifiques absorbantes, avec des capacités équivalentes ou supérieures aux matériaux métalliques, même si très peu d'études existent sur l'absorption d'énergie par les structures complexes elles-mêmes (i.e. sans absorbeur).

Cependant, le coût des essais pour valider des concepts de structures absorbantes est très élevé, et devant le développement des outils de simulation (codes éléments finis explicites par exemple) et des capacités de calcul des machines aujourd'hui, il est bien-sûr tentant de s'attaquer au problème par la simulation numérique.

Le problème n'est pas simple, étant donnée la complexité des mécanismes mis en jeu, et les modèles actuellement disponibles ne le sont que sur des domaines d'application très restreints, donc avec une prédictibilité très faible. Ce déficit peut donc être attribué à la fois à ce manque de connaissance fine des phénomènes physiques rencontrés dans le crash, mais également au fait que les temps de calcul restent encore aujourd'hui très important, limitant l'usage de la simulation à des modèles à l'échelle macroscopique, donc n'ayant qu'une représentativité relative.

Le challenge est donc de pouvoir modéliser le crash d'une structure composite et sa capacité à absorber de l'énergie à partir de la connaissance seule des propriétés mécaniques élémentaires des matériaux constitutifs de la structure. Cela nécessite une bonne connaissance des mécanismes qui pilotent la rupture et l'absorption d'énergie, dans le but de proposer des méthodes de modélisation pour le développement d'outils numériques de la simulation du crash.

Objectifs de l'étude

L'objectif de cette étude est de développer un modèle numérique du crash de plaques composites à base de fibres de carbone et de résine époxy, sous faible vitesse (<10m/s). Le domaine de vitesse est donné par le cas d'application aéronautique d'atterrissage dur, pour lequel la vitesse verticale retenue reste faible.

Ce rapport est divisé en quatre parties.

Le premier chapitre est une étude bibliographique sur le crash dans les composites.

Le deuxième présente les essais expérimentaux réalisés pendant la thèse, afin de mieux comprendre le comportement des plaques composites sous crash, d'observer finement les mécanismes mis en jeu, et ainsi de proposer des modèles. Les essais sont réalisés à différentes échelles, y compris à l'intérieur d'un MEB. Leur analyse permet de définir les modes d'endommagement à prendre en compte, et notamment de définir une nouvelle grandeur

mécanique, la contrainte moyenne d'écrasement d'un pli. Enfin, une étude sur l'influence du vieillissement humide est effectuée.

La troisième décrit les modèles d'endommagement choisis dans le cadre de cette étude pour modéliser le comportement par la méthode des éléments finis. En particulier, sont présentés les modèles et critères pour la représentation du délaminage et des différents types de fragmentation.

Le dernier chapitre présente les résultats de l'application des modèles précédemment décrits au cas du crash de plaques de stratifiés composites. Une étude d'influence est alors réalisée pour les paramètres suivants : vitesse d'écrasement, coefficient de frottement, et présence de vieillissement humide.

Chapter I

ETUDE BIBLIOGPRAPHIQUE SUR LE CRASH DES STRUCTURES COMPOSITES

Introduction

L'objectif de ce chapitre est de présenter l'état de l'art concernant le crash pour les matériaux composites. Ce chapitre est divisé en trois parties. La première présente ce qu'est le crash d'une structure composite en général, en décrivant notamment l'ensemble des mécanismes élémentaires d'endommagement dans les composites, puis en focalisant plus particulièrement sur les modes propres au cas du crash. La seconde partie passe en revue les études expérimentales réalisées sur le sujet, pour mettre en avant l'influence de différents paramètres sur la réponse des composites à l'écrasement: géométrie de la structure, propriétés matériaux, configurations d'essais ou de chargement. Enfin, la dernière section est consacrée aux modèles existants sur l'endommagement des composites, applicables au problème du crash.

Synthèse des travaux

Comportement au crash des structures composites

Si on met à part les cas de ruptures fragiles avec effondrement direct des structures composites sous crash, qui ne répondent pas à la fonction d'absorption d'énergie, il y a globalement deux types de comportements avec ruine progressive du matériau. Comme pour les matériaux métalliques (Figure F-I-1a), il existe un mode par pliage, plutôt pour les matériaux « ductiles », et un mode de ruine progressive par multi-fragmentation, plutôt pour les matériaux fragiles (Figure F-I-1b). Nous ne considèreront que ce mode, étant donné le cadre de l'étude : matériaux pour structures aéronautiques, et plus particulièrement le comportement des stratifiés.

D'un point de vue global, ce que recherche le concepteur en cas de crash, c'est l'obtention d'un écrasement progressif, avec dissipation d'énergie. L'allure de la courbe force/déplacement recherchée est donc de la forme pic de force suivi d'un plateau. La valeur moyenne du plateau et sa longueur permet de définir l'énergie absorbée. Pour pouvoir

comparer les matériaux entre eux, et notamment en regard de leur masse, une autre grandeur est utilisée : la SEA (*Specific Energy Absorption*), l'énergie absorbée par unité de masse. Elle permet en principe de classer les matériaux, mais n'est en fait pas une grandeur intrinsèque, puisque les études montrent qu'elle dépend du drapage, de la géométrie de la structure,…[BOL95, LAV96, BIS05].

D'un point de vue mécanismes d'endommagement, la rupture lors de l'écrasement des composites est bien-sûr la combinaison de l'ensemble des mécanismes élémentaires mis en jeu dans les composites en général, à savoir les ruptures de fibres, de matrice, le délaminage, les décollements fibre/matrice. La différence avec les problèmes standards de conception des structures composite est que pour le crash, on ne considère pas uniquement les premiers instants de ruine pour définir un critère de tenue. Le problème est plus complexe puisqu'on considère la rupture totale d'une partie de la structure, ce qui nécessite de prendre en compte l'endommagent jusqu'à la ruine ultime, et dans une zone étendue.

En se plaçant maintenant à une échelle légèrement supérieure, on définit généralement deux modes de rupture [HUL91]. Le premier est l'évasement des plis (Figure F-1c). Il est piloté par le délaminage et la présence de débris dans le front d'écrasement. L'énergie dissipée est donc principalement due à l'énergie de délaminage, et aux frottements entre plis, plis et débris, plis et surface de contact. Le second mode est la fragmentation (Figure F-1c). Elle consiste en la rupture de plis ou blocs de plis en débris de différentes tailles, provoqués par la combinaison d'efforts de compression, flexion et cisaillement. Ce mode se répète au fur et à mesure de l'écrasement, et dissipe plus d'énergie que le premier. La plupart des fronts d'écrasement présentent en fait une combinaison de ces deux modes [MAM05, GUI08], et c'est ce couplage entre les deux modes qui définit au final la morphologie du front d'écrasement et l'énergie dissipée. C'est également ce couplage, ainsi que la complexité des mécanismes mis en jeu, qui rendent difficile la prédiction du comportement d'une structure composite sous crash.

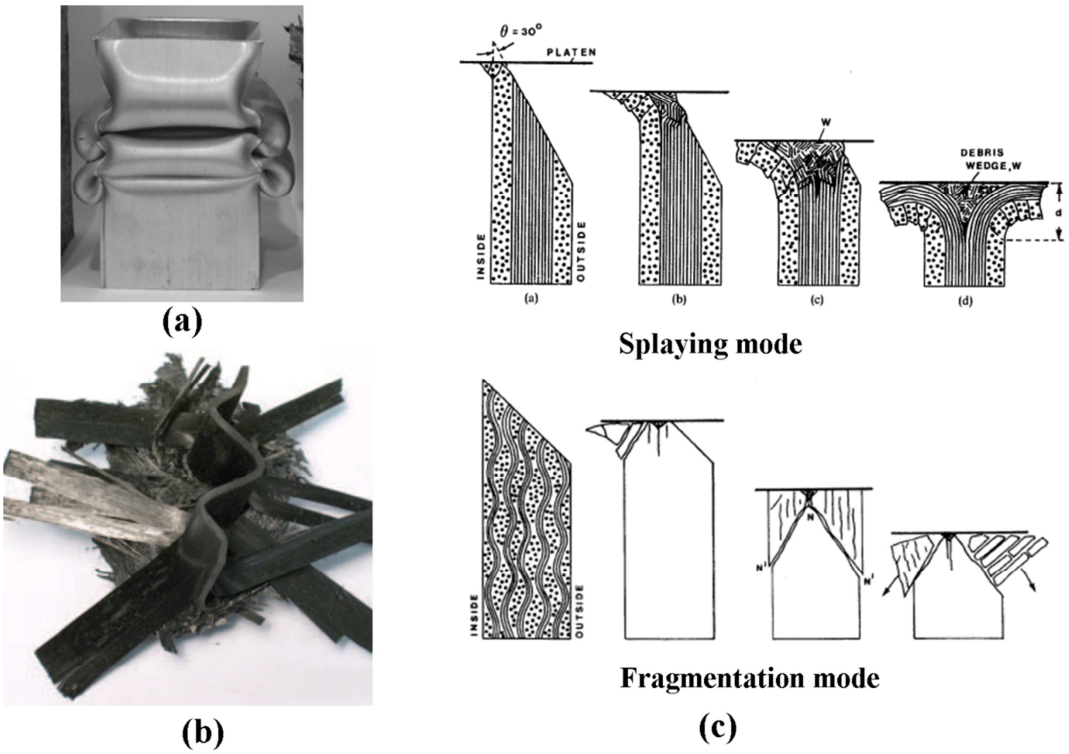

Figure F-I-1 : (a) Ecrasement d'un tube métallique [BAM10] (b) Ecrasement d'un stratifié composite de forme sinus [FER08] (c) Deux modes d'endommagement dans les composites sous crash [HUL91] : évasement et fragmentation

Etudes expérimentales

Devant la grande complexité du comportement au crash des composites, de nombreuses études expérimentales ont été menées afin d'étudier l'influence d'un certain nombre de paramètres sur la réponse au crash. On peut classer ces études en fonction des paramètres étudiés : géométrie, matériau, conditions d'essais ou de chargement.

La géométrie de la structure est bien-sûr un paramètre important. Les structures de type tube (profil à section fermée circulaire [SIG91, BIS05, ZAR08, OBR12], carrée [SCH98, JIM00, MAM05]) sont les concepts les plus performants pour l'absorption d'énergie, et ont été les plus largement étudiés. On trouve également dans la littérature des profils à section ouverte (poutre I [JIM00], sinus [HAN89, FER08]) dont les capacités sont plus faibles, mais très peu de structures réelles, étant donnés les coûts de ces essais. On trouve également des tests réalisés sur plaques [LAV96, SAV06, GUI08, DUO10], qui ont l'avantage d'être plus simples à réaliser, et de pouvoir donner plus d'informations lors des essais [GUI08, DUO10] (meilleur suivi expérimental).

Pour une géométrie donnée, les études montrent aussi l'importance du système d'initiation du crash (trigger) dans le comportement global [FAR89, FAR92, JIM00]. En

effet, la façon dont démarrent les endommagements pilote la morphologie du front d'écrasement dans la suite du processus.

Les études sur la configuration du chargement de crash (vitesse, angle d'écrasement) montrent globalement que pour l'influence de la vitesse [FAR89, HUL91, LAV96, MAM97B], on ne sait actuellement pas répondre, les résultats pouvant même sembler contradictoires sur l'augmentation ou la diminution de l'énergie absorbée. Pour ce qui est de l'angle d'attaque de la structure (angle entre l'axe de la structure et la direction du chargement) [GRE08, OCH09] il est clair que plus l'angle est élevé, plus la compétition entre l'écrasement et la rupture global de la structure en flexion, donc rupture catastrophique sans grande dissipation d'énergie tourne à l'avantage du second cas.

A l'échelle des constituants de la structure, là aussi, de nombreuses études ont été réalisées. Au niveau de la fibre [FAR92], le carbone, grâce à sa masse volumique la plus faible, est clairement le meilleur en termes de SEA, devant la fibre de verre, puis le kevlar, qui induit souvent des modes de pliage de la structure. En ce qui concerne la résine [RAM97], différents travaux semblent aller dans le même sens, montrant que les thermoplastiques donnent de meilleurs résultats, le PEEK étant la meilleure de celles étudiées [HAM95]. Enfin, l'influence du drapage du stratifié et du type de renforts (UD ou tissu) est difficile à quantifier étant donné le nombre emportant de combinaisons possibles [RAM97], et l'effet n'est pas toujours le même, pour un stratifié donné, en fonction de la géométrie de la pièce testée.

Pour conclure sur les études expérimentales disponibles dans la littérature, étant donné la grande complexité des phénomènes, et surtout des couplages ayant lieu, la plupart de ces études ont des résultats limités à un domaine restreint, souvent même limités à la simple comparaison des différents cas étudiés, sans extrapolation possible quant à une tendance franche de tel ou tel paramètre sur la capacité d'absorption.

D'autre part, il y a très peu d'études approfondies des phénomènes à une échelle fine [HUL91, FAR89], qui permettent de bien comprendre les mécanismes mis en jeu. Or les modèles doivent impérativement se baser sur de tels essais et observations pour pouvoir être prédictifs.

Modélisation

Les premières modélisations du crash remontent à la fin des années 80 [FAR89] et sont aujourd'hui de plus en plus nombreuses dans la littérature, l'intérêt étant bien entendu de remplacer progressivement les essais, coûteux. Il s'agit de modèles élément finis, le plus

souvent en explicite, étant donné le caractère fortement non linéaire et la quantité de ruptures à gérer lors d'un calcul.

De façon générale, le bon modèle pour résoudre un problème donné de calcul de structure est le modèle qui combine un choix d'échelle, de modèle d'endommagement et d'architecture qui permet d'être représentatif des mécanismes observés.

En ce qui concerne le choix de l'échelle, de nombreux modèles développés par le passé sont à l'échelle macroscopique [XIA09, FER11, OSH13, ZHA13]. Ils ont l'avantage d'être rapides en temps de calcul, mais nécessite une connaissance a priori du comportement global du stratifié, notamment de l'effort d'écrasement [DEL00], basée sur des résultats d'essais de caractérisation à cette même échelle. Ils restent donc par définition peu prédictifs. A l'opposé, quelques modèles existent à l'échelle micro [PIN05], avec les limitations classiques : temps de calcul prohibitifs, nécessité de représenter suffisamment bien l'ensemble des mécanismes à cette échelle pour pourvoir remonter aux mécanismes élémentaires d'endommagement à l'échelle du pli, qui nécessite alors un grand travail d'identification des nombreux paramètres. Entre les deux, l'échelle méso semble la plus appropriée, et est aujourd'hui la plus répandue [GUI08, SOK11].

Pour ce qui est des modéles de rupture, les mécanismes élémentaires mis en jeu dans le crash des composites étant les mêmes que pour n'importe quel problème d'endommagement des composites (délaminage, rupture de fibre, rupture matricielle), on retrouve dans les travaux un grand nombre des critères et modèles classiques de la littérature, comme ceux utilisés pour les cas d'impact [BOU09], de rupture en bord de trou,… Un accent est tout de même mis sur les critères de rupture en compression, et notamment sur la problématique de l'initiation de la rupture par micro flambage (Kink Band). D'autre part, le crash nécessitant de représenter la dégradation totale de la matière et sa propagation à une grande partie de la structure, il est nécessaire de faire appel à des modèles permettant de représenter la dégradation complète de la matière [PIN05]. Souvent, il s'agit de modèles à loi d'endommagement bilinéaire, basés sur l'énergie dissipée [PIN05, BOU12], avec éventuellement un plateau d'écrasement avant la rupture finale [FOU05, MCG08] (Figure F-I-2). On trouve également certains modèles spécifiques au problème du crash [WIL01, MCG07].

Pour représenter le délaminage, les éléments cohésifs semblent aujourd'hui l'outil le plus adapté [PAL10A, PAL10B, JOO11, SOK11, ZHA13], même s'il existe également quelques travaux mentionnant la méthode VCCT [FLE99].

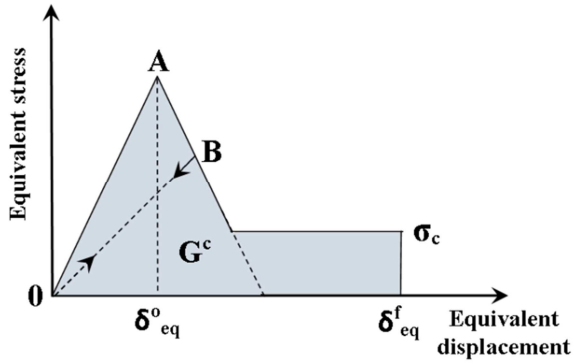

Figure F-I-2 : Loi de comportement bilinéaire en compression avec plateau [FOU05, MCG08]

Au niveau de l'architecture du modèle, l'étude bibliographique montre l'existence de différentes représentations des stratifiés : un élément coque pour représenter l'ensemble de l'épaisseur du stratifié [OSH13], empilements de coque avec éléments d'interfaces [PAL10B, SOK11, JOO10], ou bien éléments volumiques [HEI10], ces deux derniers types permettant d'obtenir de meilleurs résultats étant donné notamment la prise en compte du délaminage (Figure F-I-3). Pour initier l'écrasement, et donc représenter les trigger, différentes solutions adaptées au type d'éléments choisis sont utilisées. Pour les modèles à une coque, il s'agit en général de réduire progressivement l'épaisseur de la coque à l'extrémité, ou de déplacer les nœuds hors plan pour favoriser la rupture [HUA09].

La présence de débris, créés pendant le crash, étant importante dans le pilotage de l'évolution du front d'écrasement (formation de cales de débris favorisant l'évasement des plis), certains auteurs l'ont prise en compte dans leurs modèles, à différents degrés de finesse de représentation : débris prédéterminés [MCG10], ou formation naturelle d'une cale par accumulation des débris formés par la rupture dans les plis [JOO11].

Enfin, on trouve également des techniques spécifiques à la problématique du crash, et notamment la représentation du front d'écrasement localisé dans le ou les premiers éléments du modèle, tel que le paramètre « SOFT » de la loi MAT54 de LS-DYNA [MAM06, FER11], qui permet d'adoucir les sur contraintes dans les premiers éléments, ou la CZone, intégrée dans ABAQUS [NIX09].

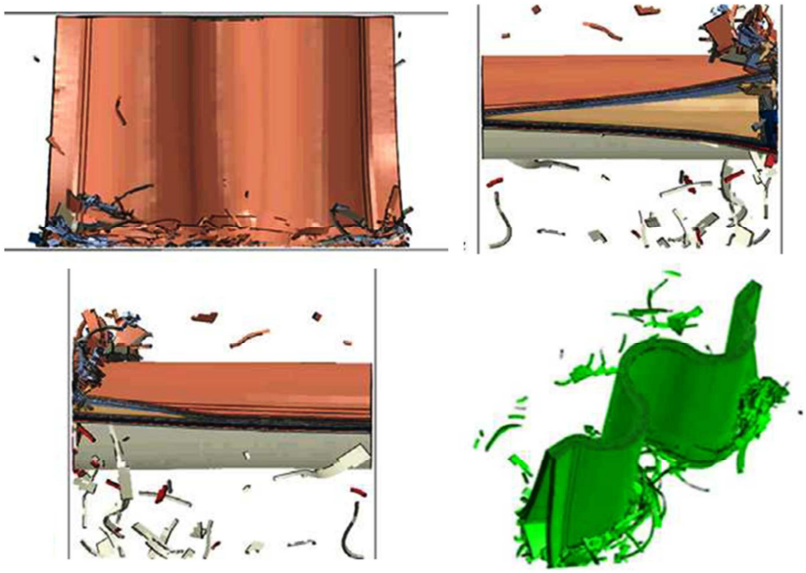

Figure F-I-3 : Ecrasement quasi-statique d'un stratifié de forme sinus [SOK11]

Conclusion

Il existe aujourd'hui de nombreuses études sur le crash des composites, et globalement, le comportement des structures simples, de type absorbeur à section fermée, est assez bien connu. Ce n'est pas le cas pour les structures plus complexes, et la prédiction de leur comportement nécessitent donc des modélisations fines. Pour cela, le développement de modèles basés non pas sur des approches macroscopiques (contrainte moyenne dans le stratifié, non prise en compte des délaminages), mais à une échelle plus fine, nécessite encore aujourd'hui une meilleure connaissance des mécanismes élémentaires. Des approches de modélisation et lois de comportement adaptées à une représentation suffisamment fine du front d'écrasement pourront alors être proposées ou adaptées de modèles existants.

Chapter II

ETUDE EXPERIMENTALE : ESSAIS ET ANALYSES DES DOMMAGES

Introduction

Ce chapitre présente des essais d'écrasement réalisés sur différents types d'éprouvettes, pour améliorer la connaissance des mécanismes d'endommagement mis en jeu, et ainsi pouvoir proposer des modèles d'endommagements adaptés au cas extrême du crash, mais également pour fournir une banque de données d'essais pour la validation de ces modèles.

Les essais, dispositifs d'essais et matériaux sont donc présentés en premier lieu, puis analysés pour mettre en lumière les mécanismes les plus importants, notamment ceux liés à la fragmentation. Une section particulière est consacrée à la contrainte moyenne d'écrasement du pli, grandeur physique importante pour la modélisation, et à sa méthode de détermination. Enfin, la dernière section présente l'influence du vieillissement humide sur le comportement du composite au crash.

Synthèse des travaux

Tests

Trois types de tests sont présentés. Il s'agit des mêmes échantillons, mais pour trois tailles, donc trois échelles différentes. Les matériaux utilisés sont :

- un UD de carbone époxy T700/M21, épaisseur de pli de 0.26 mm,
- un tissu équilibré de carbone époxy Cytec 5H (6KHTA) 977-2, épaisseur de pli de 0.35 mm,

L'étude se focalise sur des échantillons contenant uniquement des plis à 0° et 90°, avec les drapages suivants :

MATERIAU	NOM	DRAPAGE
T700/M21	T-0	$[(0°)_8]$
	T-90	$[(90°)_8]$
	T-0/90	$[(0°/90°)_4]_{sym}$
Cytec	C-0	$[(0°)_{12}]$

Le premier type de test est un test en statique et dynamique de plaques composites de dimensions 160 mm x 60 mm (Figure F-II-1a). Ces tests n'ont pas été réalisés pendant la thèse, mais lors de travaux précédents [DUO10] Ces travaux sont présentés pour deux raisons : parce qu'ils fournissent des essais pour la validation des modèles, à l'échelle d'une structure élémentaire, et parce qu'ils ont été analysés de manière plus poussée, ce qui a permis de mettre en avant l'hypothèse de l'existence d'une contrainte moyenne d'écrasement dans les plis, et ainsi de définir les deux autres types d'essais à réaliser.

Le deuxième type d'essais est un essai d'écrasement de poutre composite courte (60 mm x 10mm) en statique (Figure F-II-1b), nommé essai à l'échelle intermédiaire. Cet essai est défini pour valider l'hypothèse précédemment citée et calculer la valeur de cette contrainte moyenne d'écrasement dans les plis à 0° et 90°.

Le troisième type est le même que le second, mais réalisé à l'intérieur d'un MEB, grâce à un dispositif d'essais de compression in situ spécifiquement développé pour l'étude. Les éprouvettes sont de taille plus faible (20 mm x 2.6 to 6 mm), mais sont identiques par ailleurs. Ces essais permettent d'observer plus finement les mécanismes, entre les échelles méso et micro. Tous les échantillons sont chanfreinés en leur extrémité pour initier l'écrasement.

Ces tests sont instrumentés pour connaitre le déplacement imposé et l'effort. Ils sont également suivis par caméra (rapide pour les essais dynamiques) ou imagerie MEB pour obtenir des visualisations du front d'écrasement.

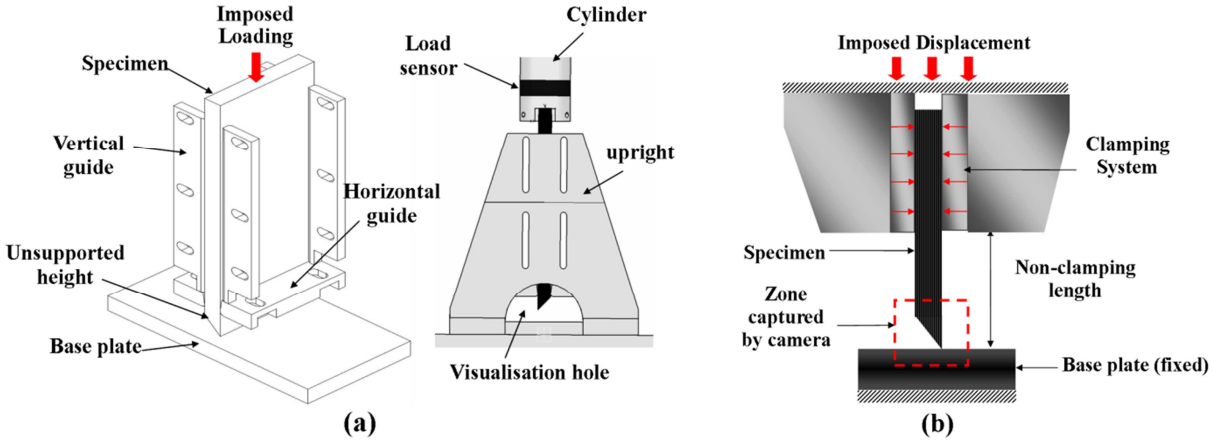

Figure F-II-1: Dispositifs d'essais d'écrasement : (a) sur plaque (b) échelle intermédiaire

Analyse de la rupture

La complexité des phénomènes mis en jeu pendant le crash rend leur modélisation complexe. L'objectif principal des observations faites pendant les essais décrits ci-dessus est

de permettre d'inventorier les différents types de dommages pour évaluer leur importance en termes de dissipation d'énergie ou de capacité de pilotage du front d'écrasement, afin de déterminer les mécanismes à représenter dans un modèle de crash et l'échelle de modélisation à adopter. Intéressons-nous d'abord aux stratifiés formés de plis unidirectionnels.

A l'échelle macroscopique, les principaux mécanismes d'endommagement sont relativement bien connus ([FAR89, HUL91]). Il s'agit du délaminage, de l'évasement des plis, de la fragmentation du stratifié, et de l'accumulation des débris provenant de la fragmentation, qui peuvent faire évoluer le front d'écrasement (Figure F-II-2).

Le délaminage peut s'initier et se propager en mode I, II ou le plus souvent en mode mixte. Il n'est pas forcément localisé au niveau des interfaces entre plis, et peut donc apparaître au cœur d'un pli, aussi bien à 0° qu'à 90°.

Lorsque les délaminages se propagent sur des longueurs suffisantes, ils peuvent aboutir à l'évasement de plis ou blocs de plis (multi-délaminés ou pas). Si rien ne vient perturber ces plis (frottement excessif ou blocage), ils peuvent s'évaser ainsi jusqu'à la fin de l'essai, sans autre endommagement apparent. Sinon, des ruptures de plis peuvent arriver : c'est un cas particulier de fragmentation.

La fragmentation regroupe en fait un ensemble de mécanismes différents. On peut le diviser en deux familles (Figure F-II-2b) :

- la fragmentation localisée en extrémité de pli, là où le matériau est en contact avec le milieu sur lequel il s'écrase, et qui donne des débris de petite taille (0 à 0.5 mm)
- et par opposition, la fragmentation qu'on appellera « en cœur de pli » qui correspond à la rupture d'un pli ou d'un bloc de plis sous l'effet d'une combinaison de compression, flexion et cisaillement. Les débris sont alors de taille plus importante (> 0.5 mm).

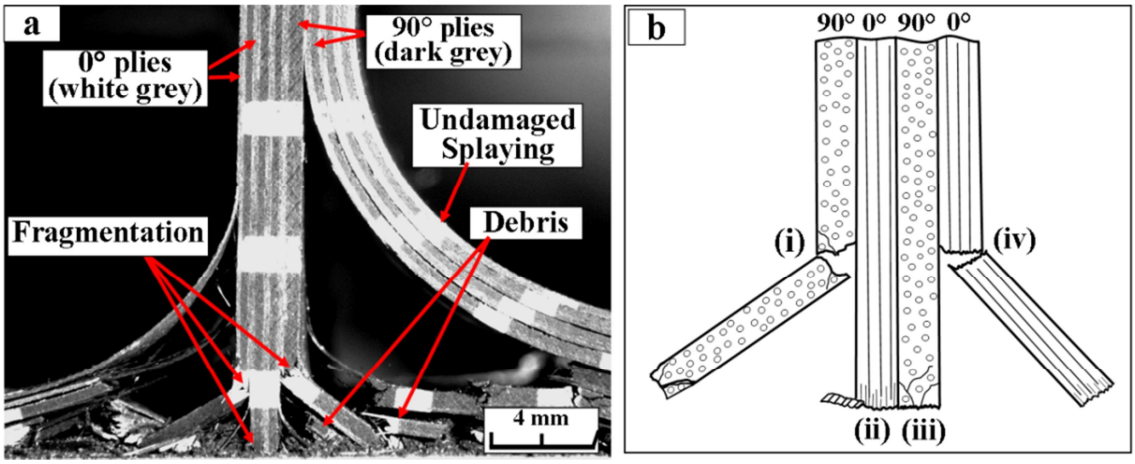

Figure F-II-2 : Les différents endommagements : (a) observation à l'échelle macro [DUO10] - (b) les différents types de fragmentation

L'observation au MEB permet de comprendre l'origine de la fragmentation localisée.

Dans les plis à 90°, il s'agit en fait de la création d'un réseau de microfissures, le plus souvent orientées à environ 45°, qui aboutissent à la formation de débris de taille comprise entre 0 et 0.5 mm (environ deux fois l'épaisseur du pli) (Figure F-II-3). Les plus petits débris, semblables à de la poussière, sont en général évacués lors de l'avancée du front d'écrasement, alors que les plus gros peuvent provoquer l'évasement des plis à 0° adjacents (Figure F-II-3c). Ce dernier point est particulièrement important, car ce mécanisme pilote l'évolution du front, donc doit être pris en compte dans les modèles.

La fragmentation localisée des plis à 0° est plus complexe. Elle semble provenir du micro-flambage de fibres et paquets de fibres à l'extrémité du pli, comme l'atteste la présence de débris de forme caractéristique de kink-band. Cependant, ces kink-band ne doivent pas être confondues avec celles observées lors d'un essai de compression en cœur de pli, puisqu'ici, elles apparaissent en bout de plis, là où, avant flambage, le matériau présente un faciès chaotique, et est déjà localement micro-délaminé. Les débris provenant de ce mécanisme d'endommagement sont de l'ordre du dixième de mm, et le plus souvent évacués lors de la propagation de l'écrasement.

La fragmentation localisée, aussi bien dans les plis à 0° que dans les plis à 90°, est à l'origine de la contrainte moyenne d'écrasement du pli décrite plus loin dans ce chapitre. C'est également un point très important de l'analyse des essais, essentiel à prendre en compte pour la modélisation.

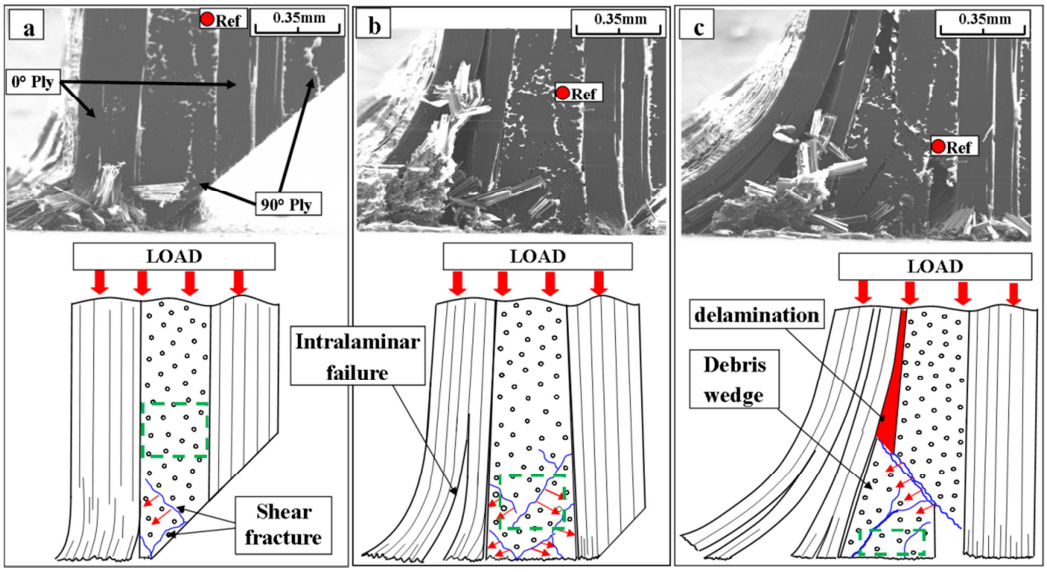

Figure F-II-3 : Fragmentation localisée : formation d'une cale de débris dans un pli à 90°

La fragmentation « en cœur de pli » présente différentes origines. On trouve principalement de la rupture de plis ou blocs de plis par combinaison de flexion et compression, mais également la rupture de blocs de plis par compression et cisaillement. Dans ce dernier cas, on trouve alors dans les plis à 0° touchés des débris de type kink-band, dus à une rupture en kink-band de compression piloté par du cisaillement. Le plus souvent, ce cisaillement dans les plis à 0° provient de la formation de fissures dans les plis à 90° adjacents.

Concernant les stratifiés formé de plis de tissus, les phénomènes observés sont globalement les mêmes : délaminages, kink-band, rupture en flexion des plis… Cependant, étant donné le croisement des chaînes et trames, les dommages intra-laminaires ne se propagent pas tous dans la totalité de la profondeur de l'échantillon, comme observé dans les UD.

Contrainte moyenne d'écrasement du pli

La notion de contrainte moyenne d'écrasement du pli est présentée dans une section à part à cause de son importance dans le comportement au crash.

Une analyse plus poussée des essais sur plaques stratifiées de plis UD réalisés par Duong [DUO10] a permis de montrer que la force d'écrasement semblait proportionnelle au nombre de plis écrasés, ce qui sous-entend qu'il est possible de définir une contrainte moyenne d'écrasement du pli ou d'une portion de pli. Cette observation est originale car, jusqu'à maintenant, il a pu être prouvé que, dans certains cas, l'écrasement d'un stratifié se faisait à force constante, mais pas au niveau du pli.

Les essais à échelle intermédiaire ont donc été réalisés dans le but de vérifier si l'écrasement se faisait bien à contrainte constante, et de calculer cette contrainte. Les essais sous MEB permettent également de faire les mêmes analyses.

La mesure de la contrainte est basée sur la mesure de la surface en contact pendant l'écrasement, sachant que cette surface peut évoluer lors de l'écrasement. Plusieurs images sont analysées par essai, pour avoir un nombre important de points de corrélation. Pour chaque image, sont prises en compte : la force d'écrasement totale sur le stratifié, la surface en contact de l'ensemble des plis à 0°, et la surface de contact de l'ensemble des plis à 90°. La contrainte moyenne d'écrasement du pli n'étant a priori pas la même pour les deux orientations de plis, le modèle proposé est le suivant : l'effort soutenu par le stratifié est la somme des efforts dans les plis à 0° et dans les plis à 90°. Est donc négligée la force due aux plis en évasement ([GUI08]), ce qui donne :

$$F = \sigma_{0°} S_{0°} + \sigma_{90°} S_{90°} + F_{splaying} \qquad \text{(Eq. F-II-1)}$$

Pour chaque type d'essai (0° pur, 90° pur, ou stratifié 0°/90°), une régression linéaire au sens des moindres carrés (LMS) est réalisées sur l'ensemble des points de mesure pris en compte, c'est-à-dire sur les triplés de valeur (F, $S_{0°}$ et $S_{90°}$), afin de déterminer les contraintes moyennes $\sigma_{0°}$ et $\sigma_{90°}$. Les résultats montrent une bonne concordance des efforts théoriques (calculés à partir des valeurs de contraintes du modèle de régression) et des efforts mesurés (Figure F-II-4), validant ainsi le modèle, c'est-à dire:

- que l'effort d'évasement peut être négligé
- qu'il est possible de définir une contrainte moyenne d'écrasement du pli pour les plis à 0° et 90°.

De plus, les valeurs obtenues pour les deux directions sont très proches : $\sigma_{90°}$ = 270 MPa, et $\sigma_{0°}$ = 276 MPa.

Le résultat à 90° n'est pas étonnant, puisque la fragmentation localisée, à l'origine de cette contrainte moyenne, se fait par microfissurations dans la résine, comme pour un essai de compression pure sur pli à 90°.

Par contre, pour les plis à 0°, la valeur obtenue est beaucoup plus faible que la résistance en compression. Comme évoqué plus haut, cela provient du fait que le phénomène n'est pas le même. Même s'il s'agit ici aussi d'un problème de micro-flambage, les conditions appliquées aux fibres ou paquets de fibres en extrémité de plis (multi-délaminés, fissurés) ne sont pas les mêmes que pour la formation des kink-band classiquement observées en cœur de pli.

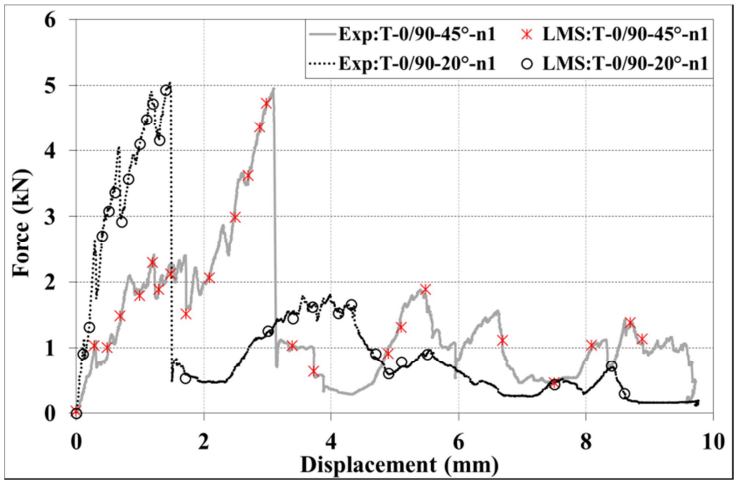

Figure F-II-4 : Corrélation entre essais et modèle LMS : stratifiés T-0/90 à l'échelle intermédiaire

Notons tout de même que ce n'est pas parce qu'un pli peut soutenir une contrainte moyenne d'écrasement que ce pli va nécessairement le faire. Il se peut que lors de l'écrasement, ce pli subisse également de l'évasement, donc de la flexion, et il y aura alors compétition entre différents modes de ruine : fragmentation localisé en bout de pli, à contrainte constante, ou rupture en flexion/compression au cœur du pli. C'est d'ailleurs très critique pour les plis à 90°, les modes de rupture étant très proches. D'autre part, les plis pouvant être multi-délaminés, il est possible qu'une partie d'un pli seulement soit en fragmentation localisée.

La même étude sur les stratifiés de tissus donne des résultats analogues. Bien-sûr, la distinction entre 0° et 90° n'a pas lieu d'être, et une seule contrainte moyenne d'écrasement du pli est calculée. La valeur obtenue est proche de celles des UD : 272 MPa.

Influence du vieillissement humide

Les structures composites utilisées en aéronautique sont exposées au vieillissement (humide, UV,…). Il est connu ([SHE77A, SUR06, RAY06, CUN08, SHI10]) que le vieillissement humide diminue les capacités des matériaux composites, essentiellement par dégradation de la résine. Le crash mettant en jeu de nombreux phénomènes liés à la tenue de la résine (délaminage, micro-flambage lors de la fragmentation localisée,…), il est intéressant de regarder quelle peut être l'influence du vieillissement sur le comportement au crash.

Les essais précédents (échelle intermédiaire et MEB) ont donc été répétés sur des éprouvettes provenant du même lot de fabrication, mais ayant subi un vieillissement humide jusqu'à saturation.

L'observation des essais montrent que les mêmes mécanismes apparaissent, et qu'il est difficile de chiffrer une différence (nombre de plis en fragmentation, taille de délaminage,…). Cependant, on observe une légère augmentation de la force du plateau dans les courbes effort/déplacement.

Au niveau de la contrainte moyenne d'écrasement du pli, par contre, on observe une diminution de presque 10%, ce qui est sensible (Figure F-II-5).

Cette observation n'est pas forcément contradictoire avec la hausse de la valeur du plateau d'effort, les couplages entre délaminage et fragmentation étant ce qui pilote véritablement l'évolution du front d'écrasement, donc du nombre de plis réellement écrasés.

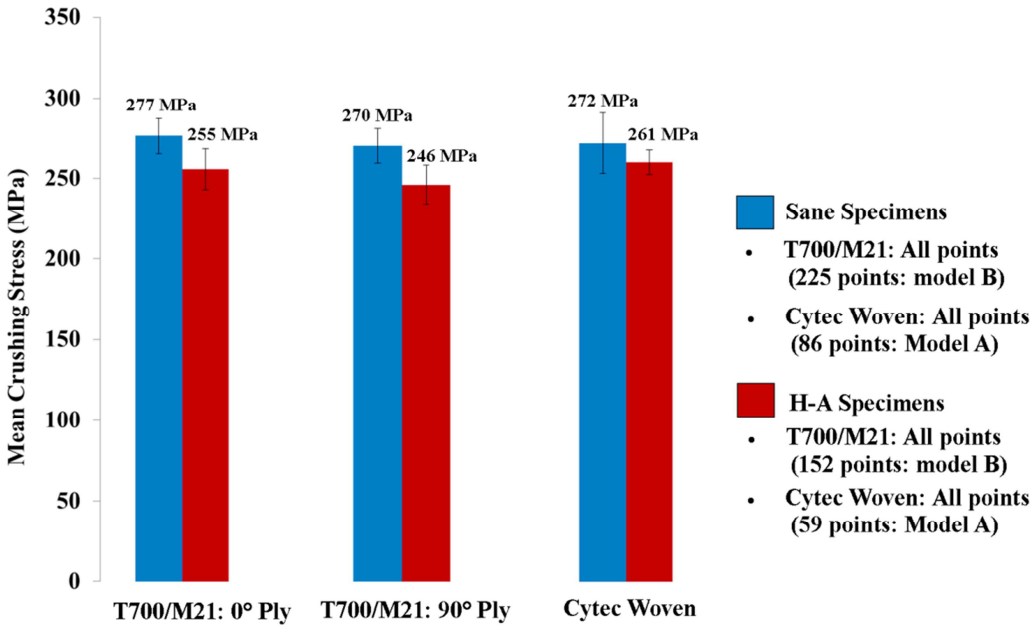

Figure F-II-5 : Contrainte moyenne d'écrasement du pli: comparaison entre matériau sain et matériau vieilli

Conclusion

Lors de cette étude expérimentale, de nouveaux tests ont été proposés, à différentes échelles. Les tests aux échelles les plus fines ont permis de mettre en avant les mécanismes intervenant lors du crash de plaques, aux échelles micro et méso, mettant ainsi en avant les phénomènes essentiels à prendre en compte pour pouvoir modéliser l'écrasement.

Outre les classiques dommages de délaminage et de rupture des plis, il a été mis en évidence un mécanisme de fragmentation localisé en bout de pli, aussi bien dans les plis à 0° que dans les plis à 90°. Une explication a été donnée pour ces deux phénomènes, et il a surtout été démontré que lors de cette fragmentation, le matériau soutien un effort proportionnel à sa surface de contact. Une nouvelle propriété mécanique a donc été proposée : la contrainte moyenne d'écrasement du pli, intrinsèque au matériau, et indépendante du drapage choisi.

Une étude a également été réalisée sur des éprouvettes après vieillissement humide, montrant notamment une baisse légère de la contrainte moyenne d'écrasement du pli.

L'ensemble de ces analyses d'essais permet de définir à la fois l'échelle pertinente pour la modélisation de l'écrasement des plaques composites, mais également les phénomènes principaux à représenter pour permettre des simulations réalistes. En outre, ces essais forment également une base de données pour la validation ultérieure des modèles.

Chapter III

MODELE D'ENDOMMAGEMENT

Introduction

Dans ce chapitre, sur la base des observations faites lors des essais présentés au chapitre précédent, des modèles sont proposés pour représenter les phénomènes physiques à prendre en compte dans les simulations.

Il s'agit tout d'abord des modèles permettant de traiter les différents niveaux de fragmentation : au cœur du pli et localisé en extrémité, avec leur critères associés. On définira notamment le concept de « free face crushing » pour la fragmentation localisée.

L'implémentation des modèles est alors explicitée, puis des calculs élémentaires réalisés pour les valider.

La manière de gérer le délaminage est ensuite présentée, qui constitue la dernière brique permettant de définir le modèle complet de crash sur plaque décrit et utilisé au chapitre IV.

Synthèse des travaux

Modélisation de la fragmentation

Etant donné les dommages observés lors des essais, le modèle envisagé est basé sur des éléments volumiques cubiques, de dimension égale à l'épaisseur du pli (voir le chapitre suivant pour plus d'explications).

Comme il a été mentionné au chapitre précédent, l'un des dommages prépondérants dans le crash est la fragmentation. Elle a lieu à deux niveaux différents : à l'intérieur du pli, et en son extrémité. C'est cette dernière qui représente l'apport le plus original de ces travaux.

La modélisation de l'écrasement localisé en bout de pli est en effet plus complexe. Dans les plis à 0°, il s'agit de représenter l'effet du micro-flambage de fibres et paquets de fibres, suivi de formation de débris, et de leur évacuation. L'observation à l'échelle mésoscopique de ces phénomènes montre qu'il suffit de représenter un écrasement continu

sous contrainte constante : la contrainte moyenne d'écrasement du pli. Dans un modèle éléments finis, on choisit donc de le représenter par l'écrasement successif des éléments consécutifs du pli. Il faut alors régler trois questions : la loi de comportement à utiliser, l'élimination des éléments au cours de l'écrasement, et le fait que le comportement en bout de pli n'est pas le même qu'en cœur de pli.

Le concept de « free face crushing » est alors défini. Il s'agit de ne donner la possibilité à un élément de s'écraser que s'il est à l'extrémité du pli, donc qu'il a une face libre dans une direction donnée. Les éléments suivants suivent eux une loi de comportement différente (voir plus loin). Une fois totalement écrasé, l'élément est éliminé et l'élément suivant prend alors les propriétés d'un élément « free face crushing » et peut s'écraser, assurant la continuité de l'écrasement. Ce principe est illustré sur la Figure F-III-1. La loi de comportement associée est une loi pseudo plastique à contrainte constante. Pour adoucir le passage d'un élément à l'autre lors de la disparition du premier, une décroissance linéaire de la contrainte est appliquée juste avant l'élimination. Il s'agit bien-sûr d'un artifice pour représenter l'aspect continu de l'écrasement par un modèle discret.

Dans les plis à 90°, les mécanismes ne sont pas les mêmes (microfissurations), mais aboutissent également à une contrainte moyenne. Ainsi, on peut appliquer exactement le même modèle. Une différence existe néanmoins dans le traitement du déplacement transverse dans l'élément écrasé. Pour les plis à 0°, ce déplacement est faible, alors que dans les plis à 90°, finissent par se développer des cales de débris. Ces cales sont représentées, à l'échelle de l'élément, par une déformation transverse. Ceci permet d'initier le délaminage entre plis à 0° et 90°, et l'évasement éventuel des plis à 0° adjacents (voir la Figure F-II-3).

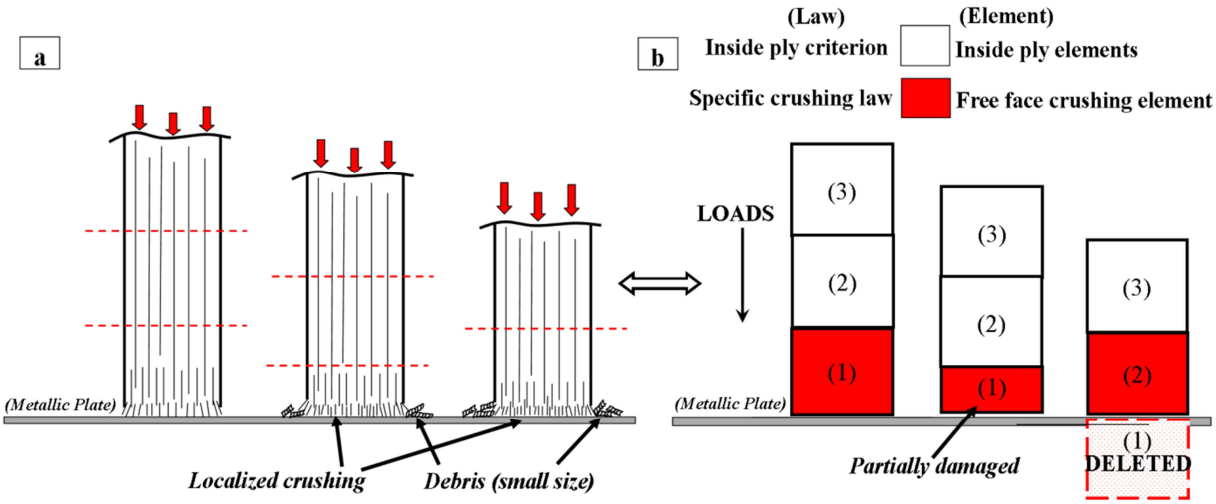

Figure F-III-1: (a) Schéma de la fragmentation localisée (b) Concept de « Free face crushing »

Concernant la fragmentation par rupture au cœur du pli, elle est gérée de façon plus classique, par élimination de l'élément lorsqu'un critère de rupture est atteint.

Pour les plis à 90°, on utilise le critère suivant (Eq. F-III-1) avec rupture fragile. L'énergie dissipée dans une telle rupture étant négligeable face aux autres sources de dissipation d'énergie, dès que le critère est atteint dans un élément, cet élément est éliminé.

$$\left(\frac{\langle \sigma_t \rangle^+}{Y^T}\right)^2 + \left(\frac{\tau_{tz}}{S_C}\right)^2 = 1 \qquad \text{(Eq. F-III-1)}$$

Pour les plis à 0°, donc pour représenter la rupture des fibres, qui dissipent beaucoup d'énergie, on utilise la mécanique de la rupture, avec dissipation de l'énergie de création d'une fissure répartie dans l'ensemble de l'élément volumique. Pour passer de la surface au volume, et rendre le critère indépendant du maillage, on introduit dans le calcul une longueur caractéristique de l'élément [BAZ83]. La loi est présentée dans la Figure F-II-2, appliquée aux 8 points d'intégration, mais pilotée par un paramètre d'endommagement unique dans l'élément [BOU09, HON13].

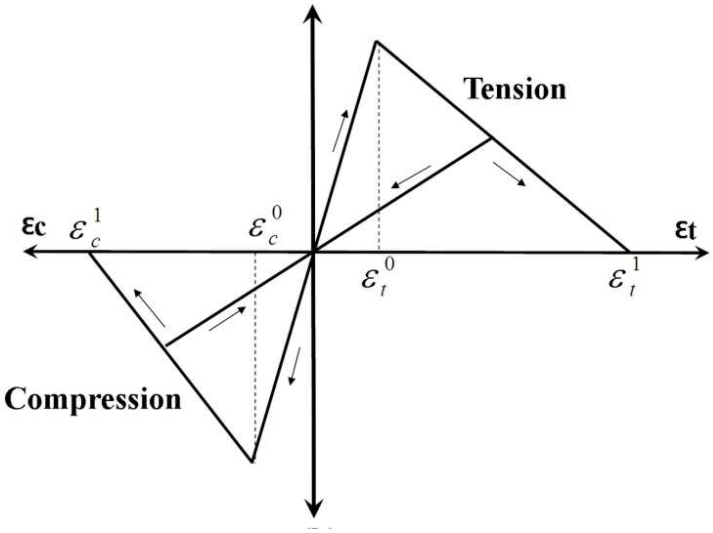

Figure F-III-2 : Loi d'endommagement dans le pli

Implémentation et validation

La part de l'implémentation dans le travail est relativement importante puisque les lois utilisées, à la fois pour le concept « free face crushing » et pour la rupture à l'intérieur de plis nécessite la discussion entre les différents points d'intégration d'un élément, voir entre éléments.

Une fois implémentées, ces lois on été testées sur des structures élémentaires: élément seul ou série de 10 éléments.

Ces tests ont montré la possibilité de représenter le comportement observé lors des essais, notamment la continuité de la fragmentation localisée (Figure F-III-3), et également la compétition entre les deux niveaux de fragmentation lorsqu'un pli est soumis à la fois à de la compression (favorisant l'écrasement localisé) et de la flexion (favorisant la rupture en cœur de pli).

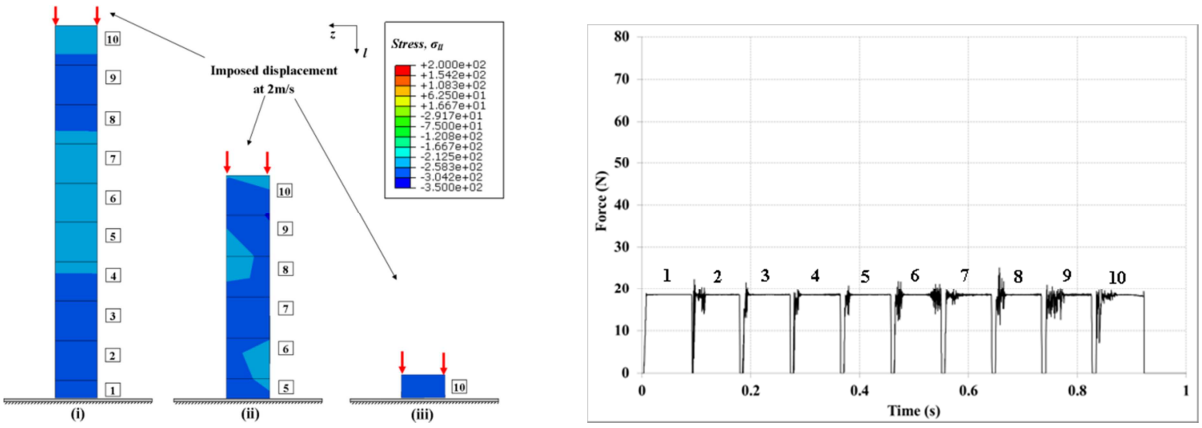

(a) **(b)**

Figure F-III-3 : Validation du concept de « free face crushing » sur 10 éléments d'un pli à 90° (a) visualisation de l'écrasement (b) Effort d'écrasement au niveau du contact

Modélisation du délaminage

Le délaminage est modélisé par des éléments cohésifs, avec une loi classique de séparation en traction [ABQ09]. Cette méthode est aujourd'hui couramment utilisée dans le calcul de structures composites ([PAL10A, SOK11, BOU12]). Comme le délaminage observé dans les essais se fait en mode mixte, la loi utilisée prend en compte ce couplage ([CAM03]), à la fois pour l'initiation et pour la propagation.

Conclusion

L'idée principale de ce travail est l'introduction d'un concept de « free face crushing » associé à une loi spécifique dans une modélisation par éléments finis, pour représenter l'écrasement localisé observé en extrémité de pli. L'implémentation est réalisée dans Abaqus, et les simulations sur des cas élémentaires montrent la faisabilité du concept. Une loi est également proposée pour la rupture en cœur de pli, et la possibilité de représenter la compétition entre ces deux niveaux de fragmentation est confirmée. Enfin, le modèle de délaminage utilisé pour les simulations décrites au chapitre suivant est lui aussi présenté. L'ensemble sera appliqué dans le chapitre suivant au cas du crash de plaques composites.

Chapter IV

MODELISATION NUMERIQUE: APPLICATION AU CRASH DE PLAQUES

Introduction

Ce chapitre présente l'application des modèles développés au chapitre précédent au cas d'écrasement de plaques composites présenté au chapitre 2, et plus précisément aux essais plaques en dynamique et aux essais à l'échelle intermédiaire en statique.

La première partie présente le modèle éléments finis développé, la deuxième sa validation à partir de certains des essais, puis une analyse des mécanismes d'absorption d'énergie est faite dans la partie 3. Enfin, les parties 4 et 5 étudient respectivement l'influence du vieillissement humide et des frottements sur la réponse au crash grâce au modèle.

Synthèse des travaux

Modèle éléments finis

Le modèle est développé à l'échelle du pli, qui nous semble la plus appropriée au regard des mécanismes observés expérimentalement. Sont modélisés à la fois les essais plaques (à 2 m/s, 5 m/s et 9 m/s) et les essais à l'échelle intermédiaire, avec les conditions aux limites associées (Figure F-IV-1), pour des stratifiés $([0°/90°]_4)_{sym}$. Chaque pli du stratifié est représenté par un élément 3D à huit points d'intégration dans l'épaisseur, et un seul élément de 0.25 mm dans la largeur de l'échantillon (modèle pseudo 2D). Les plis sont séparés par des éléments cohésifs d'épaisseur nulle, et un pré-délaminage est imposé en éliminant le premier élément de chaque interface.

Pour le contact, un modèle simple de Coulomb est utilisé, avec un coefficient de frottement de 0.15, identifié en comparant la forme d'évasement de certains plis entre essais et simulations.

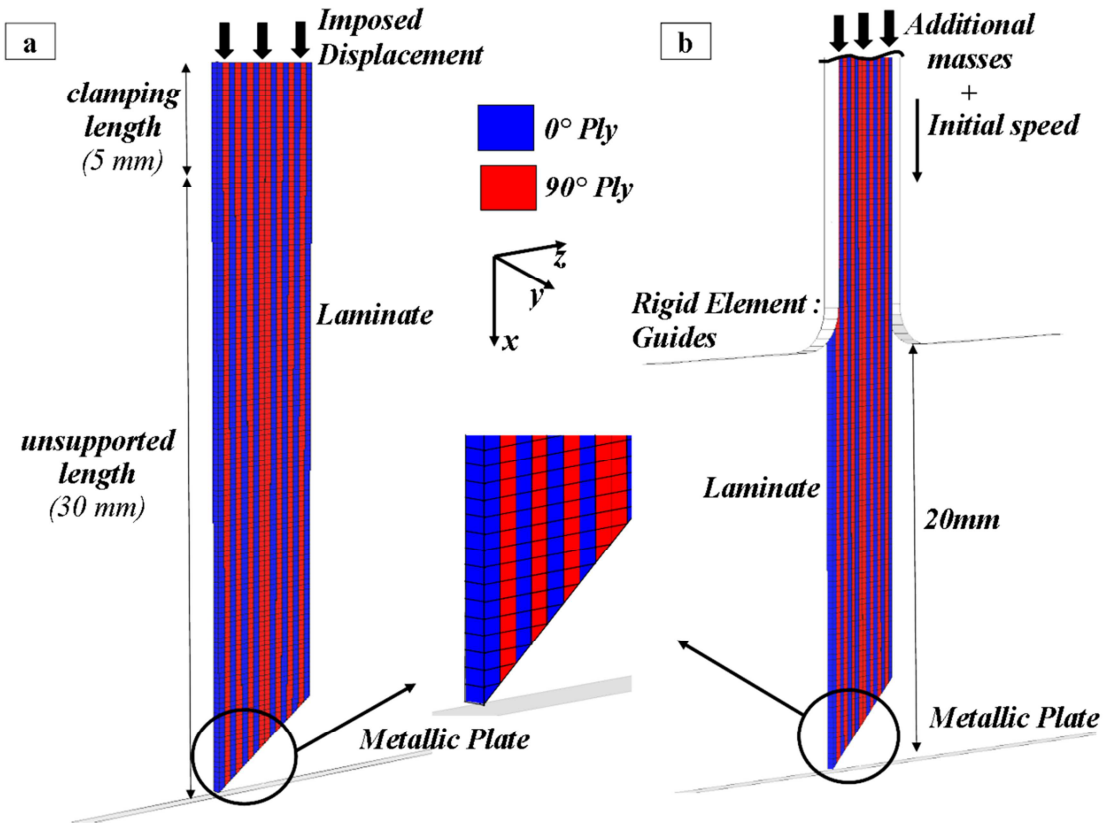

Figure F-IV-1 : Description du modèle : (a) Test à échelle intermédiaire en quasi-statique (b) Test plaque en dynamique

Validation du modèle

Globalement, la morphologie du front d'écrasement est bien représentée, le modèle permettant effectivement de bien représenter les mécanismes observés expérimentalement : évasement, rupture dans les plis, fragmentation localisée, création de débris. La Figure F-IV-2 présente une comparaison entre les images des deux essais quasi-statiques à échelle intermédiaire et la simulation numérique. Il est bien-sûr difficile de faire une comparaison essai/calcul concernant le nombre de plis en fragmentation localisée stable, sachant que, déjà, la dispersion entre les essais est importante ; mais globalement, l'ordre de grandeur est bon.

Concernant les courbes effort/déplacement (Figure F-IV-3), une très bonne corrélation est obtenue dans la phase transitoire (augmentation initiale de l'effort suivie de la grande chute d'effort). Dans la phase de plateau, les résultats sont également satisfaisants, même si pour les essais dynamiques, on observe des chutes d'effort un peu grandes, dues à des ruptures trop fragiles dans les plis en flexions. Globalement, les quantités d'énergies absorbées sont donc également très proches de celles calculées dans les essais.

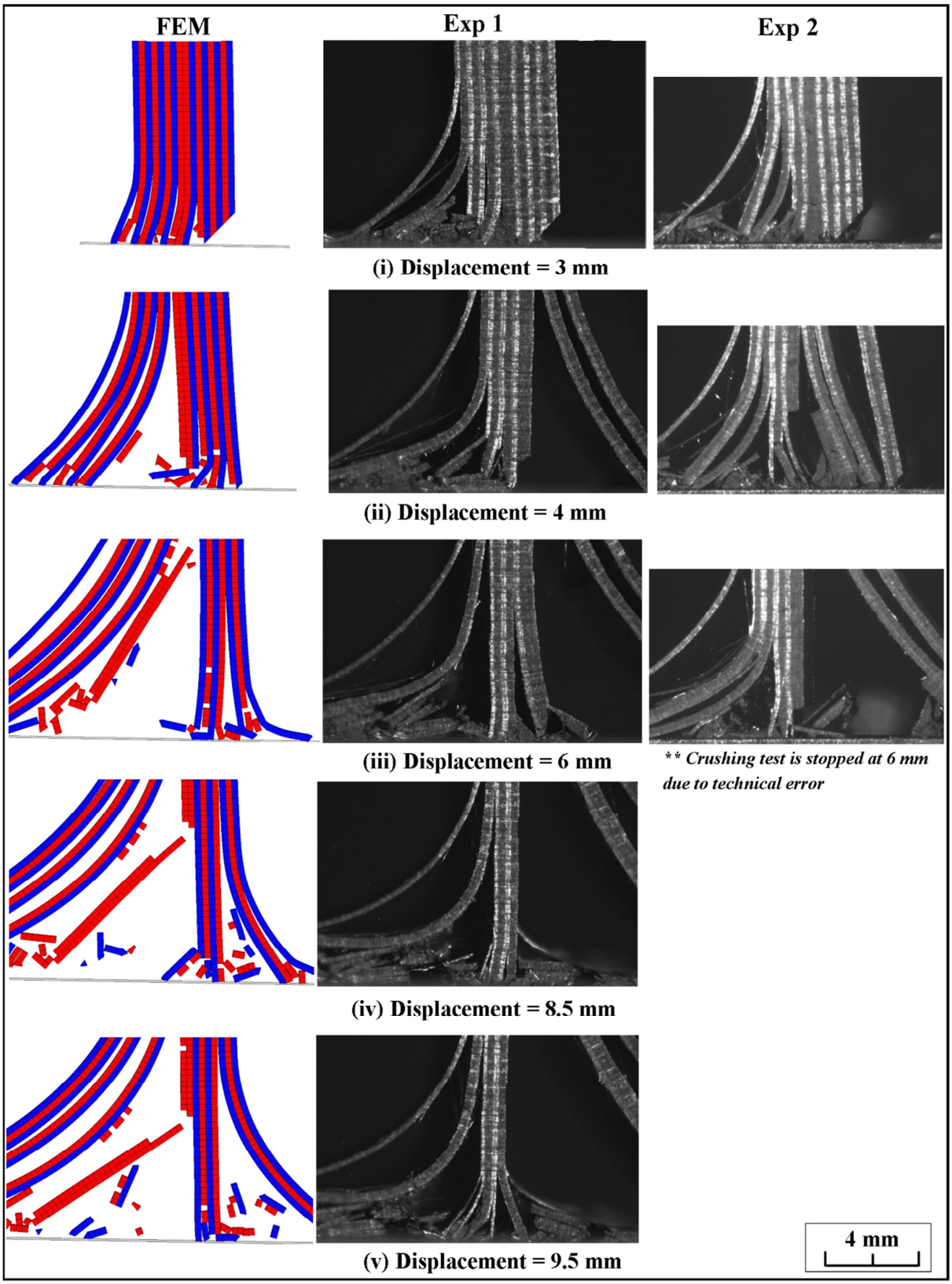

Figure F-IV-2: Comparaison des morphologies du front d'écrasement pour la simulation numérique et les deux essais quasi-statiques à l'échelle intermédiaire

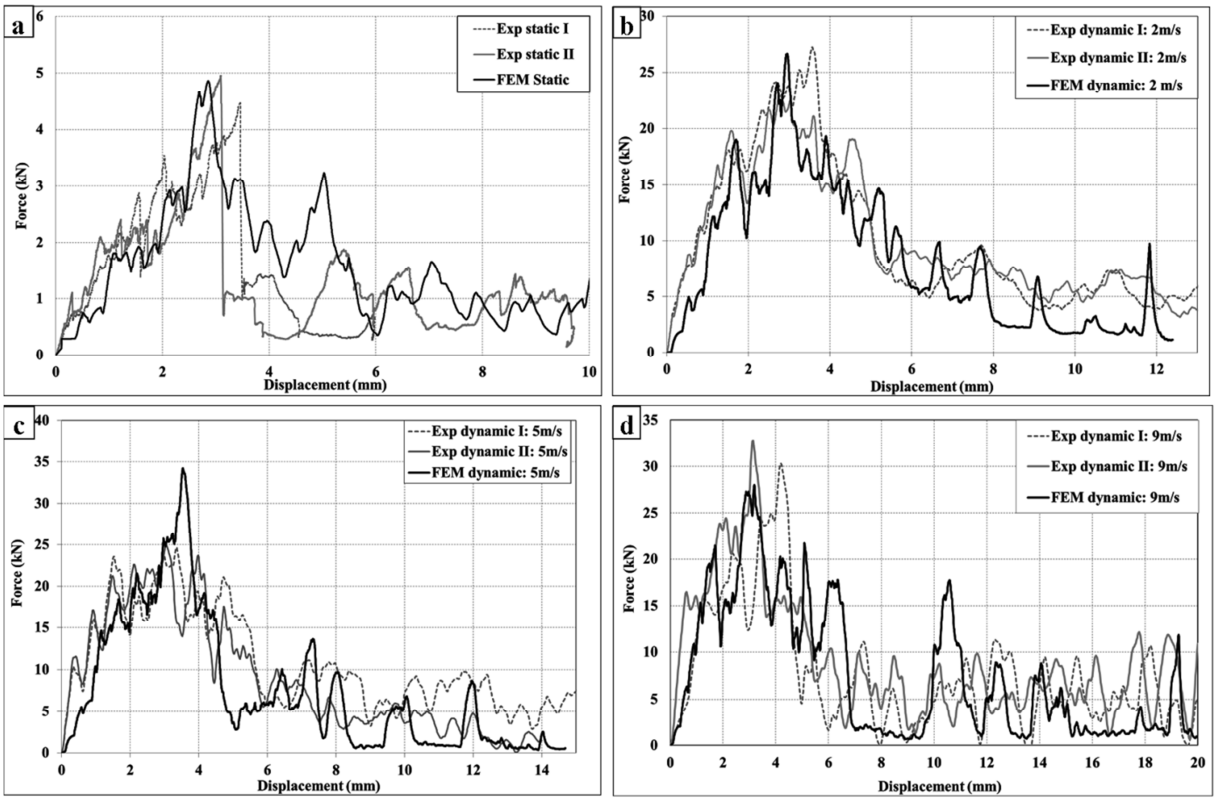

Figure F-IV-3: Corrélation essais/calculs : courbes efforts/déplacement pour (a) Echelle intermédiaire en quasi-statique (b) Plaque à 2m/s (c) Plaque à 5m/s (d) Plaque à 9m/s

Compétition entre les mécanismes d'absorption d'énergie

L'énergie dissipée pendant le crash l'est par différents mécanismes. L'avantage de la modélisation sur les essais est de pouvoir quantifier la part de chacun : rupture dans les plis (à 0°, 90°), frottement, délaminage. La Figure F-IV-4 montre que la plus grande part de l'absorption est due aux ruptures dans les plis, et en particulier dans les plis à 0°. La quantité d'énergie passant en frottement est également importante, supérieure même à celle du délaminage. En regardant plus précisément les énergies liées à la rupture dans les plis, les résultats (Fig F-IV-5) montrent en outre que la part due aux ruptures « en cœur de plis » est faible par rapport à la fragmentation localisée (inférieure à 10%), et que cette dernière est plus importante pour les plis à 0° que pour les plis à 90°, les plis à 90° ayant tendance à casser très tôt en flexion.

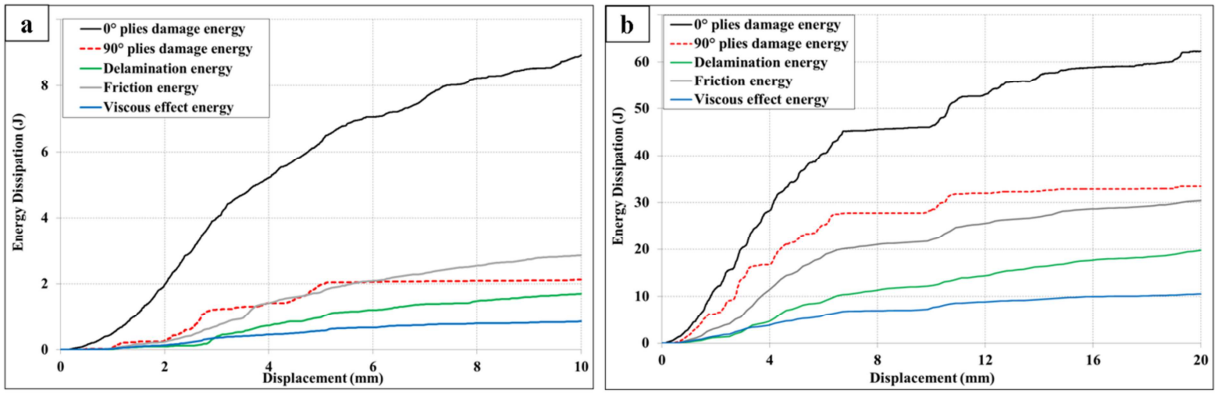

Figure F-IV-4: Evolution des différentes énergies lors de l'écrasement:
(a) Echelle intermédiaire en quasi-statique (b) Plaque à 9m/s

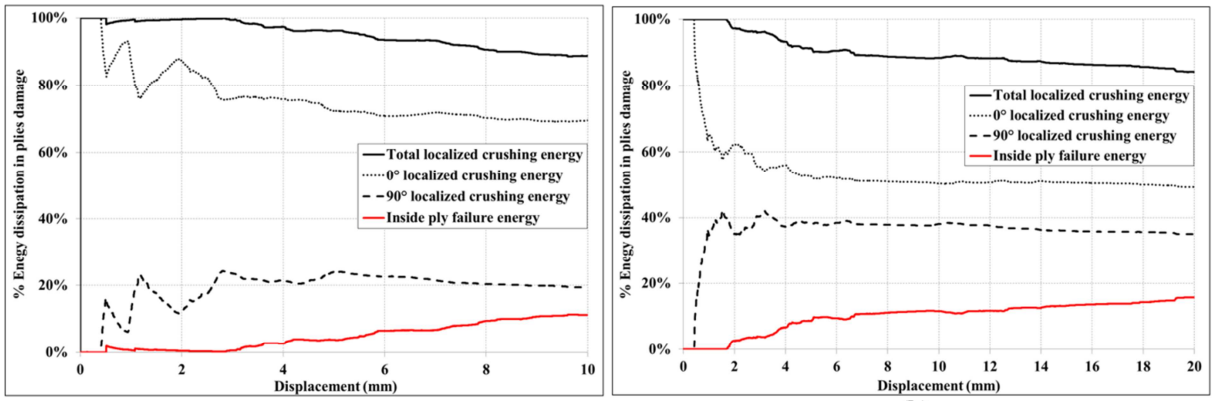

Figure F-IV-5: Répartition de l'énergie dissipée dans la rupture des plis entre les différents plis et les différents types de fragmentation (a) Echelle intermédiaire en quasi-statique (b) Plaque à 9m/s

Influence du vieillissement humide

La même simulation est lancée pour le test avec vieillissement humide quasi-statique. Globalement, les paramètres matériaux liés à la rupture dans la résine sont diminués de 10%, ainsi que la contrainte moyenne d'écrasement du pli à 0°.

Les morphologies observées sont alors très semblables à celles des essais, et également à celles de la simulation sur éprouvette saine. Il est donc difficile de conclure quant à une éventuelle augmentation du nombre de plis en fragmentation localisée, ou du nombre de plis évasés, même si au niveau de la courbe effort/déplacement, on observe globalement les mêmes tendances entre éprouvettes saines et vieillies que dans les essais.

Une analyse de la répartition des énergies dissipées montre en outre dans la simulation que la part de l'énergie dans les plis à 0° augmente légèrement, alors que celle dans les plis à 90° diminue. Ceci peut s'expliquer par la plus faible résistance des plis à 90°, plus affectés par

la diminution de leurs caractéristiques mécaniques, mais cette hypothèse reste à prendre avec précaution étant donné les nombreux couplages entre mécanismes mis en jeu.

Influence du frottement

Le modèle de frottement utilisé étant assez simple, une étude de sensibilité sur la réponse des stratifiés au crash a été réalisée en faisant varier le coefficient de frottement de 0.1 à 0.3.

L'influence de ce frottement est relativement faible dans la phase d'initiation, mais devient importante dans la phase de plateau, qui génère plus d'évasements de plis. De manière générale, un coefficient faible provoque beaucoup d'évasement, et un coefficient trop fort limite les délaminages et conduit à une rupture du stratifié par flexion globale de l'ensemble.

Conclusion

L'application des modèles développés au chapitre précédent au cas du crash, dans une modélisation pseudo 2D des essais, montre leur capacité à représenter les principaux mécanismes d'endommagement observés : évasement, fragmentation localisée et fragmentation en cœur de pli. Cela permet d'obtenir une bonne corrélation à la fois pour la morphologie du front d'écrasement et pour les courbes effort/déplacement.

A partir du modèle, il est alors possible d'analyser la répartition des énergies dissipées en fonction des mécanismes mis en jeu, et c'est de loin la fragmentation localisée qui absorbe le plus d'énergie.

L'influence de vieillissement humide observée par simulation est faible, du même ordre de grandeur que pour les essais.

L'influence du frottement quant à elle est assez importante, puisqu'il peut modifier sensiblement les mécanismes à l'échelle du pli et même du stratifié.

CONCLUSION ET PERSPECTIVES

Il est aujourd'hui nécessaire de dimensionner certaines structures composites au crash, comme dans le domaine aéronautique. Mis à part pour certaines structures simples comme les absorbeurs de crash de type tube, il est difficile, aussi bien expérimentalement (coût des campagnes d'essais, nombre de paramètres d'entrée important) que numériquement (limitation des modèles existants, méconnaissance des mécanismes fins à représenter) d'effectuer des prédictions sur les capacités d'absorption d'énergie des structures. C'est pourquoi, dans cette thèse, nous avons proposé une approche couplée essais/calculs pour améliorer la compréhension des phénomènes mis en jeu lors du crash des composites, et développer un modèle capable de représenter ces phénomènes.

Dans un premier temps, des essais d'écrasement de stratifiés $(0°)_n$, $(90°)_n$ et $[(0°/90°)_n]_{sym}$ à différentes échelles, incluant des essais sous MEB, ont été réalisés pour deux matériaux (UD carbone-époxy et tissu carbone-époxy).

Les premières observations ont permis d'affiner la classification usuelle des modes d'écrasement (fragmentation et évasement des plis), en divisant le mode de fragmentation en deux sous-modes : la fragmentation localisée à l'extrémité du pli, c'est-à-dire au niveau de la zone de contact, et, par opposition, la fragmentation au cœur du pli. Cette dernière est relativement classique, puisqu'elle consiste en fait en la rupture de plis ou blocs de plis sous une combinaison de compression, flexion et cisaillement. La fragmentation localisée est quant à elle beaucoup plus originale, et les essais ont révélés que les plis à 0° et 90° sous écrasement localisé ne pouvaient soutenir qu'une contrainte de compression maximum d'environ 270 MPa. Cette observation a donc permis de définir une nouvelle grandeur intrinsèque du matériau : la contrainte moyenne d'écrasement du pli, et les essais d'identification associés.

L'observation au MEB de cette zone d'écrasement a également permis de déterminer quels mécanismes y étaient mis en jeu. Pour les plis à 0°, cette contrainte est le résultat de micro-flambages de paquets de fibres prédélaminés au niveau de la surface de contact, alors

que pour les plis à 90°, il s'agit de multi-fissuration matricielle en cisaillement. Au sein du stratifié, il a également été mis en avant que la coexistence des mécanismes dans ces deux orientations de plis avait une influence sur l'évolution du front d'écrasement, les multi-fissurations dans les plis à 90° entrainant la formation de cales de débris pouvant piloter l'évasement des plis à 0° adjacents, réduisant ainsi le nombre de plis en fragmentation.

Une campagne d'essais a ensuite été réalisée sur les mêmes types d'éprouvette, après vieillissement humide. Il est difficile de conclure sur l'influence du vieillissement sur la réponse des échantillons, les écarts entre essais sains et vieillis étant relativement faibles comparés à la dispersion au sein même des essais sains. Cependant, il est apparu clairement que la contrainte moyenne d'écrasement du pli était influencée par le vieillissement, avec une baisse sensible d'environ 10% pour les deux directions (0° et 90°), et de 4% pour les tissus.

A partir de ces observations, un modèle d'endommagement a été proposé pour simulation sous éléments finis. Il est basé sur un concept appelé « free face crushing », qui consiste à considérer qu'un élément en bout de pli subit un écrasement localisé, avec un tenue inférieure à la tenue du pli plus loin, et qu'au fur et à mesure de l'écrasement, cet élément se déforme sous contrainte constante (loi pseudo plastique), égale à la contrainte moyenne d'écrasement du pli, puis est éliminé lorsque totalement écrasé. L'élément suivant se voit alors attribuer la même loi de comportement, et ainsi de suite au cours de l'écrasement de la structure. Pour prendre en compte le pilotage de l'évasement des plis à 0° par les cales de débris dans les plis à 90°, une expansion de l'élément en « free face crushing », dans le sens transverse, est imposée lorsqu'il est écrasé. Pour les autres endommagements (rupture en cœur de pli et délaminage), des modèles plus classiques sont utilisés.

Ce modèle d'endommagement est appliqué à la modélisation des essais statiques et dynamiques présentés avant, et donne des résultats très satisfaisants, puisqu'il permet de représenter les principaux mécanismes évoqués ci-dessus, validant ainsi les choix effectués. La simulation permet en outre de faire des analyses sur la répartition des énergies absorbée par mécanisme d'endommagement, là où les essais ne le permettent pas. Il s'avère que c'est la fragmentation localisée qui dissipe le plus, et surtout dans les plis à 0°.

Le modèle, appliqué aux essais avec échantillons vieillis, ne permet pas de donner une tendance franche sur l'influence du vieillissement, mais semble tout de même aller dans le sens des résultats d'essais.

Perspectives:

Bien entendu, les travaux réalisés durant cette thèse ne constituent qu'un pas vers une modélisation au crash des structures composites, et beaucoup reste à faire.

En termes d'études expérimentales, il semble important d'augmenter progressivement notre compréhension du crash en incorporant des mécanismes non encore étudiés, comme le comportement des plis à 45°. Des essais sont actuellement programmés pour effectuer des observations sous MEB, afin de voir notamment s'il existe également un écrasement localisé dans les plis à 45°, seuls ou au sein d'un stratifié.

Une question qui s'est également posée pendant cette thèse est l'influence de la vitesse sur la réponse au crash. D'après les observations « macroscopiques » réalisées sur les essais plaques (courbes effort/déplacement, morphologie globale du front d'écrasement), il semble que l'influence soit faible. Cependant, certains signes laissent à penser qu'il pourrait y avoir une influence sur un paramètre précis : la contrainte moyenne d'écrasement du pli. Mais le passage de l'essai existant, en statique, à un essai à une vitesse de quelques mètres par seconde est complexe (problème d'acquisition de l'effort en dynamique) et nécessite le développement d'un essai spécifique.

Enfin, dans les structures plus complexes qu'une plaque apparaissent souvent des modes d'endommagement par déchirement. Il serait donc intéressant de définir des essais pour étudier les mécanismes mis en jeu dans ce mode, pour pouvoir également proposer ensuite les modèles associés.

En ce qui concerne l'aspect numérique, un modèle est toujours confronté à certaines limitations… Dans le cas de la modélisation développée au cours de cette thèse, il semble notamment que la rupture « au cœur du pli » nécessite, pour les plis à 0° comme pour les plis à 90° des améliorations. En particulier, le cisaillement qui accompagne la compression et la flexion est mal pris en compte, ce qui pourrait expliquer les pics d'efforts importants dans la phase de plateau, qu'on ne retrouve pas de façon aussi accentuée dans les essais.

Enfin, le modèle pseudo 2D développé n'est qu'un premier pas, et ne permet pas de modéliser un stratifié classique avec des plis à 45°. Le modèle sera donc prochainement étendu en 3D complète en intégrant le concept de « free face crushing » au modèle DPM (Discrete Ply Model) développé par Bouvet et al ([BOU12, HON13]), qui a montré sa capacité à simuler des problèmes d'impact, problèmes mettant en jeu les mêmes mécanismes que ceux observés lors du crash (mis à part la fragmentation localisée, spécifique au crash).

Experimental and Numerical Investigation of CFRP Composite Laminates under Crushing

ABSTRACT

A challenge in numerical simulation of crashworthiness is to be able to predict the crush damage modes, their evolution during crushing and the energy absorbed in any composite structure from a limited number of material properties. The aim of this study is to improve the understanding of the elementary mechanisms involved in the crushing of CFRP laminates made of unidirectional plies and to develop a numerical model.

Crushing tests are performed at different scales (macro, micro), and lead to the definition of a new essential material property: the mean crushing stress that a 0° or 90° ply can support, and its associated characterization method. Tests analyses also show that to correctly represent the material behavior during crushing (splaying, fragmentation…) it is necessary to choose a mesoscale model.

The Finite Element model developed in this thesis is based on five main ideas: 1-Meshing of each ply of the laminate; 2-Use of cohesive elements to represent delamination and plies splaying; 3-Possibility to represent failure of plies into big-sized fragments; 4-Representation of the localized crushing of plies, at their extremities, with the introduction of a free-face-crushing concept associated to a specific criterion based on the mean crushing stress; 5-Representation of contacts between plies, plies and impacted base, plies and debris.

This physically based model is then applied to the simulation of the crushing of laminated plates. From elementary material properties of the ply, it allows to predict the force, the main failure mechanisms and the phenomenology observed during crushing experiments.

TABLE OF CONTENTS

INTRODUCTION

Since 1970's, composite materials are progressively replacing metals in aircraft structures design. This is due to their technical advantages in comparison to the conventional materials especially on its high strength to weight ratio, durability, as well as the adaptability to specific applications. For example, in the commercial aircraft the use of composite materials in structural design is becoming more significant as illustrated in Figure 1. Since it was first introduced in the aircraft A300B in 1972 to substitute metallic materials for the fairings of vertical tail plane, composite materials have substituted more parts and components as a result from the advancement in research and positive experiences. Currently, the latest commercial aircraft, A350 XWB consists of 53% composite materials in their design with both fuselage and wing structures made primarily of carbon fiber-reinforced polymer (CFRP) [AIR06]. This tremendous evolution can also be seen in other vehicle structural design such as the formula one cars, boats, helicopters etc. For instance, current structural design for the formula one cars include more than 75% of carbon fiber in its construction.

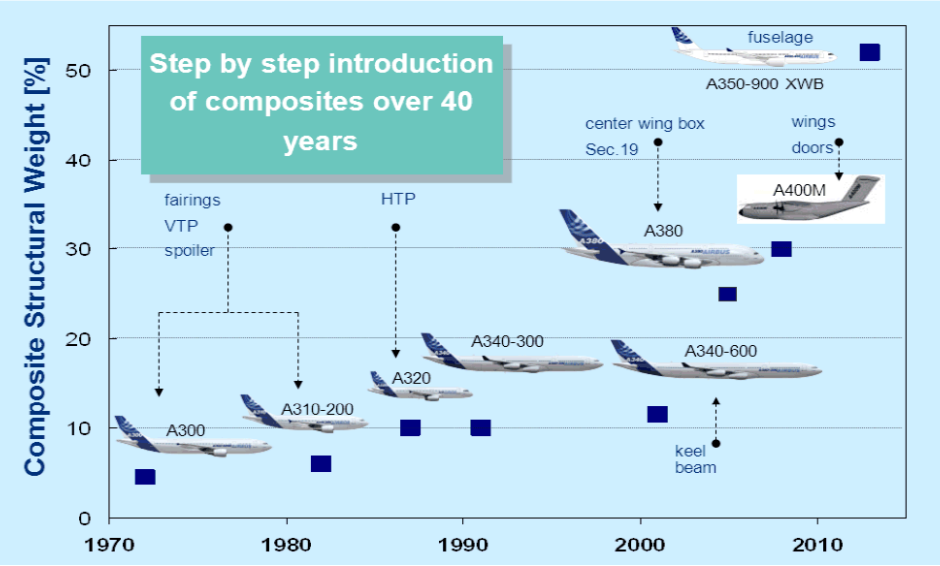

Figure 1: The growth in use of composite material in Airbus aircraft [AIR06]

However, the vehicle structures may be subjected to extreme loads level such as in the case of hard landing of an aircraft resulting from landing gear failure (Figure 2a) or the collision in formula one car during a race (Figure 2b). Indeed, for safety reasons, the structures are also designed to withstand crash. In the case of hard landing for example, the structures (mainly lower part of fuselage) have to absorb the energy by deformation or phasing out of certain elements of the structure. With metallic structures, this function is quite natural by plastic deformation of the lower part of the fuselage resulting from local buckling and progressive folding that absorbs the energy during the crash. On the other hand in composite structures, the energy absorption is associated with brittle-type factures, resulting in the destruction of the structure in the crush zone. Therefore, the behavior of composite structures on the crashworthiness response is a major concern while specific design is necessary for the energy absorption part.

Figure 2: (a) Hard landing of Air Canada plane *(www.strangedangers.com)* (b) Collision in formula one car during racing *(www.grandprix247.com)*

Nevertheless, the specification and complexity of composite structures fractures modes make it difficult to predict its behavior when subjected to the crush loads as it related to great numbers of parameters such as geometry, laminate sequences, mechanical properties, contact and friction etc. [HUL91, MAM97A, BAR10]. This will require a comprehensive understanding of their crushing behavior. The aim is to demonstrate their ability to provide an equivalent or improved level of safety and crashworthiness as compared to the conventional metallic materials.

For that reason, many researches on composite crashworthiness have been done for the last 30 years with a wide range of knowledge and information gained concerning composite structure crushing behavior. These studies have proved that with specific design, composite structure can become an excellent energy absorbing component such as crash absorber because of its ability to absorb an equivalent or higher energy than those found in

metallic structures [RAM97, BAM10]. But this is not the case for complex composite structures (i.e. without absorber).

The crashworthiness test programs used to validate design variants through experimental works increase drastically the design costs. Meanwhile, the increase in performance of computer resources and new explicit finite element codes has given the opportunity to use such tools to address the design issue and the crashworthiness problem by developing numerical modeling in order to minimize experimental tests costs. Nevertheless, the capability of existing numerical models to describe the initiation and progression of a crushing mode right up to the point of final failure is still limited. One of the reasons is due to insufficient information to describe the complex nature of failure mechanisms in composite structure during crushing. It involves fiber fracture, intra- and inter-laminar matrix cracking, fiber–matrix debonding, delamination etc. that take place at different length of scales [FAR89]. Therefore, limitations in numerical models can also result from the choice of modeling scale related to the competition between computational time and a fine mesh model. This is because calculation times are still very important and constraining the model at the macro-scale only allows to obtain relative representativeness.

Hence, the challenge in composite crashworthiness modeling is the ability to predict crushing damage modes, their evolution during crushing and the energy absorption from elementary material characterization data in order to have a predictive numerical model in composite crash absorbers, but also in complex composite structures (self-crashworthy component). This requires a deep understanding on crushing behaviors and the mechanisms that drive the failures to occur during the crushing tests in order to introduce new modeling methodology to support the development of numerical model in composite crashworthiness studies.

Objective of the Study

The objective of this study is to develop a physically-based numerical model for CFRP laminated plates subjected to low velocity crushing (<10 m/s) based on elementary material mechanical characteristics. The velocity range is set with respect to the aeronautical application of hard landing (*CS§25.473«landing load conditions and assumptions»*), in which the vertical velocity still remains low. Besides that, the materials used in this study are CFRP UD and woven fabrics laminates, materials classically used in the aeronautics field. Moreover, in order to observe damage mechanisms at elementary scale, laminated plate structure is used. In fact, none of the elementary structures (like tube) are able to represent a real structure. For that reason, a simple specimen (plate) is preferred in this study to observe mechanisms and propose numerical models.

The scopes of the study can be summarized as follows:

Experimental works:

- An investigation on the damage mechanisms based on numerous physical observations made during experimental crushing tests of composite plates including microscopic observation of the failure mechanisms
- An investigation on ply mean crushing stress characterization of CFRP plies inside a laminate under compressive crushing mode
- A study of the influence of humid ageing on the crushing performance of CFRP laminated plate including observation on the failure mechanisms and estimation of mean crushing stress.

Modeling works:

- Determination of the modeling approach and the appropriate modeling scale, in order to numerically represent the mechanical phenomena involved in the progressive crushing of composite plates
- Introduction of new constitutive laws and fragmentation modeling concepts
- A study of influence on the humid ageing, crushing speeds and friction coefficient on the crushing performance

Thesis Structure

This thesis is divided into four chapters. A brief overview of each chapter is presented in this section as follow:

CHAPTER I Literature review on composite structure crashworthiness

A general review on composite structure crashworthiness is presented. This chapter is separated into three main parts of discussion. The first part is the general review on the crushing behavior of composite structures. The second and the third parts are review on experimental and numerical modeling studies on composite crashworthiness respectively.

CHAPTER II Experimental tests and damage analysis

This chapter presents the experimental tests carried out in this study for better understanding on the behavior of composite plates under crash including details observation on the mechanisms involved. The tests are performed at different scales, including micro-scale inside a scanning electron microscope. The analysis allows the identification of damage mechanisms present at the crush front including the definition of a new mechanical quantity which is the ply mean crushing stress inside a laminate. Finally, a study on the influence of humid ageing is also carried out.

CHAPTER III Physically-based damage modeling

This chapter describes the damage models used in this study to model the crushing behavior by finite element method. The damage modeling can be divided into two types in general, modeling of fragmentation and modeling of delamination. All the failure criteria used for the delamination and different kinds of fragmentation are presented.

CHAPTER IV Numerical modeling: Application to plate crushing

This last chapter presents the results of the application of the physically-based damage models described above on the crushing test of composite laminated plate. A study of influence is then performed for the following parameters: crushing speeds, friction coefficients and the presence of humid ageing.

Chapter I

LITERATURE REVIEW ON COMPOSITE STRUCTURE CRASHWORTHINESS

This chapter presents a bibliographic study on composite structure crashworthiness. Crashworthiness is one of the more important aspects in the vehicle structural design related to the crash-absorbing components responsible to absorb impacts or crashes energy in a controlled manner and bringing the safety.

Metallic structures such as metal, aluminum etc. have proved their ability in absorbing high impacts or crashes energy mainly through plastic deformation under local buckling and progressive folding as shown in Figure 1-1. However, for weight optimization especially in aerospace or automotive industries, the introduction of composite material for weight optimization can be an alternative.

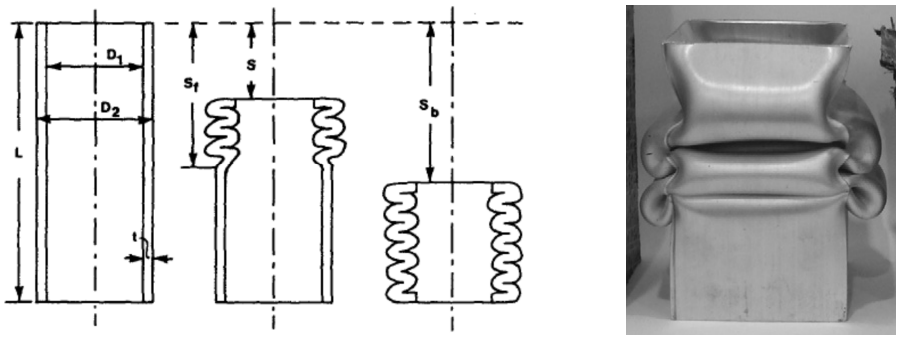

Figure 1-1: Progressive folding in metallic structure: An illustration [HUL91] and real test [BAM10].

As a result, these metallic materials are being replaced with new materials like CFRP due to the fact it is lighter and stronger [MAM05, MAM06]. Therefore, the use of composite materials in crashworthy structures design requires the designers to have a comprehensive understanding of their behavior subjected to crash loads. For that reason, various composite structures with different geometrical designs, fiber architectures and boundary conditions have been experimentally and numerically studied to optimize the crashworthiness ability of the composite structures. A detailed review on damage mechanisms, failure modes, experimental and numerical crush modeling developments will be presented in this chapter.

Generally, this chapter is separated into three main parts of discussion; the general behavior of composite structures when subjected to crushing load, review on experimental studies and numerical modeling studies of composite crashworthiness. The objective is to understand the mechanisms of energy absorption in composite material and to know the state of the art in composite crashworthiness study up to this date.

1.1 Crushing Behavior of Composite Structures

Unlike the plastic deformation in metallic structures, composite materials such as glass fiber reinforced plastics (GFRP) and CFRP composites when subjected to crushing loads may experience a wide variety of interacting fracture modes associated to energy absorption. Basically, these fracture modes depend on mechanical properties of constituent materials, structures geometries and the testing configurations. In general, there are two types of progressive collapse in composite crashworthiness namely progressive crushing for the brittle-type composite materials such as CFRP, and progressive folding for the ductile-type composite materials such as Kevlar. Nevertheless, only the progressive crushing behavior will be reviewed in details as the material used in this work (aeronautics) is CFRP based materials.

Figure 1-2 shows a typical load-displacement curve of composite material collapse under progressive crushing. In this curve, maximum load is generally defined as the peak load obtained during the initiation of crushing process. Thereafter, the crushing process turns into progressive crushing that is characterized by a relatively constant force (plateau) with eventual oscillations and P_{avg} is defined as the plateau average force. Using this value, two primary properties interesting for assessing crashworthiness of a composite material or structure in a particular application can be determined.

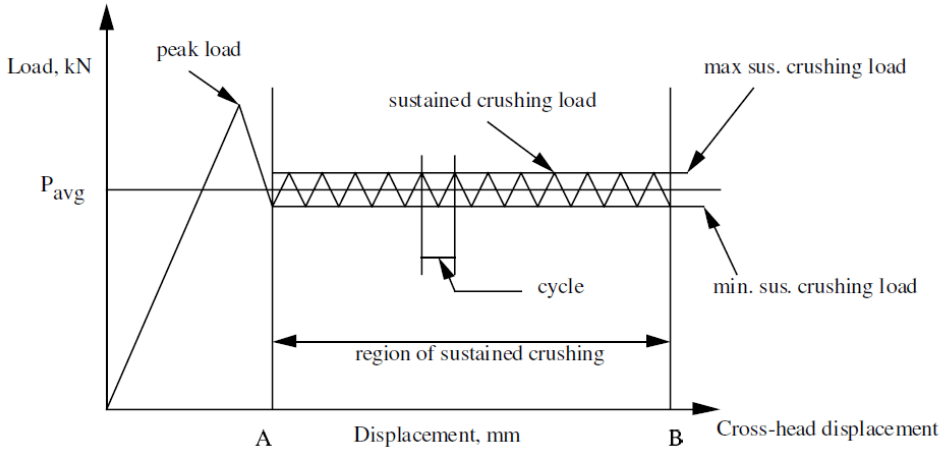

Figure 1-2: The typical load-displacement response [DAN00]

The first property is the sustained crush stress defined as P_{avg} divided by the cross sectional area of the specimen, *A*. It is normally used to compare with the compression strength to establish the percentage of the compression strength of the test coupon at which progressive crushing will occur [BAR10]. The second quantity of primary interest is the specific energy absorption (SEA) that is a formulation to measure the crashworthiness capability of a composite material/laminate which is also dependent on the global geometry of the structure. It is defined as the energy absorbed in the crushing plateau (refer to Figure 1-2) per unit mass of crushed material:

$$SEA = \frac{E_{plateau}}{M_{Crush}} = \frac{P_{avg}}{\rho . A} \qquad \text{(Eq.1-1)}$$

With: $E_{plateau}$: energy absorb in crushing plateau
M_{crush}: mass of the crushed material
P_{avg}: average load
ρ: material density
A: cross-sectional area

The amount of SEA for a given composite material for instance carbon-epoxy in three different studies [BOL95, LAV96, BIS05] is relatively wide depending on many factors such as laminate design, thickness, cross-section shape etc. Besides these factors, SEA also depends on the damage mechanisms and crushing modes present when the composite structures are subjected to crash loads. Different kinds of damage modes will result in different amount of SEA [FAR89, GUI08]. Detail review on damage mechanisms and crushing modes will be presented in the following section.

1.1.1 Damage Mechanisms

The crushing responses of composite structures are described in term of their damage mechanisms or crushing modes. The damage mechanisms in composite structures during progressive crushing generally involve different types of classical failure. The difference with the standard design issues of composite structures is that for the crash, it does not only consider the first moments of failure to define a criterion. The problem is more complex as it is considered a total rupture of a part of the structure which requires taking into account the damage until the ultimate failure, and in a wide zone.

In general, different structural geometries and materials give different damage mechanisms that usually can be categorized into three different scales as follow:

1) Micro-scale failure

Micro-scale damage occurs at intra-laminar and propagates through the ply thickness of the composite laminate. Typically, it can be categorized according to fiber and matrix failures as described in [MAT95]:

a) ***Fiber failure:*** In composite crushing, fiber failure can be classified into two kinds. The first one is fiber breakage due to the tensile stresses in fiber direction. The second failure is fiber micro buckling and kinking, accompanied by matrix fragmentation which is observed in uniaxial compression tests with loading in the fiber direction. It is largely affected by the matrix shear behavior and the weakness of the fiber-matrix interface.

b) ***Matrix failure:*** As with fiber failure, matrix failure can also be characterized into two kinds; tensile matrix cracking and shear matrix cracking. Tensile matrix cracking is a formation of micro-cracks of resin occurred under transverse tension load due to macro-cracks along the fiber-matrix interface. It crucially depends on the transverse tensile strength and shear strength of the lamina. Shear matrix cracks or also known as matrix crushing can also come from macro-cracks along the fiber-matrix interface but the formation of micro-cracks of resin is initiated under in-plane shear and transverse compression. In general, failure occurs at an angle with the loading direction and it is associated to the transverse compressive strength and shear strength of the composite material.

2) Meso-scale failure

Meso-scale failures on the other hand take place at ply level as a result from the micro-scale damages. For instance delamination between laminate and ply breakage that can be described as follow:

(a) ***Delamination:*** The formation of delamination is a result from the inter-laminar failure that normally occurs when plies with different fiber orientations are separated. The initiation of delamination usually is induced by the matrix cracks formation [FLE99, PIN05]. Delamination is recognized as one of the critical aspect of crushing behavior and may significantly influence the energy absorption capability of the composite structure or laminate [FAR89, HUL91, FLE99, FLE06]. Theoretically, there are three pure modes of inter-laminar failure namely opening, shearing and tearing which are modes I, II and III respectively. Nevertheless, in the real event of impact, crash or

buckling cases, the inter-laminar failure mode of composite structures is usually a combination of these three basic modes.

(b) ***Ply failure:*** This failure is a result from the fiber or matrix failures discussed before that propagates through the ply thickness.

3) Macro-scale failure

This damage concerns the global failure of composite laminate or structure resulting from the micro- and meso-scale failures. It can be described as the crushing mode that is presented in details in the following section.

1.1.2 Crushing Mode (Macro-scale)

Composite structures when subjected to crushing loads exhibits multiple modes controlled by the damage mechanisms discussed in the previous section. In earlier 90's, Hull [HUL91] have described the main crushing modes present during progressive crushing. In general, Hull has classified the crushing process into two main failure modes. The first one called splaying mode (Figure 1-3a) in which bundle of bending delaminated lamina splay on both sides of a main crack. The delamination failure in most of the time occurs in tension (mode I) and shear (mode II). Failure may also involves the fracture of plies in tension, compression, and shear parallel and normal to the fiber directions which leads to the plies splitting and broken fibers as reported in [HUL91, GUI08]. The broken fibers and resins trapped at the crushing zone can lead to the formation of debris wedge on the surface of the crushing platen as shown in Figure 1-3a-i. Energy is mainly absorbed by delamination, rupture of fibers and friction which involves plies/plate friction, plies/debris friction and plies/plies friction.

The second failure mode is called fragmentation mode (Figure 1-3b) in which the plies sustain multiple short length fractures due to pure compression, transverse shearing or sharp bending which leads to the formation of small fragments in the crush zone. Different materials and test conditions will form different fragment shapes. For the fragmentation mode in Figure 1-3b-I, Hull [HUL91] concluded that it is critically dependent on the shear failure processes in the laminate. The pure fragmentation crushing test in [GUI08] also exhibits the same shear failure process as shown in Figure 1-3b-ii. The energy is absorbed mainly through the multiple short fibers breakages and the failures growth of inter-and intra-laminar matrix cracks.

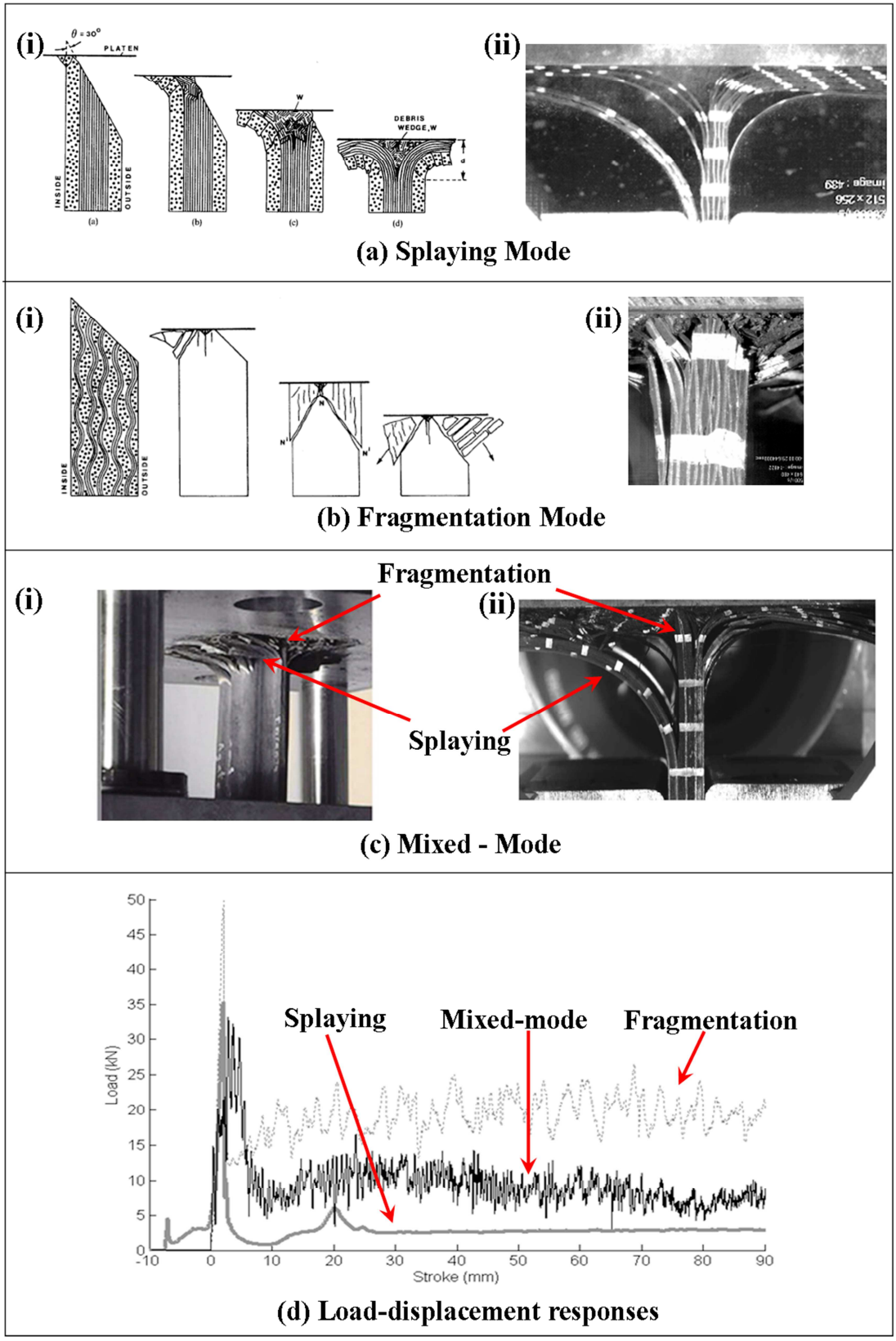

Figure 1-3: The overview of crushing modes. *Image (i) in (a and b) is taken from an illustration of tube crushing [HUL91] while image (i) in (c) is taken from crushing test of sine-wave shape [SOK11]. Image (ii) in (a, b, and c) is taken from a crushing test of plate [GUI08].*

As with Hull, Farley and Jones [FAR89, FAR92] have described the same failure modes, but named it with different terminologies for example lamina bending for splaying mode, transverse shearing mode and brittle fracturing mode are a combination for fragmentation mode. They also added local buckling mode in the classification of crushing mode. This local buckling mode is normally observed in ductile fiber-reinforced materials like Kevlar [KIM10] as shown in Figure 1-5a-ii and also other fiber-reinforced such as GFRP [TAH09, ABD06] which crushed under progressive folding as exhibited by conventional metallic structures (Figure 1-1). Local damage, fiber breaks or inter-laminar cracks may occur but remain restrained in each fold.

Nevertheless, in recent studies the terminology splaying and fragmentation mode have become more commonly used and these two modes are commonly observed in the brittle-type fiber reinforced materials such as CFRP [GUI08, GRE08, OCH09, DUO10]. In addition, crushing mode of most of composite structures is a mix of these two modes (Figure 1-3c) [MAM05, GUI08]. Mamalis et al [MAM05] reported the crushing mode changes from one mode to another on the same structure of square tubes fabric carbon / epoxy. According to Hull [HUL91], this is because in the crushing processes there is always a competition between different micro-fracture mechanisms which determines the eventual crush mode. For example, if splaying did not occur the stresses in the crushing zone will build up until the critical value for shear fracture is reached. In fact, the appearance of different crushing modes and different levels in energy absorption depends on many factors that will be discussed further in the following section.

Figure 1-3d shows the load-displacement response of three different crushing modes for a given material and laminate design. It can be seen that, the fragmentation mode exhibits higher average crush load than the splaying mode. Thus, according to the SEA formulation (Eq. 1-1), fragmentation mode provides higher energy than splaying mode.

1.1.3 Summary of Failure and Crushing Mode

This review has shown that the composite crushing behavior is very complex as it involves various damage mechanisms such as delamination, fiber breakage, formation of debris etc. Furthermore, this behavior may vary with different type of materials, structure geometry and boundary conditions. For that reason, extensive experimental studies have been done in order to improve the understanding concerning the composite crushing behavior and this will be discussed in the following section.

1.2 Experimental Study of Composite Crashworthiness

In this section, a review on the different types of tests from the literature is presented. In general, different types of tests deliver different levels of energy absorption and crushing morphology. These differences are basically influenced by many parameters that can be divided into three main categories namely, structure geometry, testing configurations and laminate design.

1.2.1 Structure Geometry

Many studies have proved that the structure geometry is an important parameter which significantly influences the appearance of different crushing modes and energy absorption capability [JIM00, FER09, PAL11, LAU12]. This is including the use of initiator systems (triggers) to initiate and drive the crushing process. Extensive test campaigns were conducted to investigate the influence of different triggers and specimen types described in the literature is discussed here to highlight the advantages and limitations of each.

1.2.1.1 Trigger Mechanisms

Trigger normally affects the initial formation of the crush zone and the force-displacement response [FAR89, FAR92]. The function of trigger is to form stress concentration on the edge to initiate localized failure in order to avoid the loads transfer to the whole structure [LAU12]. As shown in Figure 1-4a-ii, the absence of trigger can cause a catastrophic failure resulting in a sudden drop of force and thus low-energy absorbed. Hence, the influences of different triggering mechanisms have been investigated intensely by many researchers in order to improve the crushing performance and it is still an interest subject for some researchers in recent investigations [GUI08, PAL10A, PAL10C, PAL11].

Proper selection of triggering mechanism will help in optimizing the SEA because different types of trigger will deliver different failure mechanisms. For that reason, many types of triggers have been tested such as edge chamfering or bevel, tulip [JIM00, PAL10A, PAL10C, PAL11], steeple [GUI08, JOO11], notch [LAV96] and metallic pointer [GUI08]. Guillon [GUI08] has used three different trigger types, metallic pointer, steeple and edge chamfering in order to drive formation of three different modes, pure splaying (Figure 1-3a-ii), fragmentation mode (Figure 1-3b-ii) and mixed-mode respectively (Figure 1-3c-ii).

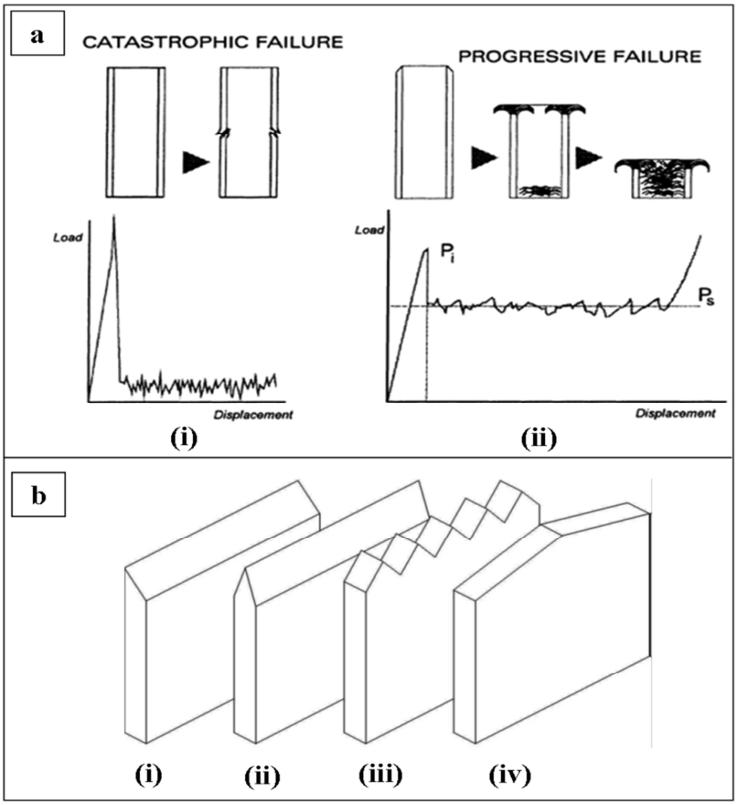

Figure 1-4: (a) The effect of trigger mechanism [JIM00] (b) Typical type of triggers in literature: (i) 45° edge chamfering (ii) Steeple (iii) Notch (iv) Tulip [BAR10]

Nevertheless, the effect of triggering mechanisms cannot be treated independently because it is always interacting with the structure geometry. For that reason, Palanivelu et al [PAL10D, PAL11] has investigated different triggers on different cross-sectional shapes. They found that circular composite tube with edge chamfering absorbed energy 7-9% higher than tulip type. But, the result for the square shape composite is the opposite. The use of tulip type triggering has shown an increment of 16.5% of SEA.

For edge chamfering trigger type, the difference in chamfering angles will influence the morphology of crush zone as reported by Sigalas et al [SIG91] which also leads to different energy absorbing capabilities [JIM00]. For small angle in chamfering, the failure process begins with fiber bending and subsequent formation of internal cracks while for larger chamfering angles, the failure is initiated by the formation of a long circumferential crack nucleated at the loadings point [SIG91]. Jimenez [JIM00] on the other hand, used two different chamfering angles 30° and 60° on the same composite box and has shown 25% difference in SEA level. In general, many researchers have used the 45° edge chamfering due to its stability and simplicity in manufacturing as shown in Figure 1-4b-i.

1.2.1.2 Specimen Type

There are many types of specimen that have been observed in the literature. In general, it can be classified into three types which are closed-section profile or tubes, self-supporting web and plate. The evaluation on these three different types of geometry in term of crushing mode and energy absorption capability is discussed in this section.

- **Closed-section Profile**

Closed section profiles such as circular, square tube or other tubular elements achieved good results with high stability of the crushing front and absorb high impact or crash energy [DUB98]. For that reason, it has been extensively used in composite crashworthiness study, especially the circular [SIG91, BIG05, ZAR08, OBR12] and square [SCH98, JIM00, MAM05] sections because it is more representative of industrial structures. Some authors also worked on a variety of more complex structures that often corresponds to the industry needs [OBR12] and design optimization such as choice of materials, triggers and structure dimensioning [ABD06, OCH 09, PAL11].

However, closed-section profile in general exhibits complex crushing modes and it is difficult to observe the damage mechanisms during the crushing tests because, most of the time, the tube wall or fronds are bending both inward and outward from the tube as shown in Figure 1-5a. Therefore, post-mortem analysis needs to be done in order to investigate the damage mechanisms that take longer time as the specimen need to be cut and observed under the microscope (for better observation) [KIM11]. Besides that, the observation is limited only to the damage state at the moment when the crushing process is stopped.

Hull [HUL91], Sigalas et al [SIG91] and McGregor et al [MCG10], discuss in details the crushing mechanisms for composite tube as illustrated in Figure 1-5b. Most of the time, the crushing modes observed are transverse shearing, splaying modes and local buckling (in some cases). In general, the transverse shearing for composite closed-section profiles is characterized by a wedge-shaped laminate cross section (Figure 1-5b-i) while the splaying mode is characterized by very long inter-laminar, intra-laminar, and parallel-to-fiber cracks [HUL91], [KIM11]. Figure 1-5b-ii summarizes the forces acting at various locations of the crushing zone and the debris wedge [MCG10].

In term of energy absorption capability, many studies have shown that circular tube provides better SEA compared to the other closed-section shapes [BAR10]. For example, Palanivelu et al [PAL10D] have tested three different cross-section shapes in their study; circular, square and hexagonal. They found that only circular tube was able to have

progressive crushing while the rest crushed catastrophically for aspect ratio t/D (thickness to diameter) or t/W (thickness to width) 0.045. By increasing the aspect ratio to 0.083, all shapes are crushed progressively with circular tube absorbing 30.4kJ/kg, the highest energy compared to the square (12.3kJ/kg) and hexagonal (16.4 kJ/kg) shapes. In fact, this study has shown that the fracture mechanisms are influenced by the structure dimensions that lead to the determination of overall energy absorption capability.

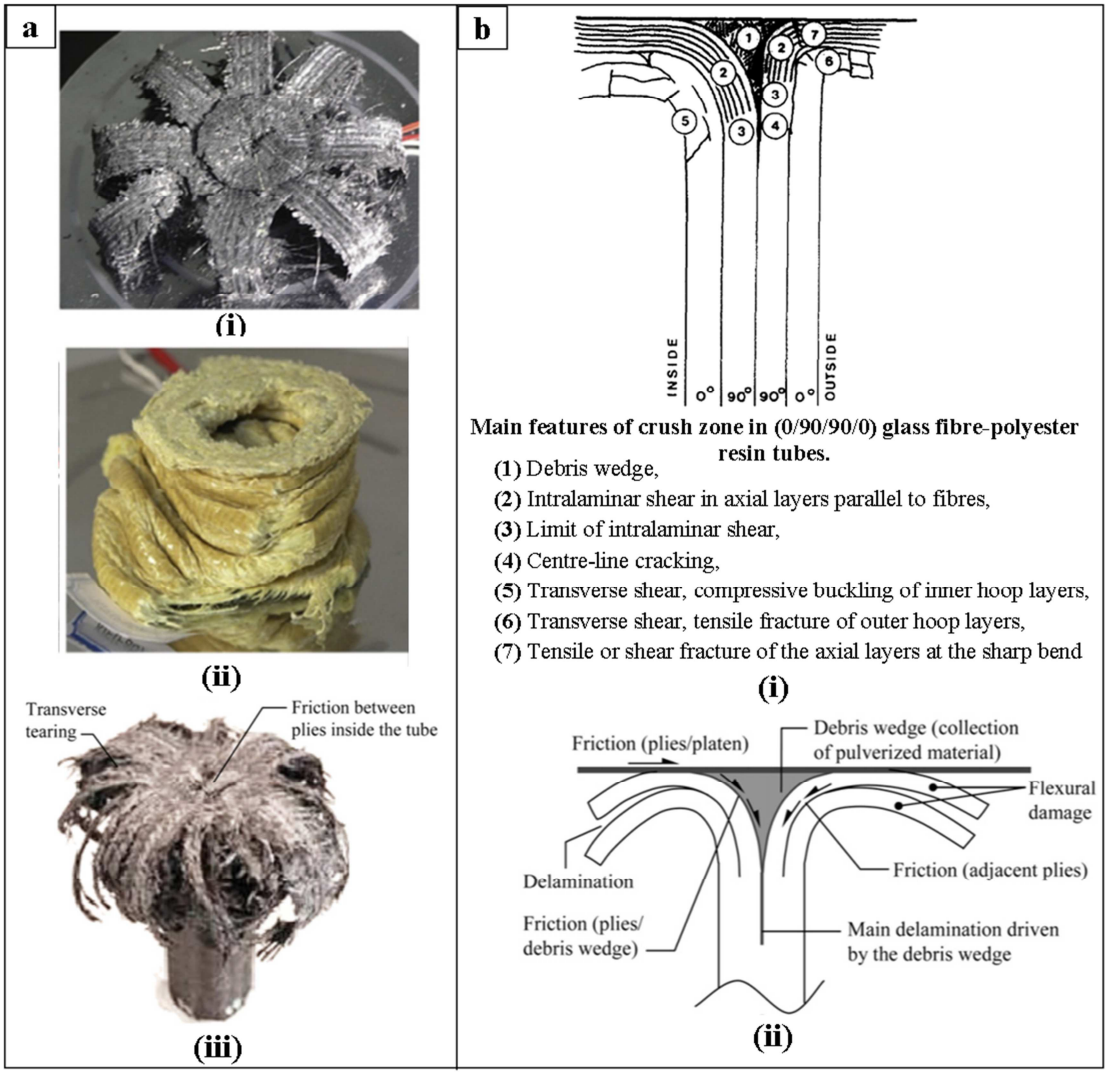

Figure 1-5: (a) Post-crash of composite tubes (i) UD carbon-epoxy [KIM11] (ii) Kevlar [KIM11] (iii) Braided carbon-epoxy [MCG10] (b) Summary of (i) failure mechanisms [HUL91] and forces [MCG10] of tubes crushing in the crush zone

- **Open-section Profile**

Open section profiles such as self-supporting web, I-column etc. on the other hand present a lower stability and complex behavior as well. Its design is also related to the industrial needs and is more complex to manufacture [FER08, JOO11].

For the self-supporting web, there are many different shapes that have been tested in the literature such as hat-shape (Figure 1-6c) [JOO11], omega-shape [JAC11] and the widely studied sinusoidal (Figure 1-6a) [HAN89, FER08]. For a given material, Hanugaud et al [HAN89] tested sinusoidal specimens with different triggers and different number of waves (different widths). The results have shown that the sinusoidal specimen is robust to the geometric shape. While Feraboli et al [FER08] reported high sine shape provides better stability and energy absorption than low sine shape.

In general, open-section profiles provide different crushing morphologies depending on the global shape as shown in Figure 1-6. Most of the open-section profile specimen in this figure experience mixed-mode crushing failures. For example, in the hat-shape (Figure 1-6c), splaying mode is induced by an internal delamination that generates an internal debris wedge to drive the crushed plies petalled away from the center line while the fragmentation mode induced by large transverse strain [JOO11]. In term of energy absorption capability, it is often reported that open-section profile absorbs lower energy than closed-section profile [JIM00]. However, Feraboli et al [FER09] has reported that small corner stiffener is more efficient in absorbing energy per unit mass than square shape stiffener for the front bumper design in cars.

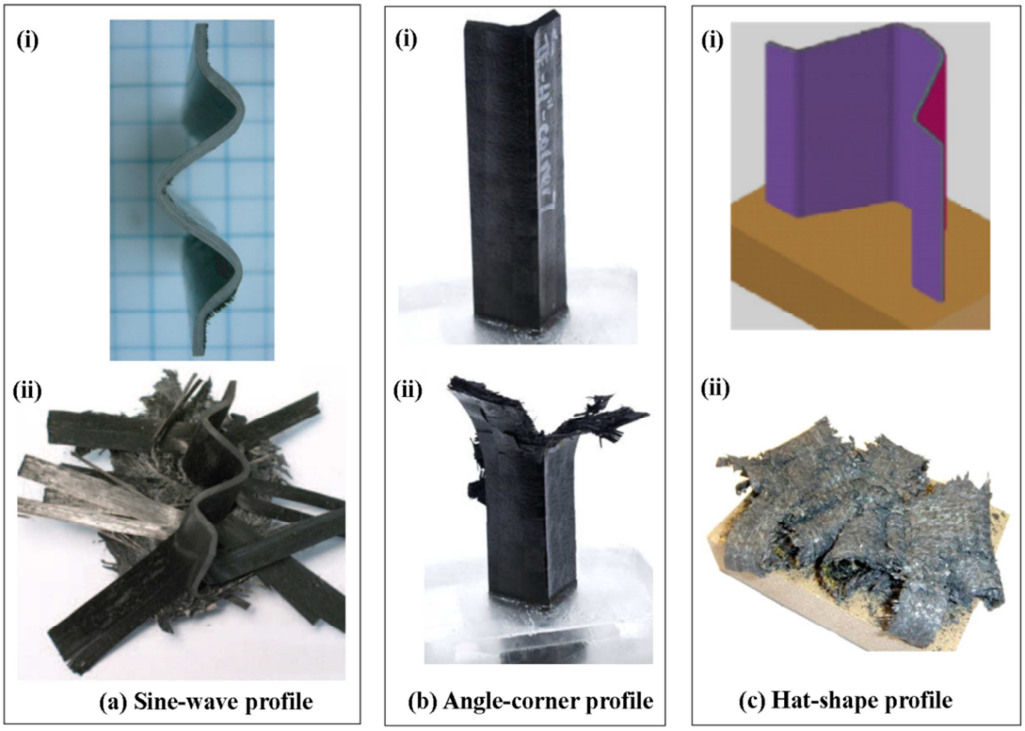

Figure 1-6: Crushing behavior of open-section profile (a) sine-wave profile [FER08], (b) Angle-corner profile [FER09] (c) Hat-shape profile [JOO11].

- **Flat Plate**

In the literature, less studies has been reported concerning crushing tests of flat plate coupon [LAV96, GUI08, DUO10, SAV06]. Normally, flat plate coupons are used for elementary test to study the effects of different materials, stacking sequences, trigger mechanisms etc. which significantly reduced the costs and materials. For instance, Lavoie and Kellas [LAV96] used flat plate coupon to study the effects of structure dimensioning and laminate design with different materials on the crushing behavior as well as energy absorption capability. For development of numerical models, composite plates are often used to obtain input data for computational models.

The crushing plate has the advantage of being simpler to manufacture. However, it absorbed low energy compared to the other geometry shapes that normally have fronds or petals during the crushing which can dissipate a lot of energy (Figure 1-5). Therefore, flat plate cannot represent the real energy absorber [GUI08]. But the development of composite crashworthiness test programs commonly relies on the pyramid test or building block approach. Then, the composite plate is useful at the elementary scale testing to study some specific behavior or to investigate some mechanical properties for material characterization before going into detail design of sub-component or component testing [GUI08, DUO10].

In addition, the crushing tests of composite plate are complicated since it can have global buckling when subjected to compressive load. As a result, it requires a specific test fixture to support it during the crushing tests. Some researchers [LAV96, DAN00, DUB98, SAV06], have proposed a test fixture that manage to avoid global buckling but the specimen is being forced to tear around the specimen supports (see Figure 1-7a). Such tearing introduced parasite energy absorption. Therefore, an innovative test fixture has been proposed in [GUI08, FER08] to overcome this limitation by providing a path for the crushed, splayed laminate and debris to escape during the crushing test (see Figure 1-7b).

The composite plate may exhibits different types of crushing mode; pure splaying, pure fragmentation or mixed of these modes, which depend upon the trigger mechanisms (refer to Figure 1-3a-ii, 1-3b-ii, 1-3c-ii). Guillon [GUI08] reported that pure fragmentation is hard to obtain in composite plate, because outer plies often crush in splaying mode. Most of the crushing front exhibit mixed modes crushing. The drawback of mixed mode crushing is some plies can slip out, so the number of plies in fragmentation changes during the crush. This causes irregularity and dispersion on the crush load curve and crushing morphology.

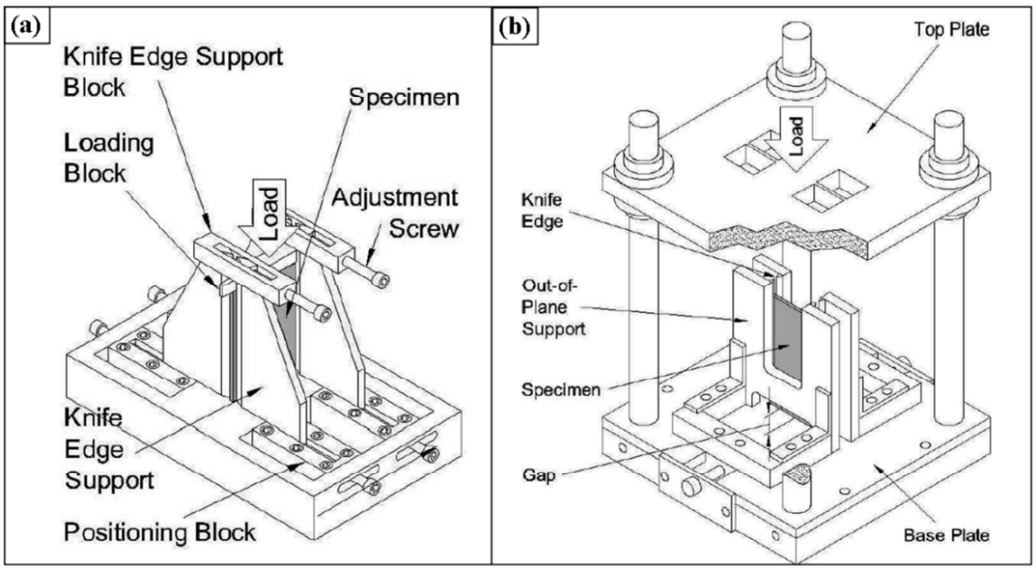

Figure 1-7: Crush test fixture design of (a) Savona and Hogg [SAV96] (b) Feraboli [FER08]

1.2.2 Testing Configurations

Numerous studies have been done in optimizing the SEA by changing the testing configurations such as crushing speed and the angle directions of applied loading.

1.2.2.1 Crushing Speed

Early studies by Hull [HUL91], Farley and Jones [FAR89] on the effect of crushing speed rates up to 15 m/s on the tubular type structures have brought to the conclusion that crushing speed did not affect energy absorption. However, recent investigations of the effects of crushing speed on the composite structures have come out with two different conclusions. The crushing tests on the carbon/epoxy flat plate done by Duong et al [DUO10] have shown no influence of crushing speeds (20 mm/min up to 9 m/s) on the SEA while Jackson et al [JAC11] has found a reduction around 6%-15% in SEA with the increasing testing rates on other carbon/epoxy omega-shape composite structure. They have concluded that the reduction is due to a subtle change in fragmentation mode with more debris ejected from the specimens.

Other studies in the middle of the 90's have also reported that for some composite materials, energy absorption is a function of crushing speed. Most of the studies have shown an increment in dynamic crushing rates had substantially reduced the energy absorption. For example, the crushing tests of carbon/epoxy tubes (knitted fabric) done by Ramakrisna [RAM97] has shown a reduction of 20% in SEA with the increment of crushing speed ranging from 0.001 (quasi-static) up to 12 m/s. This is perhaps due to the reduction of mode I fracture toughness and the friction with the increase in crushing speed [JAC11]. Similar behavior is

observed too in the crushing tests of composite flat plate coupons done under different speeds (from 2.5mm/min to 7 m/s) by Lavoie and Kellas [LAV96]. Composite plate that is crushed at higher speeds exhibited more splaying plies due to the drop in matrix stiffness.

Nevertheless, some composite materials have demonstrated the opposite behavior. Mamalis et al [MAM97B] have made crushing tests for a given square-shape with two different materials, glass/polyester and glass/vinylester. They also made another study but were only using glass/polyester with square cone shape (square frusta) [MAM96A]. Both studies are conducted with different crushing speeds (ranging from 0.0002 m/s to 8.0 m/s). Overall results of SEA have shown a 15% decrease for glass/polyester material but a 20% increase for glass/vinylester material. The analysis has shown that the difference in SEA results is due to the different values of the dynamic friction coefficients, higher for glass/vinylester and lower for glass/polyester with the increase of crushing rates that indicates the friction coefficients of different materials were affected by strain rate in different ways.

From the discussion above, it is hard to conclude on the effect of crushing speed on the SEA value since it interacts with the material behavior and the geometrical shape as highlighted in [FAR89]. However, for the composite tubes crash under axial crushing, Mamalis et al [MAM97A] has reported that the increasing or decreasing of SEA due to the effect of crushing speed depends on the material properties.

1.2.2.2 Angle of Loading Direction

In contrast to the effect of crushing speed, the study of different load directions on the crushing performance has rarely been reported in the literature. An investigation on the influence of angle between loading and specimen's axis is carried out by Ochelski et al [OCH09]. They study the effects of crushing loading at two different angles (0° and 20°) on the composite tube and cone made of carbon/epoxy. A slight change of crushing mechanisms and SEA is reported for the cone-shaped specimens but circular tube specimens loaded at 20° angle has failed under global buckling.

In another study, Greve et al [GER08] have made an axial and oblique (15°, 20°, 25° and 30°) crash tests on short thin-walled tubes made from cylindrical continuous carbon fiber reinforced composites (CCFRC). They also made an oblique crash at angle 15° on long circular tube specimens. In general, all the short specimens have crushed progressively but the energy absorption capability getting lower with the increment of the oblique angles as the competition between global bending of the tube and the local fragmentation at the crush front

is getting higher. Similarly in [OCH09], long circular tube specimens have failed under global bending fracture in the contact zone between the tube and the support ring.

Based on this review, it can be said that the SEA is widely dependent on the load angle. Crushing mechanisms on the other hand depends on the geometrical shape and dimensions. Short length specimen is recommended to be used for high angle loading in order to avoid general buckling or bending fracture.

1.2.3 Laminate Design

Many attempts to draw the relationship between the crushing behavior and the laminate design which involve different types of fibers, matrices and stacking sequences have been reported in the literature. All these three parameters may influence significantly the energy absorption capability and the crushing behavior of the laminate.

1.2.3.1 Effect of Fiber Type on the Crushing Performance

In general, there are three main composite fibers widely used in composite crashworthiness studies: carbon fiber, glass fiber and aramid fiber (Kevlar). As mentioned before, carbon and glass fibers are progressively crushed in splaying and fragmentation modes [RAM97, OCH09] whereas Kevlar is crushed by progressive folding [FAR89, KIM11]. Ramakrishna [RAM97] conducted a series of crushing tests with different materials, carbon (AS4)/PEEK, carbon (IM7)/PEEK and glass (S2)/PEEK tubes under crushing tests. The results have shown that all tubes crushed progressively in a splaying mode. Kim et al [KIM11] on the other hand, compared carbon/epoxy and Kevlar/epoxy tubes under crushing tests. Similarly, carbon tubes exhibit complex behaviors with both splaying and fragmentation modes while Kevlar tubes failed under buckling mode with good post-crush integrity.

In term of energy absorption, Farley and Jones [FAR92] have concluded that carbon delivers the highest SEA, followed by glass and Kevlar. This conclusion have been validated in many studies showed the used of different fibers have influence in energy absorbing capability due to the materials properties [MAM97A, RAM97, OCH09, KIM11]. For example, Ochelski et al [OCH09] reported that the higher value of SEA in carbon/epoxy material is due to higher mechanical properties such as modulus young in tensile and compression as compared to glass/epoxy materials. Kim et al [KIM11] also found the same result when comparing between carbon/epoxy and Kevlar epoxy. Besides that, the SEA

results in the study of Ramakrishna [RAM97] have shown that carbon fiber exhibits higher SEA because of its low density compared to the glass fiber.

Apart from the use of common fibers, some researchers tried to hybridize them and compared it with the common fibers. Kim et al [KIM11] tried to evaluate circular tubes made of carbon-Kevlar and Kevlar-carbon hybridization. They showed the addition of Kevlar in the carbon tubes has improved the post-crush integrity by mean the crushing mode has changed from brittle fracture to local buckling and of course reduced a little bit the SEA value. Similarly, contrast behavior is obtained when adding carbon into Kevlar tubes. This is to say, hybridization tubes, the crushing mode and SEA is dependent on the types of fibers in the axial direction. Chiu et al [CHI99] also observed the same behavior of carbon-Kevlar hybridization tubes. Hence, in the vehicle design, if energy absorption capability and post-crush integrity are simultaneously required, carbon-Kevlar hybridization would be the best choice.

1.2.3.2 Effect of Matrix on the Crushing Performance

Regarding the matrix types, it is often the choice between a thermosetting matrix i.e. epoxy, vinylester etc. and thermoplastic i.e. polyetheretherketone (PEEK), polyimide (PI), polyarylsulfone (PAS) etc. Some studies reported that the SEA has a strong correlation with mode I and Mode II inter-laminar fracture toughness (GIc and GIIc) of the matrix: higher GIc and GIIc of laminate will absorb higher energy [RAM97, SAV06B, HAD09, GHA09]. As reported, tougher matrix gives higher GIc [RAM97, GHA09].

Ramakrishna [RAM97] studied extensively the behavior of thermoplastic matrices. He found that PEEK resin presented the toughest fracture toughness and absorbed highest SEA compared to the others thermoplastic resins. Hamada et al [HAM 95] in other study found that the PEEK resin provides better SEA than epoxy resin due to the higher fracture toughness and good strength of the fiber-matrix bonding. However, because of its complexity of nature, it is more difficult to impregnate the fibers which require special equipment and techniques. This can increase the manufacturing cost. For that reason, thermosetting matrices which are easier to manufacture has been widely used especially epoxy resin. Besides that, it has excellent resistance towards corrosion and good fatigue strength. Farley and Jones [FAR89] have demonstrated that an increase in matrix failure strain of epoxy resin causes an increase in energy absorption capability with brittle fibers but it reduces with ductile fibers. Larger failure

strain normally reduces the inter-laminar cracks which promote more fiber breakages to performed fragmentation mode that absorb higher energy.

1.2.3.2 Effect of Fiber Architecture on Crushing Performance

Like the other influences discussed before, crushing behavior and SEA are also sensitive to fiber architecture. Its influence can be present in many ways such as varying fiber orientation, fiber contents or lengths, woven or UD fibers etc. Ramakrishna [RAM97] tried to summarize all the influence of these choices with composite tube using carbon and thermoplastic matrices. It is noted that there is a strong interaction between these parameters.

In term of stacking sequence, Ramakrishna [RAM97] found that the SEA and crushing behavior is a function of the angle of fiber lay-up. The SEA values for carbon/PEEK tubes increases as the angle increases from 0° to 15° due to the reduction in the length of longitudinal cracks by mean of the fracture toughness is improved that control the crack growth process. In the same time, micro fracture processes like fiber failure and frond splitting have increased. However, Farley and Jones [FAR89] have demonstrated that for carbon/epoxy tubes with cross-ply laminate [0°,±θ], that SEA decreases as the angle increases but for laminate [±θ], a non-uniform trend of SEA is recorded as shown in Figure 1-8. This is due to the percentage of material crushed in each mode which varies with ply orientation.

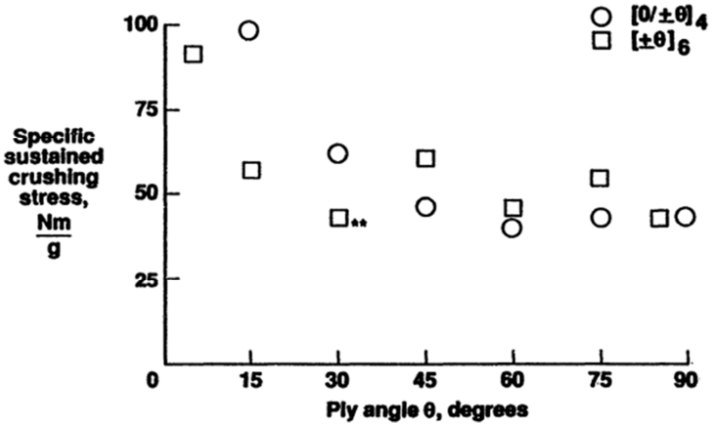

Figure 1-8: Effect of ply orientation on the energy absorption capability of T300/934 carbon-epoxy tubes [FAR89]

For the same laminate but made from glass fiber and Kevlar, Farley and Jones [FAR89] found an increment of SEA as the angle increased up to 60°. According to their report, this is because of the predominant crushing mode of lamina bending and local buckling in glass/epoxy and Kevlar/epoxy tubes respectively. Besides that, the lateral support to axial fibers of these tubes is increased with the increasing angle.

In terms of the fiber contents and lengths, Mamalis et al [MAM97A] reported that short fibers exhibit lower stiffness than the long fiber and an increase in fiber contents may improve the SEA. However, the addition of fiber contents may not always necessarily improve the SEA as the material density is increased as well.

Different fiber architectures such as UD, braided and woven have been widely tested in the crashworthiness study to optimize the SEA and crushing behavior. Ramakrishna [RAM97] has reported that for a given material (carbon/PEEK), all these architectures exhibit almost the same crushing behaviors (brittle fracturing under splaying and fragmentation modes). Only the woven and knitted architectures always have the transitions in crushing modes between fragmentation and splaying as it depends on the weft and warp directions. Besides that, it is noted that different fiber architectures deliver different SEA values, with UD architecture demonstrating the highest SEA followed by woven and braided.

1.2.4 Summary of Experimental Studies

In the absence of reliable predictive numerical simulation, experimental test campaigns are still the best way to improve the crash behavior of composite structures. A wide range of investigations have been made to optimize the crushing performance of composite structures. This involves numerous trials on varying many parameters that could influence the composite crashworthiness. It can be seen in some cases, a slight change in configurations may cause a complete change in the crushing process. Therefore, it is difficult to establish clear trends of the crushing behaviors since these trials are often made to understand on the specific domains in which does not lead to general conclusions.

Macro-scale tests are insufficient to understand the mechanisms that drive the failure to occur during the crushing tests. Ideal for understanding of the mechanisms involved would be microscopic observation of composites during the crushing test is done. There is very few study of the crushing behavior at lower scale.

1.3Numerical Modeling of Composite Crashworthiness

Parallel to the development in experimental works, numerical simulations have been proposed to model composite crushing as a part of the design process for the development of crashworthy components. In fact, the interest in current studies of composite crashworthiness [MCG07, XIA09, HEI10, FER11, ZHA13, OSH13] have focused more on the development and simulation of the crushing behavior using finite element model analysis as a solution to

substitute the expensive experimental programs [PIN04]. Different approaches and methodologies have been introduced to improve the numerical modeling of composite crashworthiness with varying degrees of success. This extensive development of numerical models has been motivated by the advances in computer resources and finite element software.

Literary wise, the numerical modeling of composite crashworthiness was initiated in 1989 by Farley and Jones [FAR89] concerning the prediction of the crushing response of circular composite tubes. The developed model is a quasi-static numerical model and based on a virtual crack extension technique since the main feature of the model is the ply separation. Their model is able to simulate the failure mode observed in experiment with ply separation but the laminate crushing stress is not well-predicted. Since then, many efforts have been made by many researchers to improve the numerical modeling of composite crashworthiness in various aspects such as the choice of constitutive models [FEL06, XIA09], delamination technics [PIN04, FLE06], triggering mechanisms [MCG07, PAL10A] etc. in order to properly predict the crushing morphology, specific energy absorption (SEA) and force-displacement curve, as experimentally observed.

To adequately describe the crushing morphology in the numerical modeling which involves large deformation and non-linear behavior, the use of non-linear analyses via an explicit code is seems more appropriate to describe the initiation and progression of a crushing mode failure [PIN04, HEI10, JOO11]. Besides the integration scheme, the development of crushing modeling also depends on the choice of modeling scales, damage models and the methodology that will be presented in the following sections.

1.3.1 Modeling Scale

As discussed before, crushing phenomenon in composites generally involves failure modes different than those observed in conventional metallic materials which take place at different length scales [MAM97A]. Therefore, it is necessary to define a scale on which the material can be described properly without going into excessive details. Three main modeling scales classically classified are macro-, micro- and meso-scale.

- ***Macro-scale (structure scale)***: Some of the models developed in the past [XIA09, FER11, OSH13, ZHA13] are based on global test characterizations that take place at macro-scale (structure scale) making the model strongly dependent on the global laminate behavior, as an example in Figure 1-9a [DEL00]. Even though this

methodology makes modeling simpler and decreases computational time, any precise failure modes or interface damages, for example delamination cannot be predicted. Normally, the macro-scale is used for larger scale structure since the main motivation of the modeling is to predict the energy absorption capability with roughly prediction on the global damage of structure in the crushing zone. That is to say, this scale is more favorable for the structure-level modeling.

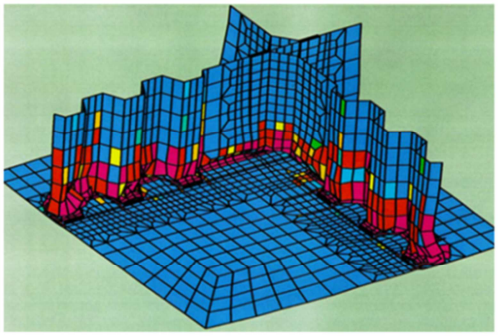

(a) Macro-scale: Dynamic-crash simulation on corrugated sub-floor box

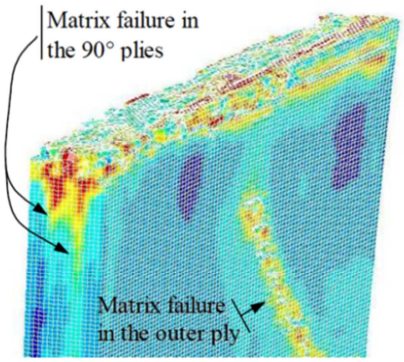

(b) Micro-scale: Quasi-static crushing of composite column with $(45/0/90/45)_S$

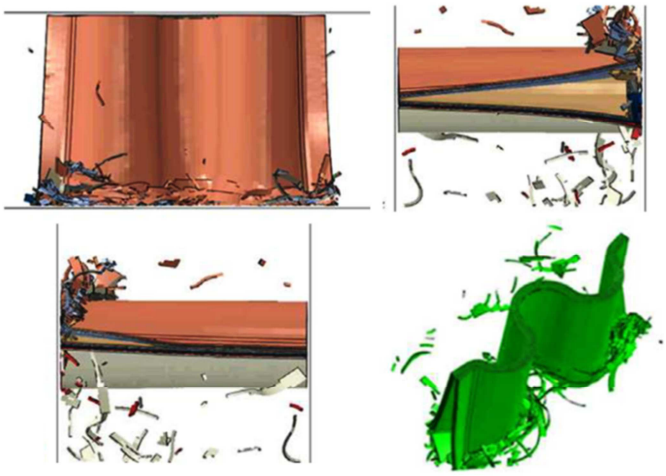

(c) Meso-scale: Quasi-static crushing of composite sine-wave laminate $(0/90)_{2S}$

Figure 1-9: Examples of crushing modeling: (a) macro-scale [DEL00], (b) micro-scale [PIN05] and (c) meso-scale [SOK11]

- ***Micro-scale (fiber scale)***: Concerning models using micro-scale approach, physical representation of such a complex phenomenon is difficult, and even if it is possible, detailed physical parameters and internal variables concerning each kind of damage involved [LAU07] are needed which are very difficult to obtain. The modeling motivation is concerns more on the comprehensive study of the physical mechanism at fiber or matrix level such as fiber-matrix debonding [CAP06], fiber friction effect [RAO07] etc. rather than designing a composite part or structure. Furthermore, it requires high computational time that would restrain study cases only to small structures.

- ***Meso-scale (ply scale)***: Between macro- and micro-scale, the meso-scale (ply-scale) approach, commonly used in composite modeling [ALL97, LAD00] seems to be the appropriate one. This is an intermediate scale between micro-and macro-scale associated with the thickness of the layer and of the different inter-laminar interfaces [ALL97]. Although it requires more detailed laws as compared to macro-scale models, it nonetheless has the potential to capture most of the physical phenomena occurring at the crushing front such as the propagation of delamination, fiber failure, matrix cracking and debris accumulation [GUI08, SOK11].

1.3.2 Failure Modeling

Failure criteria are used to represent sudden failure of the ply or to introduce a progressive failure through damage evolution. Various approaches have been used to predict well the damage mechanisms. Most of the failure models used in crushing modeling is based on conventional failure criteria (Tsai-wu [TSA71], Hashin [HAS80], Chang-chang [CHA87] and Matzenmiller [MAT95]) with varying degrees of success in simulating the crushing behaviors of composite structures. In general, most of them are strength-based failure criteria and have been proposed since 1971 [TSA71] with the aim to accurately predict the onset of composite material failure. Recent works in numerical modeling have focused less on the role of delamination and put more attention on improving the intra-laminar failures [FER11, OSH13]. Nevertheless, there are also several researchers that recognize the importance of delamination in the crash behavior and keep trying to enhance the modeling of delamination [FEL99, PIN04, FEL06]. The review of failure modeling is classified into two categories, intra-laminar failure and delamination modeling.

1.3.2.1 Intra-laminar Failure

Predicting the intra-laminar failures of composite is complex as it involves fiber failure and matrix cracking either under tension, compression, shear or combination of these loads. For the damage initiation or sudden failure of the ply, there are two types of failure models reported in the literature called non-physically and physically-based failure criteria [PIN05]. A non-physically based failure criteria is defined as a dependent function of all components of the stress tensor from which it determines the global state of the material. It is relatively simple to use but it does not specifically consider the failure modes observed in composite materials or non-phenomenological. For example, the Tsai-Wu criterion [TSA71] used quadratic stress-based equation to predict the global failure of composite as expressed in eq. (1-2) for three dimensions case.

$$\frac{\sigma_{11}^2}{X_T X_C}+\frac{\sigma_{22}^2+\sigma_{33}^2}{Y_T Y_C}+\frac{\left(\sigma_{12}^2+\sigma_{13}^2+\sigma_{23}^2\right)}{{S_C}^2}-\frac{\left(\sigma_{11}\sigma_{22}+\sigma_{11}\sigma_{22}\right)}{\sqrt{X_T X_C Y_T Y_C}}-\frac{\sigma_{22}\sigma_{33}}{Y_T Y_C}$$
$$+\sigma_{11}\left(\frac{1}{X_T}-\frac{1}{X_C}\right)+\left(\sigma_{22}+\sigma_{33}\right)\left(\frac{1}{Y_T}-\frac{1}{Y_C}\right)\geq 1 \qquad \text{(Eq.1-2)}$$

With X_T and X_C: longitudinal tensile and compressive strength
Y_T and Y_C: transverse tensile and compressive strength
S_C: shear strength
σ_{ij}: stress tensor

Physically-based failure criteria on the other hand distinguish between failure modes, aiming at describing the physics of the failure process. The maximum stress and maximum strain criteria can be considered the simplest physically-based failure criterion that has been used not only in crashworthiness modeling [PIN05] but also in impact modeling [BOU09] for predicting the fiber tensile failure.

Maximum stress / strain failure criterion:

$$\sigma_l \leq X_T \quad / \quad \varepsilon_l \leq \varepsilon_l^0 \qquad \text{(Eq.1-3)}$$

With: σ_l: current longitudinal stress
ε_l: current longitudinal strain
ε_l^0: tensile failure strain in fiber direction

Among the physical based failure criteria exist in the literature are Hashin failure criteria [HAS80]. It has been widely used to predict failures in composite laminate [GUI08, PAL10A, ZHA13] because of its capability to distinguish the damage initiation in various failure modes in each constituent (fiber and matrix) separately. This criterion used quadratic

interaction equation to propose four failure modes that are separately considered between tension and compression failures:

Tensile fiber failure:

$$\left(\frac{\sigma_{11}}{X_T}\right)^2 + \frac{\left(\sigma_{12}^{\ 2} + \sigma_{13}^{\ 2}\right)}{S_C^{\ 2}} \geq 1 \qquad \text{(Eq.1-4)}$$

Compressive fiber failure:

$$\frac{\sigma_{11}^2}{X_C^2} \geq 1 \qquad \text{(Eq.1-5)}$$

Tensile matrix failure:

$$\frac{1}{Y_T^{\ 2}}(\sigma_{22} + \sigma_{33}) + \frac{1}{S_T^{\ 2}}(\sigma_{23}^{\ 2} - \sigma_{22}\sigma_{33}) + \frac{\left(\sigma_{12}^{\ 2} + \sigma_{13}^{\ 2}\right)}{S_C^{\ 2}} \geq 1 \qquad \text{(Eq.1-6)}$$

Compressive matrix failure:

$$\frac{1}{Y_C}\left[\left(\frac{Y_C}{2S_T}\right)^2 - 1\right](\sigma_{22} + \sigma_{33}) + \frac{1}{4S_T^{\ 2}}(\sigma_{22} + \sigma_{33})^2 + \frac{1}{S_T^{\ 2}}(\sigma_{23}^{\ 2} - \sigma_{22}\sigma_{33}) + \frac{\left(\sigma_{12}^{\ 2} + \sigma_{13}^{\ 2}\right)}{S_C^{\ 2}} \geq 1 \qquad \text{(Eq.1-7)}$$

With: S_T: transverse shear strength and the rests are the same notations as for Tsai-Wu criterion (Eq. 1-2).

Nevertheless, some studies have reported that the stress interactions in this failure model do not always fit the experimental results, especially in the case of compressive failure of fiber or matrix [DAV03, PIN05]. Furthermore, it also did not consider the effects of in-plane shear in the compressive fiber failure that reduces significantly the effective compressive strength of a ply [DAV03].

Besides Hashin failure criterion, several other failure models have been proposed in the literature for general prediction on the failure in composite laminate. Chang–Chang failure criterion [CHA87] for example has been proposed in 1987 in which a modified version of the Hashin failure criterion [HAS80] was suggested to include the non-linear shear stress-strain behavior in the tensile fiber mode equation. This failure model has been established in LS-DYNA commercial code and has been used in many crashworthiness modeling studies [FLE06, ZAR08, HUA09]. In general, as reported in World Wide Failure Exercise [DAV03, PIN05] most of these conventional damage models are unable to capture some failures in regard to compressive loading on the fiber and matrix in which there are great interest in the

crashworthiness modeling for example in simulating the fiber and matrix under compressive crushing mode.

Based on this report, various efforts have been done by several researchers to enhance the existing failure criteria. Among them are Dàvila and Camanho [DAV03], and Pinho [PIN05] that have proposed failure criteria for matrix and fiber compression based on Mohr-Coulomb criteria (Eq.1-8) proposed in [DAV03] and Eq.1-9 proposed in [PIN05]. The idea of their works is to take into account the interaction between the stresses and the angle of the fracture plane that was found oriented at 0° and 53°±2° (Figure 1-10a). Furthermore, they have also proposed the formulation of fiber kinking in compression (Figure 1-10b) based on a micro-mechanical model and coupled with the failure criterion matrix.

$$\left(\frac{\langle|\tau_T|+\mu_T\sigma_n\rangle}{S_T}\right)^2+\left(\frac{\langle|\tau_T|+\mu_L\sigma_n\rangle}{S_L}\right)\geq 1 \qquad \text{(Eq.1-8)}$$

$$\left(\frac{\tau_T}{S_T-\mu_T\sigma_n}\right)^2+\left(\frac{\tau_L}{S_L-\mu_L\sigma_n}\right)^2\geq 1 \qquad \text{(Eq.1-9)}$$

With: τ_L and τ_T : longitudinal and transverse shear stresses acting on the fracture plane

μ_L and μ_T : internal material friction in longitudinal and transverse directions

S_L and S_T: longitudinal and transverse shear strengths

σ_n : Stress normal to the fracture plane

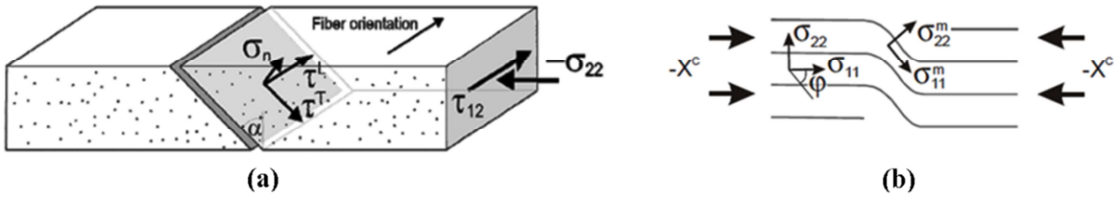

Figure 1-10: (a) Angle of fracture plane of a UD lamina subjected to transverse compression and in-plane shear (b) Fiber kinking in UD lamina subjected to longitudinal compression [DAV03]

Some of the numerical models in the literature only considered the damage initiation by using one of the failure criteria explained before to account for failure mechanisms at crush front. Once failure is detected, the relevant elastic properties are reduced to zero over a fixed number of time steps. This approach is unrealistic as the post-failure behavior is completely disregarded [PIN05]. In order to model damage propagation, damage variables are defined to degrade linearly the relevant stress components to zero as shown in Figure 1-11a [PIN05]. The positive slope of the stress-displacement curve prior to damage initiation corresponds to linear elastic material behavior while the negative slope after damage initiation is achieved by

evolution of the respective damage variables according to the damage evolution of different failure modes. In general, final degradation of material is depending on the energy dissipated G^c which corresponds to the area under the curve (0AC).

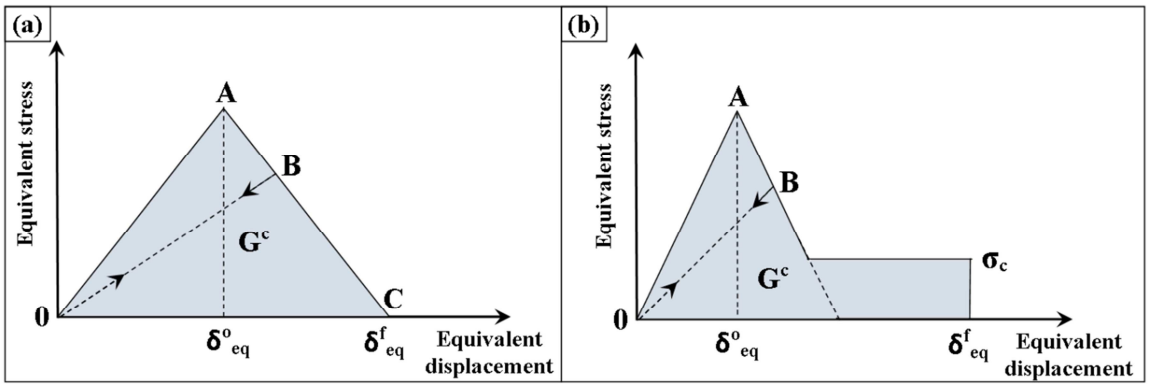

Figure 1-11: Damage evolution (a) linear degradation after initiation [PIN05, BOU12] (b) Additional constant crushing phase [FOU05, MCG08]

Nevertheless, in some studies of crashworthiness modeling [FOU05, MCG08] a constant crushing phase as example shown in Figure 1-11b has been added into the damage evolution of fiber compression failure, particularly to have better representation of fragmentation crushing mode and force-displacement curve. Generally, the constant plateau is characterized from the laminate mean crushing stress, σ_c. Thus, this type of damage model is dependent on the global behavior of laminate which does not permit to have a predictive model.

There are also failure models specifically innovated for the crashworthiness study. In particular, CODAM failure model based on continuum damage mechanics initially proposed by Wiliam and Vaziri [WIL01] to analyze tensile dominated failure. Then, it has been further developed by McGregor et al [MCG08] to include compressive predictive capabilities in order to use in composite crushing of braided tubes [XIA09, MCG10]. It generally includes both damage initiation and evolution. This model has provided better results than Matzenmiller failure criterion [MAT95]. However, the compressive stress-strain response in this model depends on the estimated plateau stress (laminate mean crushing stress) measured in coupon specimens under compression. Thus, this stress is not an intrinsic parameter that makes it dependent on the global parameters of the coupon specimens. Moreover, this model is specifically proposed for the braided type composite. There is no study reported using CODAM criterion on other type fiber of architectures for example UD and woven. The coupling model between viscoplasticity and damage has also been introduced to improve the composite structure response when submitted to the high strain rate loadings (impact,

crushing...) [MAR06]. This coupling is realized through the introduction of the effective shear stress which stands for the stress that should be applied to the undamaged material to obtain the same state of deformation as the one obtained with shear stress on the damaged material. A good agreement between the experimental and numerical results is achieved but this approach only suitable for the CFRP woven type materials. Moreover, in the case of tube crushing simulation, the prediction crushing response is focused more on the brittle failure at the middle of the tube structure instead of the damage at the crushing front.

1.3.2.1 Delamination Modeling

Delamination failure is also a complex behavior to simulate. Several techniques and criterions have been introduced to improve the delamination behavior during crushing. An absence of delamination in crushing modeling may cause the prediction of SEA and deformation pattern to be different from the experimental results, as demonstrated by Palanivelu et al [PAL10A]. An extensive review on delamination modeling for the crash application has been provided by Fleming [FLE99]. In general, interface modeling technique (discrete model) has been widely used in predicting the delamination failure in crash modeling since early 1990's [WIS10].

In the context of crash analysis, three methods of delamination modeling are reported in the literature, stress-based failure models, virtual crack closure technique (VCCT) and cohesive zone model (CZM). As reported in [FLE99], the stress-based criterion is the easiest to implement by using the equation as follow:

Stress-based criterion:

$$\left(\frac{\sigma_N}{\sigma_{Nc}}\right)^{a_n}+\left(\frac{\sigma_S}{\sigma_{Sc}}\right)^{a_s}\geq 1 \qquad \text{(Eq.1-10)}$$

With: σ_N: normal stress acting on the interface surface
σ_S: shear stress acting on the interface surface
σ_{Nc}: normal failure stress
σ_{Sc}: shear failure stress
a_n/a_s: parameter governing the interaction between the failure modes

Normally, it is assigned with tiebreak contact interface that widely used in composite tubes crash modeling [XIA09, HUA09, MCG10]. Nevertheless, the failure property is hard to define and basically obtained through experimental correlation. Furthermore, it is often reported that the results are likely to be mesh-dependent. Thus, a fracture mechanics based

criterion is recommended that depends on the critical energy release rate such as virtual crack closure technique (VCCT) and cohesive zone model [FLE99, WIS10].

VCCT method is commonly used to calculate strain energy release rates in the model and predict delamination growth. The method is based on the assumption that the energy required for an infinitesimal amount of crack extension is equivalent to the work that would be required to close the crack to its original length [FLE99]. Thus, its accuracy is also strongly dependent on the mesh size and may require mesh refinement that are incompatible with a crash modeling. Wisnom [WIS10] also reported that VCCT method may present limitation to the simulations which involve multiple failures and interact to each other. This limitation can be seen in the modeling of composite plate crushing done in [FLE99].

The cohesive failure model on the other hand received more attention lately to simulate the delamination failure in composite laminate. Pinho [PIN04] is one of the first authors that has demonstrated its potential application for crashworthiness modeling based on the procedures presented by Camanho et al [CAM03]. They simulated composite tubes crushing based on the experimental tests of Hamada et al [HAM95]. Good correlations are obtained. Following this achievement, it has been widely used in crash modeling works as reported recently in [PAL10A, PAL10B, JOO11, SOK11, ZHA13].

Cohesive failure model controls the delamination at the interface based on bilinear traction-separation laws which consider the amount of energy required to create new fracture surfaces. This model usually works with cohesive elements that are placed between different oriented plies to represent the interface and its thickness can be either infinitely thin or have a finite thickness. It also can be assigned with tie contact interface as reported in [JOO11, ZHA13].

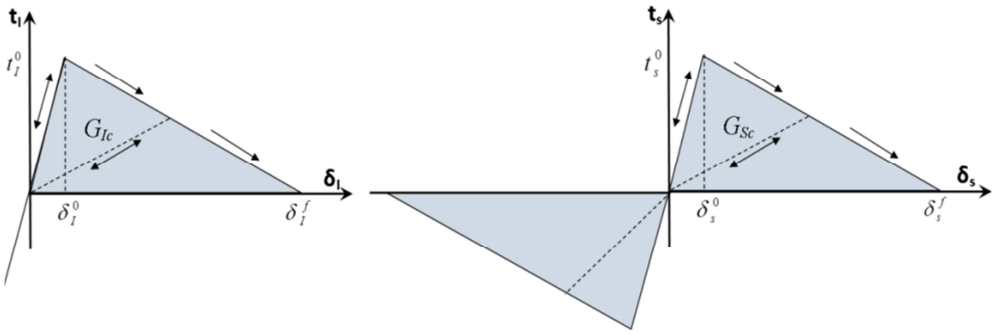

Figure 1-12: Bilinear constitutive law of pure loading mode [PIN05]

In general, the traction-separation law involves three states: a damage initiation, a damage evolution and a complete separation as shown in Figure 1-12. The damage initiation is referring to the starting of the degradation of the response in the material when the

maximum traction either in opening (mode I) or shear modes is reached. For example, the corresponding onset separations are as follow [PIN05]:

$$\delta_I^0 = \frac{t_I^0}{k} \ , \ \delta_s^0 = \frac{t_s^0}{k} \qquad \text{(Eq.1-11)}$$

With: t_I^0 : maximum allowable tractions in mode I
t_n^0 : maximum allowable tractions in shear mode
k : elasticity of the element

The damage then propagates until the traction reaches zero in which the energy absorbed is equal the critical energy release rate. This leads to the definition of the final separations as follow [PIN05]:

$$\delta_I^f = \frac{2G_{Ic}}{t_I^0} \ , \ \delta_s^f = \frac{2G_{Sc}}{t_s^0} \qquad \text{(Eq.1-12)}$$

With: G_{Ic}: Mode I fracture toughness
G_{Sc}: shear mode fracture toughness

Perhaps the only drawback of cohesive element is that some of the material properties are difficult to obtain from conventional experimental data as highlighted in [PIN04, FLE06]. One of the solutions often taken as reported in the literature is to simulate the delamination propagation using a Double Cantilever Beam (DCB), End Notch Flexure (ENF) and Mixed-mode Beam (MMB) specimen to indentify mode I, mode II and mixed mode I/II properties. [PRO07].

Besides the failure criteria, several approaches have been studied in crash modeling to promote the delamination in the laminate. For instance, nodes and interfaces at the edge of the model are meshed with imperfections in order to promote an initial failure as reported in [GUI08, MCG10, PAL10B]. Palanivelu et al [PAL10B] have demonstrated that the implementation of predefined seams in their models has shown an improvement by providing better deformation pattern and SEA estimation compared to the seamless models. Nevertheless, there are also studies showing that it is not necessary to know a priori where delamination occurs and yet delivers good prediction of crushing behaviors [SOK11, JOO11].

Inelastic damage mechanics for interface modeling has also been introduced recently to improve the delamination prediction by taking into account the friction effects during the damage evolution as demonstrated in [GOR10]. The main idea is the modification of strain energy parameter by introducing sliding and friction parameters. At the moment, this model

only has been implemented for the study of pull-out test and provided good agreement with the experimental results.

1.3.3 Architecture of Crash Modeling

The available crash modeling in the literature are often carried out with different methodologies and approaches that incorporate the failure criteria explained in previous section. For the representation of composite laminate, it can be modeled either in two dimensional or three dimensional. Several methodologies of laminate modeling can be found in the literature of crash modeling. For example, a stacked-shell analysis methodology has been widely used for last decades to simulate crushing behavior of composite structures especially for the composite tubes. In general, number of layers of shell elements may vary from single (continuum damage mechanics) to multiple layers (discrete). A single stacked-shell methodology [OSH13] is usually handled at macro-scale level in which the prediction of SEA and global failure of laminate or structure is the main motivation. Thus, to account for both intra-laminar (in-plane) and inter-laminar (delamination) failure mechanisms in crushing simulation, the use of multiple layers with an insertion of interface elements seems necessary as demonstrated in [PAL10B, SOK11, JOO10]. Guillon et al [GUI08] on the other hand have developed a meso-scale model using 2D continuum shell element with interface element in between to simulate the elementary damages at the ply scale. Numerical simulation for the case of pure splaying mode has delivered good results compared to the experimental works. However, the use of 2D continuum shell elements has led to problems of instability in the case of mixed-mode simulation [GUI08]. Therefore, the use of 3D solid element becomes necessary to overcome these limitations by allowing the stress distribution propagates through the element thickness. Recent studies also showed 3D solid element has been used in tube crushing [HEI10]. Nevertheless, the performance of crash simulation also depends upon the representation of triggering mechanisms in the model to initiate the crushing.

For that reason, different approaches to initiate crushing have been reported in the literature. For instance plug initiator often used in the composite tubes crushing [XIA09, MCG10]. Different modeling techniques to model the chamfering trigger also have been reported. Huang and Wang [HUA09] used two-layered staked-shell model to simulate composite tube subjected to quasi-static axial crushing. Usually in the stacked-shell model, the 45° chamfer trigger is model with a gradual reduced of the thickness but Huang and Wang [HUA09] have introduced new technique to model the 45° external chamfer by translating

inward the tip nodes of each shell layer from center-line. Good agreement with experimental results is obtained in term of crushing morphology but the peak load and SEA are over estimated by the numerical model. In addition, this approach is not suitable for other types of trigger mechanism such as steeple [JOO11].

The presence of debris wedge in the numerical model to induce specific damages is also important to provide general behavior of composite crushing. Such approach has been implemented in [JOO11, MCG10]. Both studies are using stacked-shell methodology to develop the numerical model but using different technics in presenting the debris wedge. However, the approach introduced by McGregor et al [MCG10] is not suitable for a development of predictive model as they used a pre-determined debris wedge (the geometry and location of debris wedge was fixed from the beginning of simulation) to induce splaying mode at the tip of the modeled tube. In addition, this approach is only useful for crushing case where splaying mode is the main failure mode. Joosten et al [JOO11] on the other hand, introduced a new alternative to create an internal debris wedge in composite hat-shaped model. This internal debris wedge was built up from an internal delamination produced by large stresses at the tip of specimen during initiation process. This method is capable to promote the petalling mode in the simulation but the overall failure mode is not representative of the failure in experimental test. Besides that, there is no physical proof of debris wedge presented in their model.

Finally, there are also specific techniques of crush front modeling specifically developed to account for better prediction of crush front. For example, “SOFT” parameter or crush front reduction factor is introduced in LS-DYNA under material model MAT54 based on Matzenmiller criteria. SOFT parameter is used to reduce the strength of the element adjacent to the deleted element (assumed to be at the crush front). This parameter is used to avoid instability and to ensure stable crushing during the load transitions from the crush front element to the next. Cases of crushing simulations using this method are reported in literature [FER11, MAM06]. Figure 1-13a shows an example of crushing simulation using this method carried out by Feraboli et al [FER11]. However, the SOFT parameter is believed not to be related to any physical or measurable quantity. Besides that, the process of failing and deleting the elements from the mesh has created a gap and reinitiating contact produces large force spikes as shown in Figure 1-13b which is do not represent the real crushing behavior. Therefore, the crushing force often has to be “filtered” to reduce the oscillations (Figure 1-13b) before to compare with the experimental test (Figure 1-13c). Furthermore, this method is more applicable

for the larger scale or macro-scale modeling where the energy absorption and SEA prediction is the main motivation.

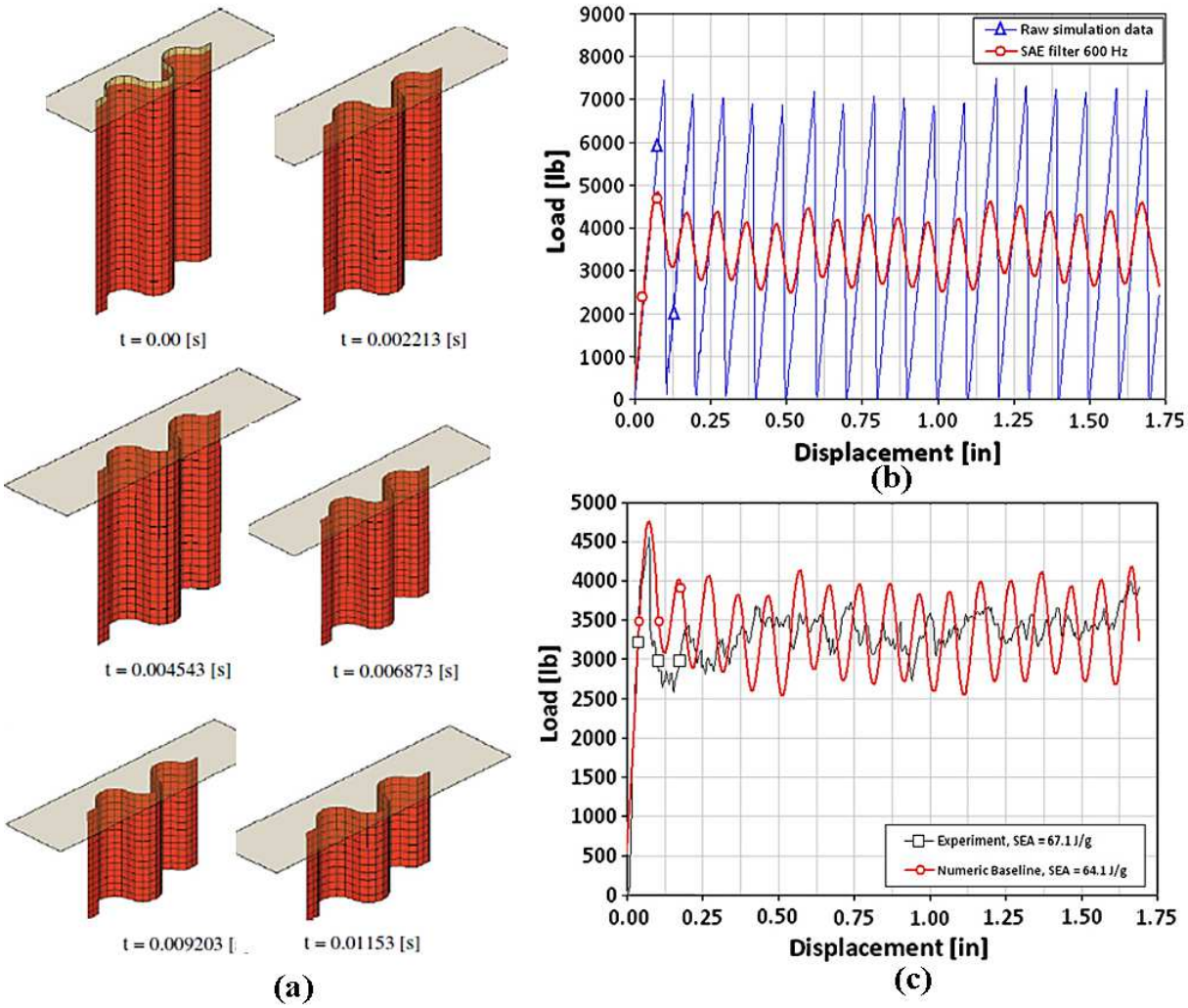

Figure 1-13: Example of corrugated composite crushing simulation using SOFT parameter [FER11] (a) crushing morphology with row element deletion (b) Filtered versus raw data of force-displacement curve (c) Comparison of force-displacement curves between experiment and simulation

CZone technology, on the other hand has been developed and incorporated as an add-on product for ABAQUS/Explicit in order to provide a predictive capability for composite structure in larger scale crash event [NIX09]. The concept of CZone is the utilization of "crush stress", a distinctive mechanical property of a composite material. This crush stress corresponds only to fiber compression stress that needs to be measured in order to be implemented with numerical model. The main idea of CZone is to predict the crushing response at the crushing front as well as the prediction of damage in regions away from the crush front. It is suitable for complex structural interaction and large scale composite structures. Acceptable correlations are reached between experimental and simulation results

on the global damage of the structure and the force-displacement curve as demonstrated by Nixon et al [NIX09] using CZone technology. Nevertheless, the value of "crush stress" can be dependent on global parameters of the tested coupons (flat plates) such as ply stack sequence, laminate thickness etc. Thus, it needs to be determined each time the laminate configurations change which increases cost and time consuming.

1.3.4 Summary of Crash Modeling

The increase in performance of computers and advance explicit code, have allowed rapid development of numerical models to provide good solutions for composite crashworthiness problems.

The crash modeling is particularly complex to develop as it involves different damage mechanisms and crushing modes that can interact with each other. Different methodologies and failure criteria have been employed with their advantages and disadvantages. However, due to complex nature of failure mechanisms in composite structures and subsequently to the lack of relevant experiments on elementary damage mechanisms, they are often too simplified or too specific to be predictive on complex structures. For example models developed at macro-scale usually used laminate mean crushing stress and no representative of delamination. Such modeling is not predictive to represent the crushing at any structure but only allows obtaining relative representativeness.

Therefore, to adequately represent crushing morphology and the SEA it seems necessary to develop numerical models at ply-scale to simulate physically the behavior of plies at the crushing front and its evolution during crushing. To do so, again an improved understanding on the elementary damage mechanisms is thus necessary to properly understand and to introduce better methodology to simulate the crush behavior. Only then, probably by using a multi-level strategy for development of macro-scale models could provide the overall failure mode of a structure based on a meso-scale model for the simulation of the crushing front.

Chapter II

EXPERIMENTAL TESTS & DAMAGE ANALYSIS

Simulating the crushing process of a composite structure must be able to describe the initiation and progression of a crushing mode right up to the point of final failure. In contrast to ductile metals, which mainly absorb energy by plasticity during crash, composite structures absorb energy through combination of fracture mechanisms, which involve fiber fracture, intra- and inter-laminar matrix cracking, fiber–matrix debonding and delamination [FAR89, HUL91], all of which at a micro or meso-scopic (sub-ply) scale. This means in order to be able to represent these mechanisms in a crushing numerical simulation, it requires a detailed finite element model at the scale of these observed phenomena.

As seen in the literature review, the limitation in previous studies is mostly due to the lack of information on the elementary damage mechanisms. Therefore, it is very important to have a close observation of the crushing process to improve the understanding of damage behaviors and the mechanisms that drive the failures to occur during the crushing tests. Furthermore, it can support the development of numerical model including an observation at micro-scopic level. Thus, in this study the experiment tests are performed to obtain some additional information regarding the material behaviors, damage mechanisms and etc., i.e. those which are required in the development of the numerical model or for material characterization.

Generally, this chapter is separated into four main sections. The first one is the explanation of the type of materials and the details of the experimental works that has been done in this thesis together with the specimen configurations. The reason to perform an additional experiment will be explained in this section and all the necessary information concerning the test procedures, methods, and equipment used in this experimental work will be described in detail. The second section concerns the details of damage mechanisms that are present during the crushing tests of composite plate from the meso- and micro-scopic point of view. The damage mechanisms explained in this chapter can be divided into two categories;

the first one is the global damages that are usually found in the literature [FAR89, HUL91] and the second one is the specific damage that is discovered during this study which is important for development of numerical model. Besides that, a new material property called as ply mean crushing stress is also introduced in the third section together with its estimation method. The 4th section concerns the influences of ageing specimen under humid conditions on the crushing performances of carbon-epoxy composite material. The discussion includes its effects on the crushing morphology, damage mechanisms, and the ply mean crushing stress as compared to the sane specimen.

2.1 Experimental Test

Three types of experimental tests have been used to observe the damage mechanisms involved in low velocity crushing plates in order to improve the understanding and also for the development of the numerical model. These tests use the same specimens but with different dimensions depending on the test set-up that will be explain further. All experimental tests, including the dynamic tests, are specifically designed to give high quality images of the front geometry to support a physical observation work in order to develop a physically-based damage modeling.

2.1.1 Materials

Two different materials are used in this study. The first material is Hexcel carbon epoxy unidirectional (UD) prepreg T700/M21. The matrix Hexflow M21 consists of a mix of duroplastic epoxy resin and thermoplastic constituents. Besides that, the matrix weight proportion is 35.5%. The thickness of ply is 0.26 mm. The second material is Cytec balanced fabric 5H (6KHTA) 977-2 carbon epoxy. The matrix Cytec 977-2 is a high-viscosity toughened resin with normal cure cycle approximately 90 minutes at 177°C/350°F and about 100 psi pressure. The mechanical properties of fabric 5H (6KHTA) 977-2 are obtained from the constructor. The ply thickness for this material is 0.35 mm.

2.1.2 Plate Crushing Test

The plate crushing test has been carried out by Duong et al [DUO10] in their study to obtain better understanding concerning the influence of the crushing speed in progressive crushing of composite laminated plates. The availability of their experimental data has given

an opportunity to make new analyses regarding the mechanical phenomena and damage mechanisms involved in the progressive crushing of composite plates.

2.1.2.1 Specimen

The specimens used in this test are 160 mm x 60 mm flat plates with different stacking sequences. For every 5 mm, a white graduation is drawn on the edge of the specimen. The trigger mechanism is a 45° chamfer machined at the bottom end of the plate. For both materials, three different laminate configurations were designed and tested. The full characteristics of the laminate configurations can be found in [DUO10]. Nevertheless, in this study only one laminate configuration from each material are used to make new analyses. The first configuration is a laminate made from 16 plies of UD prepreg T700/21 with stacking sequence $[(0°/90°)_4]_{sym}$ and named as Plate-T-0/90 while the second laminate consists of 12 plies made from Cytec balanced fabric with stacking sequence $[(0°)_{12}]$ and named as Plate-C-0. In addition, the experimental results of laminate Plate-T-0/90 are also used for the model validation. The reason for choosing these two laminate configurations is because at the moment, the new analyses works are focused on ply orientation in 0° and 90°. As it is possible to differentiate these two plies (longitudinal and transverse direction) during the tests, it will make it easier to see the mechanisms.

2.1.2.2 Test Set-up

The plate crushing test was performed using a drop tower with several different initial speed that range from 20 mm/min to 9 m/s and with a falling weight which range from 36 kg to 207 kg depending on the initial speed. This test fixture is shown in Figure 2-1 [GUI08, DUO10]. In this test, the unsupported height (gap between the metallic base and the horizontal guides) was fixed to 20 mm. The four vertical guides were designed to avoid the buckling phenomena on the plate during the crushing while the two horizontal guides ensure the boundary conditions are uniform along the plate width. The use of these guides also can avoid the tearing of the plate as observed in the classical plate crushing tests [FLE06, LAV96]. In addition, the design of this test fixture enables to observe the behaviors at both edges of the crushing front. Thus, by using high speed cameras, it allows a real-time visualization of the crushing front during the initiation and propagation of damage and correlations with the force-displacement curve. The filming speed is 20000 fps, with a

512x256 pixels resolution. Detailed explanations of this test can be found in [GUI08, DUO10].

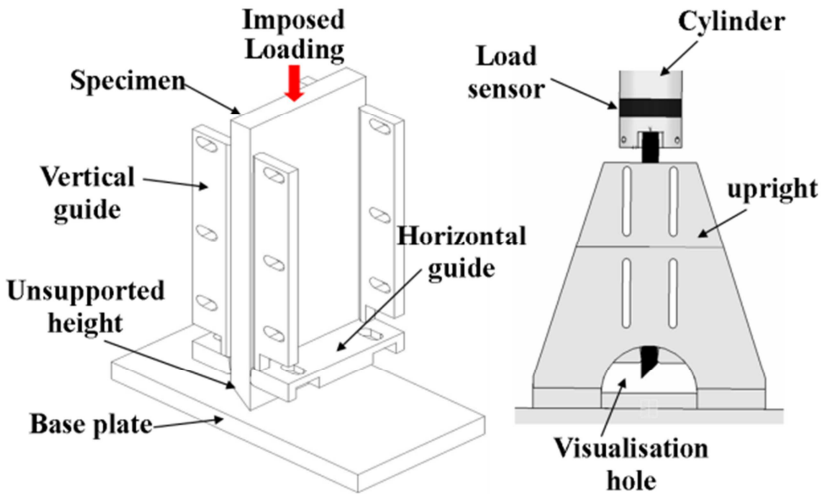

Figure 2-1: The test fixture used in dynamic crushing tests

2.1.2.3 Additional Analyses

Based on the results obtained from the plate crushing tests of laminate Plate-T-0/90 and Plate-C-0, additional analyses concerning the mechanical phenomena at the plate extremity during crushing process have been conducted. The result of these new analyses has shown that during the test, the contact area of plies having direct contact or local fragmentation with the metallic base can vary. Only this contact area is considered enable to sustain the applied force according to study by Guillon [GUI08]. The detail definition of contact area is explained in section *§2.3.1*. These contact areas are measured from the available images taken during the tests with no distinction between 0° and 90°.

The objective of these analyses is to study the relationship between the contact area and the applied force as shown in the Figure 2-2. The contact area is measured at three different regions of displacement and plotted in the same curve. It shows that different levels in applied forces have different levels of measured contact area. Therefore, it is believed that there is a linear proportionality between the applied force and the measured contact area. This relationship indicates the possibility to determine the local ply mean crushing stress inside a laminate by using an appropriate method which is important for material characterization and also for numerical modeling.

Nevertheless, these contact areas are measured according to an approximation only due to the quality problem of the images. The available images are not very clear especially at

the contact surface and make it difficult to measure precisely the contact area. Therefore, the measurement of contact areas have some dispersion as shown in the Figure 2-2b. For this reason, no further investigation has been made using this data to determine this local ply mean crushing stress. A new set of new experimental tests are performed for that purpose and explained in the next section.

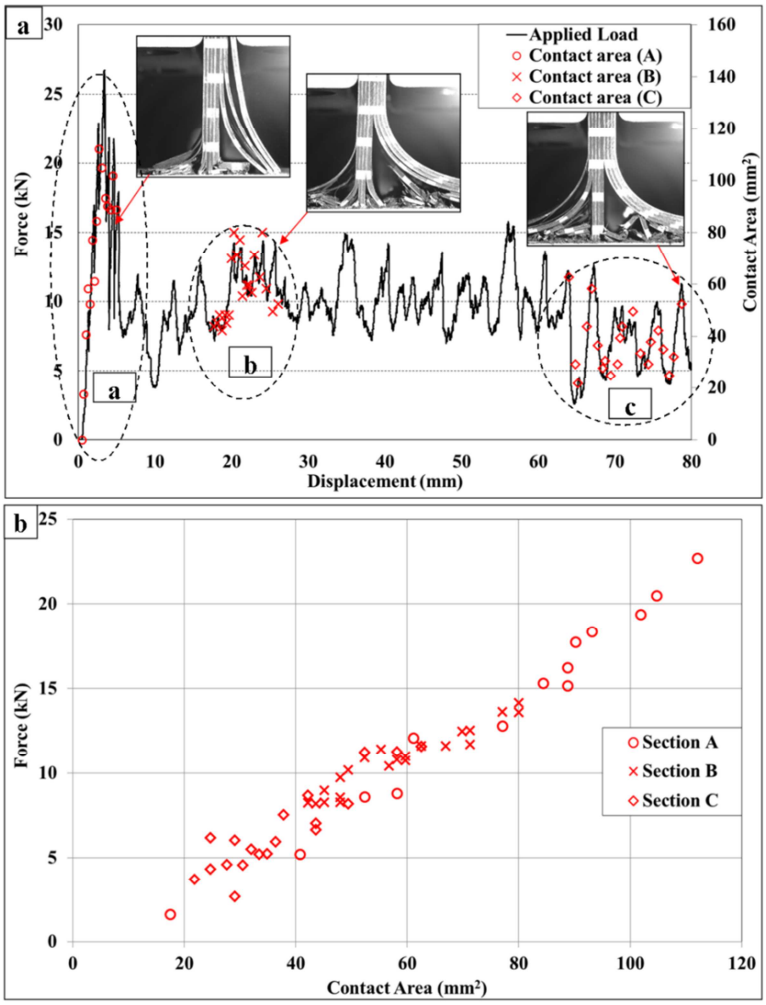

Figure 2-2: (a) The contact area of plies having fragmentation mode at three different region (b) Range of the contact area measurement

2.1.3 Medium-scale Quasi-static Crushing Test

This test is specifically introduced to design a new methodology to investigate the ply mean crushing stress (section *§2.3*) of carbon-epoxy plies inside a laminate. A series of quasi-static crushing tests are performed for different configurations of both unidirectional (UD) and woven fabric of CFRP laminates with smaller dimension (medium-scale) compared to the plate specimens in previous section. The idea for doing the same test is to ensure the crushing mechanisms are similar as observed in the experimental tests done by Duong et al [DUO10]

but more precise with close observations of these crushing mechanisms at the plate extremity. In fact, these new tests can give new experimental data that will be useful for the numerical modeling development. Besides that, the images are taken to observe precisely the global behavior and crushing mechanisms of CFRP plate under crushing load for the validation purpose with the numerical model.

2.1.3.1 Specimen

Specimens are cut out from laminated plates. There are two plates made from material T700/M21. The first one is a UD laminate made of 8 plies that is used to determine the ply mean crushing stress alone in pure longitudinal direction $[(0°)_8]$ (specimen T-0) and pure transverse direction $[(90°)_8]$ (specimen T-90). The second plate (T-0/90) is used to study the ply mean crushing stress inside a laminate specimen with laminate design consist of 16 plies with stacking sequence of $[(0°/90°)_4]$sym. Meanwhile for the Cytec balanced fabrics 5H (6KHTA) 977-2 only one plate (C-0) is used in this study with stacking sequence $[(0°)_{12}]$.

The plates from both materials are cut to produce small specimens with short length and small width varying from 8 mm to 10.5 mm. This small length (from 55 mm to 65 mm) is considered enough to have both the initiation step and a steady crushing front which gives different configurations of specimen fragmentation in the same test. Besides that, one extremity of the specimens is cut to form a chamfering-type trigger mechanism. Three different chamfering angles are used in this study as shown in the Figure 2-3c in order to have different crush morphologies at crush front and afterwards be able to determine the overall average of ply mean crushing stress of all cases.

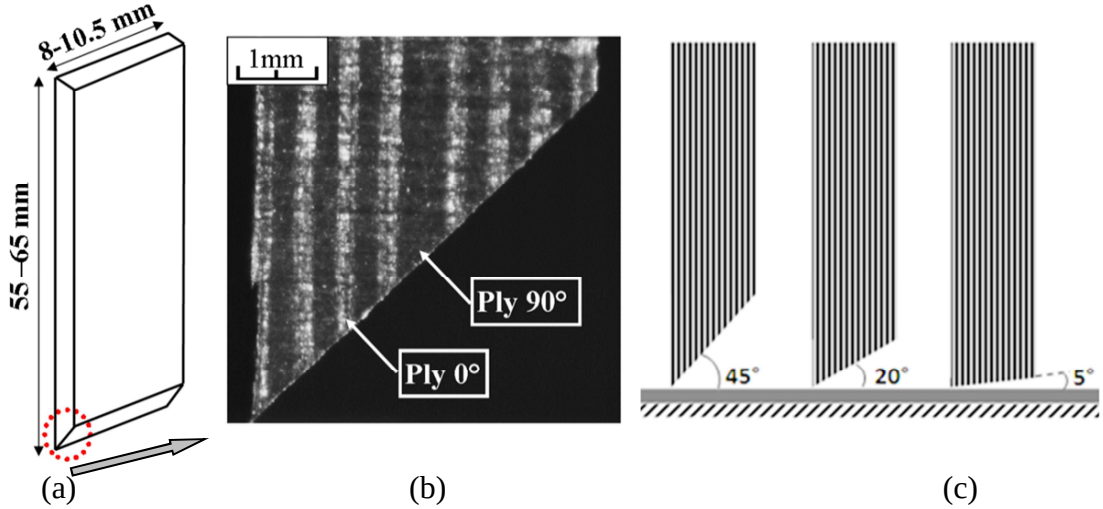

Figure 2-3: Specimen description: (a) geometry (b) T-0/90 chamfering detail (c) chamfer angles

However, for specimen T-0/90 with 5° chamfering angle (T-0/90-5°), only little crushing is observed during the crushing initiation before it turned to have too much flexion that makes the measurement of contact length became unrealistic. Apart from that, this big flexion also causes a big sudden inter-laminar crack that turns all the plies into splaying mode. Therefore, it is decided that for material T700/M21 it is not practical to make a crushing test on the specimen with 5° chamfer angle as trigger.

In general, 11 specimens are used in this study. Before the tests, all of these specimens are measured for the calculation of the cross-sectional area. The summary of all specimen geometry configurations is listed in Table 2-1. There is only few in number of specimens, but one must see that each test provides a wide range of force/surface contact configurations (as much as the number of images taken during tests).

Table 2-1: Medium-scale specimen geometry configurations

	Specimen[a]	Thickness (mm)	Width (mm)
T700/M21	T-0-20°-n1	2.11	10.23
	T-0-45°-n1	2.11	10.22
	T-90-20°-n1	2.11	10.16
	T-90-45°-n1	2.11	10.13
	T-90-45°-n2	2.11	10.13
	T-0/90-20°-n1	4,26	8,32
	T-0/90-45°-n1	4,26	8,34
	T-0/90-45°-n2	4,26	8,30
Cytec	C-0-5°-n1	4,71	8,09
	C-0-20°-n1	4,71	8,04
	C-0-45°-n1	4,71	8,14

[a]*Note: The designation of specimens was based on the code [M-S-C°-n] where; M: Material, S: Stacking sequence, C°: Chamfering angle, n: number of the specimen.*

2.1.3.2 Test Set-up

Quasi-static crushing tests are carried out for all specimens at a constant loading speed. Therefore, it is easy to control and able to observe precisely the crushing mechanisms as reported by many authors that also used quasi-static tests in their study concerning crashworthiness capability of composite structures [MAM96B, PAL11]. In this study the quasi-static crushing test is performed using Hydraulic Instron testing machine in compression testing mode. The specimens are clamped in the moving grip and the metallic base on which specimen are crushed is fixed. All tests are conducted under a displacement-controlled mode at a constant loading rate of 6 mm/min. Figure 2-4 shows the test set-up and the location of specimen.

The force-displacement data have been recorded and acquired at the rate of 100 Hz. To avoid global buckling and too much bending, the non-clamping length is limited to 30 mm for the laminate specimens and 10 mm for the thinner UD specimens. For the laminate specimens, tests are interrupted after 10 mm crushing displacement while 6 mm displacement for the UD specimens, which is considered enough to have information on the ply mean crushing stress.

Two cameras are used to capture the images of crushing process every 0.1 mm of displacement during the experiment. These two cameras are placed at both sides (front and back respectively) to have complementary information for contact area calculation. Besides that, only a small area is captured by the camera approximately 10 mm x 10 mm because only this area is important to observe for measurement of the contact length between plies and the metallic base. Image resolutions approximately 100 pixel/mm. Image acquisition is performed at the rate of 1 Hz.

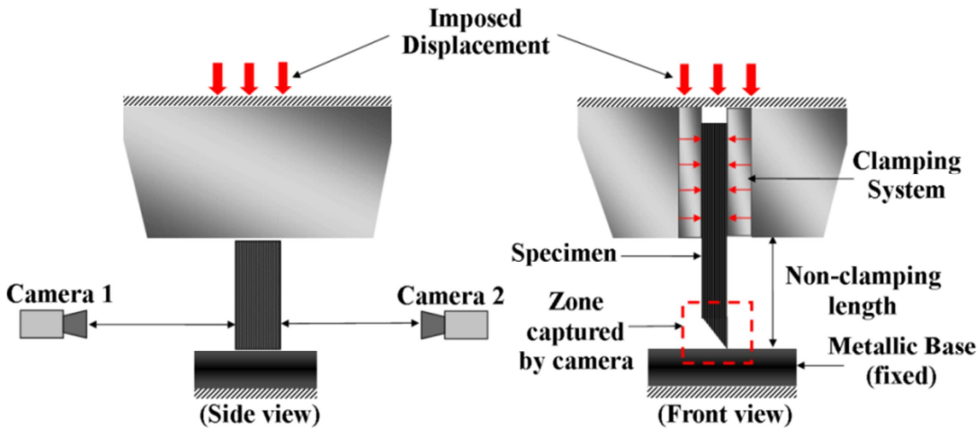

Figure 2-4: Test set-up

2.1.4 Micromechanical Crushing Test

Apart from plate and medium-scale crushing tests, additional observations are also obtained from micromechanical quasi-static crushing tests on the same CFRP laminates. The aim is to study the details on the behaviors of CFRP plates under crush loads and the mechanisms that drive the occurred main damages from a microscopic point of view. This study is done by performing the tests directly inside a scanning electron microscope (SEM) by using a special test jig in compression mode (Figure 2-5). Several crushing tests are performed on small dimension specimens, and the results of these tests have been analyzed

carefully to see in details the damage evolutions including the post mortem observations made through an optical microscope and SEM.

Besides that, the high-magnification images provided by the SEM on the crushing process at the extremity has given the opportunity to calculate the ply mean crushing stress from the microscopic point of view. This is useful to support the results of ply mean crushing stress computed from the medium-scale crushing test.

2.1.4.1 Specimen

In this test, only eight specimens are used to perform micromechanical quasi-static crushing test. The number of specimens is less than the number of specimens used in the medium-scale crushing test because only 45° chamfering trigger is considered for this study. Six of them are made from material T700/M21 (two specimens for each configuration) which are UD laminate made of 8 plies in pure longitudinal direction $[(0°)_8]$ (specimen mT-0), pure transverse direction $[(90°)_8]$ (specimen mT-90) and UD laminate of 16 plies with stacking sequence of $[(0°/90°)_4]_{sym}$ (mT-0/90). The other two specimens are made from Cytec balanced fabrics (mC-0) with stacking sequence $[(0°)_{12}]$.

The same laminate configurations have been used because the idea is to study separately in details the formation of damage mechanisms occurring in each laminate configuration during crushing process in order to provide more information for the development of numerical model:

- Fiber compression, formation of compress powder, micro-bending, intra-laminar failure including delamination and possible kink-bands in **mT-0.**
- Shear propagation of cracks, brittle fracture and matrix compression in **mT-90.**
- Mixed damage modes due to the contribution of both types of UD plies including the inter-laminar failure or delamination in **mT-0/90**.

Moreover, using the same laminates as in medium-scale crushing tests will be useful for the re-computation of the ply mean crushing stress.

As mentioned before, the dimension of specimens is designed small enough to be fitted in the micromechanical test jig. The maximum length of specimens is 22 mm and the maximum width is limited to 4 mm for specimen mT-0, mT-0/90 and mC-0, and 6 mm for specimen mT-90 in respect to the maximum capacity of the force sensor (2.5 kN).

Before conducting the tests, each specimen is polished to obtain a good finish on the surface to be visible during the test in order to improve the quality of images taken during the

test. After polishing, the specimens are measured for the calculation of the cross-sectional area and observed in the optical microscope. This is done to ensure there are no defects occurred during cutting and polishing phase. The final dimensions of the specimens are listed in Table 2-2.

Table 2-2: Micromechanical specimen geometry configurations

	Specimen[b]	Thickness (mm)	Width (mm)
T700/M21	mT-0-45°-n1	2.11	3.07
	mT-0-45°-n2	2.11	4.0
	mT-90-45°-n1	2.11	5.93
	mT-90-45°-n2	2.11	5.52
	mT-0/90-45°-n1	4,26	2.84
	mT-0/90-45°-n2	4,26	3.2
Cytec	mC-0-45°-n1	4,71	2.6
	mC-0-45°-n2	4,71	3.75

[b]*Note: The designation of specimens is the same as explained in table 1, only there is an additional of m which is stand for micro in order to differentiate with specimens in Instron test*

2.1.4.2 Test Set-up

The test jig shown in Figure 2-5a is attached inside the SEM in order to perform quasi-static crushing tests. Test jig is a mechanical device with dimensions adapted for experiments inside the SEM, originally designed for the tensile test. Therefore, in this study it has been re-designed to be able to apply a compressive load to the specimens.

Before placing the test jig inside the SEM, the specimens are clamped with additional clamping system specifically designed for this test to avoid any lateral movement of the specimen during the test. Basically, the test jig is operating under displacement-controlled mode which depends on the rotational speed of rotating device that manually controlled by an external control panel, which can provide eleven different speeds.

Nevertheless, the objective of this study is to perform a quasi-static crushing test with the aim to observe closely the damage mechanisms. Therefore, the crushing process is manually controlled at a very low speed. This allows the possibility to observe closely the damage mechanisms during crushing and to stop the crushing process in order to visualize and take images of the specimen being crushed if there are any damages occurred.

The operational system of this test jig is represented by the red arrows in the Figure 2-5a. It begins when the rotating axis is rotated in clockwise direction at a constant rotational speed (1) that makes the trapezoidal metal ingot moving forward (2). Thus, it pushed the tips

of two sliding bars to move outward (3) that makes the metallic base and the specimen being pulled oppositely (4) to move inward to perform crushing as illustrated in Figure 2-5b.

The applied force is measured by the force sensor attached to the test jig and its data has been recorded at each time the image is taken. The non-clamping length is around 14 mm for all specimens and the maximum crushing length that can be reached in this test is 6 mm which is considered enough to have initiation and progressive crushing under mixed mode crushing.

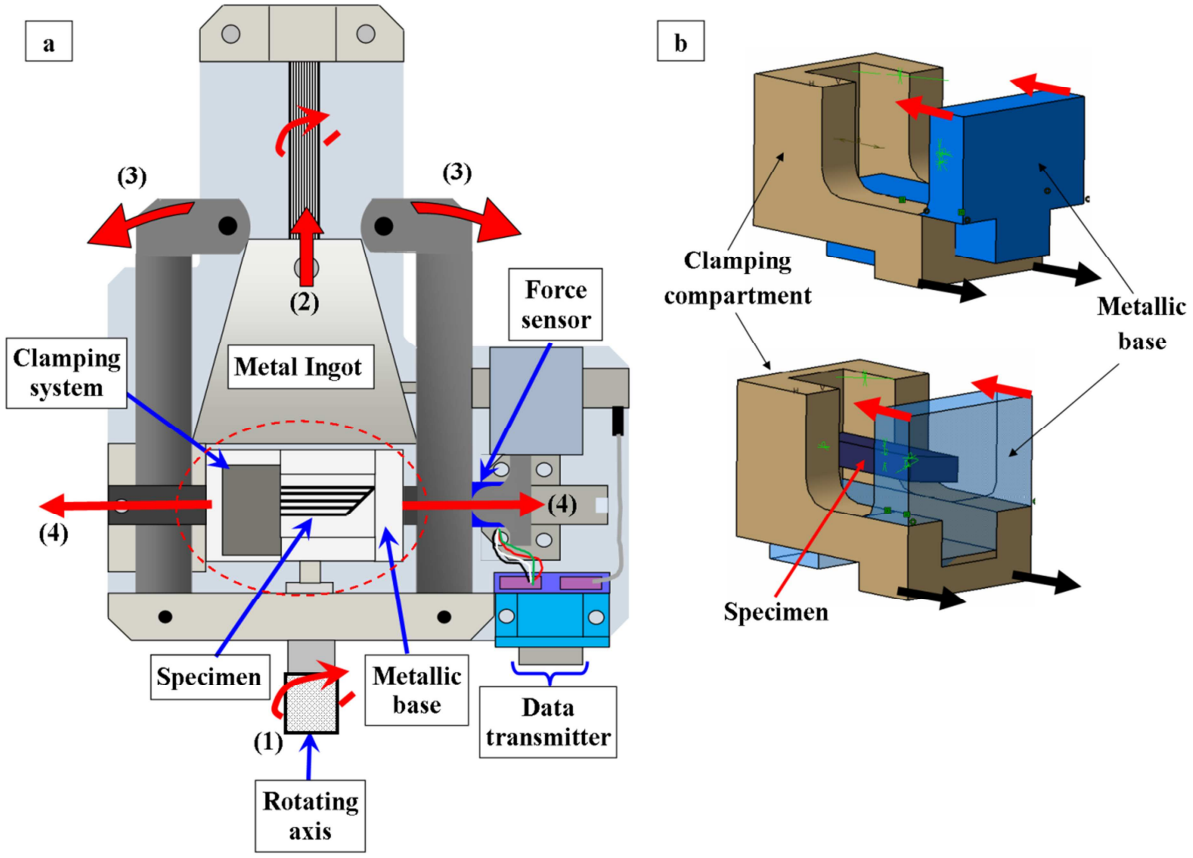

Figure 2-5: Micromechanical test jig (a) Top view (b) 3-D view of clamping compartment and metallic base being pull in opposite direction

2.1.4.3 Post Mortem Analysis

This is an additional analysis on the crushed specimen to observe any important remarks that can support the observation made on the damage mechanisms during the tests. For instance, the formation of kink-bank in the 0° plies. This includes the observation along the crushing surface in the loading direction (see Figure 2-6a) using SEM and the visualization of inner surfaces of laminate (see Figure 2-6b and Figure 2-6c) using an optical microscope. The observation is done to investigate if there are any internal damages like fiber breakages or matrix cracking that is invisible to the images taken during the tests.

The post-mortem analysis begins with the observation of the crushing surface along the width inside the SEM. Therefore, after the crushing test is done, the crushed specimens are removed from the test jig and re-located inside the SEM to observe the ruptures from different angles. Before that, to improve the vision and images quality, these specimens are coated with gold to support the reflection of electron when the specimen is being observed.

Once the SEM observation works is done, the crushed specimens are immersed in resin together with chemical hardener (catalyze polyester peroxide) and yellow coloring to avoid confusion with the matrix of the specimen (Figure 2-6b). After the hardening process, the visible surface (side surface refer to Figure 2-6b) of crushed specimen is polished to reveal the inner damages and analyzed using the optical microscope. This process is reiterated up to two or three different inner surface observations with approximately 1 mm depth are removed for each observation (see Figure 2-6c).

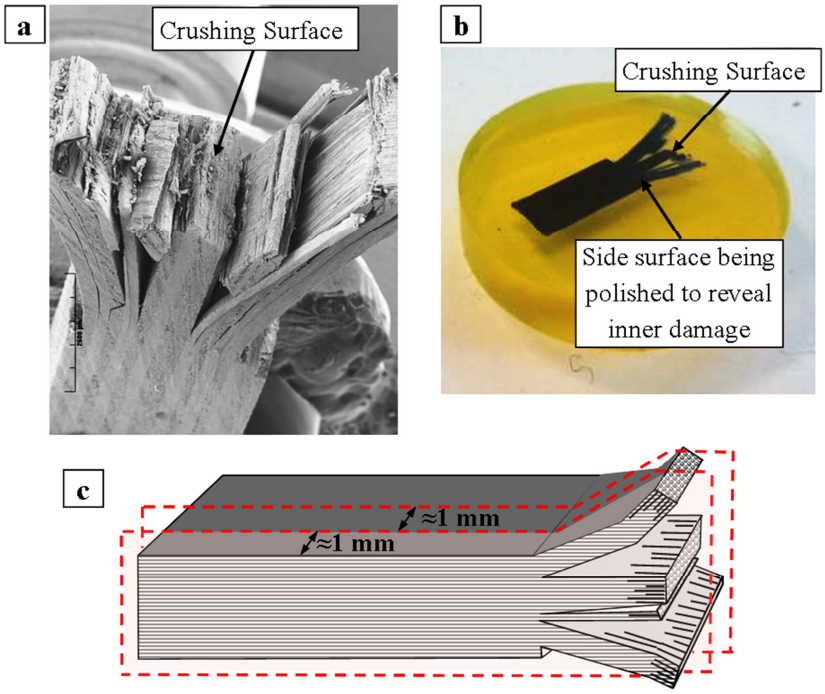

Figure 2-6: (a) Post mortem observation inside SEM. (b) Specimen post mortem preparation for inner surface observation (b) Illustration of polishing depth on the specimen width for inner damage observation

2.2 Failure Mechanisms

As described in the literature review, the failures in composite structure under crushing loading conditions are physically complex that involved failure in fibers, matrix, and at the fiber/matrix interface depending on the structure configuration i.e. geometries, laminate architectures, materials etc. [FAR89, HUL91]. However, due to insufficient observation and analyses of the damages at the elementary scale, often the understanding on the mechanisms that drives the failure to occur during the crushing tests is still inadequate. Thus, it is important to make new investigation on these mechanisms to improve understanding of the elementary mechanisms involved in the crushing of CFRP laminates and to support the development of numerical modeling.

In this study, four different types of laminate configurations and different loading conditions have been used to perform crushing test, so that different damage modes and failure mechanisms can be observed. This includes some others specific mechanisms that have never been discussed or explained in the literature. The analysis of failure mechanisms is separated into two parts between UD prepreg T700/M21 specimens and the woven fabric specimens in order to avoid any confusion between these two materials. Furthermore, the ply mean crushing stress analysis will be presented in a specific section, due to its importance in numerical modeling.

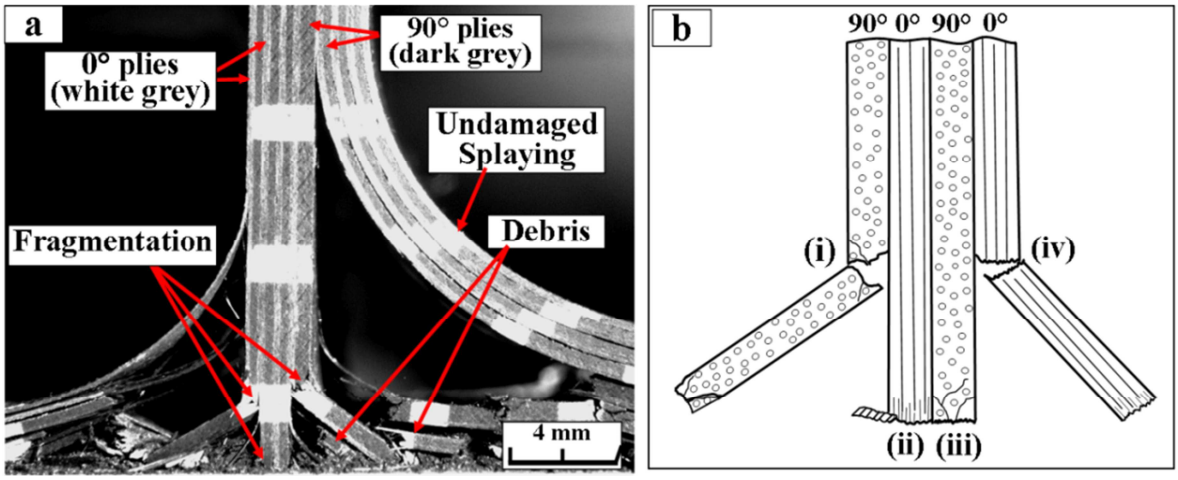

Figure 2-7: (a) Example of mixed-mode crushing in UD laminate $[(0°/90°)_4]_{sym}$ [DUO10] *(Note: white painted stripes are used to follow the plate displacement*) (b) Illustration of failure mechanisms in fragmentation modes: (i) inside ply matrix cracking (ii) 0° localized crushing (iii) 90° localized crushing (iv) inside ply fiber breakage

Generally, due to chamfering at one end of the plate, most of the specimens made from material T700/M21 experienced mixed-mode (splaying and fragmentation) crushing as

shown in Figure 2-7, an example for the case of UD laminate $[(0°/90°)_4]_{sym}$ (T-0/90 or mT-0/90). However, for the laminate pure UD 90° (T-90 or mT-90), it only endures fragmentation mode (see Figure 2-9b). The details of each crushing mode and the damage mechanisms will be explained in the following section.

Similarly, for the laminate woven fabric $[0°_{12}]$ (C-0 or mC-0), the failure analysis has shown that it has mixed-mode crushing that is very alike to the ones found in UD T700/M21 specimens as shown in Figure 2-8. The difference is in the disposition of fibers at 90° (warp and weft), which creates some discontinuities along longitudinal direction.

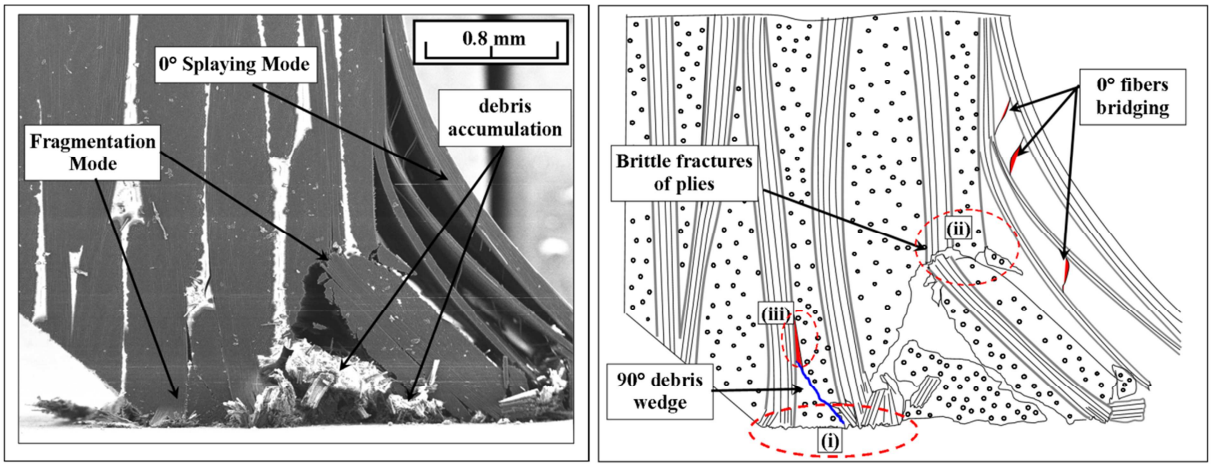

Figure 2-8: (a) Example of the main damages in woven fabric specimens (C-0 or mC-0). (b) Details of failure mechanism in fragmentation modes (i) localized crushing with fibers micro-buckling and shear micro-cracks of matrix (ii) inside ply failure, fiber breakages and matrix tensile cracking (iii) delamination initiated by debris wedge

2.2.1 Splaying

The formation of splaying mode during crushing test has been discussed extensively in the literature [FAR89, HUL91]. In general, the main failure mechanism controlling the splaying mode is the delamination. In this study, whether the specimen is made from UD T700/M21 or woven fabric, the crushing initiation ply interfaces at the tip of the specimens are subjected to high stresses. This leads to delamination and then splaying of plies as the crush zone move forward. The proportion of plies that bend on each side is varied. Initiation and propagation of delamination can occur either in pure opening (mode I), shear (mode II) or more often in combination of these two modes. Besides that, the delamination can occur at inter-laminar or intra-laminar.

However, for the case of laminate T700/M21 pure UD 0° (T-0 or mT-0) and pure UD 90° (T-90 or mT-90), most of the time, the delamination failures occur only at the intra-laminar. For example in specimens T-0 or mT-0, the delamination failures are initiated by the intra-laminar longitudinal cracks when the fibers cannot sustain the given load anymore and it starts to bend which creates high stress level inside the plies. This intra-laminar failure is characterized by a crack propagating parallel to fibers through the layers thickness and crucial for transverse matrix cracking analysis. This phenomenon creates fiber bridging as shown in Figure 2-9a. The inter-laminar fracture (crack between two plies) does not occur mainly because the intra-laminar and inter-laminar toughness can be different. This difference is due to a resin rich ply at the interface between layers which is tougher than matrix fiber interface where high residual stress can be accumulated [MOU10]. The propagation of intra-laminar fractures together with a constant increase of crushing load, leads to a splaying mode.

While for specimens T-90 or mT-90, the intra-laminar delamination occurs as a result of major shear matrix cracks due to the combination loading of compression and shear during the crushing tests. However, the propagation of this intra-laminar delamination does not lead to the formation of splaying mode but turns into global rupture as soon as it experienced bending mode during the crushing as presented in Figure 2-9b (or refer to Figure 2-28).

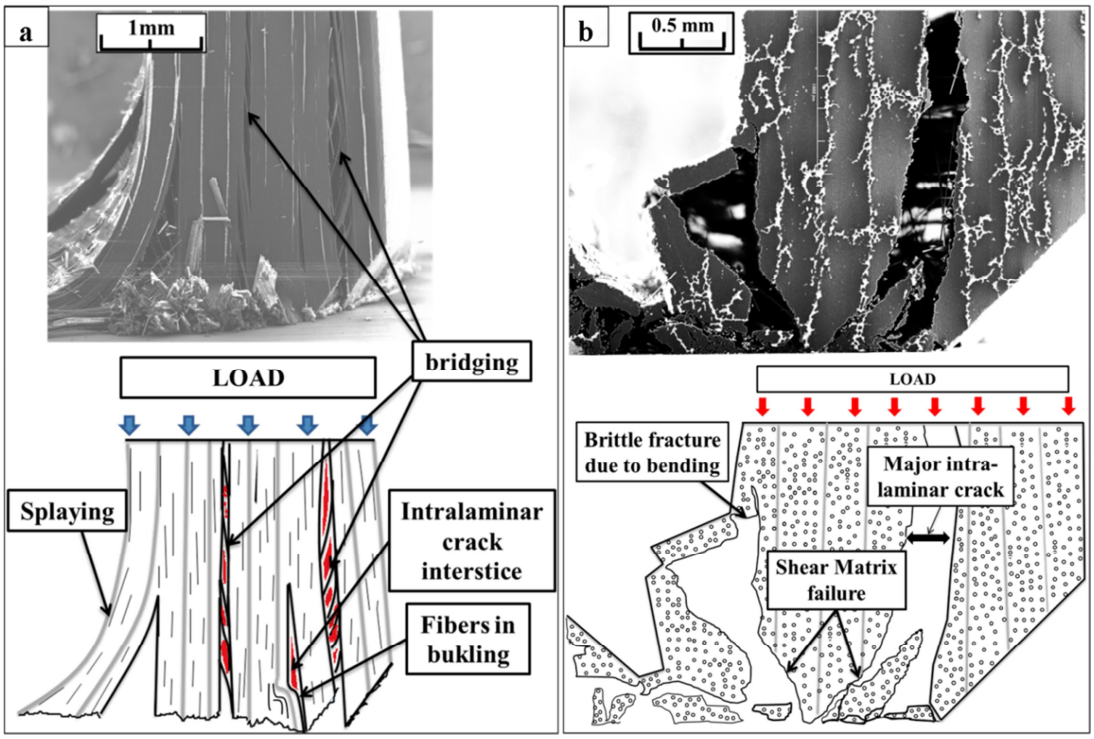

Figure 2-9: An example of intra-laminar failure during crushing of T700/M21 pure UD 0° (mT-0) and UD 90° (mT-90) (a) 0° Fiber bridging (b) 90° global rupture

2.2.2 Fragmentation

As the crushing loads are continuously applied on the specimens, plies that do not turn to the splaying mode perform fragmentation. Often in the literature, fragmentation mode has been described as a crushing mode with multiple short length fiber ruptures due to pure compression and transverse shearing that leads to the formation of small fragments in the crush zone [FAR89, HUL91]. Nevertheless, in this study the failure mechanisms involved when plies crushed under fragmentation mode is categorized according to two different scales of mechanism.

The first one is a fragmentation localized at the tip of the plies. In 0° plies both in specimens T-0 (mT-0) and T-0/90 (mT-0/90), localized fragmentation is due to micro-buckling and micro-fracture of fibers near the contact surface between plies and the metallic base as presented in Figure 2-7b (case ii), Figure 2-9a and Figure 2-10c. In 90° plies, the localized fragmentation is due to multiple shear micro-cracks at the tip of the plies as shown in Figure 2-9b, Figure 2-10c and Figure 2-12. This localized fragmentation (both in 0° and 90° plies) is the mechanism leading to the definition of ply mean crushing stress presented here after. In this study, it will be called localized crushing.

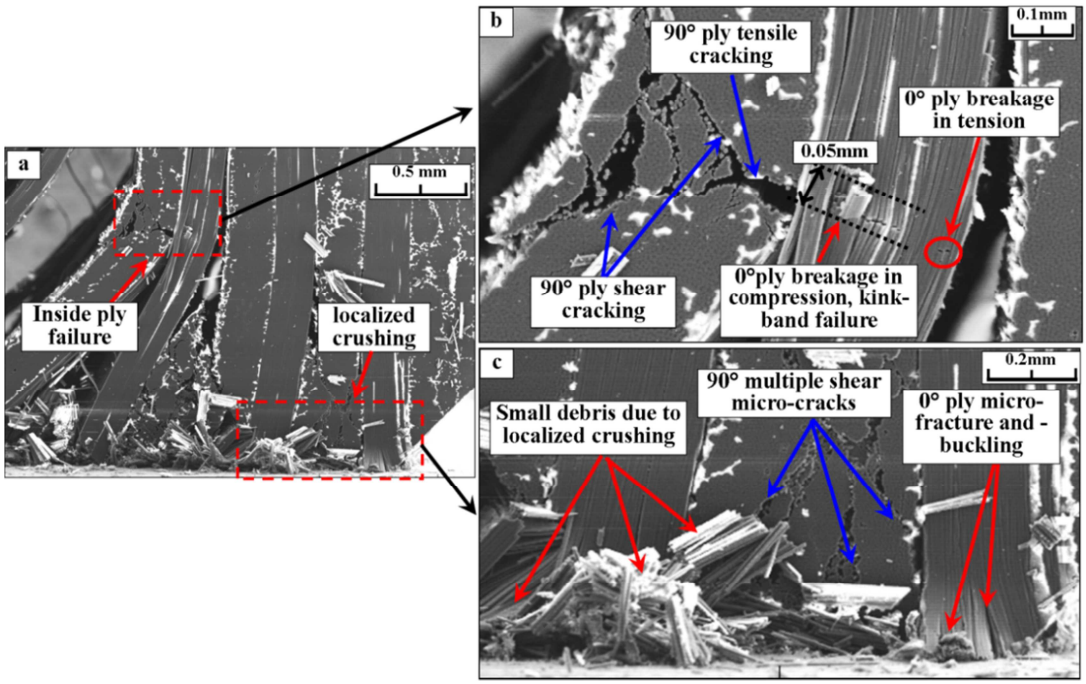

Figure 2-10: (a) Two levels of failure mechanisms in fragmentation mode (a) Inside ply failure (b) Localized crushing

The second level of fragmentation is the one induced by classical intra-laminar ply failure such as fiber breakage and matrix cracking [MAT95] as shown in Figure 2-10b. For example, fiber breakage through the ply thickness in the 0° plies is normally due to the

combination of a short ply bending and high compressive load. Furthermore, this combination loads can generate high shear force acting on the ply, leading to the fiber miss alignment (i.e. shear driven kink-bank) that will be discussed further in section *§2.2.2.3*. The brittle fracturing in 90° plies is generally caused by matrix cracks that can be divided into tensile cracking, shear cracking or the mix of tensile and shear cracking which also resulting from a combination of compression, bending, and shear loads. Contrary to localized crushing, these failures are not localized at the tip of the plies as shown in Figure 2-7b (case i and iv) and Figure 2-10. In this study, it will be called inside ply failure to differentiate from the localized crushing previously described.

It is the same case for the woven fabric specimens, where the fragmentation also happened at two different levels of scales exactly like the T700/M21 specimens. Similarly for the woven fabric specimens, the first scale will be called localized crushing which is categorized by the local fragmentation occurred at the tip of specimens with 0° plies performed multiple micro-buckling of fibers and matrix micro-cracks in 90° plies as shown in Figure 2-8b (case i). The second level will be called as inside ply failure which is specifically addressed for the failure generated by classical intra-laminar (fiber breakage, 90° brittle fracture, kink-bank formation etc.) as shown in Figure 2-8b (case ii).

Moreover, one must notice that the present of big fragments during the crushing tests is mostly due to the bending with eventual shear and compression load. If there is no bending, inside ply failure will not happen and the fragmentation mode only involves localized crushing.

2.2.2.1 Debris Accumulation

The presence of the debris during the crushing tests is a result from the fragmentation failure mode. Different kinds of failure mechanisms which occur under the fragmentation mode generate different lengths of fragments or debris. Nevertheless, for the T700/M21 specimens, the lengths of fragments are either accumulated from the pure UD specimen (T-0, mT-0, T-90, mT-90) or from the laminate UD specimen (T-0/90, mT-0/90) they are very close. The size of these fragments is measured from the available images taken during the crushing tests.

The length of fragments ejected during localized crushing of 0° plies is very small (from 0 to 0.25 mm) as shown in Figure 2-10. In 90° plies, localized crushing develops multiple micro-cracks that can lead to a macro-crack through the whole thickness of the ply,

and consequently to longer fragments: from 0 to 0.5 mm as observed in Figure 2-9 and Figure 2-12.

On the contrary, in the case of inside ply failure fragmentation (mostly due to bending) for both 0° and 90°, because failure occurs further from the extremity of the ply, the debris is bigger. The sizes are from 0.5 mm to 5 mm as shown in Figure 2-7a, Figure 2-11 (case ii and iii) and as illustrated in Figure 2-7b (case i and iv). Besides that, in the crushing tests of specimens T-0/90 (or mT-0/90), fragments made of 0° and 90° plies attached together can also be observed, as in Figure 2-11 (case i) and the length of this kind of debris is normally more than 1 mm. This is due to these debris are the result from the bending failure that often occur at higher position from the plate extremity. Further observation of this 0°/90° attached debris has shown that, the length of 90° plies debris is shorter than the 0° plies debris when they are attached together. This means that the tensile or shear cracking of 90° plies occurred first when both plies having bending at the same time. Such example can be seen in Figure 2-11 (case i).

Woven fabrics specimens also create different lengths of fragments as shown in Figure 2-8 (or see also in Figure 2-20). Similarly, the lengths of fragments can vary from 0.25 mm to 1 mm in the localized crushing. As for the debris created from the inside ply failure, the length can vary from 1 mm up to 5 mm.

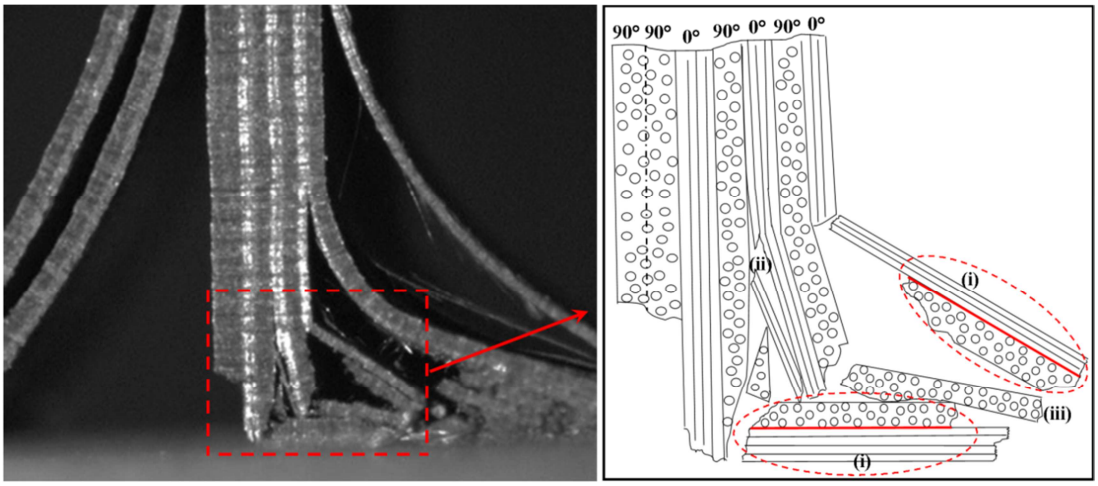

Figure 2-11: Example of big debris at crushing front (i) 0°/90° plies attached debris (ii) 0° plies debris (iii) 90° plies debris

2.2.2.2 90° Debris Wedge

During the crushing test, the accumulation of big fragments created from 0°, 90° or both plies can create a debris wedge during the crushing process which is influential in

changing the evolution of the crushing front [HUL91]. Unfortunately, from experimental observations, it seems that the slipping (and evacuation) or accumulation of debris is quite random. More specifically, debris due to localized crushing in 90° plies can have a particular role in the crushing process. Figure 2-12 shows the formation of a trapezoidal wedge at the tip of a 90° ply. The shape of this wedge, with a 45° angle crack, and its confinement between 0° plies provokes a transverse load on the 0° neighboring plies that leads to the delamination of one of the 0°/90° interfaces. If the transverse force is high enough, it can initiate the splaying of one of the 0° plies. If this is not the case, the 0° ply will be subjected to localized crushing. To the author's knowledge, this 90° debris wedge mechanism has never been discussed or explained in the literature.

The formation of 90° debris wedge can also be found in the crushing tests of woven fabric specimens as shown in Figure 2-8b and it exhibits the same behavior in initiating the delamination at the interface of the adjacent plies.

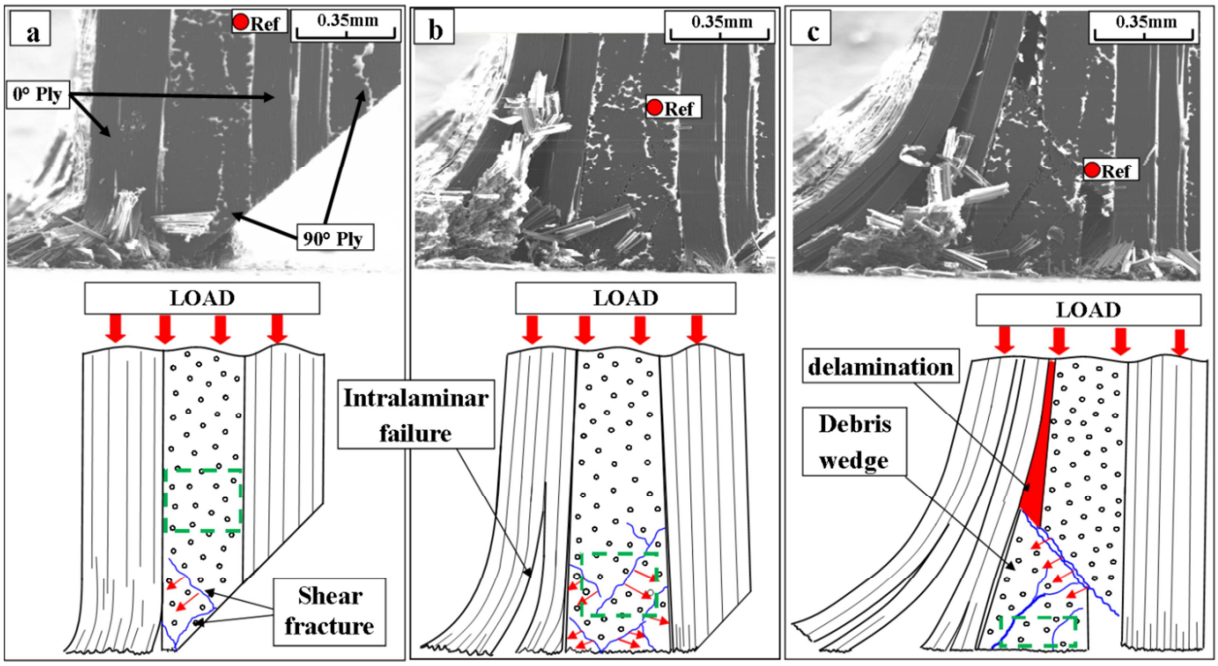

Figure 2-12: Creation of a debris wedge in a 90° ply: SEM in-situ test

In addition, the 90° debris wedges can also cause the local fibers breakage in 0° plies in bending. Based on the continuous observation made on the creation of 90° debris wedge presented in Figure 2-12, after it initiated the inter-laminar delamination, it keeps moving in the transverse direction towards the adjacent 0° ply as being pushed by the sane area. Thus, it causes misalignment on the 0° fibers in the longitudinal direction that makes the load to be no longer transmitted uniformly along the 0° ply. Subsequently, a pack of fibers is bended until the final rupture (Figure 2-13). This is not a kink-band fracture mechanism that will be

discussed in the following section. Nevertheless, it is believed that the 90° debris wedge is also the mechanism which initiates the formation of kink-bank under shear-driven compressive failure.

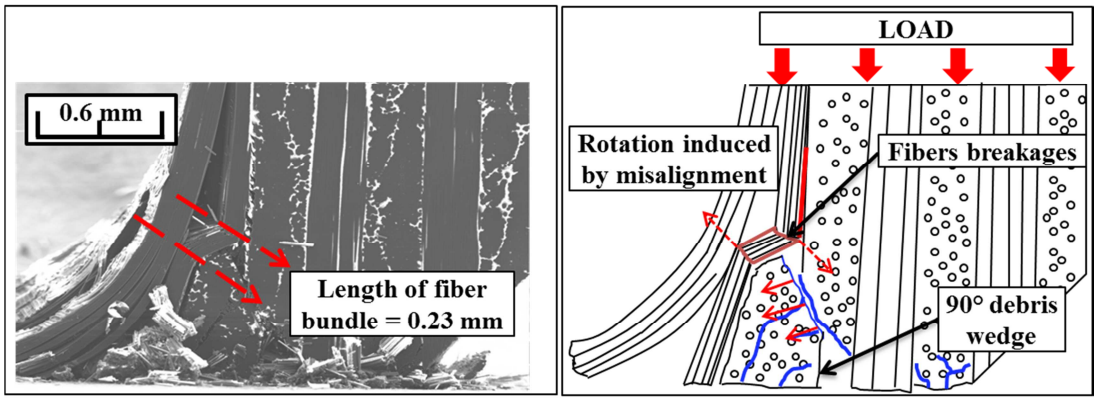

Figure 2-13: The influence of 90° debris wedge on the 0° fiber breakage

2.2.2.3 Kink-band Fracture Damage

Kink-band formation is one of the common failures normally found when the composite structures are subjected to the longitudinal compression [SCH96]. It is typically initiated in the regions of large fiber misalignment [FLEC97], free edge region where fiber rotation is introduced by the delamination of neighboring plies [PIN12], resin rich region, and a shear-driven fiber compressive failure [GUT10]. This locally initiated failure propagate under incremental load through the laminate and thus creates a narrow zone called kink-band within the 0° plies, which lose structural integrity and collapse as shown in Figure 2-14 [JUM09].

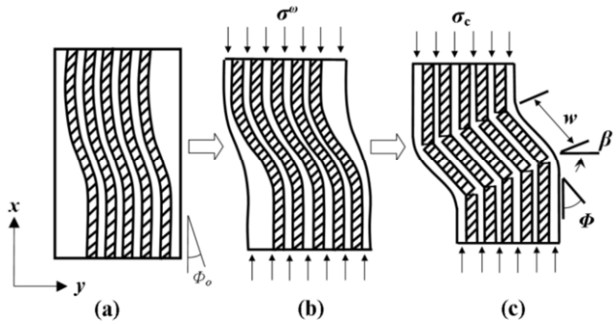

Figure 2-14*:* The typical formation of kinking failure mode on UD carbon-epoxy composites subjected to compressive loading [JUM09]

The illustration of the common kink-band failure in Figure 2-14 is normally due to high compressive stresses that lead to the rupture in the fibers [GUT10]. Besides that, Vogler and Kyriakydes [VOG01] have proven from their results that shear stress also plays a significant role in generating kink-band failure. There are many studies and discussions

concerning the formation of kink-band available in the literature review [MOR95, PIM09, FEL11]. However, most of these studies are specifically prepared with special specimens (notched, open-hole etc.) and test set-up that really dedicated to the formation of kink-band.

In this study, through the physical observation made during micromechanical crushing tests and post-mortem analysis, it has been revealed that 0° plies when crushed under fragmentation mode can lead to the formation kink-band fracture mechanism which either occurred at localized crushing as highlighted by Hull [HUL91] or inside ply failure. The kink-band failure occurs at localized crushing is observed in mT-0 specimens. This failure is identified during the post-mortem analysis both under SEM and optical microscope as shown in the Figure 2-15. They are located at the crushing front, or even in packs of debris that makes it difficult to know where they came from. Therefore, this observation has limitation in explaining the development (initiation and propagation) of the detected kink-band mechanism.

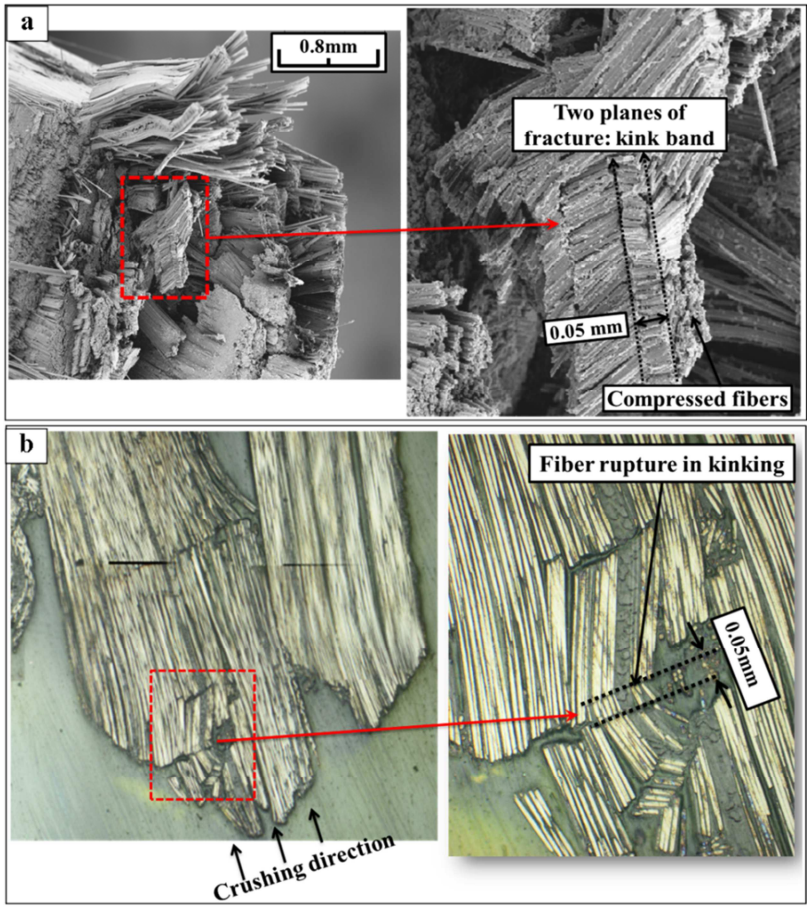

Figure 2-15: Visualization on kink-bank failure pattern on the mT-0-n2 specimen a) Post-mortem analysis under SEM b) Post-mortem analysis under optical microscope

Apart from localized crushing, the formation of kink-band failure is also observed when 0° fibers subjected to combination of global bending and high compressive load (short

ply bending) as shown in Figure 2-10b. In this case, the ply experienced both high tensile stress that leads to fiber rupture and high compressive stress resulting in fiber kinking. Similarly, this kink-band mechanism is observed in the material after failure that makes it difficult to explain on the sequence of event.

Further study on the size of the broken fibers shown in Figure 2-15 (due to localized crushing) and Figure 2-10b (inside ply failure with short ply bending) are very close to the common size of broken fibers which are normally found in the kink-band studies [JUM09, GUT10, SCH96]. For example, in the study of Gutkin et al [GUT10] and Jumahat et al. [JUM09], the sizes of the broken fibers that also made from CFRP type materials are around 0.05 mm and 0.06 mm to 0.1 mm (Figure 2-16) respectively.

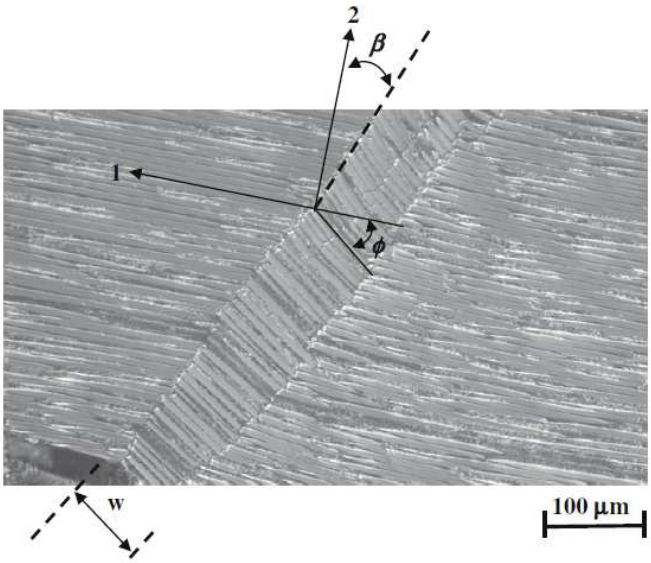

Figure 2-16: Single kinking failure on the UD HTS40/977-2 composite laminate after the initiation of micro-buckling tests [JUM09]

The kink-band formation discussed previously only acts in 0° plies. It can also be introduced by the interaction between 0° and 90° plies during crushing test of mT-0/90 that can be observed directly during the crushing tests as shown in Figure 2-17. In this case, it is believed that the presence of the 90° debris wedge during the crushing process has triggered this failure. Figure 2-17a has shown that the delamination failure has caused the short plies bending with tensile cracking in 90° ply. This makes the adjacent 0° ply having large free space on the left. While Figure 2-17b has shown that the two layers of 90° plies in the middle of the laminate endured a sudden brittle failure in shear at -45° through to its thickness to create a big 90° debris wedge and a kink-band formation that appears on the same shear fracture line. This rupture occurred so fast that it is not possible to follow the exact sequence of the initiation and propagation of this observed kink-band failure.

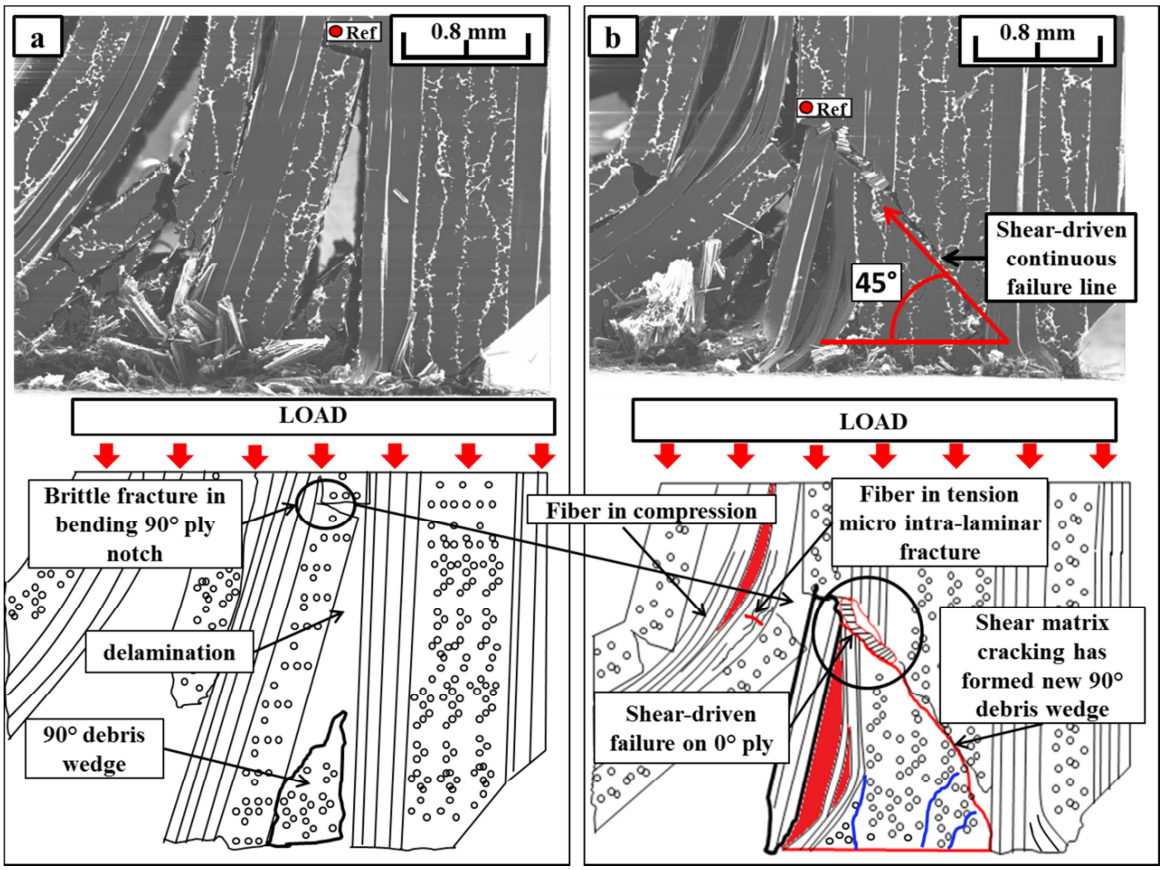

Figure 2-17: Kink-band-like failure pattern under shear-driven compressive failure

Several assumptions have been made in order to have better understanding on the mechanisms that drive this kink-band formation. This kink-band failure is probably formed under shear-driven compressive failure triggered by the 90° debris wedge. An illustration of the mechanism that drive the formation of kink band found in Figure 2-17 is presented in Figure 2-18. In image 1 (Figure 2-18), the shear crack propagates at -45° inside the 90° plies through to its thickness, which creates a debris wedge that is still attached to the adjacent 0° ply. As the crushing process continues, the sane area has pushed this 90° debris wedge moving to the left. Subsequently, it introduced high shear stresses to the 0° fibers. Therefore, by combining these high shear stresses and the high compressive loads, a shear-driven fiber compressive failure is promoted that induce small rotation on the 0° fibers (image 2 in Figure 2-18). Then, as the specimen is loaded further, the shear-driven fiber compressive failure has propagated which caused the shear crack faces to slide on each other along the -45° shear crack. According to Gutkin et al [GUT10] and Pinho et al [PIN12], these shear crack faces have promoted rupture of the fibers at one end and then, at the other. This has induced local bending on the 0° fibers resulting in more splitting and promotes kink-band formation (image

3 in Figure 2-18). After this point, the propagation is really fast, and inevitable under constant compressive load. The final failure of the structure is shown in Figure 2-18 (image 4).

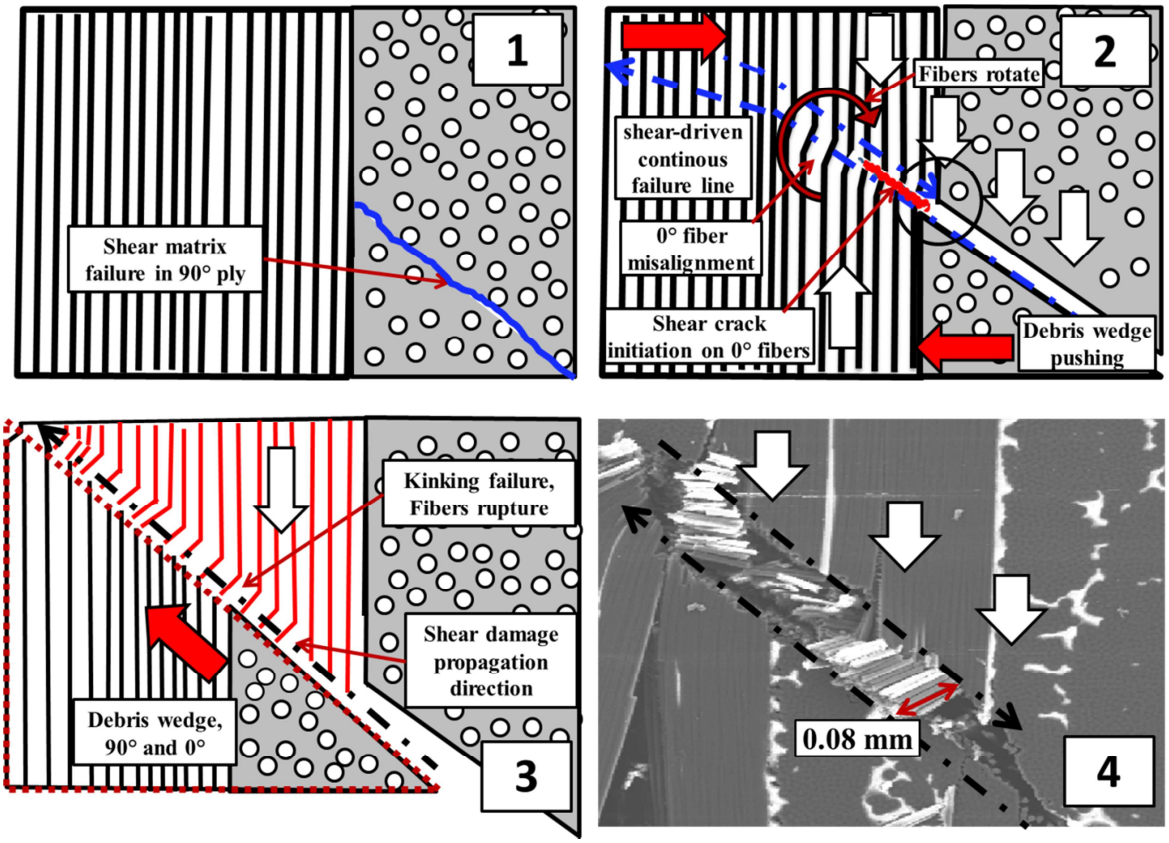

Figure 2-18: Proposed mechanism on the kink-band formation under shear-driven compressive failure. Illustration is based on the detail of Figure 2-17

This proposed mechanism is very close to the sequence of events presented by Pinho et al [PIN12] as shown in Figure 2-19. The only difference is that in their case there is no presence of 90° debris wedge and free space (delamination on the left side as in Figure 2-17a) to accelerate the formation of kink-band. Besides that, it is also different than the formation of kink-band under shear-driven fiber compressive failure done by Gutkin et al [GUT10] because in their study, they have introduced an initial notch to promote a crack tip. Once the compressive load is applied, it creates the shear stress at the crack tip to propagate the crack under shear-driven formation and then to introduce the kink band failure. This is contrary to the proposed mechanism (Figure 2-18) in this study where the shear-driven is believed to be initiated by the 90° debris wedge.

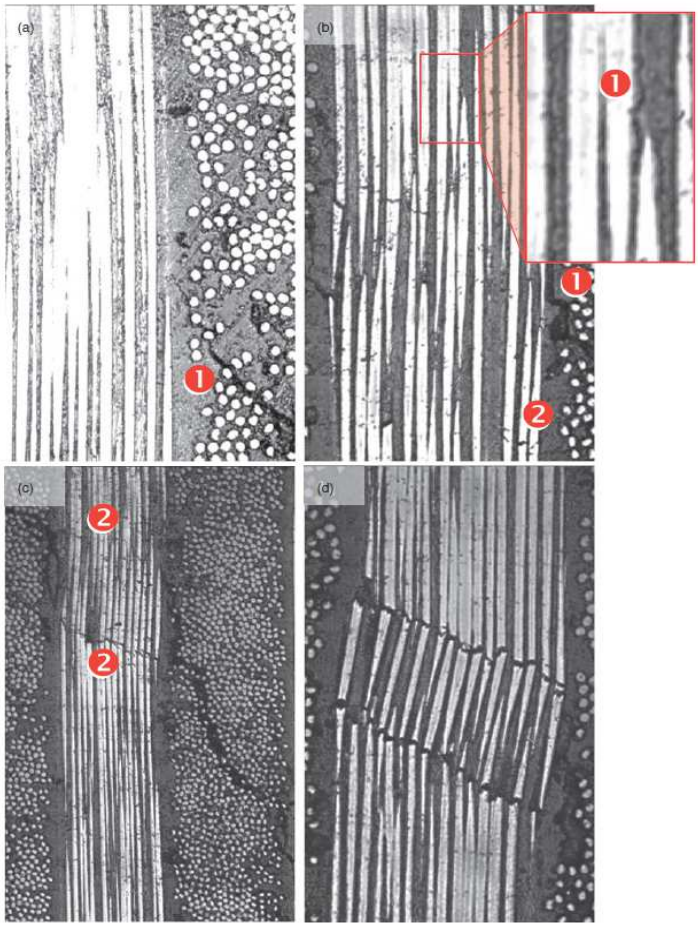

Figure 2-19: Sequence of events during kink-band formation [PIN12]. *(1) Matrix cracking (2) Fiber failure*

The same kink-band fracture pattern that was drove by shear-driven fiber compressive failure is also found in the woven fabric specimen (mC-0). In Figure 2-20a, the free space has been created by the big crack or delamination in the middle of the laminate that allows the adjacent 0° fibers to have free edge on the right side. It is believed that the 90° fibers has failed in the first place in shear and then propagates at 45° until it reaches to the adjacent interface of 0° fibers. Then, the process is assumed to be similar with the process described before (Figure 2-18). The only difference between the kink-band formation found in mT-0/90 and mC-0 is in the length of the fracture fibers. In this case the length is higher than fracture fibers mT-0/90. This is perhaps due to the difference in material properties of the fiber and the resin.

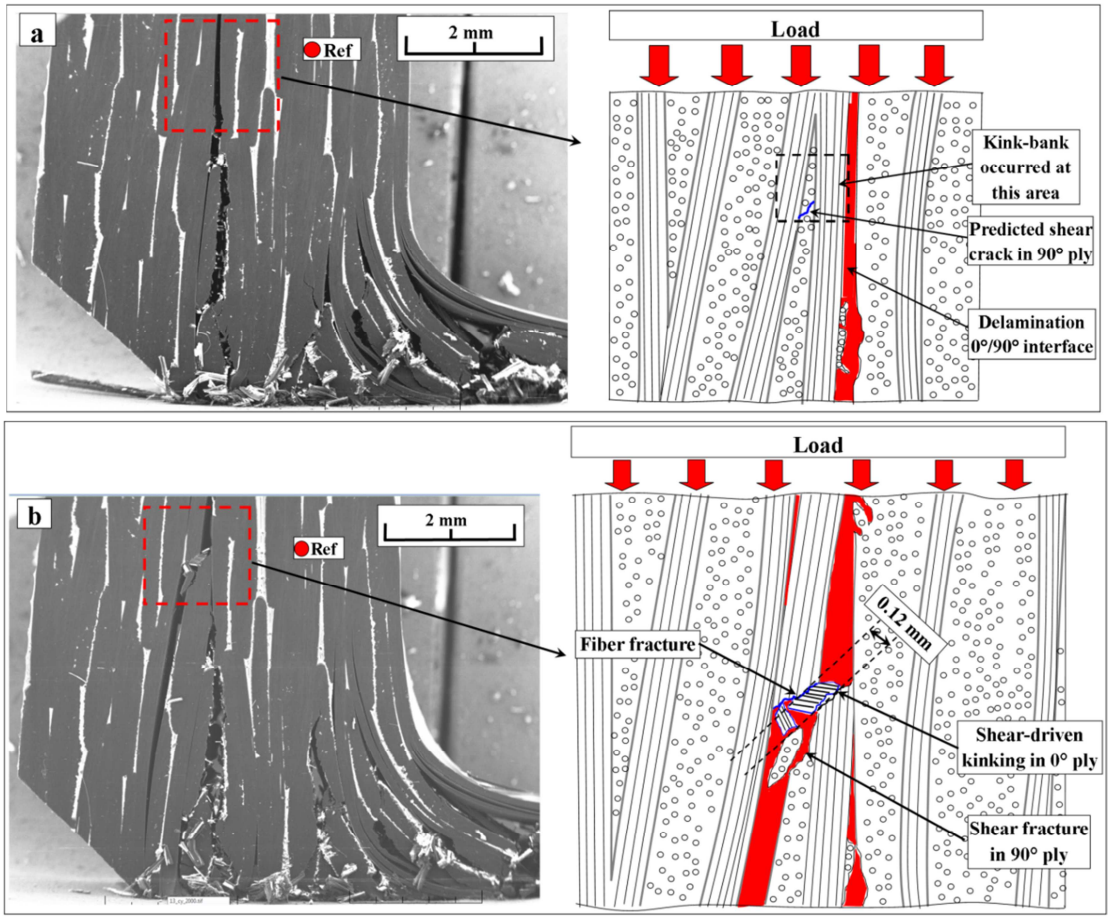

Figure 2-20: Kink-band failure pattern under shear-driven on the Cytec woven specimen (C-0 or mC-0)

2.2.3 Summary of Failure Mechanisms

Detailed observations of the failure mechanisms that controlled the crushing modes have been presented in this section. Besides that, the observation has shown that the fragmentation mode can be classified into two level scales of mechanisms namely localized crushing and inside ply failure. This classification will be useful for the numerical model development. Furthermore, this study has also revealed the formation of 90° debris wedge during localized crushing. Its presence at the crushing front is important to drive the behavior of the adjacent plies. Apart from that, this study has also demonstrated that during crushing test, kink-band fracture mechanism can exist when plies are crushed under fragmentation mode.

2.3 Ply Mean Crushing Stress

The ply mean crushing stress analyses are presented in this section due to its importance in the numerical modeling development. Failure analyses have shown that to correctly represent the material behavior during crushing, it requires a detailed finite element model at the scale of these observed phenomena. Thus, it is important to know the behavior of one ply subjected to crushing load, especially to determine the ply mean crushing stress that could be used for simulation.

From an experimental and numerical point of view, the laminate mean crushing stress is often used to understand, analyze or calculate a structure subjected to crushing. Even if the laminate mean crushing stress is defined as the mean crushing load divided by the cross sectional area, which is not a material characteristic, but a structure dependent value.

For example, Mamalis et al [MAM97A] has reported that mechanism controlling the energy absorption is dependent on the rate of applied stress, therefore it could be said that the laminate mean crushing stress is an important criteria. Barnes et al [BAR10] reported that the laminate mean crushing stress in composite structures is dependent on material and geometric parameters i.e. fiber and resin type, fiber orientations, and volume fractions of the constituent materials. But they also added that when designing an energy absorbing structure using composites the laminate crushing stress is a critical design parameter that must be known. Besides that, the laminate mean crushing stress was found considerably lower than the compressive strength.

For the last two decades many studies have investigated on the effect of the type of composite material [LAV96, KIM11], laminate design [HUL91, JOO11], specimen geometry [CZA91, JIM00, FER09], processing condition [MEL10], fracture toughness [HAM95, HAD09] or crushing mechanisms [SIG91, WAR08] on the energy absorption capabilities of structural components. But just a few discussions [MEL10, SAV06, FAR92] concerning the laminate mean crushing stress or specific sustained crushing stress (SSCS) have been done in the past.

Melo et al [MEL10] have investigated the effect of the application of vacuum on composite structures during fabrication on the energy absorption capability. According to their results, it did not produce any significant effect on laminate mean crushing stress or either compressive strength. In fact, the SEA is proved to be dependent on the cross section geometry. Furthermore, Savona et al. [SAV06] studied the relation between SSCS of glass fiber reinforced plastic (GFRP) composite plates in function of their Mode-I and Mode-II

fracture toughness properties. They found that the magnitude of the mean crush force depends on the propagation of the inter-laminar and intra-laminar cracks. Besides that, materials which have low Mode-I and Mode-II inter-laminar fracture toughness generated low SSCS and as a result, the energy absorbed during crushing is low. Farley and Jones [FAR92] used SSCS as an indicator to see the effect of ply angle [±θ] on the energy absorption capability of composite tube. Based on their results, the SSCS for ply oriented nearly 0° and 90° is close to each other for material Kevlar-934. However, these studies focused on drawing the relationship between specific energy absorption (SEA) and material properties which involve laminate mean crushing stress.

Greve et al [GRE08] on the other hand has introduced new simulation technique of phenomenological modeling based on Energy Absorbing Contact (EAC) formulation that depends on the global fragmentation stresses obtained from a series of dynamic axial and oblique impact tests on composite tubes. However, this fragmentation stress depends on the laminate lay-up, geometry (thickness) and impact angle. Thus, it needs to be determined each time the specimen and test configurations change which increases cost and time consuming.

A limitation of most of these studies is that the laminate mean crushing stress (or SEA) being a global structure and material dependent parameter, it can be used as a performance indicator, but not to predict the complex behavior of a composite structure subjected to crushing. It would then be interesting to investigate the possibility to define an elementary ply mean crushing stress, which would then be an intrinsic parameter of the material. To the author knowledge, there is no study concerning the ply mean crushing stress that has been done so far.

As explained and illustrated before in Figure 2-2, it seems there is a possibility to determine a ply mean crushing stress from the linear proportionality between the applied load and the contact length of the plies in fragmentations.

Therefore, in this section a methodology is introduced to determine the ply mean crushing stress of carbon-epoxy plies. The analysis is based on the quasi-static (instron) crushing tests performed on pure 0°, pure 90°, and mixed 0° and 90° UD laminates, and also on fabrics. Images of the crushing front taken during tests are analyzed to determine the size of the plies surface in contact during crushing. From this surface and the load, a ply mean crushing stress can be calculated for 0° and 90° plies. It has been verified that this stress is not dependent on the test configuration, which allows defining it as the mean crushing stress of a

ply. The values obtained are compared together, and to the usual compressive strength of a ply.

2.3.1 Contact Length Measurement

The aim is to calculate the ply mean crushing stress. Thus, it is necessary to define the right contact area of local crushing. The contact area is computed by multiplying the contact length with the width of specimen. The definition of contact length in this study is the direct contact between the plies and the metallic base that enable to sustain the forces.

As mentioned before, since the specimens have been chamfered at one end of the plate, most of the specimens are experiencing mixed mode crushing morphology. From the observation of Figure 2-21, the number of plies having direct contact with metallic base seems to be proportional to the force measured during the test. Thus, it would demonstrate the linear relationship between the direct contact area and the measured force.

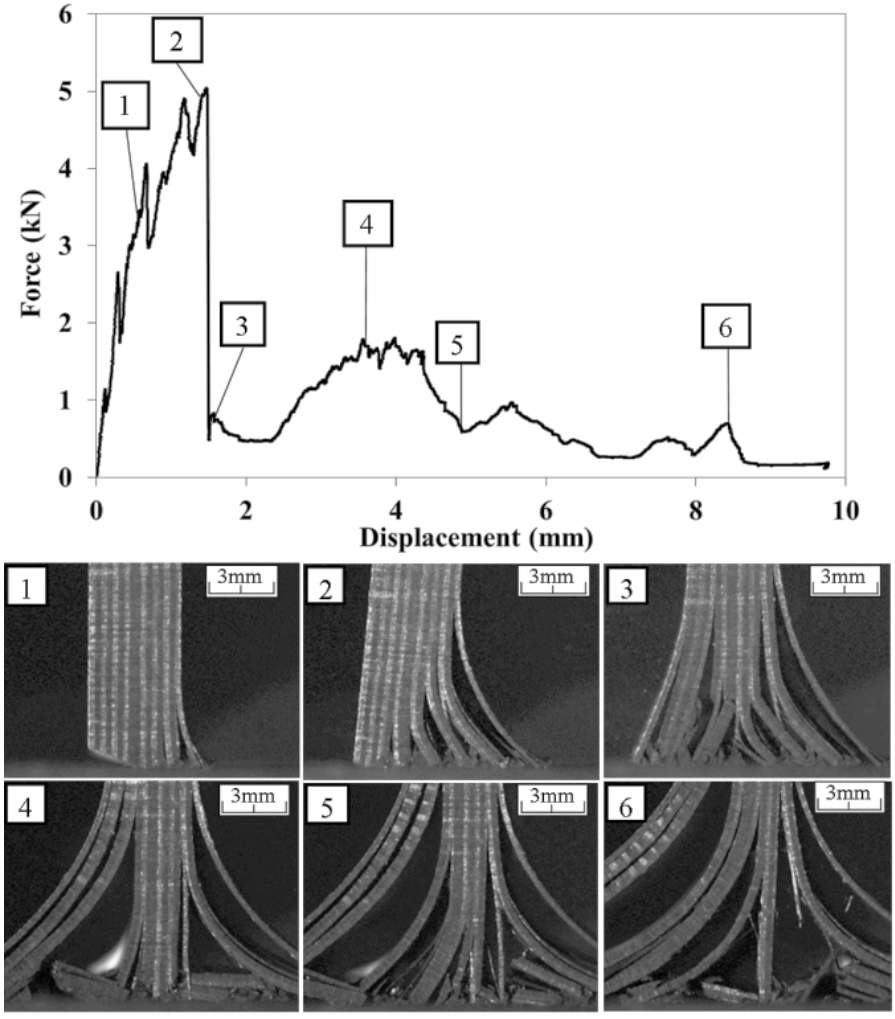

Figure 2-21: Example of force-displacement curve of T-0/90-20° test and selected pictures of the crushing front.

From the beginning to image 1 in Figure 2-21, the tip of the specimen crushes with local fragmentation (mostly) and the force grows as the contact area increases. Then, the delamination appears with splaying plies due to high transverse shear stress in plies interfaces, leading to a severe drop in the force (image 2 to 3 in Figure 2-21). Between image 3 and 4 in Figure 2-21, a mixed mode phenomenology appears with fragmentation in the middle plies, increasing the force. As well as the number of plies in fragmentation decreases from image 4 to 6 (Figure 2-21), the force correspondingly declines.

Therefore, for the contact area measurement only contact length of plies in fragmentation is counted as they enable to sustain forces as shown in Figure 2-22. In addition, there are some plies having "small bending" (short length ply bending), with still fragmentation at tip that also enable to sustain the force. Thus, the contact areas of these plies are included in the calculation (Figure 2-22a).

However, during crushing the plies in fragmentation also sustain severe damage that generates debris accumulation which reduces the contact area of plies in fragmentation. Thus, it must be careful not to include together the debris in the measurement because it makes the correlation between contact surface and the force become unrealistic as the debris has no direct contact, then no sustainable force (Figure 2-22a and 2-22d).

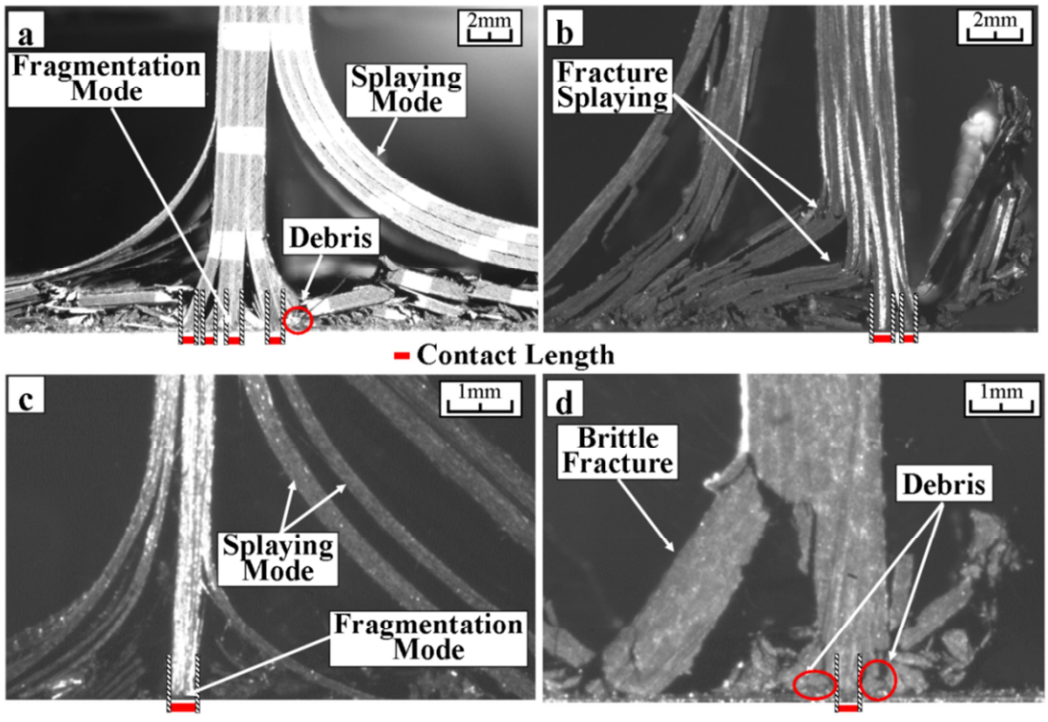

Figure 2-22: Contact length definition: (a) T-0/90 (b) C-0(c) T-0 (d) T-90

On the other hand, the contact area of plies in the splaying mode (Figure 2-22a-c) is considered negligible that will be proved after, during the ply mean crushing stress analysis.

Generally, these plies generate very low bending force. Guillon [GUI08] has made comparison tests between pure splaying mode and pure fragmentation mode. He proved that the load in pure splaying mode is very small (≤ 7%) compared to the mean crush load in pure fragmentation mode.

As the mean crushing stress is assumed not to be the same in 0° and 90° plies, for laminate specimens, contact areas of plies at 0° and 90° were measured separately in order to be able to determine the local mean crushing stress for each ply orientation.

Of course, determining the contact length from the images is not an easy task. During calculation of the contact length on certain images, it is recommended to view the image before and the image after current images to make sure not to miss any important information especially regarding the contact length at the extremity for instance to avoid including the debris into the calculation. Furthermore, the measurement is done on both side images (2 cameras) to ensure it gives same results, and help for determining the contact area.

There are some obstacles in measuring the contact length due to the quality of images, for example debris that hindering the vision, plies in contact with metallic base that are already broken at above which do not generate any forces, too much flare in the images etc. Thus, it is not possible to do the measurement for each image and the ambiguous images are removed from the calculation process.

Finally, determination of contact area is made entirely independently from the recorded data (force), not to have any bias in the method (only a few points of calculation are removed after calculation of ply mean crushing stress, for which new observations revealed mistake in the calculation of contact length). Furthermore, the deviation in the calculation of the contact length from the images is ± 1 pixel. The contact length for each specimen is calculated and plotted in function of time together with the experimental force as example in Figure 2-23. It shows similarities in the curve shapes. In the case of UD, 0° or 90°, there is clearly proportionality (see example for 0°, Figure 2-23a), but in the case of laminate (T-0/90), it is more complex to see due to the two considered parameters: contact length of 0° and 90° plies (Figure 2-23b). The ratio between contact length of 0° and 90° plies is presented in Figure 2-23b below the force curve. The ratio have shown during a test, the percentage of 0° crushed plies in the whole crushed plies can vary from 30% to 90%.

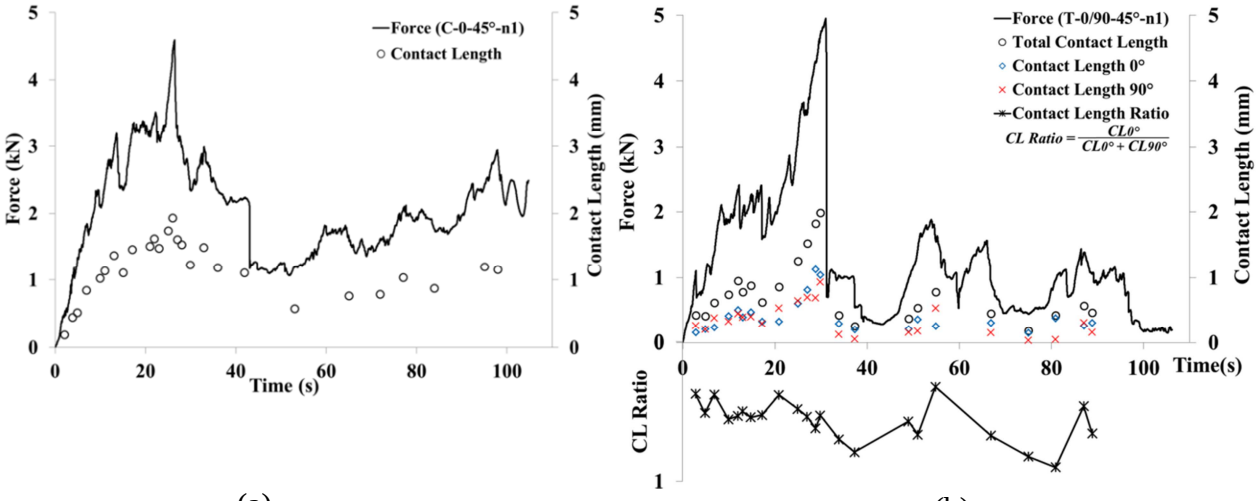

(a) (b)

Figure 2-23: Examples of contact length and force curve (a) laminate C-0 (b) Laminate T-0/90

2.3.2 Least Mean Square Analysis

From the similarity of curve shapes between force and contact length observed in the Figure 2-23, model A (Eq.2-1) is proposed to estimate the mean crushing stress of ply for the case of UD (T-0 / mT-0 and T-90 / mT-90) and balanced fabrics (C-0 / mC-0) specimens.

$$F = \sigma_{0^\circ} S_{0^\circ} + F_{splaying} \qquad (or\ F = \sigma_{90^\circ} S_{90^\circ} + F_{splaying}) \qquad \text{(Eq.2-1)}$$

Where F is the force, σ_{0° (σ_{90°) is the mean crushing stress for 0° (90°) plies, S_{0° (S_{90°) is the contact area of 0° (90°) crushing plies and $F_{splaying}$ is the splaying force.

Afterwards, the prediction model B (Eq.2-2) is introduced as an extension from model A for T-0/90 or mT-0/90 specimens since it has two parameters, crushing area of 0° and 90° ply. Therefore, the local mean crushing stress of 0° and 90° ply inside laminate can be estimated separately.

$$F = \sigma_{0^\circ} S_{0^\circ} + \sigma_{90^\circ} S_{90^\circ} + F_{splaying} \qquad \text{(Eq. 2-2)}$$

The estimation of ply mean crushing stress is done by using the least mean square (LMS) method. In both models, the prediction value of $F_{splaying}$ is very small and can be neglected for further analysis. This result has proved the contact area of plies in splaying mode can be negligible due to the reason explained in previous section. All the results of ply mean crushing stress for each case are presented in Table 2-3.

Table 2-3: Estimation of ply mean crushing stress inside laminates

Specimen (T700/M21)		**Type of crushing test**	**No. of points for LMS calculation**	**$\sigma_{0°}$ (MPa)**	**$\sigma_{90°}$ (MPa)**	**Standard deviation**
UD	T-0-20°-n1	Medium-scale	25	274	-	4%
	T-0-45°-n1	Medium-scale	24	271	-	3%
	mT-0-45°-n2	*Micromechanical*	*11*	*276*	-	*4%*
	T-90-20°-n1	Medium-scale	37	-	259	2%
	T-90-45°-n1	Medium-scale	17	-	253	1%
	T-90-45°-n2	Medium-scale	18	-	257	2%
	mT-90-45°-n1	*Micromechanical*	*9*	-	*251*	*3%*
Laminate	T-0/90-20°-n1	Medium-scale	26	288	252	3%
	T-0/90-45°-n1	Medium-scale	24	286	281	5%
	T-0/90-45°-n2	Medium-scale	23	280	275	5%
	mT-0/90-45°-n1	*Micromechanical*	*11*	*293*	*261*	*5%*
Ply mean Crushing Stress from all points			225	276	270	4%

Specimen (CytecWoven)		**Type of crushing test**	**No. of points for LMS calculation**	**$\sigma_{0°}$ (MPa)**	**Standard deviation**
Woven laminate	C-0-5°-n1	Medium-scale	23	275	7%
	C-0-20°-n1	Medium-scale	24	270	6%
	C-0-45°-n1	Medium-scale	26	269	6%
	mC-0-45°-n2	*Micromechanical*	*13*	*273*	*4%*
Ply mean Crushing Stress from all points			86	272	7%

For each test, the ply mean crushing stress analysis is made with a number of points as given in the Table 2-3 in which one data point refers to one image taken from the tests. The calculation of the last row for both parts of the table corresponds to the results of ply mean crushing stress for all tests on each material. It corresponds to a LMS executed on all points i.e. 225 data points from laminate and UD specimens of material T700/M21 and 86 data points from the woven specimens. For this calculation, the maximum error between the experimental force and the calculated force for both cases are 13% and 10% respectively, and the standard deviation are 4% and 7% respectively.

In fact, for T700/M21 specimens the domain of calculation for LMS is relatively wide, as there are pure 0° tests, pure 90° tests, mixed 0° and 90° tests (with different ratio in contact area), and different levels of crushing area in each case as shown in the Figure 2-24. All experimental data are well fitted by an interpolating plane which validates the prediction model B is suitable to be used to estimate the mean crushing stress of a ply. Moreover, Figure 2-25 shows good correlation between estimated forces from prediction models determined by LMS and force from experiment on different specimens for both materials. Thus, it can be concluded that the ply mean crushing stress is pertinent.

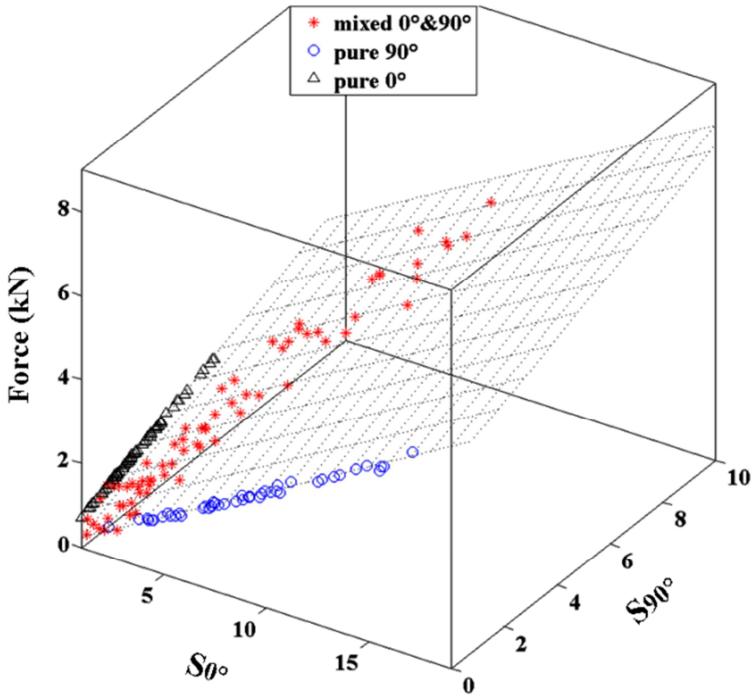

Figure 2-24: Range of contact area and global correlation for T700/M21 specimens

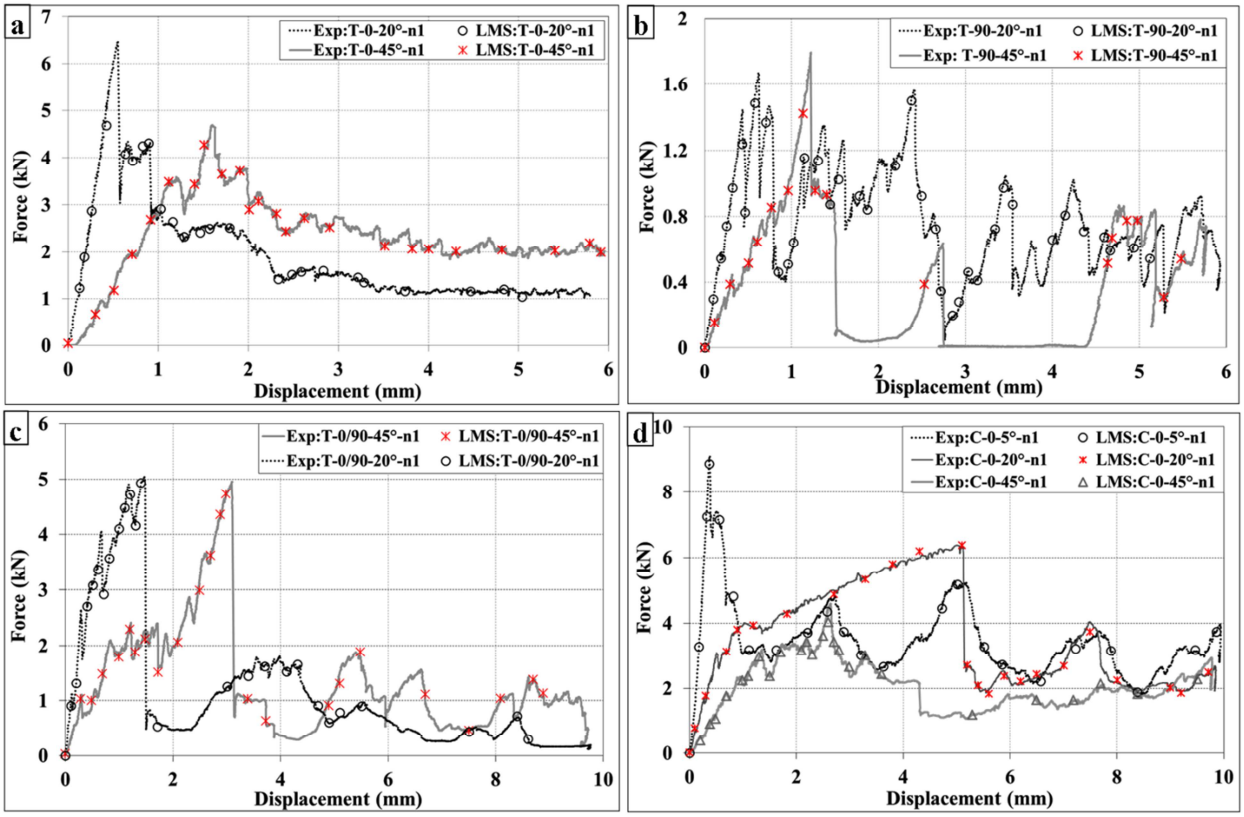

Figure 2-25: Example of experiment and LMS correlation: (a) T-0 specimens (b) T-90 specimens (c) T-0/90 specimens (d) C-0 specimens

2.3.3 Result Analysis

The proposed method works well in determining the ply mean crushing stress. From the calculations (LMS) on T700/M21, it shows that whatever the test used (only UD or laminate), the ply mean crushing stress is almost the same in each ply:

$\sigma_{0°\text{ (UD only)}} \approx \sigma_{0°\text{ (UD 0° in 0/90 laminate)}}$

(273 MPa) (280 MPa)

$\sigma_{90°\text{ (UD only)}} \approx \sigma_{90°\text{ (UD 90° in 0/90 laminate)}}$

(259 MPa) (269 MPa)

where the ply mean crushing stress values above is taken from separate LMS correlation on all T-0 specimens, T-90 specimens and T-0/90 specimens respectively. Moreover, the re-computation of the ply mean crushing stress using the data from the micromechanical tests (micromechanical test) also gives values (Table 2-3) close to the ply mean crushing stress computed from the medium-scale tests.

Besides that, by combining all data points of UD and laminate specimens, the final $\sigma_{90°}$ obtained is 272 MPa which is very close to the value of transverse compressive strength. The explanation is that in the crushing zone, the main failure mechanism is the same: shear fracture at 40° to 60°. This can be seen in Figure 2-26b, that shows the crushed surface of a 90° ply under SEM after release of the crushing load had similar shear fracture mechanism as shown in Figure 2-27. In contrast, the final $\sigma_{0°}$ obtained is 276 MPa, which is far lower compared to longitudinal compressive strength, 1015 MPa. This is due to the difference in failure mechanisms where longitudinal compressive strength is induced by kink band [SCH96] inside 0° plies, whereas $\sigma_{0°}$ is obtained from fragmentation at the extremity of the plies, where confinement of fibers is lower, and the surface is irregular, due to the presence of packs of fibers with pre-initiated inter- and intra-laminar cracks. Figure 2-26a shows the crushed surface of a 0° ply, under SEM, after release of the crushing load. The irregularities of the surface of crushing are obvious on the photography: packs of fibers and powder-like debris.

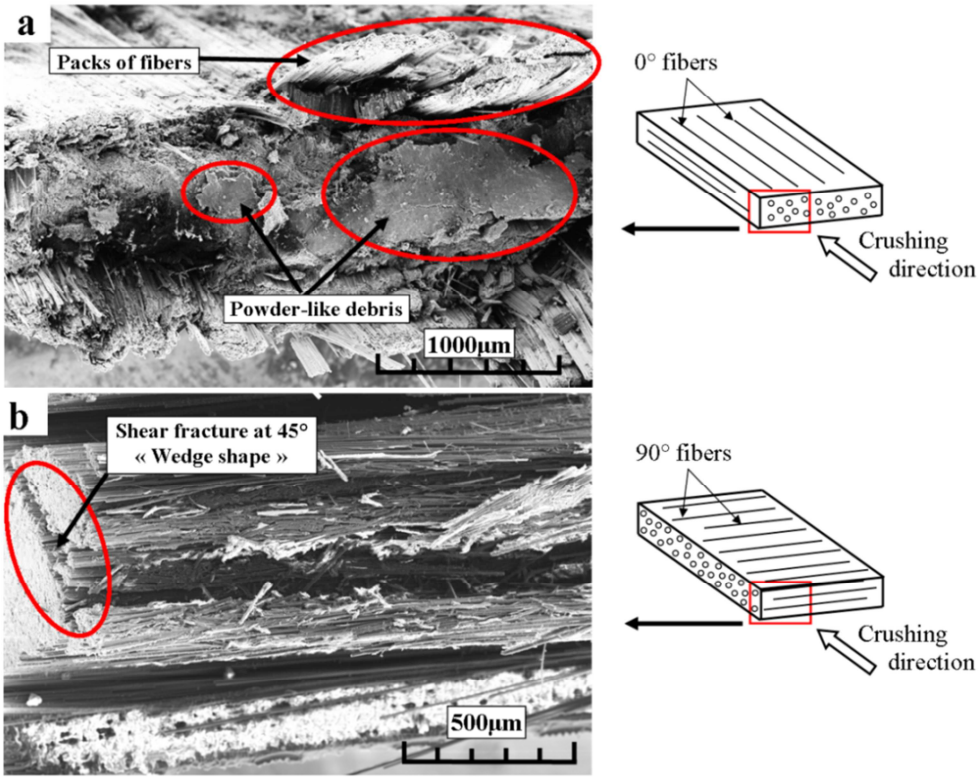

Figure 2-26: SEM observation of crushed surface: (a) T-0 specimen (b) T-90

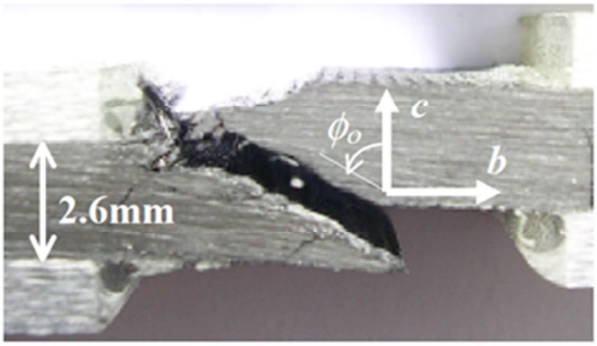

Figure 2-27: Pure transverse compressive failure, for a CFRP specimen [PIN05]

Furthermore, even if the models of calculation are different, depending on the laminate types: model A (Eq. 2-1) on UD laminates, model B (Eq. 2-2) on T-0/90 laminate, or model B on all laminates, the calculated ply mean crushing stress for 0° and 90° are comparatively always very close. It means that when a steady fragmentation is obtained during crushing in 0° or 90° plies, both plies have the same energy absorption ability. This result must be qualified by the observations made during tests. 0° plies crushing tests show the possibility for a part of the plies to create a steady fragmentation (Figure 2-28a), whereas in 90° tests, most of the time, fragmentation turns to global rupture of the ply (Figure 2-28b). In that case, the volume of material actually involved in energy absorption is then lower.

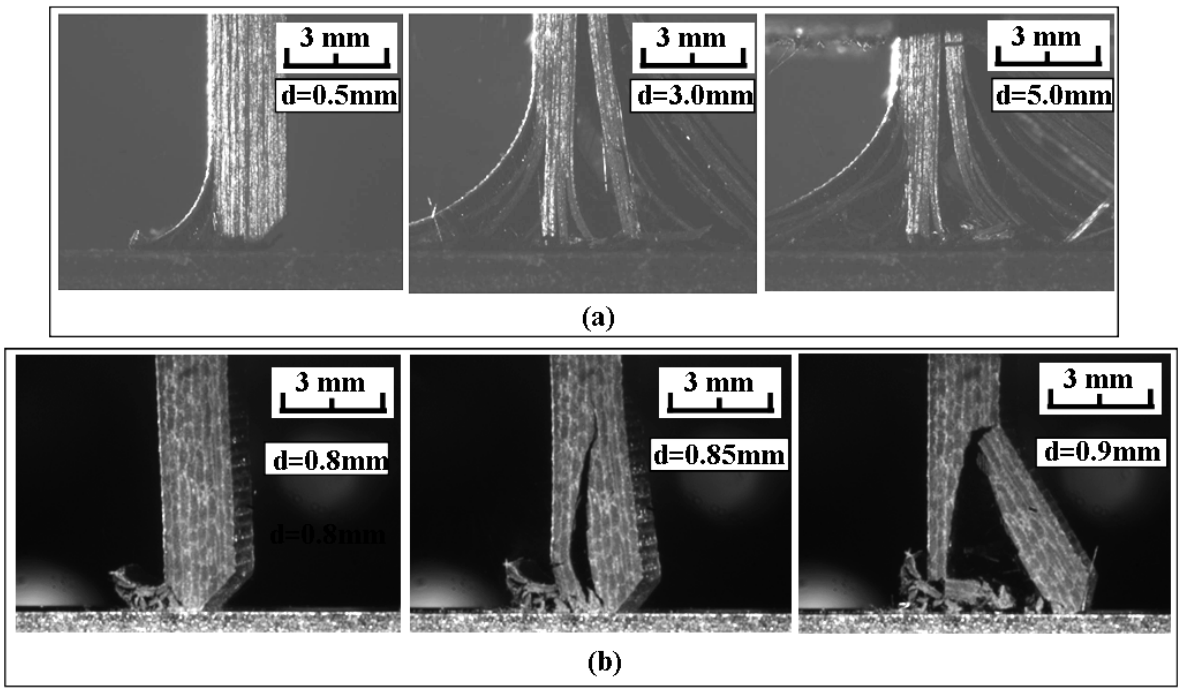

Figure 2-28: The crushing process of T700/M21 pure UD specimen (a) T-0 (b) T-90

The same method and steps are used for the analysis of laminates made of Cytec balanced fabric material (C-0). All tests are done in the warp direction of the fabric. Therefore, the model used is model A (Eq. 2-1, only one parameter). Only plies or part of plies in fragmentation are taken into account for the contact area calculation. The result of mean crushing stress for this laminate (272 Mpa) is also close to the results of ply mean crushing stress of material T700/M21 although there is no particular relation between these two materials beside both matrices are epoxy-based resin. This value is also considerably far below the compressive strength of warp plies (877 MPa).

Moreover, from the mean crushing stress obtained in this study the equivalent SEA, a frequent used parameter to specify the energy absorption capability can be computed for both materials by:

$$SEA = \frac{E_{total}}{M_{crush}} = \frac{F_{mean} \cdot L_{crush}}{\rho S L_{crush}} = \frac{\sigma_{mean}}{\rho} \qquad \text{(Eq. 2-3)}$$

Where E_{total}, M_{crush}, L_{crush}, ρ, S are the total energy absorb during crushing, the mass of the crushed material, the final crushing length, the density and cross-sectional area, respectively. While, F_{mean} is mean crushing load and σ_{mean} is mean crushing stress. Hence, for T700/M21 the calculated SEA for 0° plies is 184 kJ/kg and 180 kJ/kg for 90° plies. These SEA values are also close to the calculated SEA of Cytec balanced fabrics which is 183 kJ/kg due to the

small difference in density between these two materials. However, these SEA values are maximum that only obtained if laminates are crushed entirely in fragmentation mode which is not the case in most of tests available in the literature. Thus, these SEA results are much higher than SEA values (range from 50 kJ/kg to 95 kJ/kg) found in the literature [FAR92, BOL95, LAV96] of other carbon/epoxy types with different geometry configurations. The nearest SEA value found in literature is 194 kJ/kg obtained by Ramakrishna [RAM97], but with a different type of resin, PEEK.

In fact, the actual SEA values calculated from Figure 2-25 and the SEA results taken from [DUO10] have shown that it far lower than these ideal SEA values due to some plies are crushed under splaying mode. For example, the SEA result for specimens T-0-45°-n1 and T-90-20°-n1 is 62 kJ/kg and 18 kJ/kg respectively. While for the Plate-T-0/90 and T-0/90 specimens, the SEA results are between 19 kJ/kg and 25 kJ/kg depending on chamfering angles and crushing speeds. Similarly for Cytec balanced fabrics specimens (Plate-C-0 and C-0), the actual SEA is also far lower than its ideal value which is between 35 kJ/kg and 55 kJ/kg.

2.3.4 Summary of Ply Mean Crushing Stress Study

Based on the analyses have been made, it can be concluded that by using the proposed methodology, it is possible to determine the mean crushing stress of a ply inside a laminate that is an intrinsic parameter of the material. This is to say, when a ply is totally crushed or just partially crushed, it's the mean crushing stress is the same. Besides that, this study also demonstrate the possibility to develop new failure criterion in order to improve the fragmentation modeling especially to simulate the localized crushing and using this estimated ply mean crushing stress as the input parameter.

2.4 Humid Ageing

As we can see in the new design of aircraft, more aspect of composite materials have been included that should have a service life of 25 to 30 years in a variety of environments, which makes environmental resistance one of the most important factors in the structural design. Although CFRP composites can have a good specific energy absorption capacity from the creation of multiple damages inside the material, the effects from various environment factors i.e. temperature, relative humidity of air, water, chemical exposition etc. can cause material degradation as reported in many studies since 1960's [HAL69, BRO77, KOM83]. Generally, the degradation process is related to the chemistry of the matrix as well as the exposure time.

For example, the humid ageing phenomenon can affect the laminate strength and stiffness of CFRP composite due to plasticization of the matrix and the degradation of the fiber/matrix interface [CUN08, SHI10, SHE77A, SUR06, RAY06]. Muthirakkal et al [MUT10] have found a clear drop of mechanical properties of carbon/epoxy materials such as 21% in flexural strength, 48% in ultimate tensile strength and 18% in inter-laminar shear strength when it absorbed moisture under humidity environment (95% relative humidity (RH) and 70°C) and tested in high temperature condition. They also found the same influence of humid ageing on glass/epoxy, glass/vinylester and carbon/vinylester composites. Besides that, Cunha et al [CUN08] also added that the plasticization of matrix reduces residual stresses and increases viscoelasticity. The degradation of these material properties will influence the durability of composite materials.

From the literature point of view, the change in behaviors of CFRP composites structure in humid and thermal environments when subjected to crash load has still not been well investigated. In fact, it is very hard to find composite crashworthiness studies made on ageing specimen. Therefore, several crushing tests are performed to investigate the effect of ageing phenomenon on crushing performance of carbon-epoxy composite laminates especially to improve the understanding of its influences on the damage mechanisms and global behaviors including the ply mean crushing stress values. Besides that, the changes in some material properties can be used for the numerical model validation.

The specimens used are aged in the humid condition for certain period of time as explained in the following section. Hence, in this study the specimens used will be called as humid ageing (HA) specimen. The results of these tests will be compared with the ones given by the same tests on sane specimens

2.4.1 Specimen Preparation

In this study, only quasi-static crushing tests will be performed on the HA specimens using the same test set-up as in medium-scale and micromechanical crushing tests. The configurations (material, sizes, geometry, stacking sequence etc.) of HA specimens are exactly the same as sane specimens used in medium-scale and micromechanical crushing tests as explained in the previous section. Hence, making it possible to compare the results between crushing tests of HA specimens and the sane specimens in term of damage mechanisms and ply mean crushing stress.

In total, 16 specimens (eight specimens for each test and two specimens for each configuration) are used in this study to investigate the influence of humid ageing on CFRP composite subjected to crash load as listed in the Table 2-4. Besides that, only 45° chamfering trigger is used in this study. The same four different configurations of specimen used in the previous section are:

(1) T700/M21 UD laminate made of 8 plies in pure longitudinal direction $[(0°)_8]$ (specimen HA-T-0 and HA-mT-0 for medium-scale and micromechanical tests respectively),
(2) T700/M21 UD laminate made of 8 plies in pure transverse direction $[(90°)_8]$ (specimen HA-T-90 and HA-mT-90 for medium-scale and micromechanical tests respectively)
(3) T700/M21 UD laminate of 16 plies with stacking sequence of $[(0°/90°)_4]_{sym}$ (specimen HA-T-0/90 and HA-mT-0/90 medium-scale and micromechanical tests respectively)
(4) Cytec balanced fabrics (HA-mC-0) with stacking sequence $[(0°)_{12}]$ (specimen HA-C-0 and HA-mC-0 medium-scale and micromechanical tests respectively)

The specimens are weighed and placed in a humidity-controlled chamber at 90% RH and 80°C for a long time (until saturation). High temperature is imposed to accelerate the moisture uptake rate based on the study in [RAY06] as shown in Figure 2-29. Particular care should be taken in the measurement of the specimen dimensions and weight in order to be able to follow their growth in weight during moisture absorption. The moisture absorption of each specimen has been monitored periodically (more or less every 2 or 3 weeks), and weighted using a sensible electronic balance METTLER AT250 (precision at 0.01mg) to monitor the weight change behavior.

Generally, all the specimens are small in dimensions that give an advantage to reach faster saturation of moisture inside the specimens [MER06]. All the HA specimens are taken

out after it reaches enough saturation (more > 400 days) to perform the crushing tests. Similar to the sane specimens, the HA specimens are controlled again by observing under optic microscope and SEM in order to make sure the specimens have no defect before performing the crushing tests. All the crushing tests are carried out at room temperature.

Table 2-4: HA specimens configuration

	Specimen[c]	Type of test	Thickness (mm)	Width (mm)	Initial weight(g)	Saturated weight(g)	% weight increase
T700/M21	HA-T-0-45°-n1	Medium-scale	2.11	10.1	1.5608	1.5773	1.06
	HA-T-0-45°-n2	Medium-scale	2.11	10.22	1.6574	1.6744	1.03
	HA-T-90-45°-n1	Medium-scale	2.11	10.01	1.1518	1.1636	1.02
	HA-T-90-45°-n2	Medium-scale	2.11	10.11	1.1521	1.1634	0.98
	HA-T-0/90-45°-n1	Medium-scale	4,26	8.3	2.8808	2.9039	0.80
	HA-T-0/90-45°-n2	Medium-scale	4,26	8.3	2.8601	2.8834	0.81
	HA-mT-0-45°-n1	Micromechanical	2.11	4	0.2916	0.2948	1.1
	HA-mT-0-45°-n2	Micromechanical	2.11	4.06	0.2604	0.2630	1.00
	HA-mT-90-45°-n1	Micromechanical	2.11	5.93	0.6528	0.6594	1.01
	HA-mT-90-45°-n2	Micromechanical	2.11	5.95	0.6479	0.6547	1.05
	HA-mT-0/90-45°-n1	Micromechanical	4,26	3.88	0.8837	0.8923	0.97
	HA-mT-0/90-45°-n2	Micromechanical	4,26	3.86	1.0185	1.0285	0.98
Cytec	HA-C-0-45°-n1	Medium-scale	4,71	8.08	3.5561	3.5826	0.74
	HA-C-0-45°-n2	Medium-scale	4,71	7.98	2.8702	2.8920	0.76
	HA-mC-0-45°-n2	Micromechanical	4,71	3.81	0.8670	0.8741	0.82
	HA-mC-0-45°-n2	Micromechanical	4,71	3.82	1.1914	1.2010	0.81

[c]*Note: The designation of specimens is the same as explained in table 1 and table 2, only there is an additional of HA which is stand for Humid Ageing in order to differentiate with sane specimens*

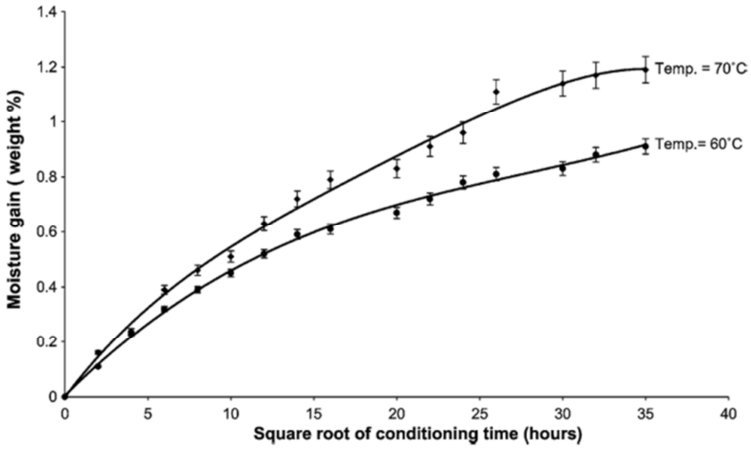

Figure 2-29: The influence of temperature on the moisture absorption in carbon/epoxy composites [RAY06]

2.4.2 Effect of Humid Ageing on the Crushing Performance

All the HA specimens are tested under crushing loads using the same test set-up of medium-scale and micromechanical crushing test done on the sane specimens as explained in the previous section. Figure 2-30 shows the example of result comparison in force-displacement curves between HA specimens (HA-T-0/90-45° and HA-C-0-45°) and the sane specimens (T-0/90-45° and C-0-45°) for medium-scale crushing tests. In general, the global shape of the curve between HA specimen and the sane specimens is very similar in both types of materials. Figure 2-31 on the other hand, presents the example of crushing morphologies comparison between the HA specimens (HA-T-0/90-45° and HA-C-0-45°) and the sane specimens (T-0/90-45° and C-0-45°) during medium-scale crushing tests. Similar to the sane specimens, all the HA specimens experienced the mixed-mode crushing as well except for pure UD 90° specimens (HA-T-90).

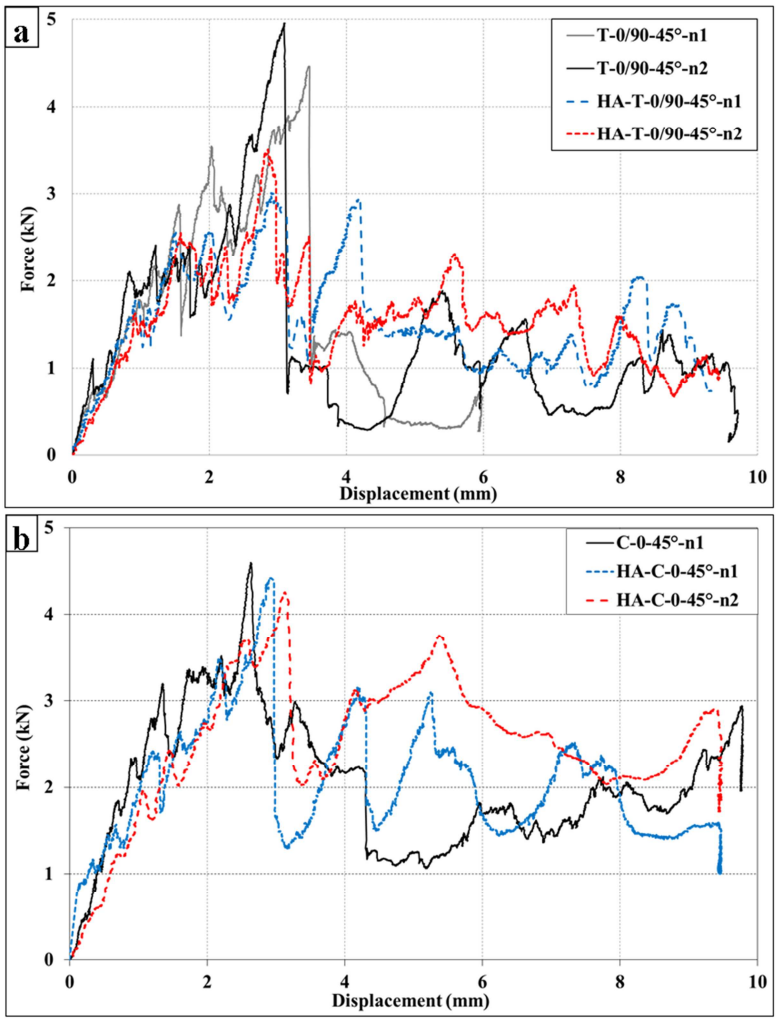

Figure 2-30: Example of force-displacement curves comparison between HA specimens and sane specimens (a) T-0/90-45° vs HA-T-0/90-45° (b) C-0-45° vs HA-C-0-45°

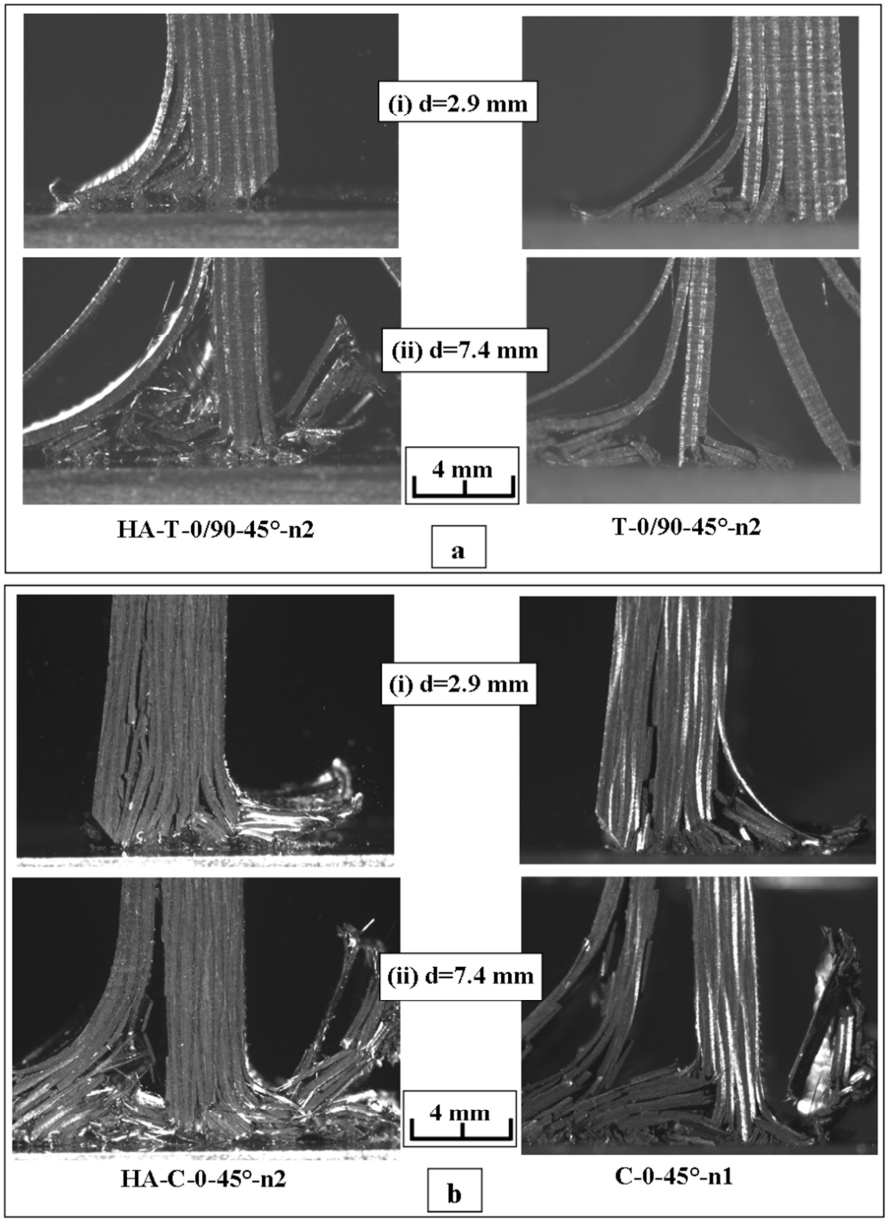

Figure 2-31: Example of result comparison of crushing morphology between HA specimen (HA-T-0/90-45°-n2) and sane specimen (T-0/90-45°-n2)

From the Figure 2-30a, one can notice that the peak force of HA specimens (HA-T-0/90) is lower than the peak force of sane specimens (T-0/90). Referring to Figure 2-31a (image i), this is due to more plies on the left in HA-T-0/90 that are broken and bended caused by the trans-laminar shear fracture as oppose to the T-0/90 specimen that have more plies crushed in fragmentation mode. However, this is not the case in the Figure 2-30b where the peak force of HA specimens (HA-C-0) are close to the peak force of sane specimen (C-0). As can be seen in Figure 2-31b (image i), both specimens (HA-C-0 and C-0) have almost the same portion of plies crushed in fragmentation mode. Concerning the mean crushing force, it can be observed in Figure 2-30 that the mean force of HA specimen is higher than the sane

specimen in both cases. According to the crushing morphology in Figure 2-31 (image ii), this is due to HA specimen having more plies in contact to perform a stable fragmentation mode compared to the sane specimen. But, it is hard to conclude the variation of forces in Figure 2-30 and whether the difference in crushing morphologies in Figure 2-31 are due to the degradation in fiber matrix bond strength affected by the moisture content [PIT96] or it is just due to the dispersion of the tests in HA or sane specimens.

In term of damage mechanisms, according to the observation made during the crushing tests on the HA specimens, there are no big differences compared to the sane specimens which has endured several kinds of damage mechanisms as discussed in the previous section either for T700/M21 specimens or the Cytec balanced fabric specimen. All main damage mechanisms (splaying, fragmentation, debris) including the specific failure mechanisms such as 90° debris wedge and kink-band formation under shear-driven, found in the crushing tests of sane specimens can also be seen during the crushing tests of the HA specimens. Besides that, it is difficult to see the effect of humid ageing on the inter-laminar fracture toughness because it seems like both specimens have the same level of delamination even tough as reported in the literature that the inter-laminar fracture toughness of composite material is normally affected by the moisture and temperature [RUS85, HUT99].

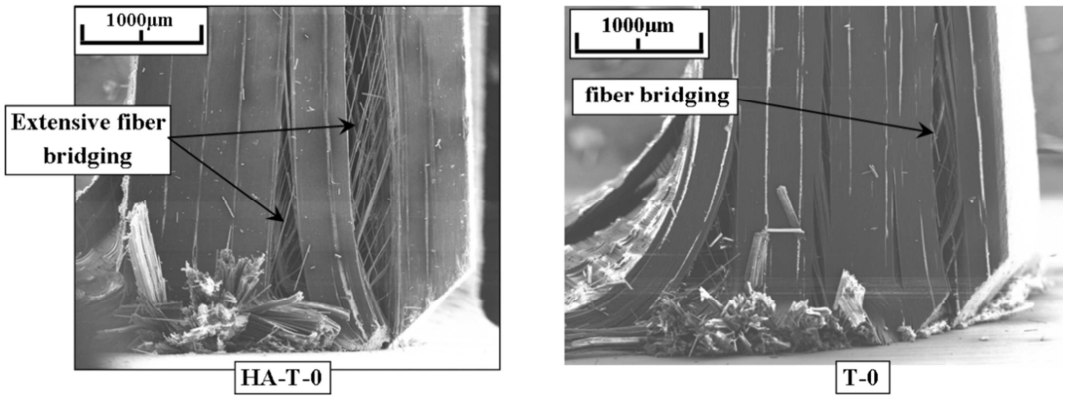

Figure 2-32: Comparison of fiber bridging behavior between HA specimen (HA-T-0) and sane specimen (T-0)

Nevertheless, there are small differences that can be noticed concerning the damage behavior found in the HA compared to the sane specimens. For example, in all crushing tests of HA-T-0 (or HA-mT-0), the intra-laminar failures is observed to create more fiber bridging than the sane specimen (Figure 2-32). The crushing tests performed on HA-T-90 (or HA-mT-90) has shown that three (1 in micromechanical and 2 in medium scale) out of four tests failed under major tensile cracking due to bending which caused the global rupture of plies as shown in Figure 2-33a. Moreover, all crushing tests of pure UD 90° have exhibited multiple tensile

cracking before turns into global rupture. The same behavior can also found in the 90° plies inside the HA-mT-0/90 specimen (Figure 2-33b) when it experienced bending mode. This multiple tensile cracking failure has not been observed during the crushing tests of sane specimens. It could be related to the decrease in the tensile strength of 90° plies as reported in the literature [SHE77A, SHE77B].

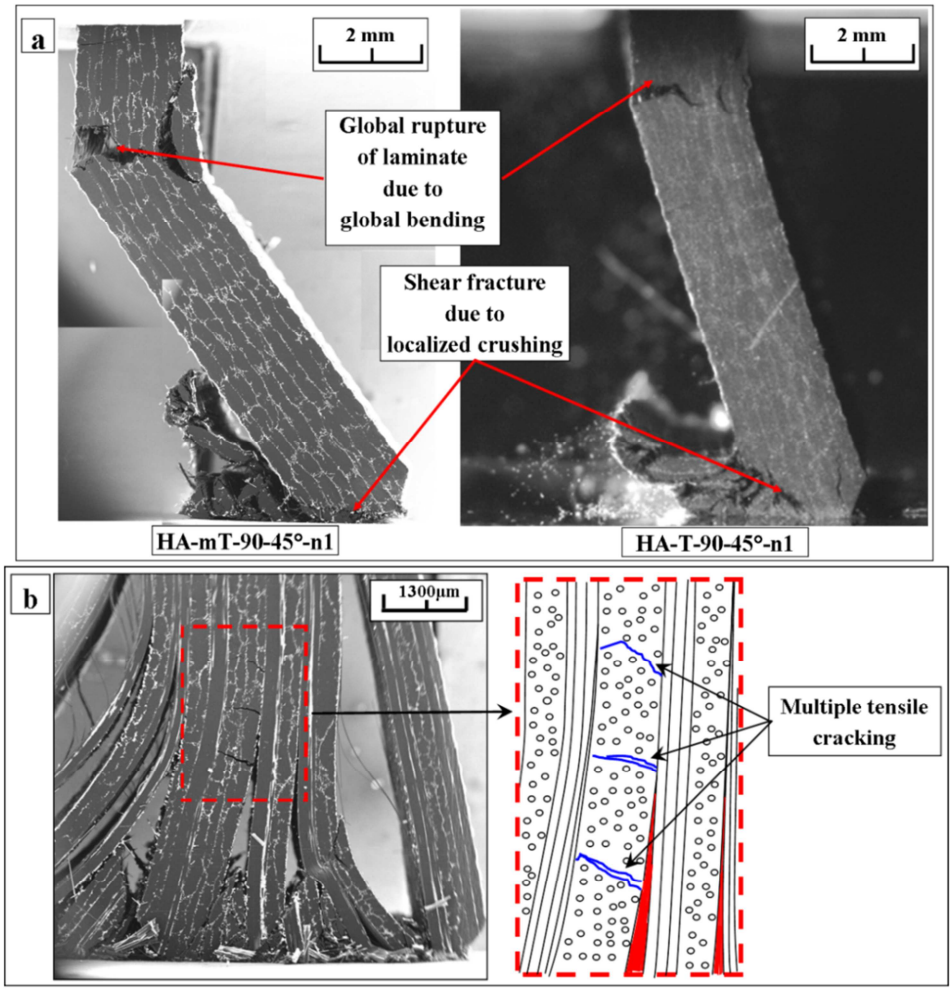

Figure 2-33: The example of failure on HA 90° plies (a) The global ruptures of pure UD 90° specimens (HA-mT-90 and HA-T-90) (b) multiple tensile cracking of 90° plies inside laminate HA-T-0/90

2.4.3 Effect of Humid Ageing on the Ply Mean Crushing Stress

The aim of this analysis is to verify either humid ageing degradation will influence the ply mean crushing stress estimated in section *§2.3* or not. In this section, the ply mean crushing stress of the HA specimens are estimated using the same method (LMS) as used for the sane specimens.

The results of ply mean crushing stress of each HA specimen are listed in Table 2-5. Similarly, the ply mean crushing stress is analyzed for each test with a number of points and

the last row in both parts of the table corresponds to the results of ply mean crushing stress for all tests on each material. In this calculation, the maximum error between the experimental force and the calculated force for both materials are 13% and 9% respectively, and the standard deviation are 5% and 6% respectively. Figure 2-34 shows the example of the good correlation between estimated forces from prediction models and experimental force on different configuration of specimens and tests.

Table 2-5: Ply mean crushing stress computation for HA specimens

Specimen (T700/M21)		**Type of crushing test**	**No. of points for LMS calculation**	**$\sigma_{0°}$ (MPa)**	**$\sigma_{90°}$ (MPa)**	**Standard deviation**
UD	HA-T-0-45°-n1	Medium-scale	17	260	-	6%
	HA-T-0-45°-n2	Medium-scale	14	250	-	4%
	HA-mT-0-45°-n1	*SEM Test*	*12*	*260*	-	*6%*
	HA-mT-0-45°-n2	*SEM Test*	*11*	*254*	-	*2%*
	HA-T-90-45°-n1	Medium-scale	13	-	242	1%
	HA-T-90-45°-n2	Medium-scale	11	-	242	2%
	HA-mT-90-45°-n1	*SEM Test*	*9*	-	*242*	*2%*
	HA-mT-90-45°-n2	*SEM Test*	*19*		*245*	*1%*
Laminate	HA-T-0/90-45°-n1	Medium-scale	18	257	250	5%
	HA-T-0/90-45°-n2	Medium-scale	14	256	247	3%
	HA-mT-0/90-45°-n1	*SEM Test*	*14*	*252*	*244*	*1%*
Mean Crushing Stress from all points			152	255	246	5%

Specimen (CytecWoven)		**Type of crushing test**	**No. of points for LMS calculation**	**$\sigma_{0°}$ (MPa)**	**Standard deviation**
Woven laminate	HA-C-0-45°-n1	Medium-scale	21	258	3%
	HA-C-0-45°-n2	Medium-scale	19	264	6%
	HA-mC-0-45°-n1	*SEM Test*	*12*	*264*	*2%*
Mean Crushing Stress from all points			52	262	6%

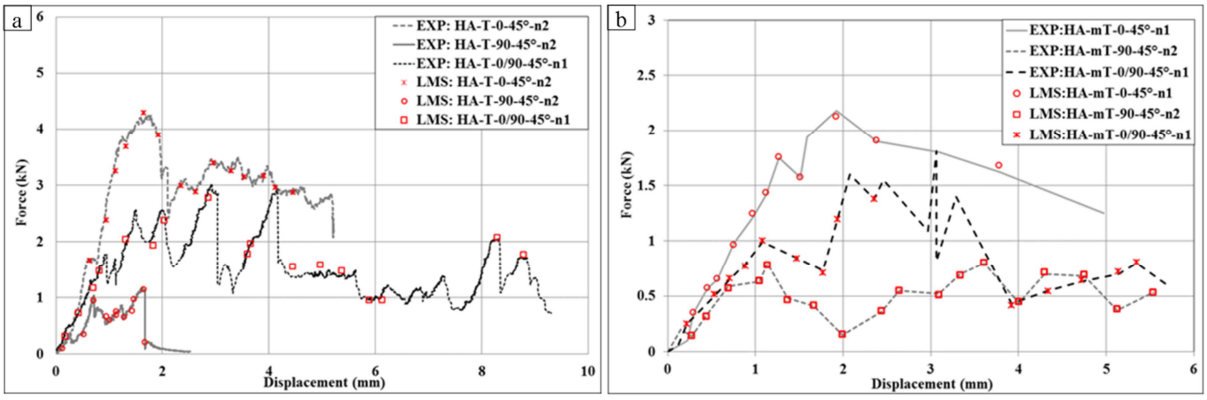

Figure 2-34: Example of experiment and LMS correlation: (a) Medium-scale crushing tests (b) micromechanical crushing tests

From the results obtained, it is quantitatively proven that there are drops of ply mean crushing stress of CFRP material after it has been exposed to the humidity environment.

Figure 2-35 shows the comparison of ply mean crushing stress results between HA specimen and the sane specimen for both, T700/M21 and Cytec balanced fabric materials. For the T700/M21, the degradations in ply mean crushing stress of 0° and 90° plies are 8% and 9% respectively. Meanwhile for the Cytec balanced fabric, the degradation of ply mean crushing stress is less than the T700/M21 material in which the drop is only 4% compared to the sane specimen.

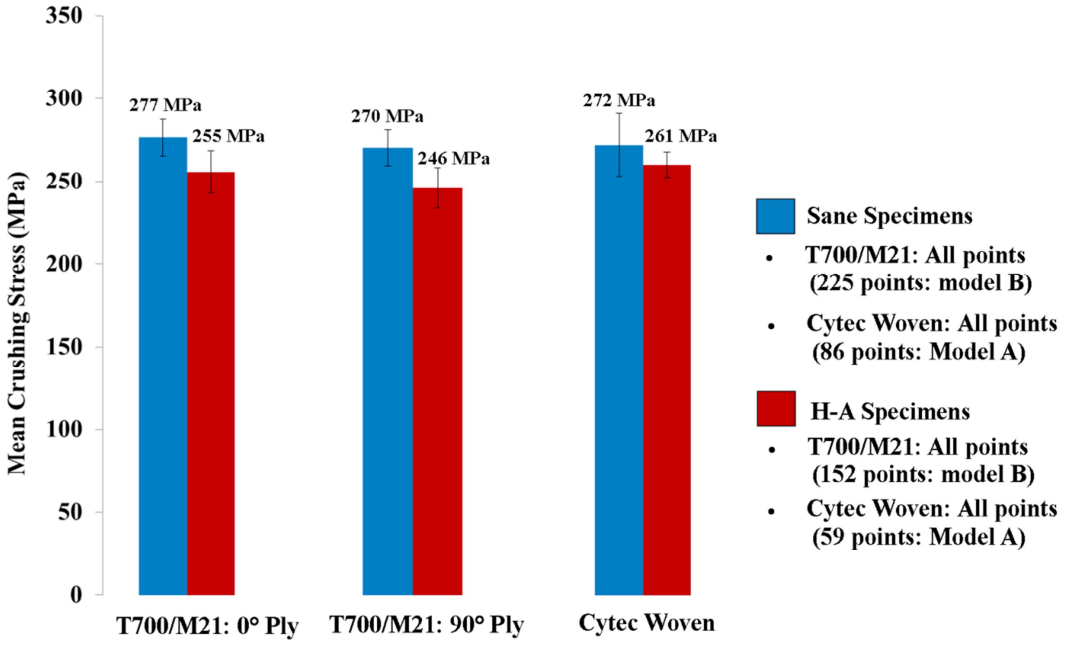

Figure 2-36: Comparison of ply mean crushing stress values between sane specimens and HA specimens

Based on these results, it is proven that the humid ageing degradation has some influence on the ply mean crushing stress. This degradation of ply mean crushing stress is close to the 8% reduction of compressive strength of carbon UD tape/epoxy 8552 composite when submitted to the salt spray chamber [CUN08].

2.4.4 Summary of Humid Ageing Study

The effects of humid ageing on the crushing performance of carbon-epoxy composite laminates have been carried out using medium-scale and micromechanical crushing tests. All the results have been compared with the crushing test of the sane specimens. In term of failure mechanisms and crushing morphology, there are no big differences observed between the HA specimen and the sane specimens. In term of degradation in the material properties, for the moment, this study only focuses on the degradation in the ply mean crushing stress properties that show a small drop i.e. 8% and 9% is estimated for 0° and 90° plies of T700/M21 material respectively while 4% for Cytec balanced fabric.

2.5 Conclusion

In general, the experimental works done in this study are useful for the development of numerical model. The real-time visualization during the tests and the post-mortem analysis have provided essential information regarding the mechanical phenomena involved in the progressive crushing of composite plates. In this study, the failure mechanisms involved in the fragmentation mode have been categorized in two level scales of mechanisms namely localized crushing and inside ply failure. Besides that, the detailed observations of the failure mechanisms has revealed the formation of 90° debris wedge mechanism that never been demonstrates in the literature. It plays a significant role in triggering other failure mechanisms such as delamination and kink-band failure to the neighboring plies during the crushing test.

Besides that, an investigation to determine the ply mean crushing stress inside a laminate has been done with a simple methodology based on analyses of images. The qualitative agreement between the correlation of force/surface analysis by LMS and the experimental data is demonstrated. It shows that it is possible to calculate ply mean crushing stress for plies that are being crushed in a fragmentation mode with the proposed test and calculation method since the correlation is done all along the crushing progression and not at a specific point of the test. For 0° and 90° plies of T700/M21 material, the values calculated in pure 0° (or 90°) or in 0°/90° laminate are the same, which allows to say that, at least for beam-like or plate-like structures, the value of ply mean crushing stress is an intrinsic parameter of the material, even if it does not involve that during crushing, all plies, or even all the thickness of a ply will crush in a fragmentation mode. These test and calculation method could then be used as a test characterization of material for the purpose of crushing simulation. From a numerical point of view, this study demonstrates the potential to deliver essential data regarding the magnitude of ply mean crushing stress to perform numerical simulations of crushing at a meso-scopic scale using the ply mean crushing stress of a material as an input parameter.

Concerning the humid ageing problems, the influences on the crushing performances of CFRP composite materials are not so obvious. The humid ageing specimens still demonstrated the same damage modes observed in the sane specimens besides the multiple tensile cracking in the 90° plies. As explained before, this might be due to the degradation in global strength of composite material as proven in the re-computation of ply mean crushing stress of the humid ageing specimens that there is a drop in the value of ply mean crushing stress which proved the composite material degradation.

Chapter III
PHYSICALLY-BASED DAMAGE MODELING

Based on the physical observation made on the damage mechanisms in experimental works (see chapter II), a physically-based damage modeling is developed and explained in this chapter with the objective to have predictive models able to represent the observed failures mechanism that take place at the ply-scale. Generally, the damage modeling explained in this study can be divided into two types namely modeling of fragmentation and modeling of delamination.

As can be seen in the previous chapter, the failure progress in composite structures subjected to crash load is very complicated compared to the conventional metallic materials. Thus, to physically represent each of these observed failures that occurred at the ply-scale, it is necessary to use different failure criteria. Most of the failure criteria used in the recent years are based on conventional failure criteria with varying degrees of success in simulating the crushing behaviors of composite structures. However, these conventional criteria have limitations in simulating the complex phenomena of damage mechanisms during crushing. For instance, there is no criterion for localized crushing reported in any conventional failure criteria. As such, the possibility to represent the competition between the two failure mechanisms in fragmentation mode (localized crushing and inside ply failure) normally cannot be achieved. Therefore, an improvement in damage models is necessary to predict better the failures mechanisms that occur in the fragmentation mode as highlighted in [BIS05].

In this study, a new concept of fragmentation modeling is introduced namely “free-face-crushing concept” with unconventional failure criteria in order to have better prediction on the fragmentation mode. A key benefit of this concept is that difference kind of failure mechanisms such as fiber breakage, matrix cracking, and localized crushing that occurs at the ply scale can be simulated at the same time to account for the competition between these

failures mechanisms. This is including a new damage law which specifically developed in this work to simulate the localized crushing mechanism.

Meanwhile for the modeling of splaying mode, a delamination damage modeling based on the classical law of traction-separation in ABAQUS software is used which implemented with the cohesive elements. Details on the constitutive laws and the modeling strategy will be explained in this chapter.

3.1 Fragmentation Criterion and Modeling

As explained in chapter II (see section *§2.2.2*), crushing plies that experienced fragmentation mode normally will have a competition between damaged under localized crushing and inside ply failures. The main damage mechanisms in localized crushing is micro-buckling of fibers and multiple shear cracking for 0° and 90° plies respectively that occur just near to the contact surface. This is the mechanisms that lead to the definition of the ply mean crushing stress. On the other hand, the damage mechanisms for inside ply failure is caused by the fiber breakage and matrix cracks due to a combination of compression, bending and shear that occur away from the plate extremity during progressive crushing. Due to these two different behaviors of fragmentation, the fragmentation criterion and modeling is separated into two sub-sections namely localized fragmentation and inside ply fragmentation to make possible to differentiate between these two modeling that will be explained further.

3.1.1 Localized Fragmentation

Physically, localized fragmentation involves a continuous crushing with small size debris evacuation as illustrated in Figure 3-1a. Therefore, the need to represent this continuous damage with finite element may cause a complexity. Furthermore, this behavior is very specific that it only occurs at the extremity, with a ply mean crushing stress. Thus, to overcome these two difficulties, a free-face-crushing concept is introduced in the model together with a new failure criterion specifically developed to rule the crushing behavior at the extremity based on ply mean crushing stress. This criterion is imposed for 3D element and plane strain modeling.

3.1.1.1 Free-face-crushing concept

In order to represent the localized crushing with small debris and a constant ply mean crushing stress, elements at the extremity of plies (i.e. having free face in the direction of

crushing) will have a different behavior than the others (see section §3.1.1.2). For elements behind, namely inside ply elements, classical failure criteria are applied (see section §3.1.2).

The operating principle is illustrated in Figure 3-1b. Initially, only the 3D element at the extremity of the ply is a free-face-crushing element (1). Once subjected to compression, it will be crushed (see next paragraph for the localized crushing law applied). Once totally damaged, it will be deleted, and the next element behind (2) will become a free-face-crushing element, and its behavior law will automatically change from inside ply to localized crushing criterion. Here, it is important to represent the total crushing before deleting the element to take into account the energy dissipated. Of course, the use of discrete elements with deletion to represent a continuous mechanism leads to limitations in the model that will be discussed further.

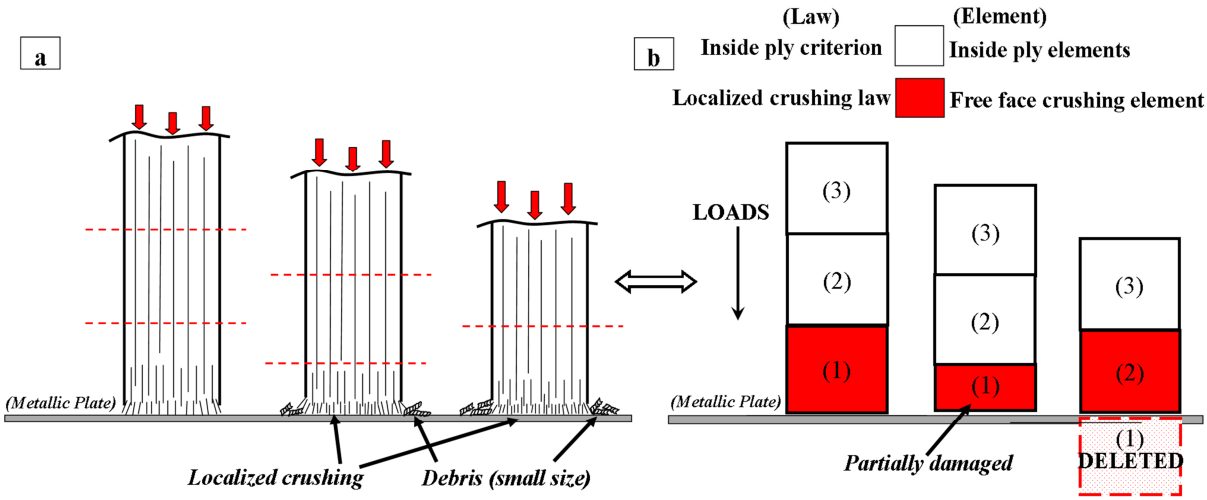

Figure 3-1: Illustration of (a) localized fragmentation in 0° plies (b) free-face-crushing concept

3.1.1.2 Localized Crushing Law

The implementation of this criterion in the model, especially in the free-face-crushing elements, is the main idea in this study. This criterion is based on the mean crushing stress that a ply can sustain, for each direction (0° and 90°) computed in the chapter II. The behavior (Figure 3-2a) is similar to an elasto-plastic stress-strain constitutive law but only for the free-face-crushing elements in compression. As mentioned before, the ply mean crushing stress of 0° plies (277 MPa) and 90° plies (270 MPa) used in this criterion are intrinsic parameters of the ply, independent from global parameters such as laminate lay-up, geometry, chamfering angle etc.

The same type of criterion is also used by Greve et al [GRE08] in their phenomenological modeling based on Energy Absorbing Contact formulation and the results

have shown good agreement with the experimental tests. However, their criterion depends on the global fragmentation stress of the laminate, obtained from a series of dynamic axial and oblique impact tests that makes it dependent on laminate material, lay-up and thickness. As a consequence, the global fragmentation stress needs to be identified for each test configuration, which increases test costs and time consuming. The same limitation is also found in other phenomenological crush modeling like the CZone ABAQUS crushing approach [NIX09]. Besides that, despite using the same type of criterion, the modeling principal in those studies is totally different with the free-face-crushing concept introduced in this work. For example, the Energy Absorbing Contact formulation is principally depending on the master-slave segments intersection and penetration [GRE08]. In addition, both phenomenological models mentioned here are suitable for larger scale composite structures, where the energy absorption and global failure of the structure is the only main motivation, and not the precise representation of damage occurring at sub-ply scale.

In the localized crushing law (Figure 3-2a), the local crushing ($|\varepsilon| > \varepsilon^0$) starts when the compression stress of the element in the crushing direction reaches the ply mean crushing stress. Once the crushing is initiated, the element is compressed at the constant ply mean crushing stress until it reaches ε^c. The use of discrete elements, with deletion at the end, to represent the continuous crushing behavior raises the problems of excessive distortion before deletion and peak force release at deletion. To solve these problems, after reaching ε^c, a linear decrease of the stress is applied in order to smooth the force release and in this study it will be called as MCS linear decrease. The maximum allowable compression strain (ε^f) needed to delete the element is set to 95%. The localized crushing law is implemented in both 0° and 90° plies according to their local axis and ply mean crushing stress (Figure 3-2b).

The pseudo-plastic strain is computed as the sum of the of pseudo-plastic strain increment during the loading. Therefore, the pseudo-plastic strain increment needs to be computed at each increment of time using the formulation below:

$$\Delta\varepsilon_n^{iP} = \Delta\varepsilon_n \quad if \quad \varepsilon^0 > \varepsilon_n \geq \varepsilon^c \qquad \text{(Eq. 3-1)}$$

$$\Delta\varepsilon_n^{iP} = \left(H - \frac{\sigma_{MCS}}{\varepsilon^c - \varepsilon^f} \right) \times \frac{\Delta\varepsilon_n}{H} \quad if \quad \varepsilon^c > \varepsilon_n \geq \varepsilon^f \qquad \text{(Eq. 3-2)}$$

Where ε_n, $\Delta\varepsilon_n$ and $\Delta\varepsilon_n^{iP}$ are the strain, strain increment and the plastic strain increment normal to the loading direction. H is the material stiffness in the loading direction (H_{ll} for 0° element and H_{tt} for 90° element).

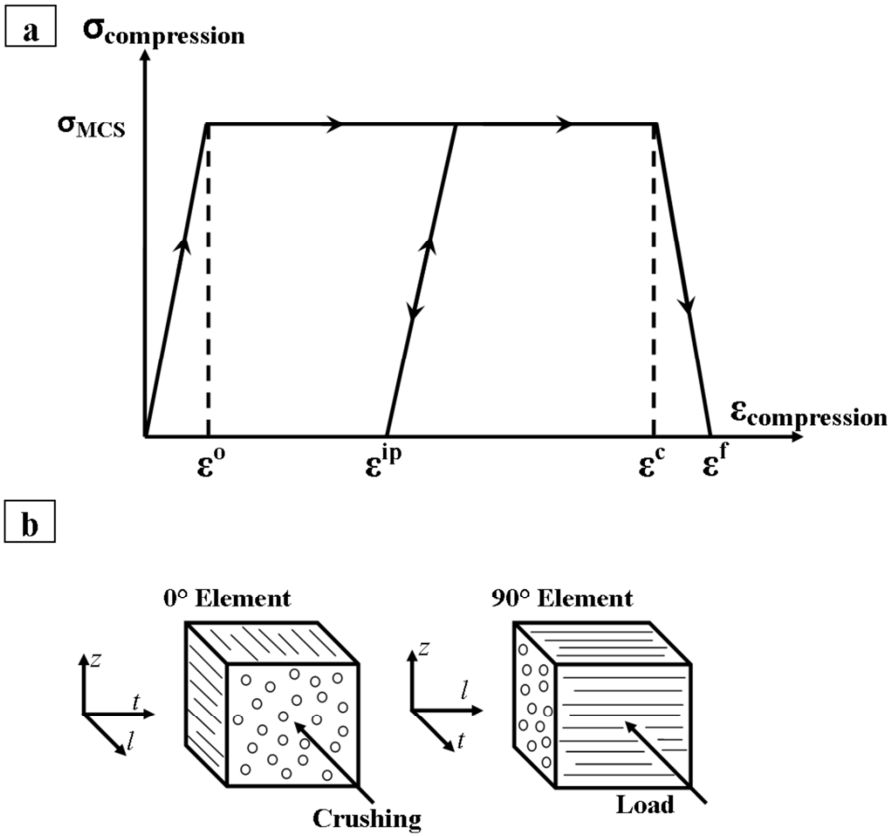

Figure 3-2: (a) Localized crushing law - (b) Local axis of 3D elements

For the 0° plies, the continuous localized crushing with small debris are continuously ejected from the crushing front as illustrated in Figure 3-1b. Therefore, the pseudo-plastic strain is only imposed in the loading direction for 0° plies. Contrary to the smallest debris from 0° plies, the debris wedge due to localized crushing in the 90° plies (Figure 2-12 in Chapter II) remains in the crushing front, and can initiate the delamination and splaying of adjacent 0° plies. Therefore, to represent this phenomenon, a pseudo-plastic deformation is imposed in the transverse direction (in laminate thickness or z-direction) of 90° plies, with a volume conservation rule to take into account the constant volume of the debris. However, even with a constant volume, the transverse expansion needs to be limited to avoid unrealistic expansion and premature delamination around the element. In practice, the expansion can be stopped after 15% to 45% compression without affecting significantly the results in terms of global crushing morphology. In this study, this transverse deformation is then stopped when the compression strain of the element in the loading direction reaches 40%, only to enable the initiation of an eventual splaying (fig. 6c).

The pseudo-plastic transverse deformation law can be expressed as:

$$\Delta\varepsilon_{zz}^{P} = -\Delta\varepsilon_{tt}^{P} \quad \textit{only true if} \quad \left|\varepsilon_{tt}^{P}\right| < \varepsilon_{40\%} \qquad \text{(Eq. 3-3)}$$

Where, ε_{tt}^{P} and $\Delta\varepsilon_{tt}^{P}$ are the pseudo-plastic strain and pseudo-plastic increment of 90° element in the loading direction, while $\Delta\varepsilon_{zz}^{P}$ is the pseudo-plastic increment of 90° element in the laminate thickness.

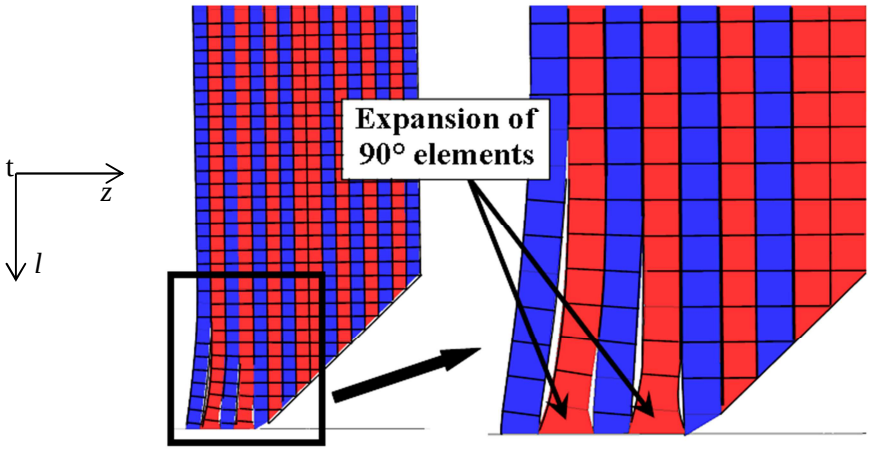

Figure 3-3: Example of 90° elements pseudo-plastic deformation in transverse z-direction during the crushing simulation

3.1.2 Inside Ply Fragmentation

The inside ply fragmentation criterion is implemented to simulate inside ply failures of plies during crushing on the inside ply elements (Figure 3-1). In this study, this criterion is used only to simulate the two main failure modes: fiber failure and matrix cracking. This is to say, for the moment it cannot represent all the ruptures seen in the experimental study, for instance, a shear-driven kink-band.

3.1.2.1 Fiber Failure

Experimental observations show that most fiber failures are due to a combination of bending and compression in the 0° plies, leading to the two different modes of fiber rupture in the same ply: compression and tension, as shown in Figure 2-10 (Chapter II). In addition, fiber breakages normally induce large energy release rates [PIN05]. Thus, it is essential to dissipate well this energy for the overall calculation of dissipated energy during the plate crushing (see Figure 4-8 in chapter IV). For that reason, a fiber failure model developed by Bouvet et al [BOU09, HON13] in the case of impact on laminates is used in this work. They introduced an approach to dissipate the fracture energy in an element defined as a function of the strain state at eight integration points. So, an energy release rate per unit area of crack can be obtained by dissipating energy throughout the volume of an element using the formulation

in Eq 3-4 based on crack band theory [BAZ83], with a characteristic element length. This approach enables to have a mesh-size independent model.

$$\int_V \left(\int_0^{\varepsilon^1} \sigma \, . \, d\varepsilon \right) . dV = S.G_I^f \qquad \text{(Eq. 3-4)}$$

Where σ (ε), ε^1, S, V are the stress (strain) in the fiber direction, failure strain in the fiber direction, element's cross section normal to the fiber direction and element's volume, respectively. G_I^f is the fracture toughness for opening mode (mode I). This equation works even if tension and compression states occur at the same time in one element in order to represent bending behavior in the element: compression at certain integration points, tension for the others. Thus, at each time increment, the choice of damage calculation depends upon the critical loads, either in tension or compression and the damage evolution is computed taking into account the energy dissipated in both states (G_{It}^f and G_{Ic}^f have different values).

Apart from that, the strain at the integration points is extrapolated at the nodes by using the shape function to account for the strain increment at the nodes due to element bending. The damage initiation is governed by maximum strain failure criterion. The element damage initiates when any one of the strain at the nodes exceed the damage initiation point. This condition can be written as:

$$\underset{node=1}{\overset{8}{Max}} (\varepsilon^{node}) > \varepsilon_t^0 \; \textit{if damage initiate in tension or} \qquad \text{(Eq. 3-5)}$$

$$\underset{node=1}{\overset{8}{Min}} (\varepsilon^{node}) < \varepsilon_c^0 \; \textit{if damage initiate in compression} \qquad \text{(Eq. 3-6)}$$

Where ε_t^0 or ε_c^0 is the strain in the fiber direction at the damage initiation point and the ε^{node} means the strain at the nodes. In addition, when this condition is met, all the eight integration points are established in the damage initiation state.

Afterwards, the element damage propagates using linear degradation of stress-softening (either in tension or compression states) that calculates according to the longitudinal strain as defined in Eq. 3-7:

$$damage = \frac{\varepsilon^1 . \left(\varepsilon^m - \varepsilon^0 \right)}{\varepsilon^m . \left(\varepsilon^1 - \varepsilon^0 \right)} \qquad \text{(Eq. 3-7)}$$

Where ε^1 is calculated using Eq. 3-4 and ε^m can be either the maximum strain if critical loads are in tension state or the minimum strain if critical loads are in compression state between the eight integration points which is calculated at each time increment. Thus, the calculated

damage will be common, and degraded for all eight integration points. Details of this criterion can be found in [BOU09, HON13].

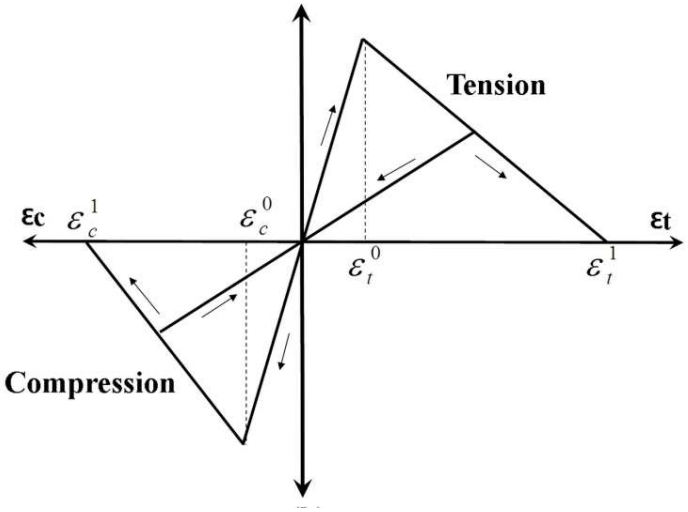

Figure 3-4: The fiber failure constitutive law

The stress tensor of orthotropic elasticity in terms of the elastic stiffness matrix (both for tension and compression) can be specified as

$$\begin{Bmatrix}\sigma_{ll}\\ \sigma_{tt}\\ \sigma_{zz}\\ \sigma_{lt}\\ \sigma_{lz}\\ \sigma_{tz}\end{Bmatrix} = \begin{bmatrix}(1-d)H_{11} & (1-d)H_{12} & (1-d)H_{13} & 0 & 0 & 0\\ & H_{22} & H_{23} & 0 & 0 & 0\\ & & H_{23} & 0 & 0 & 0\\ & & & (1-d)H_{44} & 0 & 0\\ & sym & & & (1-d)H_{55} & 0\\ & & & & & (1-d)H_{66}\end{bmatrix} \begin{Bmatrix}\varepsilon_{ll}\\ \varepsilon_{tt}\\ \varepsilon_{zz}\\ \varepsilon_{lt}\\ \varepsilon_{lz}\\ \varepsilon_{tz}\end{Bmatrix} \quad \text{(Eq.3-8)}$$

Where *[H]* is the stiffness matrix of lamina computed using the orthotropic elastic properties from Table 4-1 in Chapter IV and *d* is the damage variable.

3.1.2.2 Matrix Cracking

Matrix damage is essentially created by the transverse stress (σ_t) and the out-of-plane shear stress (τ_{tz}).Therefore, the following criterion is used to determinate the failure in 90° elements:

$$\left(\frac{\langle\sigma_{tt}\rangle^+}{Y^T}\right)^2 + \left(\frac{\tau_{tz}}{S_C}\right)^2 = 1 \quad \text{(Eq.3-9)}$$

Where $\langle\sigma_{tt}\rangle^+$, τ_{tz} are the positive transverse stress and the shear stress in (tz) plane, respectively. Moreover, $\langle\sigma_{tt}\rangle^+$ value is the maximum transverse stress among the eight nodes

of each element, extrapolated from the eight integration points. While τ_{tz} is the average value of eight integration points. This is done to account for the bending behavior in elements. Damage evolution is not considered in this criterion since it induces very low energy compared to fiber failure, and can thus be neglected [BOU12, HON13].

3.1.2.2 Element Deletion

In this inside ply failure modeling (fiber failure or matrix cracking), once an element is fully degraded, it is deleted. The deletion of inside ply elements is imposed for the creation of big fragments (debris) during the simulation because they can be accumulated in wedges that can influence the crushing front evolution. However, it will cause a loss of mass and debris in the numerical model. Considering the size of debris in experiments as compared to the size of an element, and the first simulation results, deletion of elements in these simulations seems acceptable.

3.2 Implementation of Fragmentation Modeling

As mentioned before, the fragmentation modeling is ruled via a free-face-crushing concept in order to make possible the competition between the localized crushing and the inside ply failures during a crushing test. For that reason, a communication system between neighboring elements of the same ply needs to be introduced in the model for the identification of element (free-face element or inside ply element). Furthermore, through this communication system, a particular element is able to determine the states of the element below it (existed or deleted), and accordingly it will activate or not the localized crushing law.

3.2.1 Description of Fortran Routine

The modeling of fragmentation discussed before is developed in a FORTRAN Vectorized User-Material (VUMAT) subroutine written for use with ABAQUS/Explicit finite element modeling software that provides the ability to integrate with this subroutine to simulate the damage behavior. Through this subroutine, it enables to create an external variable to update the status of the “free-face” element using the communication system explained above. Besides that, it makes possible to calculate the damage with the eight integration points together in the fiber failure criterion.

The routine scripts are written based on the ABAQUS manual [ABQ09]. In this study, 20 solution-dependent state variables (SDVs) are defined in developing this modeling. Generally, ABAQUS provides the strain increment for each integration point as an input to VUMAT. After that, using the given constitutive law in each case (localized crushing law or inside ply failure), VUMAT calculates the stress increment in each integration points and then compute the internal energy and dissipation energy. Before VUMAT send all these information to the ABAQUS Solver for update the simulation progress, it verifies the degradation status of element. If the element is fully degraded, VUMAT will delete it. Figure 3-5 below summarizes the VUMAT operation for the fragmentation modeling.

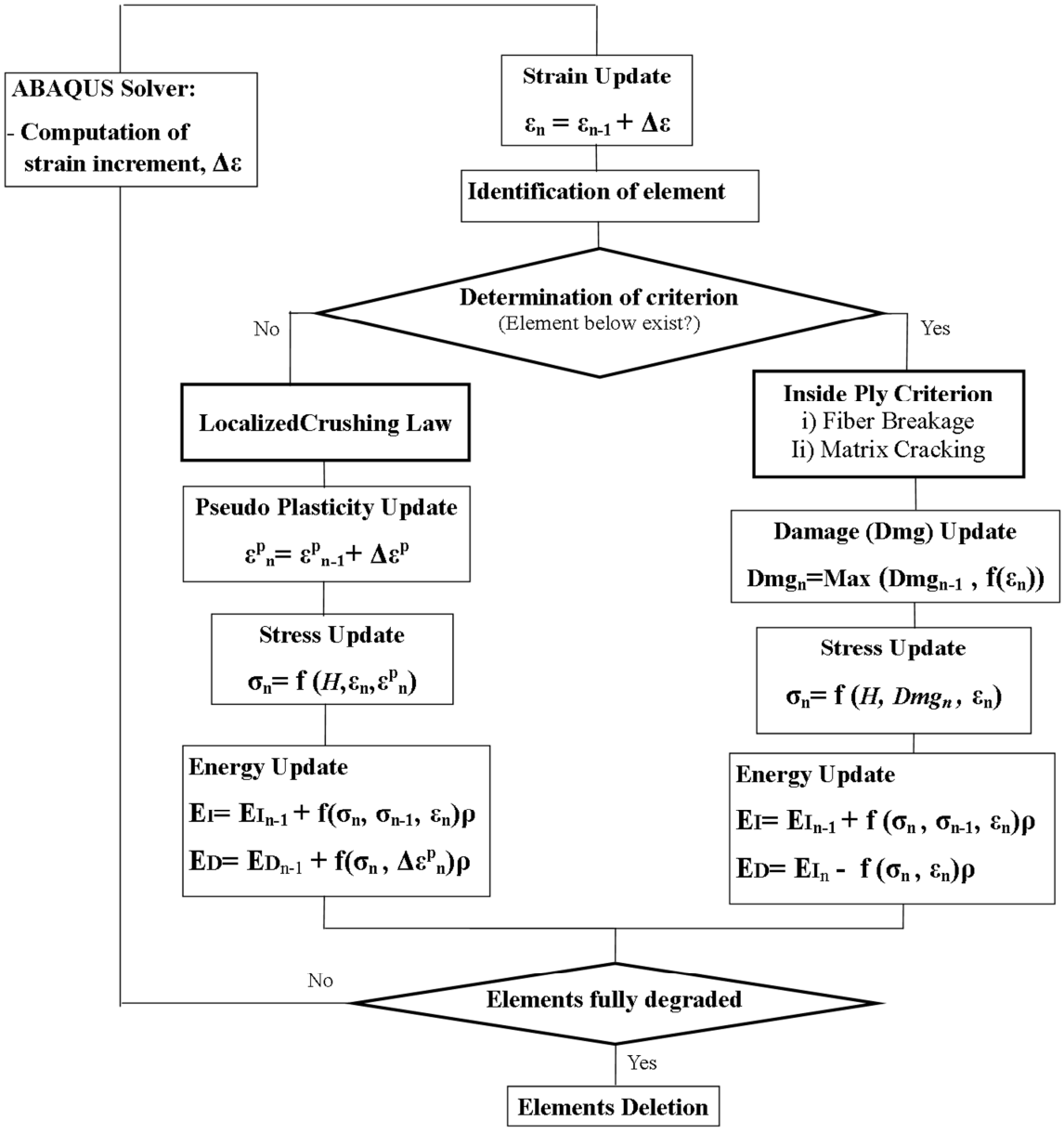

Figure 3-5: Diagram of VUMAT operation

3.2.2 Validation

Three different elementary simulations have been done to verify the fragmentation criterion and modeling. The first two simulations are concerning the verification of the implementation of free-face crushing concept and localized crushing law for crushing test of one and 10 elements respectively. The third simulation on the other hand is concerning the competition between the localized crushing and the bending mode during a crushing test. All the simulations are performed under displacement-controlled mode with different displacement rate according to the type of simulation. The type of element used in all simulations is the same, which is C3D8I, a 3D incompatible mode element with eight nodes full integration. This is the same type of element used in plate crushing simulation in Chapter IV. The incompatible modes element is used to improve the behavior in bending, even with only one element in the thickness [ABQ09]. In fact, both elements are stable to predict well the localized crushing but when come to the prediction of large splaying or bending behavior, C3D8I performed better than C3D8. The dimension of element is 0.25 mm edges in all these elementary simulations. The material input properties used for the failure criteria are based from material UD T700/M21 as listed in the Table 3-1.

Table 3-1: Material properties of T700/21

Parameters	Symbol	Values
Elastic data		
Density (kg/m^3)	ρ	1500
Longitudinal modulus:		
Tensile (GPa)	E_{lt}	130
Compressive (GPa)	E_{lc}	100
Transverse modulus (GPa)	E_t	9
Shear modulus (GPa)	G_{lt}	5
Poisson's ratio	ν_{lt}	0.33
Material Strength		
Transverse tensile strength (MPa)	Y^T	75
In plane shear strength (MPa)	S_C	110
Fiber Failure (Mode I)		
Tensile strain at damage initiation	ε_t^o	0.016
Compression strain at damage initiation	ε_c^o	-0.012
fracture toughness in tension (N/mm)	G_{It}^f	133*
fracture toughness in compression (N/mm)	G_{Ic}^f	40**
Interface fracture toughness		
Mode I (N/mm)	G_I	0.6
Mode II / Mode III (N/mm)	G_{II}/G_{III}	2.1
*Note: *Material T300/913 ([16])*		
*** Predicted value in this work*		

3.2.2.1 Localized Crushing Law Validation

- **One element crushing test**

Crushing test of one element of 0° and 90° plies is carried out to validate the behavior of plies when having localized crushing. The nodes at the top of the element are imposed with displacement at constant rate of 0.25m/s to perform crushing with a fixed metallic base. The initial gap between the element and the metallic base is 0.01mm. The crushing is performed until the element is totally crushed and deleted.

Figure 3-6 and Figure 3-7a show that both 0° and 90° elements have managed to deliver the theoretical stress flow as shown in Figure 3-2a. Both elements are compressed constantly at ply mean crushing stress, 277 MPa and 270 MPa for the 0° and 90° element respectively as soon as the elements get into crushing state ($\varepsilon > \varepsilon^{o}$) as displayed in Figure 3-6 and Figure 3-7a. These stresses are degraded linearly after the elements are compressed 90% (ε^{c}) (see Figure 3-6-a-iii) and they have been deleted immediately after reaching 95% (ε^{f}) of compression strain without having any excessive distortion and penetration problems.

For the 90° element, the transverse deformation in the laminate thickness (z-direction) is also verified as displayed in Figure 3-6b and Figure 3-7b. Figure 3-7b shows that, in zone I the element is in the elastic region and once the crushing is initiated (zone II), the element is being compressed in the loading direction together with transverse deformation in laminate thickness. This transverse deformation is stopped when the compression strains in loading direction reaches 40% and remains constant until the element reaches the maximum compression strain (95%) and deleted (Figure 3-6b-iii).

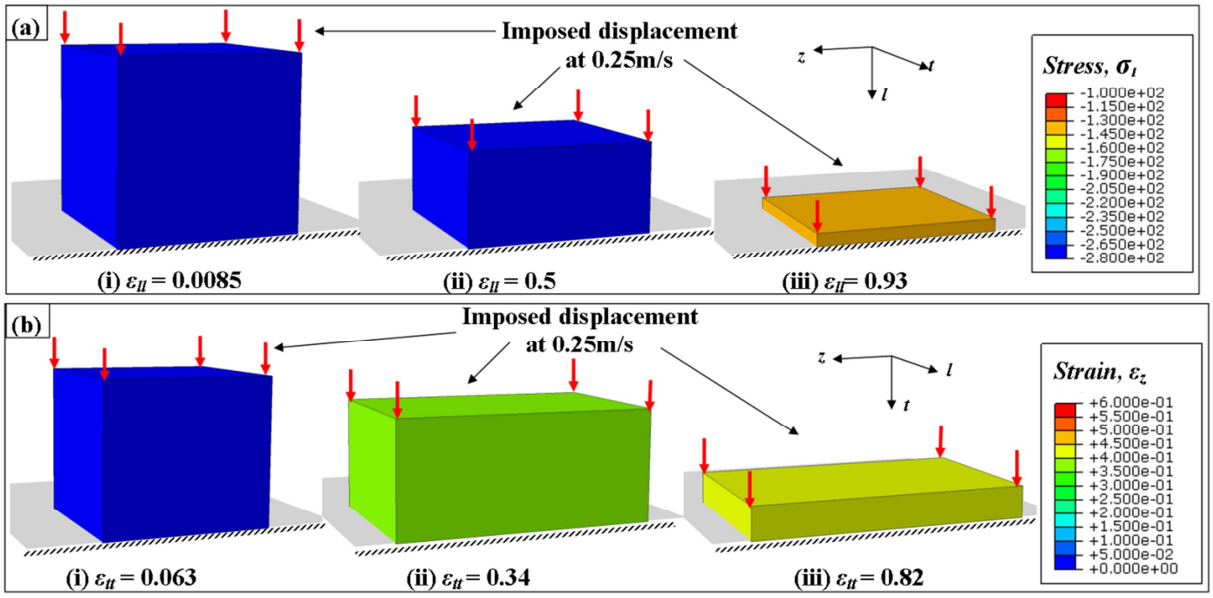

Figure 3-6: Crushing sequence (a) 0° element (b) 90° element

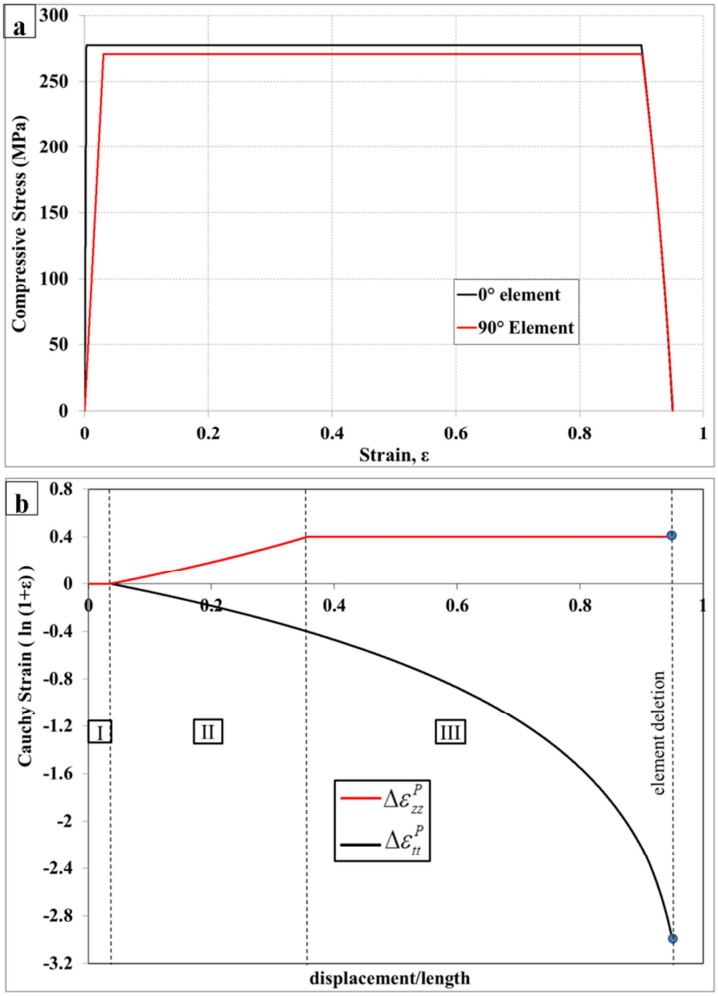

Figure 3-7: (a) Stress-strain profile in localized crushing (b) Plastic deformation in 90° element

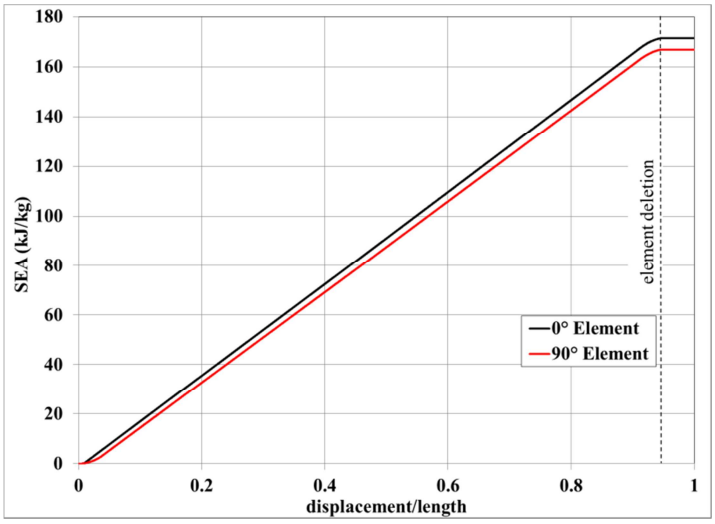

Figure 3-8: The results of SEA in modeling of pure crushing

In term of SEA, Figure 3-8 shows that 0° element is able to deliver 171kJ/kg and 167kJ/kg for 90° element. These prediction SEA values are close to the maximum SEA

values calculated in section *§2.3.3* for plies having steady localized crushing. The main difference between the prediction and maximum SEA values is only due to the fact that the element is constantly compressed at a ply mean crushing stress just up to 90% of total strain before the stress is reduced linearly and deleted at 95% of total strain.

- **10 elements crushing test**

The second elementary simulation is a crushing test of single beam of 10 elements (short length) as a representation of a ply as shown in Figure 3-9. Similarly, in this study the nodes at the top of the beam are imposed with displacement at constant rate of 2 m/s. The metallic base is fixed and the initial gap with the first element is 0.01mm.

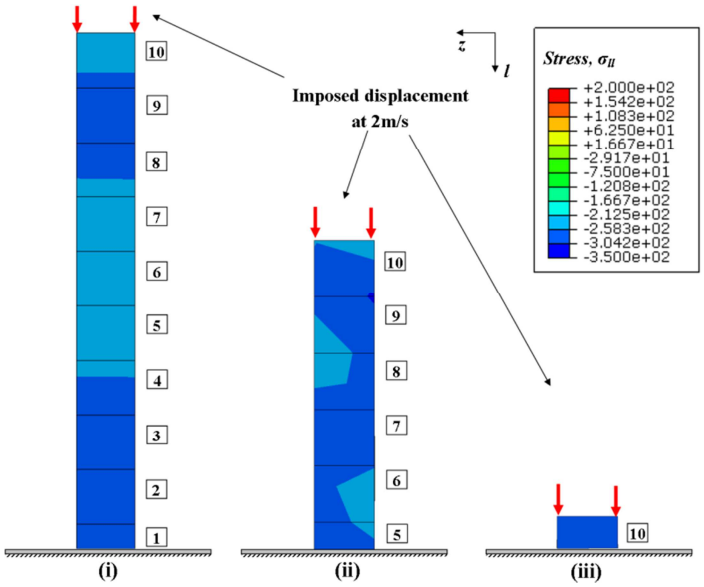

Figure 3-9: The example of deformation morphology in10 elements of 0° ply during crushing tests

In theory, the deletion of front element (using localized crushing law) at 95% compression will create small gap to the next element to come into contact with the metallic base. As mentioned before, this will cause a sudden peak force release as well as the stress (see Figure 3-10a) that will induce waves that could cause damages to the inside ply elements that should not occur and sometimes if the tensile load from this wave is high enough, it can cause the deletion to the inside ply elements especially in 90° element. This condition is unrealistic and can lead to problems in criterion determination.

Therefore, as mentioned before, the idea to implement MCS linear decrease just before the element deletion in the localized crushing law is one of the solutions to reduce this effect. In order to verify the effectiveness of this idea, two simulations have been made with and without implementation of this MCS linear decrease as for comparison and the results are

presented in Figure 3-10. As can be seen in Figure 3-10b, the stress release after the element deletion is reduced when localized law is implemented with the MCS linear decrease just before the deletion. Besides that, this idea also helps to prevent the penetration problem between the elements and the metallic base as shown in Figure 3-10a. The high peak of force and crushing stress are recorded just before the first element is deleted due to the penetration between the free-face element and the metallic base even though the element deletion is set at compression strain 95%. Therefore, when element no. 2 come into contact with the metallic base using inside ply criterion (since the free-face element (still existed), it causes the drastic increase of stress in the remaining elements that will cause drastic increase in total force as well. Nevertheless, this is not the case for the simulation with the implementation of the MCS linear decrease as demonstrated in Figure 3-10b. Hence, this study has proved that the idea to decrease linearly the crushing stress just before the deletion in the localized crushing law is necessary to reduce the induced waves and to prevent the penetration problem. Moreover, for the inside ply element of 90° plies, the transverse stress is filtered before the calculation of the criteria to avoid the remaining tension wave problems.

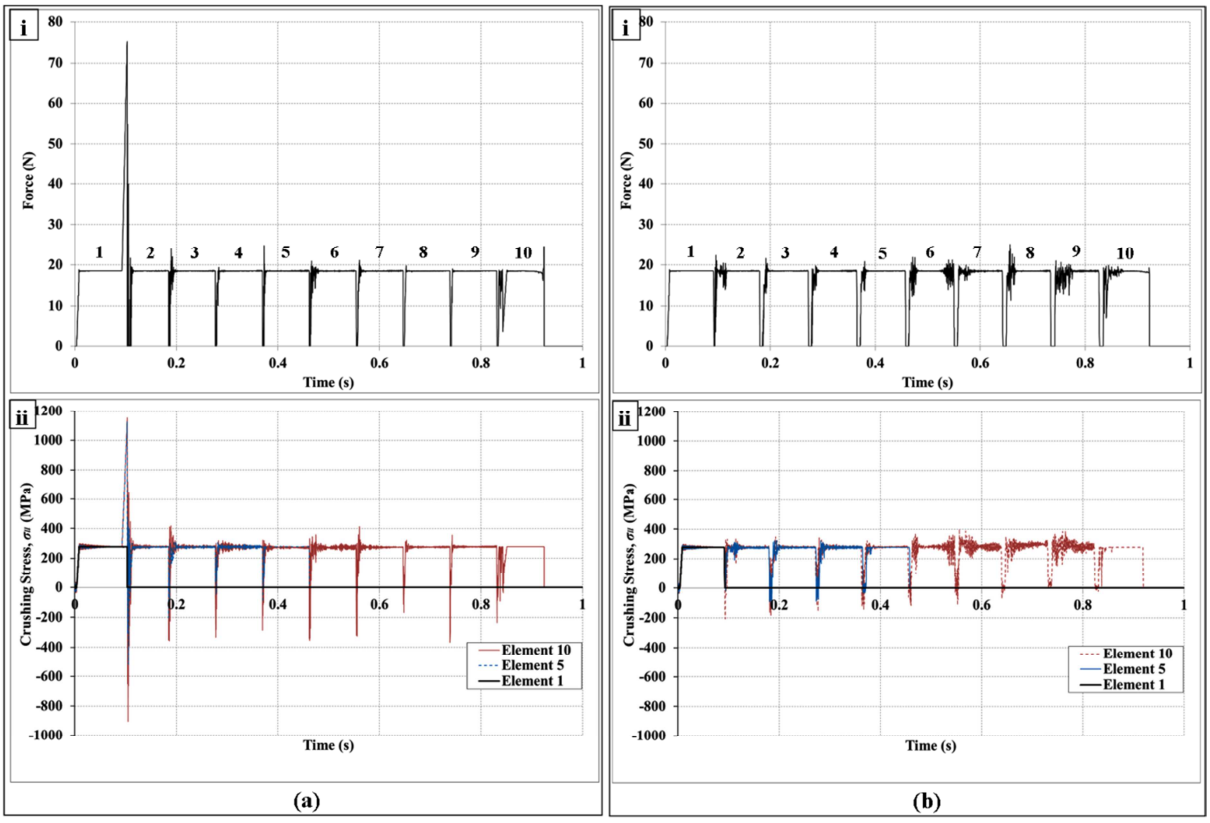

Figure 3-10: The comparison of contact force and crushing stress of 10 elements of 0° ply during crushing tests (a) Without implementation of MCS linear decrease (b) with implementation of MCS linear decrease

Besides that, Figure 3-9 and Figure 3-10b has shown that all the 10 elements are deleted due to localized crushing at the same level of stress (ply mean crushing stress). This demonstrates the effectiveness of free-face crushing concept to simulate a continuous localized crushing as illustrated in Figure 3-1.

3.2.2.2 Competition between Localized Crushing and Bending

In this simulation, a single composite beam of 20 elements (longer length) has been subjected to crash load under displacement controlled mode at constant rate of 2 m/s in loading direction. The displacement is imposed on the nodes at top of the beam. In addition, a small transverse displacement (0.025 mm) is imposed in the middle of the beam along z-direction at the beginning of the simulation, just to initiate a bending mode during the crushing process (see Figure 3-11-i). Similarly, the gap between the fixed metallic base and the first element is 0.01 mm. The objective of this study is to verify if this modeling able to simulate the competition between the localized crushing and inside ply failure when plies have a combination of compression and bending at the same time during the crushing test. Figure 3-11 show an example of this test on pure 0° composite beam.

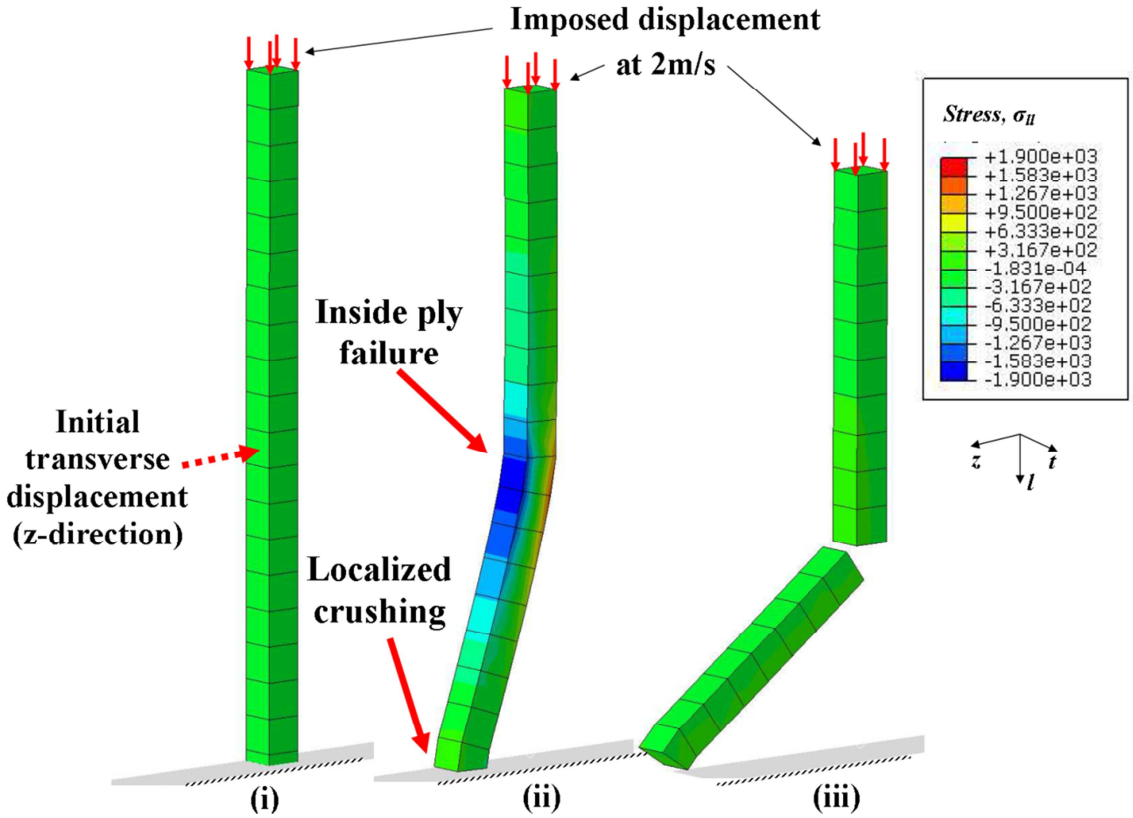

Figure 3-11: The competition between localized crushing and fiber breakage during simulation of crushing test

Since the beginning in Figure 3-11, the beam has been crushed on the metallic base with the element at the extremity endures localized crushing according to localized crushing law and at the same time elements at the middle of the beam starts to experience bending mode (Figure 3-11-i). As the crushing is continues, the bending at the middle of the beam is also getting greater as displayed in Figure 3-11-ii. Finally, the element that have been imposed with transverse displacement in the middle of the beam is deleted according to the inside ply failure criterion (fiber breakage) because it cannot sustain anymore the bending load which continues to increase as the compression loads are constantly applied to the beam to perform the crushing with the metallic base (Figure 3-11-iii).

The estimation of the energy dissipated due to the fracture of inside ply element under combination of bending and compression is compared to the energy dissipated by full crushing of an element as presented in Figure 3-12 in order to have a first idea of the importance of inside ply energy associated to localized crushing energy. Zone I in the Figure 3-12 is the energy dissipated mainly due to localized crushing (see Figure 3-12-i) while the zone II is energy dissipated from a combination of bending (75%) and localized crushing (25%) at the same time (see Figure 3-11-ii). In zone III, the energy is dissipated mainly from the bending failure during the breakage. During this moment, element at the end of the beam did not perform any localized crushing but only sliding on metallic base. No energy has been dissipated in crushing element since no friction is applied in this simulation. The amount of energy absorbed remain the same after the breakage as there is no more crushing and additional loads applied on this composite beam.

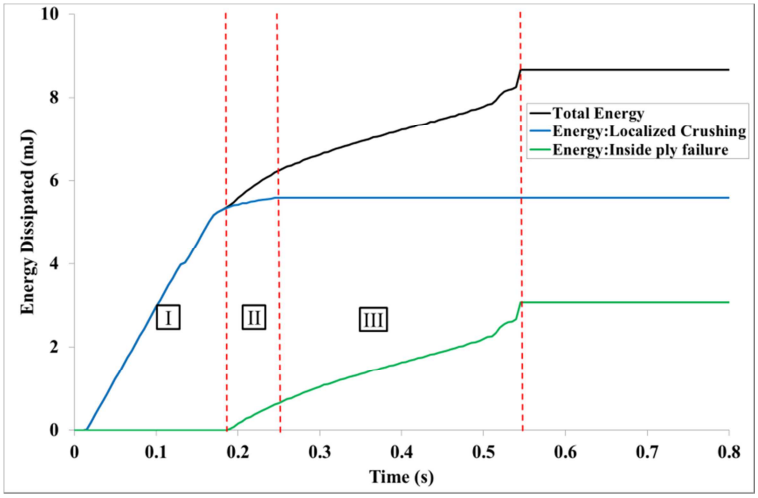

Figure 3-12: Dissipated energy repartition between localized crushing and inside ply failure during crushing tests of a single row of composite beam

3.3 Modeling of Delamination

The adaptation of delamination modeling in this study is essential to represent the mixed-mode crushing especially in representing the laminate splaying during initiation and progressive crushing. Therefore, the traction-separation damage model in Abaqus software is used to govern the initiation and propagation of delamination between the plies. This kind of modeling with cohesive elements is quite usual to be used in numerical simulations of composite structure [PAL10A, SOK11, BOU12,].

As observed in experimental test, the delamination can be occurred either in pure opening, pure shear or mixed modes. Thus, to adequately represent the delamination prediction, the mixed-mode delamination model [ABQ09] as shown in Figure 3-12 will be used in this study that based on procedures presented by Camanho et al [CAM03].

The damage initiation of delamination failure is predicted by using the quadratic nominal stress criterion (Quads Damage) response as presented in Eq. 3-10.

$$\left\{\frac{\langle\sigma_n\rangle}{\sigma_n^o}\right\}^2+\left\{\frac{\sigma_s}{\sigma_s^o}\right\}^2+\left\{\frac{\sigma_t}{\sigma_t^o}\right\}^2=1 \qquad \text{(Eq.3-10)}$$

Where $\sigma_n^o, \sigma_s^o, \sigma_t^o$ are maximum stresses in the normal to the interface, the first and the second shear directions respectively. The Macaulay brackets ($\langle\ \rangle$) indicate that the stress state is not valid for pure compression. Damage initiates when quadratic interaction of nominal stress ratios reaches a value of one. By applying this criterion, the initiation of delamination could occur either in pure opening (normal to the thickness direction), pure shearing mode or mixed modes.

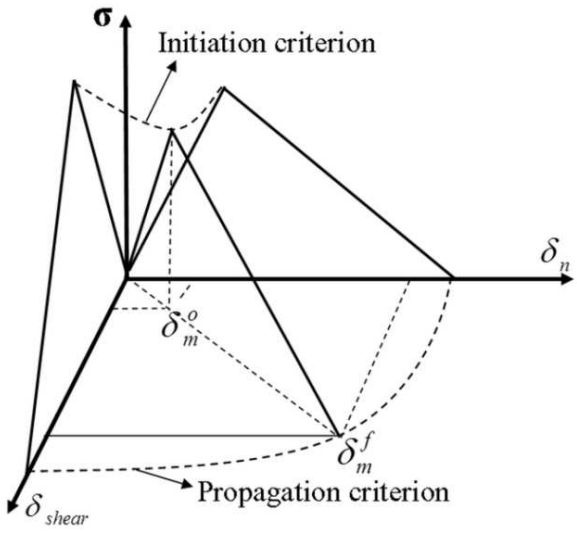

Figure 3-13: Constitutive law for cohesive elements in mixed mode [CAM03]

The evolution of the damage is defined by the dissipated energy due to failure. This is ruled by linear softening response with the power law criterion in order to take into account the mixed-mode behavior. Besides that, power law criterion often known to provide a conservative simulation of delamination in epoxy matrix composites [CAM03]. This criterion is established in term of an interaction between the energy release rates. The linear decrease is calculated and so, the dissipated energy is equal to the energy release rate at interface in each mode.

$$\frac{G_I}{G_{IC}} + \frac{G_{II}}{G_{IIC}} + \frac{G_{III}}{G_{IIIC}} = 1 \qquad \text{(Eq. 3-11)}$$

where G_I, G_{II}, and G_{III} are the energy release rate of delamination in mode I, II and III respectively. While G_{Ic}, G_{IIc}, G_{IIIc} represent the critical energy release rate of delamination in mode I, II and III, respectively.

3.4 Conclusion

The main idea of this work is the introduction of a free-face-crushing concept in the model. This concept allows the use of two main failure criteria at the same time to represent the phenomenology of localized crushing apart from classical inside ply failures in the fragmentation mode. The implementation of the free-face-crushing concept in ABAQUS with the localized crushing law coming from ply mean crushing stress experimental observation is proven to be efficient for elementary element or row of elements. The competition between the two fragmentation failure modes is also possible to perform. The modeling of splaying mode on the other hand is adapted from the existing delamination model provided in ABAQUS software. However, the initiation of splaying still depends on the “pseudo-plastic” deformation in 90° elements under localized crushing law. The physically-based damage modeling presented in this chapter will be used in the chapter IV to simulate the crushing test of composite plates under low velocity.

Chapter IV

NUMERICAL MODELING: APPLICATION TO PLATE CRUSHING

Numerical modeling of composite plates subjected to low velocity crushing loads is carried out and discussed in this chapter. Two types of numerical modeling are developed in this study. The first one is a numerical modeling of the medium-scale quasi-static crushing tests (FEM static) while the second type is a numerical modeling of plate crushing under dynamic loading with different initial speeds 2 m/s, 5 m/s and 9 m/s (FEM dynamic). Both models are based on the same laminate staking sequence $[(0°/90°)_4]_{sym}$.

Both numerical models are simulated using a non-linear analysis via explicit code and the simulation is based on the physically-based damage modeling explained in the previous chapter. The parameters required in the numerical simulations are elementary material characteristics, identified at the ply scale (see Table 3-1 in section *§ 3.2.2*).

The goal of this study is to develop a numerical modeling of composite plates crushing that is able to represent the crushing morphologies with all main damage mechanisms, force-displacement curves and re-compute the energy absorption as experimentally observed. Besides that, the numerical modeling of these crushing tests could improve the understanding of the phenomena, in the sense that to quantify the importance of each mechanism of energy dissipation and to simply study the influence of material and experimental parameters on the crushing response.

Generally, this chapter is divided into five main sections. The first one is the description of the developed finite element models including the choice of scale, element types, contact formulation etc. The second part focuses on the modeling validation with the experimental results on the crushing morphology, force-displacement curve and total energy absorbed. After that, more detail concerning the competing energy absorbing mechanisms during crushing test are explained in the third section. The fourth and fifth sections concern the study of influence of material and experimental parameter under humid ageing conditions

and the effects of friction coefficient in plate crushing respectively via numerical modeling. Details on the results of these simulations will be explained in this chapter.

4.1 Finite Element Model

4.1.1 Model Description

Finite element models of the previously described tests; medium scale static crushing test and dynamic plate crushing test have been developed in ABAQUS Explicit. Taking into account the experimental observations, the choice of the model scale is essential for accurate representation of the mechanisms involved in the development and the propagation of a crushing front in laminates. Because global mechanisms (fragmentations, splaying, fiber ruptures, debris accumulation etc.) occur at the ply scale, it will be considered as the scale for the model (meso-scale). Therefore, the finite element models are developed based on ply-by-ply basis in which each ply of the laminate is meshed with one 3D element (C3D8I, full 8 points integration) in the thickness. To reduce the calculation time, only 80 mm length of the plate is modeled for plate tests, which is considered long enough to represent the sliding inside the vertical guides. The rigid vertical guides and the metallic base are modeled using analytical rigid bodies. For the medium-scale crushing tests, only 5 mm of the clamped part of the specimen is represented by using the mathematical constraint (Figure 4-1).

Only one element of 0.25 mm width is used to represent the whole width of the plate and plane strain conditions are assumed, making the solution effectively 2D. This is consistent with the experimental observations that show little variation across the width. The dimension of each element is 0.26 mm in the ply thickness and 0.25 mm in the other two directions.

To be able to predict delamination growth and splaying mode as observed during experiments, 8 nodes 3D cohesive elements (COH3D8) with zero thickness are used to model 0°/90° plies interfaces. The first interface element of each interface (i.e. at the specimen extremity) is removed to initiate delamination.

For each model, boundary conditions and loadings are imposed to match the experimental test as illustrated in the Figure 4-1. The constant displacement rate in medium-scale static test modeling is artificially increased from 6 mm/min (experimental test) to 2 m/s to reduce the calculation time in the explicit simulations. This increase in speed shall not affect the results of simulation, according to the results of the study of Duong et al [DUO10]. Using the same specimens, they found no visible influence of crushing speeds (from 20 mm/min to 9 m/s) on the energy absorption and force-displacement curve. For the dynamic

plate crushing modeling, an additional mass is added on the top nodes of the plate to represent the falling weight according to the same mass imposed in the experimental test which is 207 kg for the simulation with initial speed 2 m/s and 5 m/s, and 36 kg for 9 m/s.

Based on current simulation results, calculation times are approximately 3.75 hours for a simulation of medium-scale static test and 6.5 hours for the simulation of plate crushing for the case when initial speed is 9 m/s, on 8 CPUs with parallel loops.

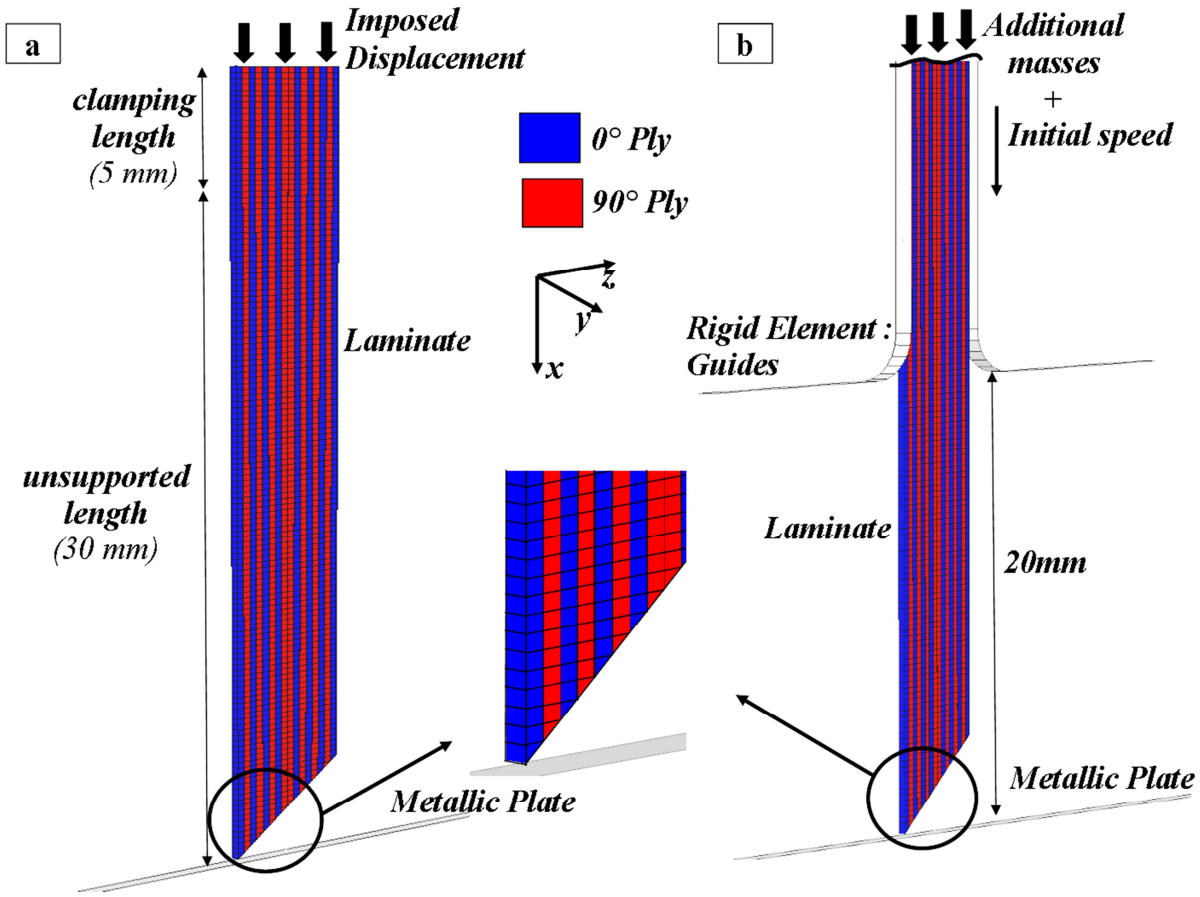

Figure 4-1: Model lay-up: (a) Medium-scale static (FEM static) (b) Plate crushing (FEM dynamic)

4.1.2 Contact Formulation

Friction plays an important role during crushing, especially friction between the crushing surface and the metallic base (during splaying), and as friction relates to debris accumulation and debris wedge formation. The available general contact formulation with classical friction model based on Coulomb approximation is used to simulate the contact behavior between all exterior surfaces [ABQ09]. Since the friction coefficient has a great influence on the crushing process [PIN04], it is necessary to have a good estimation of it.

The friction coefficient value is identified from a series of elementary simulation tests (both static and dynamic models) that focus on the friction behavior of the external splaying plies in order to have an approximation of friction coefficient between the ply and the metallic base. Simulations are done with different friction coefficients from 0.05 up to 0.3. Then, for a given crushing displacement during the crushing initiation, the radius curvature and horizontal displacement of external splaying plies are compared with experimental results, as presented in Figure 4-2. Evidently, the simulation with friction coefficient μ=0.15 shows better agreement with the reference case. Based on this approximation, the friction coefficient μ=0.15 is assumed for all exterior surface interaction contacts i.e. ply and ply, ply and metallic base, and ply and the debris (**Contact Inclusions, ALL EXTERIOR*) even though it is not true for all cases. Based on current simulation works, friction coefficient μ=0.15 is set in both medium-scale static and dynamic plate crushing models (**Surface Interaction, Friction =0.15*). In this work, static and kinetic coefficients of friction are assumed to be the same.

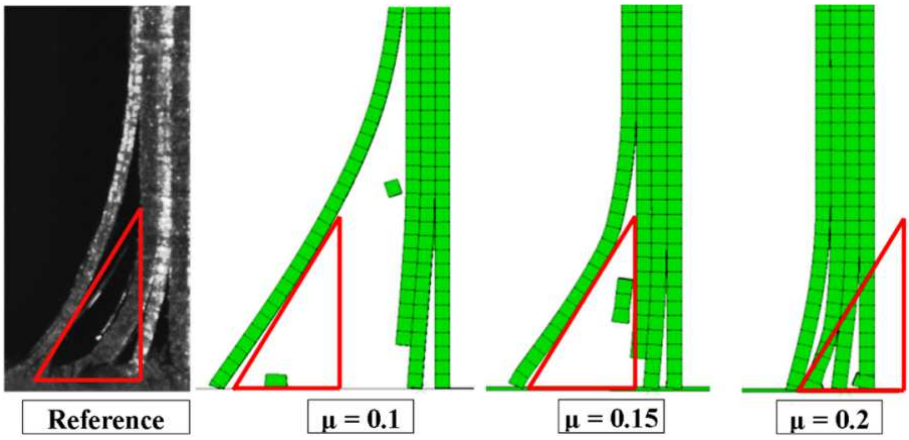

Figure 4-2: Simulation for friction coefficient identification

4.2 Modeling Validation

4.2.1 Comparison of Crushing Morphologies

Four simulations of $([0°/90°]_4)_{sym}$ laminated plate are performed under crushing with different loadings and boundary conditions (one FEM static of medium-scale static test, three FEM dynamics of plate crushing test with different crushing speeds 2 m/s, 5m/s and 9m/s). For each configuration, the experimental tests are carried out twice and the availability of the experimental results has given the opportunity to validate the simulations results.

Figure 4-3 presents the crushing morphologies of both medium-scale static and plate crushing (for the case v_0=9 m/s) models, compared with the experimental tests. Globally, the numerical models in both tests are able to represent the mixed crushing mode including the

important characteristic features of the crushing mechanisms of composite such as the splaying, localized crushing at plate extremity, inside ply failures due to bending, shear and their coupling, debris creations and the propagation of the multiple delaminations.

The development of a specific wedge resulting from localized crushing of 90° elements in the numerical model is effective in initiating the delamination of 0°/90° interfaces and then drives the adjacent 0° plies to an eventual splaying. A stable progressive crushing due to localized crushing in central plies can be observed in both cases, like in experiments morphologies (Figure 4-3a- iv and Figure 4-3b image iii-v).

Concerning the debris due to inside ply failure in 0° and 90° plies (fragments from localized crushing cannot be represented, according to the localized fragmentation modeling in *§ 3.1.1*), the debris sizes obtained from model are relatively close to the ones measured in experimental tests (refer to chapter II, *§ 2.2.2.1*). For the simulation of medium-scale static test, debris sizes are between 0.5 mm and 2.0 mm for most of the time which are close to the experimental results (0.5 mm–2.5 mm), as illustrated in Figure 4-3a. Nevertheless, one can notice that there is a big debris of 90° plies (7.0 mm in length) resulting from the breakage of two 90° plies at the middle of the laminate as shown in Figure 4-3a-iii. This big debris is unrealistic compared to the experimental result and the breakage of this plies is due to the over-prediction of the numerical model. In the plate crushing tests, the debris size is in the range of 0.5 mm to 5 mm for the experiments and 0.5 mm to 4.0 mm for the numerical model. This validates the choice made for the representation of fragments by the means of inside ply elements deletion.

While all major damages are well represented, during the transition phase from initiation to the progressive crushing, the numerical models show minor differences in terms of crushing morphology correlations. For example, in Figure 4-3a-ii and -iii, the model simulates well the multiple delaminations on the right side as in the experimental test but the delamination length is slightly under-predicted in the numerical model. Consequently, both models have differences in the number of plies involved in splaying or localized crushing, compared to experiments during the steady state of crushing (see Figure 4-3-iv and -v). Nonetheless, this does not affect much the result of force-displacement curve in numerical model. Crushing of composite plates involves significant displacements, rotations and geometric transformations that lead to large dispersion in global morphology of crushing processes, as verified experimentally. For example, the number of plies in fragmentation mode can vary significantly although tests are performed under the same condition [DUO10]

(see the comparison between Exp 1 and Exp 2 in Figure 4-3 for both medium-scale and plate crushing test).

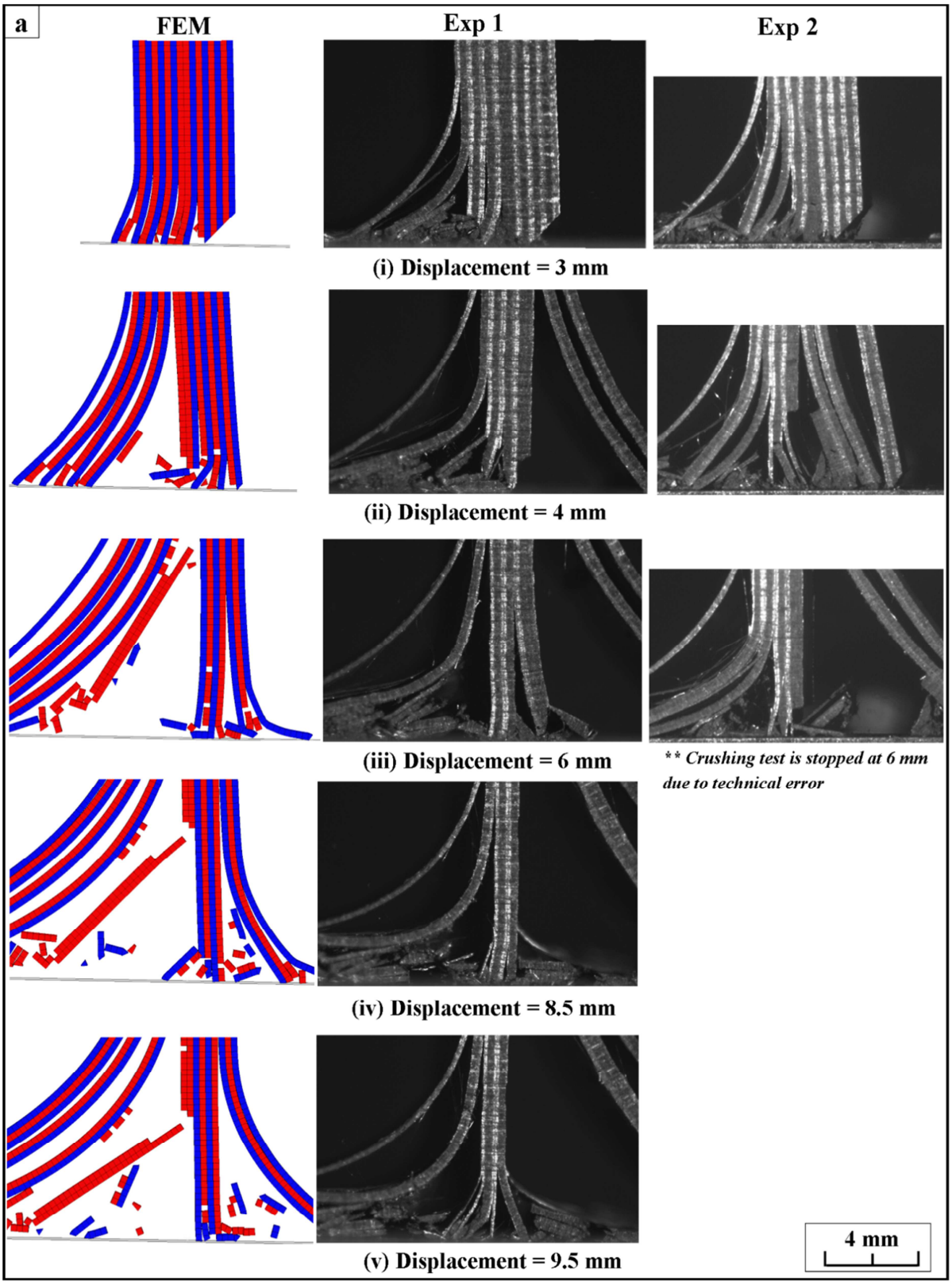

Figure 4-3: (a) Example of mixed-mode crushing morphologies comparison between simulation and experiment for medium-scale static test

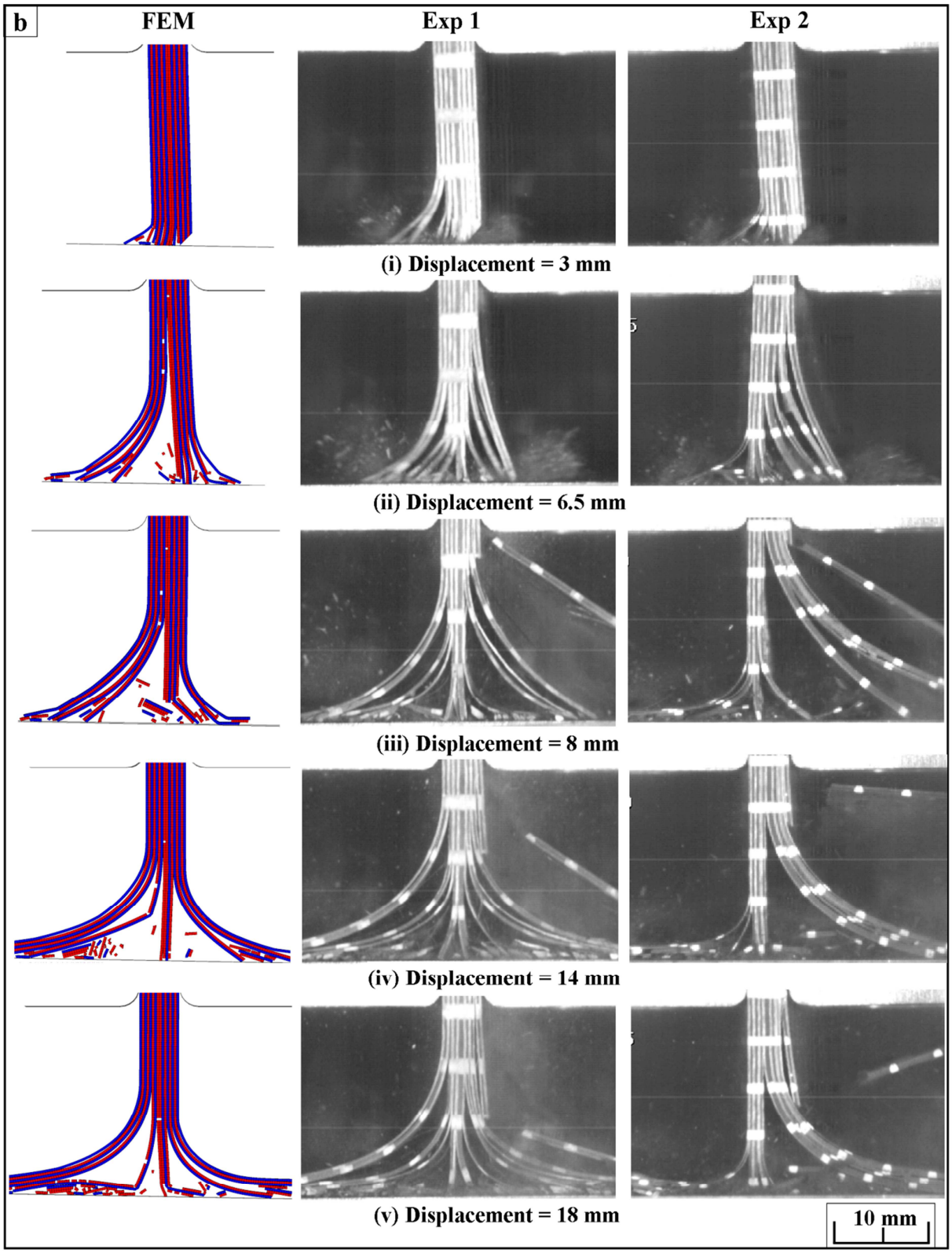

Figure 4-3: (b) Example of mixed-mode crushing morphologies comparison between simulation and experiment for plate crushing test (Vo= 9m/s)

4.2.2 Comparison of Crushing Forces

Force-displacement curves from the models and experimental tests are displayed in Figure 4-4 for comparison. The curves from experiments and numerical models comparatively are close to each other which mean that the main phenomena are well represented by the model i.e. the curves initiation and the maximum forces obtained for both static and dynamic models are close with experimental forces as a result of the implementation of specific laws in the models. After that, all curves show a transition to a steady crush load (plateau after peak force) as in experimental tests.

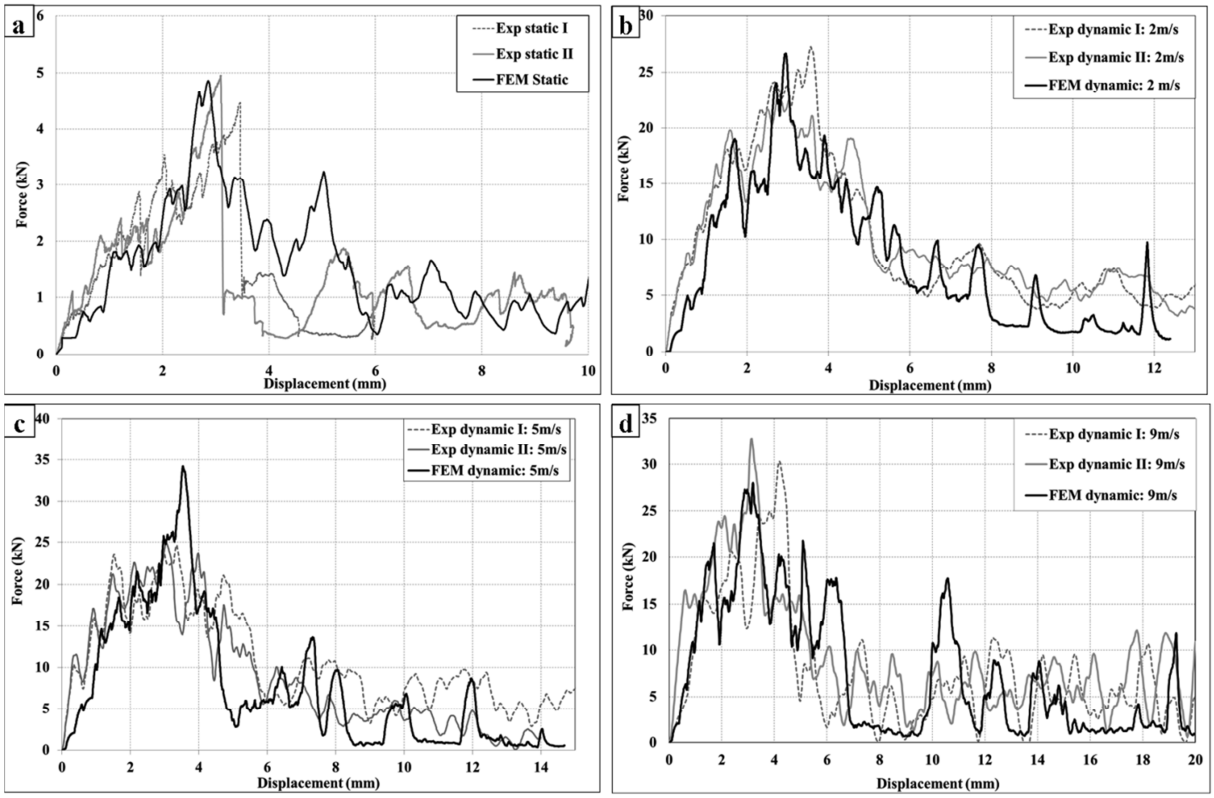

Figure 4-4: The comparison between the experimental and numerically predicted force-displacement curves for (a) medium scale static test (FEM static) (b-d) plate crushing (FEM dynamic) with initial speed (b) 2 m/s (c) 5 m/s (d) 9 m/s

The differences observed in the force curves between 3 mm and 5 mm of displacement in the medium-scale static model compared to the experimental tests is a result of under-prediction of the delamination length (Figure 4-3a-ii) by the numerical model as discussed before. Similarly, the plate crushing models slightly under-predicts the steady state crushing load as the number of plies involved in fragmentation mode is less compared to the number of plies in experimental tests. Furthermore, to reduce calculation time, the numerical model for dynamic plate crushing tests is solved for only the first 12 mm, 15 mm and 20 mm crushing length for the plate crushing simulation with initial speed 2 m/s, 5 m/s, and 9 m/s respectively.

This length is considered enough to represent both initiation step and steady progressive crushing (plateau).

Besides that, there is a slight difference of initial slope in the force-displacement curves between the experiment and numerical test of dynamic plate crushing. This may be due to the dynamic response of the force sensor during the experimental tests. Another reason can also be the influence of crushing speed on the value of mean crushing stress of a ply calculated in section *§2.3* which can be considered as the perspective of the study that will be discussed in details. Moreover, in this study both experiment results and the simulations results are filtered using a digital low-pass filter at the frequency of 1000Hz and 4000Hz respectively. The numerical results are filtered to remove the numerical noise of explicit analysis crushing simulation.

4.2.2.1 Details of Dynamic Crushing Force

As seen in the previous section, acceptable correlations are reached between experiments and simulations. For further analysis, it is interesting to have force-displacement curves of dynamic plate crushing simulations (FEM dynamic) on the same graph for comparison purposes as presented in Figure 4-5. As displayed, these three curves are comparatively close to each other which show that there is no influence of initial speeds as observed in experimental study [DUO10]. However, the peak force in the simulation with initial speed of 5 m/s (FEM dynamic: 5m/s) is higher than the other two simulations. This is due to the over-prediction of the peak force at crushing displacement between 3 mm and 3.5 mm in the simulation with initial speed of 5m/s as compared to experimental results (see Figure 4-4c and Figure 4-6). Further explanation will be given in the following section.

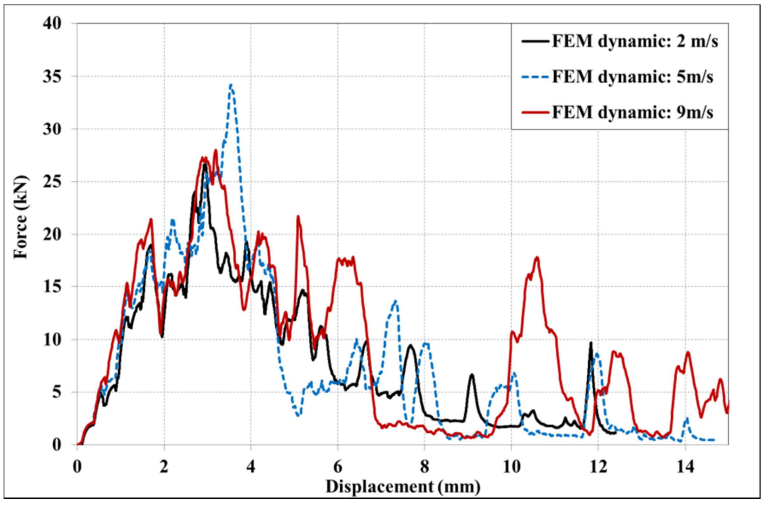

Figure 4-5: The comparison between the plate crushing (FEM dynamic) simulations

The oscillations of the force curves in all cases during the steady crushing state are resulting from the competition between the localized crushing and the inside ply failure mechanisms when the plies are in the fragmentation mode. The breakage of the plies (0° or 90°) resulting from bending failure (inside ply failure) has caused the force drops to the minimum. Moreover, it creates a gap between the main structures and the metallic base. The new contact between metallic base and the main structure after crossing the gap has produced an impact that induces a sudden increase of force which is believed to be depending on the gap distance and crushing speed. This phenomenon is repeated during all the steady crushing state described as the force plateau with eventual oscillations. In order to have better observation and understanding, it is interesting to see in details the correlation between the crushing force and the crushing morphology.

4.2.2.2 Physical Correlation of Crushing Force

In this section, a detailed correlation between mechanical phenomena during crushing and the force-displacement curve is presented in Figure 4-6 for both medium-scale static and plate crushing (Vo=5m/s) simulations. The correlation only focuses on the crushing initiation since the mechanical phenomena is clear and easy to observe. General observation has shown that the force drops in the simulation curves occurred at almost the same displacement as in the experimental curves. This is to say, the crushing phenomena is well represented by the numerical models.

For the medium-scale crushing simulation (Figure 4-6a), from the beginning to Image A (Figure 4-6a), the element at the tip of the specimen (0° free-face crushing element) is crushed under localized crushing mechanism and the force start to grow. Then, the breakage of 90° element is observed due to a small bending in 90° plies that leads to a small drop in the force. As the crushing process continues, the plate exhibits multiple delaminations as a result of the implementation of transverse deformation on the 90° free-face elements (Image B and C in Figure 4-6a). In addition, the breakages of 90° plies due to bending can also be observed, leading to more drops in the force. Nevertheless, the force continues to rise as more plies are in contact with the metallic base. During this period, only small drops in force is observed as the results from the new interface delamination (Image D in Figure 4-6a). After that, there is a high force drop caused by the multiple breakages of plies and the fast propagation of an existing delamination (Image E in Figure 4-6a) induced by the global bending of the laminate.

As with the medium-scale crushing simulation, plate crushing simulation (Vo=5m/s) also exhibits almost the same crushing behaviors throughout the crushing process with only small differences in term of the mechanical phenomena as presented in Figure 4-6b. The difference can be seen in Image B (Figure 4-6b), where despite having the same phenomena of multiple delaminations, the combination of compression and bending loads (short length bending with the tip element having localized crushing) during crushing has caused the breakage of exterior 0° ply. This breakage has not been seen in the medium-scale static simulation. Moreover, one can observe that the maximum force in this simulation curve is higher (36%) than the experimental curves. The major force drop is also delayed as compared to the experimental curves. This can be due to the plate crushing model that has under-predicted the global bending of the laminate which delayed the appearance of the big crack on the right side of the laminate (Image E in Figure 4-6b). Nevertheless, this difference will not affect much of the total energy absorbed that will be explained in the following section.

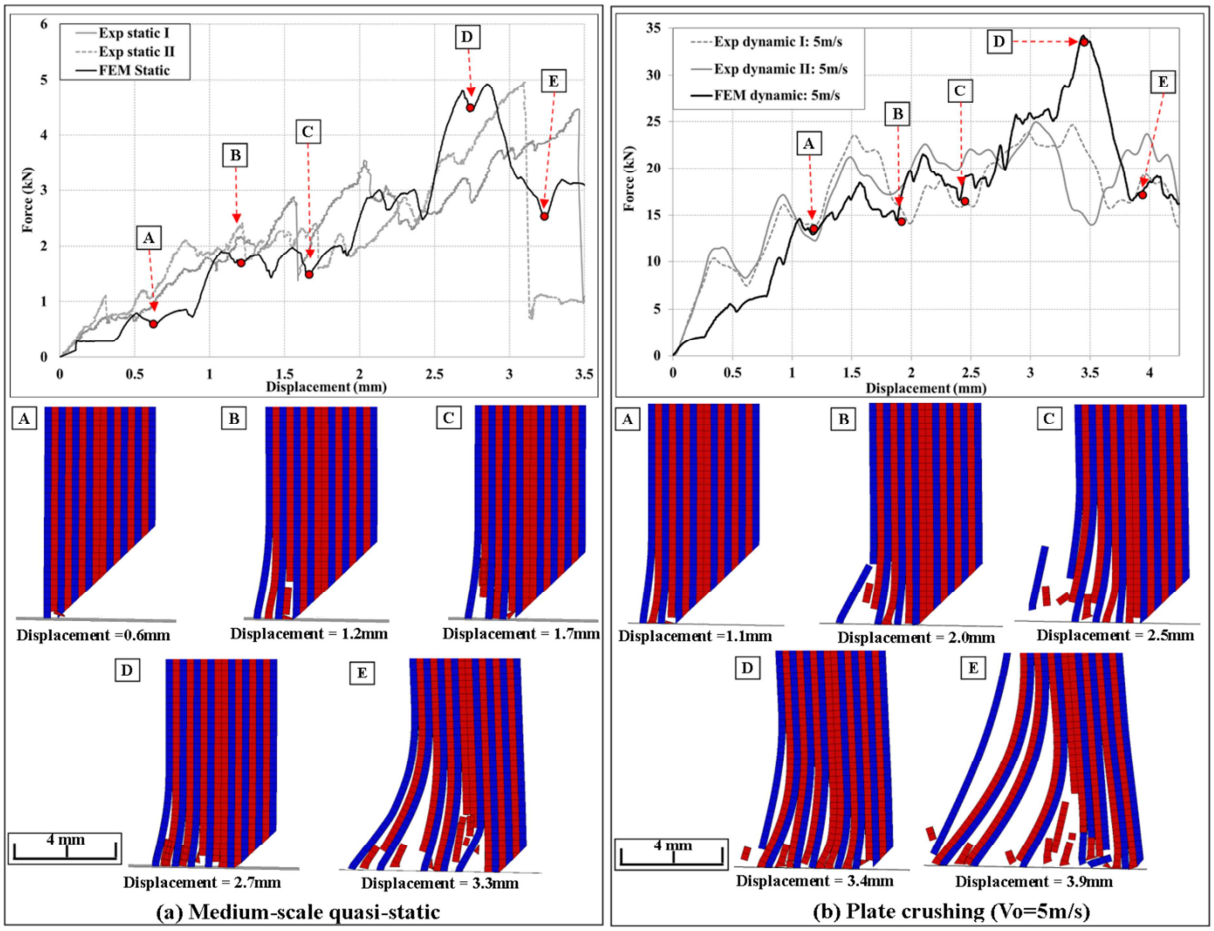

Figure 4-6: Simulation correlation of crushing phenomenon

4.2.4 Comparison of Energy Absorption

The evolution results of the total energy absorbed between numerical and experimental, which is calculated as the total area under the force-displacement curves in Figure 4-4 with respect to the real width of the specimen, are shown in Figure 4-7. As with force-displacement curve, the estimation of total energy by the numerical models correlates well with the experimental curve. The energy is dissipated by various mechanisms that will be discussed further in the next section.

For the medium-scale crushing test, the big discrepancy between the simulation and the experimental curve is due to the same reason discussed before (force at 5 mm of force-displacement curve in simulation is higher than in the experiment). Similarly, the comparison results for the plate crushing tests have shown that in all cases the discrepancy is observed at the end of the curves as a result of under-prediction of the numerical models on the steady state crushing load. However, by taking into account the complexity of the fracture modes in the laminated plate crushing and the dispersion in tests, the overall correspondence between the numerical and experimental results is considered to be acceptable [PIN04].

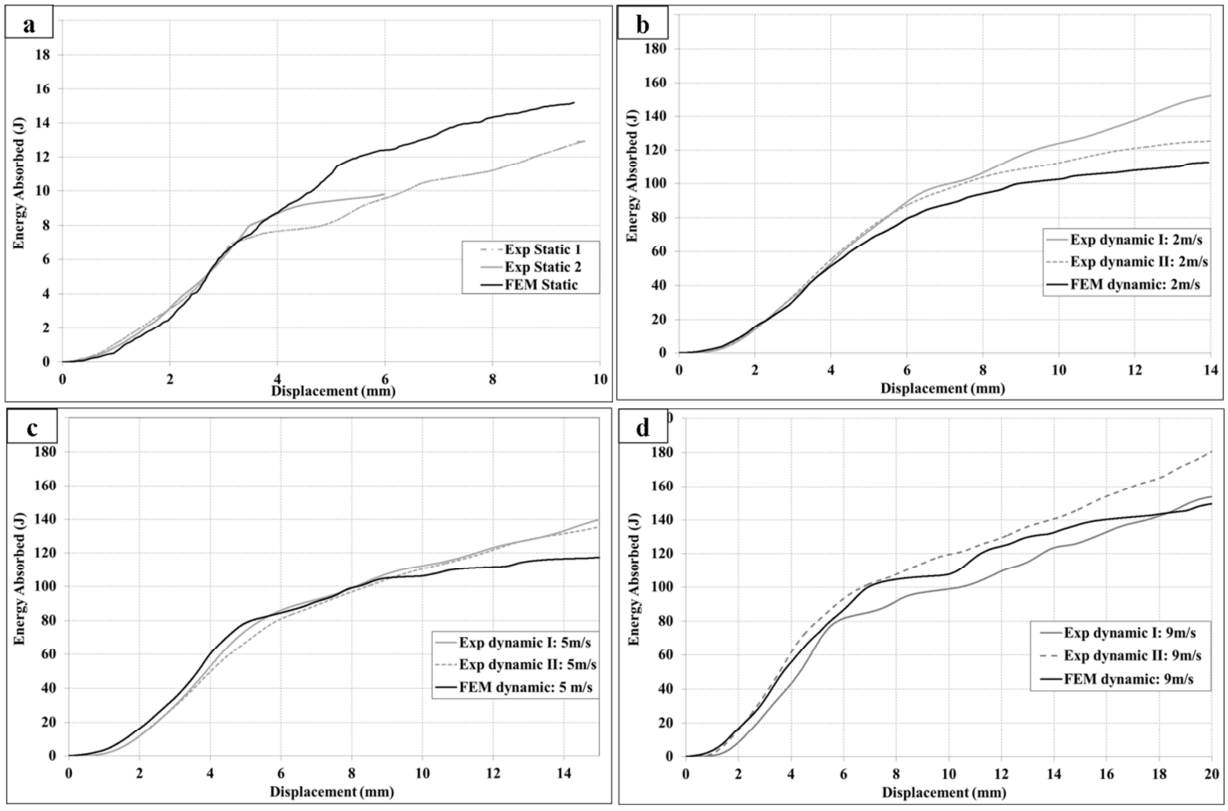

Figure 4-7: The comparison between the experimental and numerical results for absorbed energy versus displacement for (a) medium scale static test (FEM static) (b-d) plate crushing (FEM dynamic) with initial speed (b) 2 m/s (c) 5 m/s (d) 9 m/s

4.3 Competition of Energy Absorbing Mechanisms

4.3.1 Contribution of Various Energy Absorbing Mechanisms

The total energy absorbed presented in Figure 4-7 is generally dissipated through various mechanisms presence during the crushing tests. One of the advantages of numerical simulations over the experimental tests is that simulations allow one to measure, categorize and provide insight into the competing energy absorbing mechanisms of the structure in which not permissible through experimental testing. The energy absorbed during the crushing simulation of the composite plates is categorized into energy absorbed through (a) damage in 0° and 90° plies; (b) delamination; (c) friction; and (d) viscous effect.

The evolution of energy dissipation represented by each of these mechanisms during the crushing tests is presented in Figure 4-8 for each static and dynamic (9 m/s) simulation. Starting from the beginning of crushing process, the energy is absorbed mainly through plies damage mechanism especially via 0° plies damage that dissipated higher energy than 90° plies damage throughout the crushing process. This is because 0° plies have endured more localized crushing than inside ply failure which is contrary to 90° plies, that often turn into global rupture of the ply when having localized crushing. Furthermore, the energy absorbed by 0° plies damages can be divided into two categories, which are energy absorbed via localized crushing and inside ply failures that will discuss further in details. For 90° plies, no energy is considered for the inside ply failure as the breakage only involved matrix cracking due to bending that dissipate very low energy and can be neglected [BOU12, HON13].

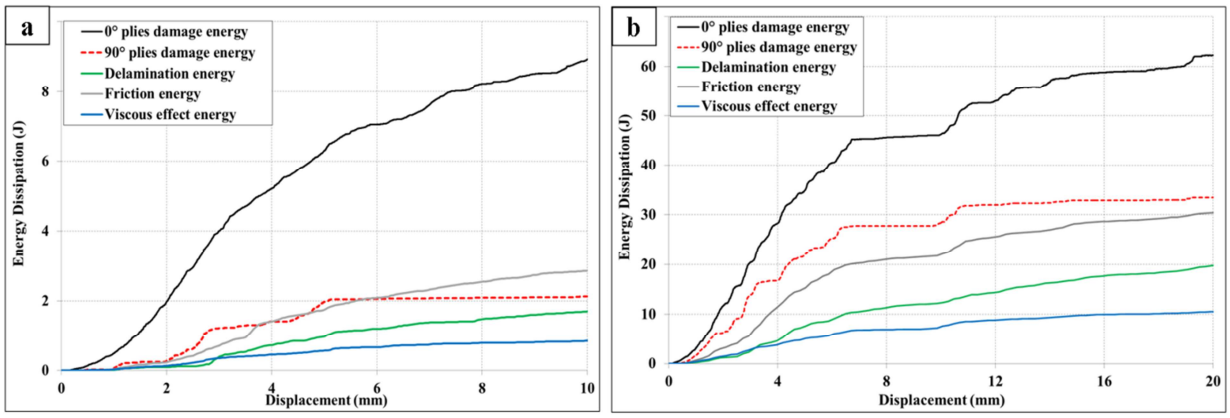

Figure 4-8: The evolution of energy absorbed through various mechanisms during crushing tests of (a) medium scale static (FEM static) and (b) plate crushing (FEM dynamic) for the case $V_0 = 9m/s$

Delamination energy on the other hand is significant and important to accurately capture the crushing morphology of mixed-mode crushing plate although it provides less

energy absorption than the energy absorbed through the friction mechanism from the beginning of the crushing. In fact, one can notice in Figure 4-8a, the energy absorbed through friction mechanism is larger than the energy absorbed via 90° plies damage during the steady state crushing process. Perhaps this is because of the over-prediction in the static simulation on the big breakages of two 90° plies as compared to the experimental test that cause the volume of 90° plies involved in energy absorption is to be lower (see Figure 4-3a-iii,-iv and -v).

Regarding the energy absorbed through viscous effect, it does exist even if when no viscous material property is defined. In order to mitigate the propagation of eventual stress waves, a global viscous coefficient needs to be specified [ABQ09]. So, to ensure the model reproduces the real test, viscous energy must remain at low enough level. With respect to that, the variation of energy dissipated by viscous is always less than 10% from the total energy absorbed.

Furthermore, a constant phase of energy absorbed via plies damage (both in 0° and 90° plies) is recorded in Figure 4-8b between displacement from 6.7 mm to 9.5 mm (during transition phase). This is due to big breakage of plies in fragmentation mode at higher point from the plate extremity as shown in Figure 4-3b-iii. Subsequently, the force drops drastically to the minimum as no direct contact occurred between plies and metallic base during that period (see Figure 4-4d). As a result, there was no augmentation in the energy absorbed through the plies damage. Thus, the energy absorbed during this period are mainly due to delamination and friction as splaying mode continues to grow that relates to the friction between the splaying plies and the metallic base.

The summary of the energy absorbed through each of these mechanisms at different crushing speeds is presented in Figure 4-9. It can be observed that the energy absorbed via 0° plies gradually decreases with the increase in the loading speed which is contrary to the energy absorbed via 90° plies (except in dynamic simulation with initial speed 2 m/s) that progresses with the increase of loading speed. Based on the simulations results, this trend is due to the plies in the fragmentation mode tend to have more inside ply failure caused by bending mode with the increase in the crushing speeds. Moreover, the inside ply failure also caused by the high impact due to the new contact between the main structure and the metallic base after crossing the gap created during the plies breakage. This has reduced the volume of 0° plies that were to the localized crushing. It similarly goes for the 90° plies, but it is observed during the steady state crushing, the number of 90° plies evolved in fragmentation

mode increases with the rise in the crushing speed (see Figure 4-3 for the comparison). This leads to the increment in the total energy absorbed of the 90° plies damage. Other than these two significant changes, Figure 4-9 demonstrates that the crushing speed does not influence the relative levels of energy absorbed through delamination, friction and viscous effect.

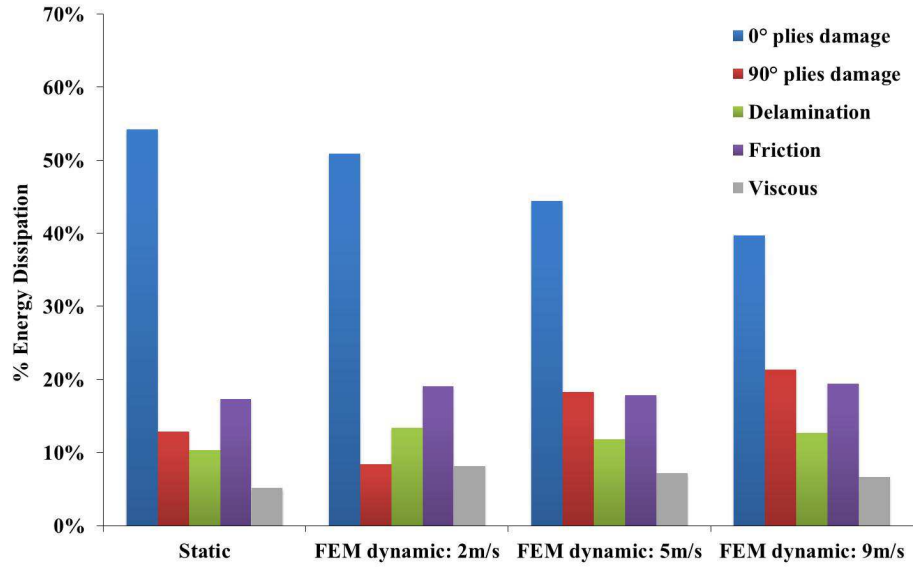

Figure 4-9: The relative comparison of energy absorbed through various mechanisms at different crushing speeds

4.3.2 Detail of Energy Absorption in Plies Damage

As observed in experiment, plies damage can occur at two levels; localized crushing at plate extremity and inside ply failure that occurs at higher position from the plate extremity. Therefore, the results from simulations also allow one to categorize the energy absorbed via plies damage into energy absorbed through localized crushing and inside ply failures mechanisms. Figure 4-10 shows the percentage variations of these two mechanisms in absorbing the energy during the crushing process. Precisely, the energy absorbed through localized crushing also can be categorized between 0° and 90° plies. However, concerning the inside ply failure mechanism, only failure in 0° plies is considered since as mentioned before the matrix cracking failures in 90° plies dissipate very low energy and can be neglected as compared to energy dissipated by fiber breakages in 0° plies.

As presented in Figure 4-10, the energy absorbed through plies damage in both cases most of the time is contributed by the localized crushing (>80%) compared to the inside ply failures (< 20%) especially during the crushing initiation when the chamfer part of the plate is crushed under pure compressive loads. The flux in 0° and 90° localized crushing during the

initiation (displacement ≤ 3mm) is related to the breakages of 90° plies due to small bending during the initiation (as example refer to Figure 4-6) that creates a gap to the next element to perform localized crushing with the metallic base.

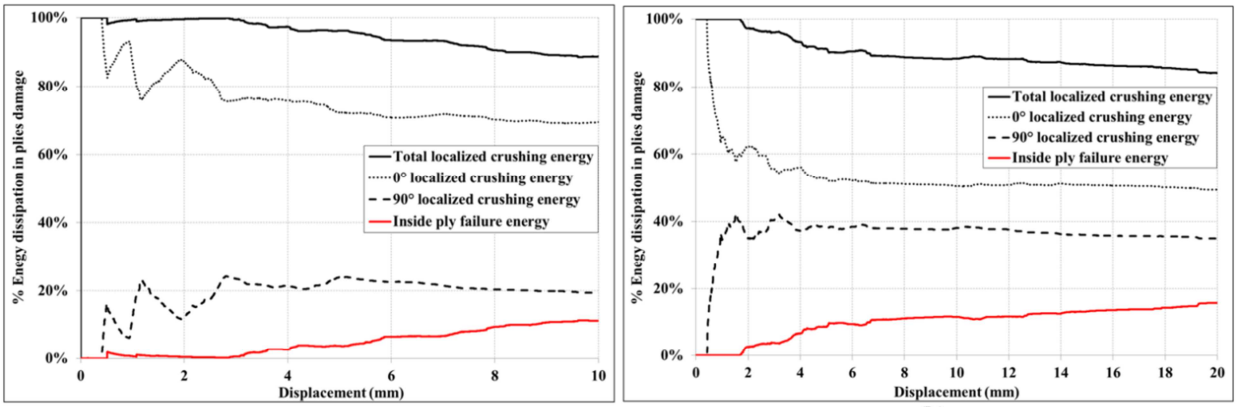

Figure 4-10: The comparison between energy absorption through localized crushing (0° and 90°) and inside ply damage mechanisms in (a) medium scale static test (FEM static) (b) plate crushing (FEM dynamic) for the case V_0=*9 m/s*

Once the plies on the left side of the laminate start to bend (see Figure 4-3a-i and 4-3b-i), only then the energy absorbed by the inside ply failures is accounted but it is still very low compared to the energy absorbed via localized crushing. As the plate crushing continues with mixed-mode crushing behavior that involves complex damage mechanisms (splaying, localized crushing, bending, and their coupling) as shown in Figure 4-3, the competing energy absorbing mechanism between localized crushing and inside ply failure also continues to rise until the end of crushing test as shown in the Figure 4-10.

Regarding the energy absorbing mechanism in localized crushing, it is always observed 0° plies dissipate more energy than 90° plies even though both plies have the same energy absorption ability (as mean crushing stress of both plies is close to each other). As expected from the experimental observation, this is due to the ability of 0° plies to perform a steady localized crushing while 90° plies often turn into global rupture of the ply. Thus, the volume of 90° plies evolved in localized crushing is actually lower since the beginning of the crushing test although in Figure 4-3b-iii, -iv and -v of the plate crushing, it was shown that the number of 90° plies in fragmentation mode is higher than 0° plies. Moreover, the different percentage variation in 0° and 90° localized crushing between medium-scale static (Figure 4-10a), and plate crushing (Figure 4-10b) tests is due only to the difference in the number of plies evolves during steady fragmentation as displayed in Figure 4-3.

4.4 Influence of Humid Ageing

From the experimental observations, it shows that the humid ageing (HA) has small influence on the crushing morphology and reduces the ply mean crushing stress values of 0° and 90° plies. These small changes in the material properties have given the opportunity to the numerical model to re-simulate the medium-scale static crushing test by taking into account all of these changes to verify the robustness of the model. The simulation is carried out with some modifications made on the material properties according to the physical observations and the results obtained in the experimental tests.

The ply mean crushing stress values for both 0° and 90° is reduced by 10% according to the drop in ply mean crushing stress of the experimental results (a reduction of 8% and 9% in 0° and 90° plies respectively). Taking into account the influence of HA on the inter-laminar fracture toughness [CAN02] and fiber matrix bonding strength [KUM10], the properties of interface fracture toughness (mode I and mode II) and in-plane shear strength in Table 3-1 are also reduced by 10% in this simulation. The rest of the material properties, boundary conditions, loading and contact properties remain the same as for the medium-scale static crushing simulation before.

The overall comparisons between this new simulation (FEM static HA) and experimental results are presented in Figure 4-11 consisting the crushing morphology, force-displacement curve and the energy absorption analysis. In general, the numerical and experimental results agreed well with each other. For example, a comparison of crushing morphologies in Figure 4-11a has demonstrated an acceptable correlation between the simulation and experimental results. However, the comparison in Figure 4-11a-iv has revealed that the simulation has predicted less number of plies in fragmentation as compare with the experimental result. This is perhaps due to the limitation of the current numerical model. According to the Figure 4-11a, the HA simulation has also shown a difference in term of delamination length on the right side of the laminate after the transition phase although it managed to deliver multiple delaminations as observed in the experimental test.

Nevertheless, it does not affect much the result of the force-displacement curve. As shown in Figure 4-11b, a close match between simulation and experimental force-displacement curves is obtained. Both the peak and steady crushing force are close to each other. The drop in simulation force after 7.7 mm is due to the difference in the number of plies in fragmentation mode predicted by model. Finally, a comparison between the

simulation and experimental energy absorption also shows that they are comparatively close to each other as shown in Figure 4-11c.

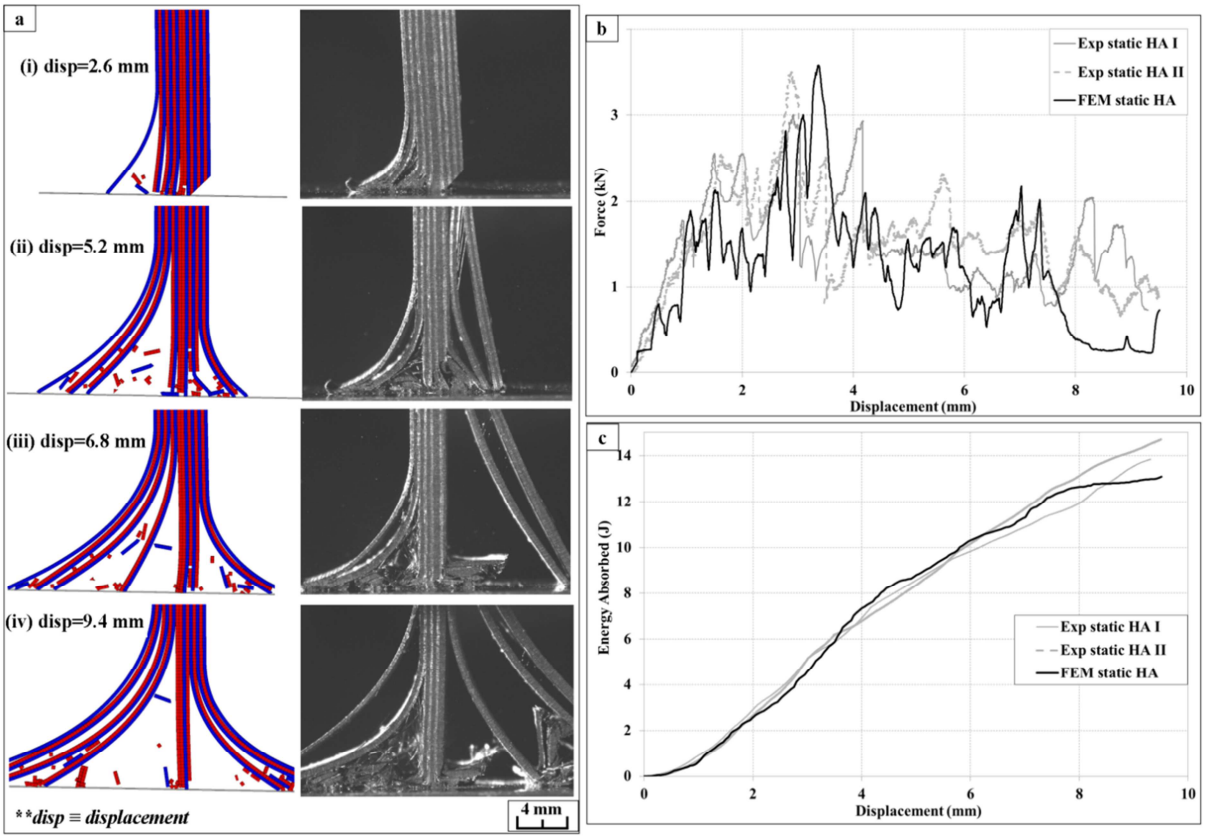

Figure 4-11: Comparison between the experimental and numerical results under influence of humid ageing in term of (a) crushing morphology (b) force-displacement curves and (c) energy absorbed

Taken into account the changes made on some material properties mentioned before, the numerical model has demonstrated its capability to represent the same effect of HA as observed in experimental results. Moreover, the results of this simulation (FEM static HA) are also compared with the results of the previous simulation of medium-scale static test (sane condition) in section *§ 4.2* for the verification purpose. Therefore, overall comparisons between the simulation of HA and the previous simulation (FEM static (sane)) are presented in Figure 4-12.

In general, one can notice some differences in term of the crushing morphologies as presented in the Figure 4-12a although both simulations exhibit almost the same mechanical phenomena. The difference in the force-displacement curves can also be observed in Figure 4-12b. Nevertheless, at the beginning of the crushing process (displacement ≤ 1.8mm), the force curves for both simulations are very close to each other. Only after this crushing displacement, the difference between these two simulations can be seen in both crushing

morphologies and the crushing forces. The drastic drop of crushing force at the displacement of 2.1mm in HA simulation is due to multiple plies breakage which is not the case for the sane simulation (Figure 4-12a-i and Figure 4-12b). As crushing continues, more plies in both simulations have made contact with the metallic base that increases the forces. But the peak force for the HA simulation is far lower than the sane simulation which is about 29%. The difference between these peak forces shows the effect of reducing the mentioned material properties before to account for the influence of the HA.

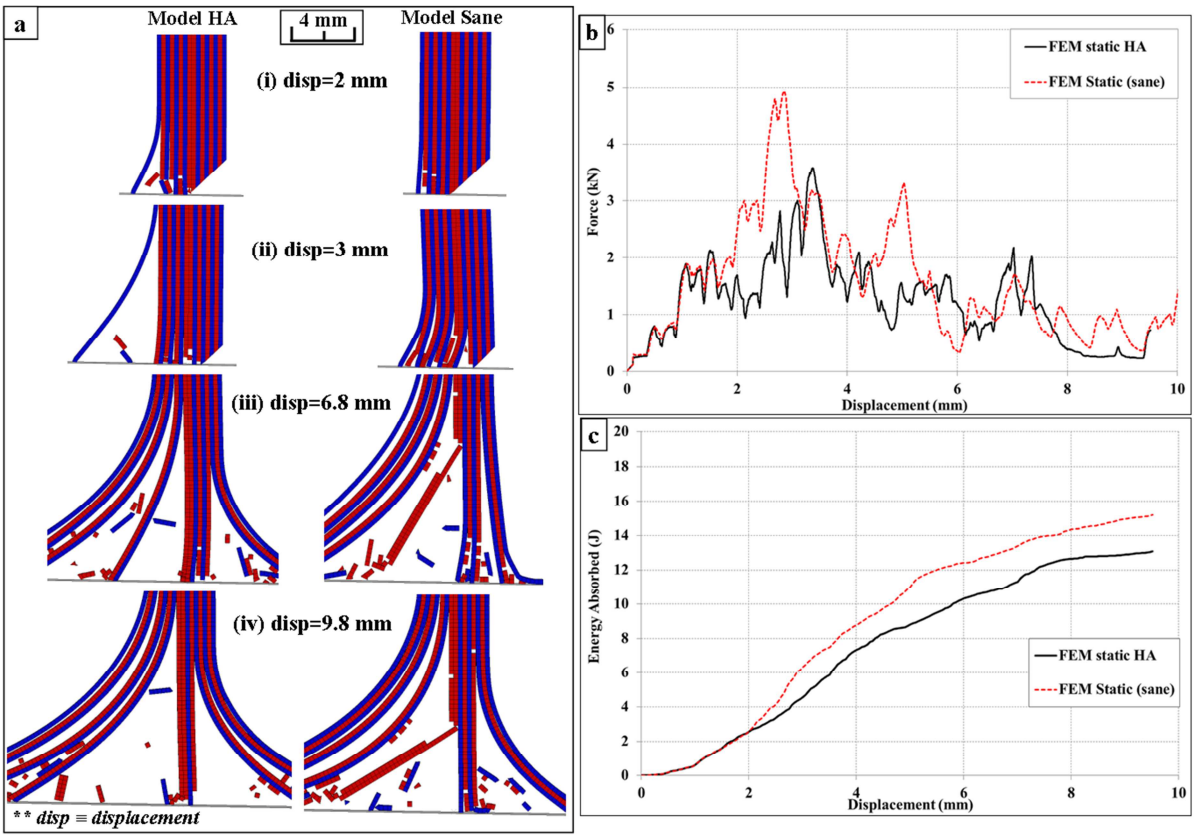

Figure 4-12: Comparison of result simulation between simulation with (FEM static HA) and without (FEM static sane) influence of humid ageing (a) crushing morphology (b) force-displacement curves and (c) energy absorbed

Once crushing process has turned into mixed-mode crushing or steady crushing state, the number of plies performed fragmentation mode in HA simulation is observed higher than the sane simulation (Figure 4-12a-iii). But the crushing forces for both curves in Figure 4-12b are close to each other. This may be due to the reduction of 10% in the ply mean crushing stress values for the HA simulation. At the end of the crushing process (displacement $\geq$ 8mm), both models have predicted almost the same number of plies in fragmentation mode and the crushing forces remain close to each other (Figure 4-12a-iv and Figure 4-12b). The difference in the crushing morphologies and the force-displacement curves discussed here will lead to

the difference in total energy absorbed between these two simulations as presented in Figure 4-12c.

This comparison has shown that the medium-scale static model is able to reproduce the same mechanical phenomena as predicted in the previous simulation (*§ 4.2*). However, the general crushing morphology is different when taken into account the effects of reducing the ply mean crushing stress, fracture toughness and the shear strength. This is to say for the moment, this model is robust to reproduce the same crushing behavior under different conditions.

Additional information from simulation results regarding the influence of HA on the competing energy absorbing mechanisms is presented in Figure 4-13. This figure demonstrates that the HA does not affect much the relative levels of energy absorbed by the competing mechanisms, other than a slight increase in the percentage of the energy absorbed via 0° plies damage (3%), friction (2%) and as expected a small decrease in 90° plies damage (4%). Although the properties of interface fracture toughness are reduced by 10%, the percentage of energy absorbed through delamination failure has not changed, which is similar to the energy absorbed via viscous.

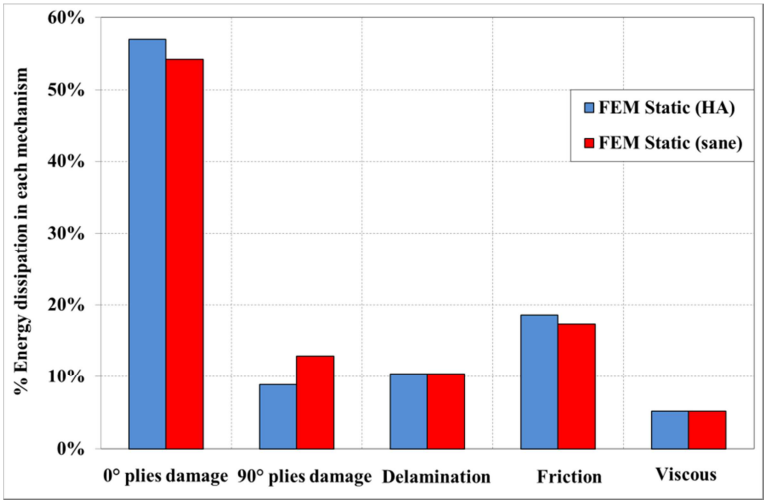

Figure 4-13: Comparison of relative energy absorbed through various mechanisms between simulations with (FEM Static HA) and without (FEM Static sane) influence of humid ageing

4.5 Influence of Friction Coefficient

Previous analyses on the competing energy absorbing mechanisms have shown that apart from the plies damage mechanism, friction mechanism had the ability to absorb higher energy than other mechanisms during crushing. Therefore, it is believed that changing the coefficient of friction in crushing tests may have significant effects on the performances of composite plate under mixed-mode crushing.

Based on the performance of medium-scale static model, several simulations with different friction coefficients, 0.1, 0.15 (reference), 0.2, 0.25, 0.3 are carried out to investigate the influence of friction mechanism on the global crushing morphology, force-displacement curve and energy absorbing mechanisms of composite plate under mixed mode crushing. The summary for each global crushing morphology of the tested friction coefficients at different displacement is displayed in Figure 4-14 (simulation with μ=0.15 can be referred in Figure 4-3a, Figure 4-6 and Figure 4-12). In general, the crushing morphology varies from one to another with the changes in coefficient of friction especially in simulation with μ=0.3. In the case of μ=0.3, after the chamfered part is crushed, the crushing process has turned into global bending of the laminate due to too high friction forces at the metallic base that cause the delaminated plies unable to slip and perform splaying mode. Therefore, the result from this simulation will not be taken into account for the further analysis and discussion.

Referring to Figure 4-14, the results of simulations have demonstrated that the increasing of the friction coefficient in the crushing test has made the plies on the left side of the plate hard to slip and leads to splaying mode during the crushing initiation. This phenomenon has made the existing delaminations difficult to propagate. As the crushing continues, all of the simulations undergo mixed-mode crushing with splaying mode starts to perform on the right side of the plate except for the simulation with μ=0.2 that still propagates under fragmentation mode with multiple inside plies failures.

The influences of friction coefficient on the crushing performances are more obvious during the steady state crushing. For example by reducing the friction coefficient to μ=0.1, the crushing process becomes unstable with plies that undergo steady crushing has turned into splaying mode once the interfaces on the right side have large delamination. As a result, the crushing force drops drastically and remains at the minimum level as shown in Figure 4-15. Apart from that, crushing simulation with higher friction coefficient (μ=0.2) has demonstrated a steady crushing state with more plies in fragmentation mode which resulting in high crushing force. However, the model predicts dissimilar trend for the simulation with friction

μ=0.25 as shown in Figure 4-14. It exhibits less plies in fragmentation as compared to the simulation with μ=0.2. This has led to the drop in the crushing force.

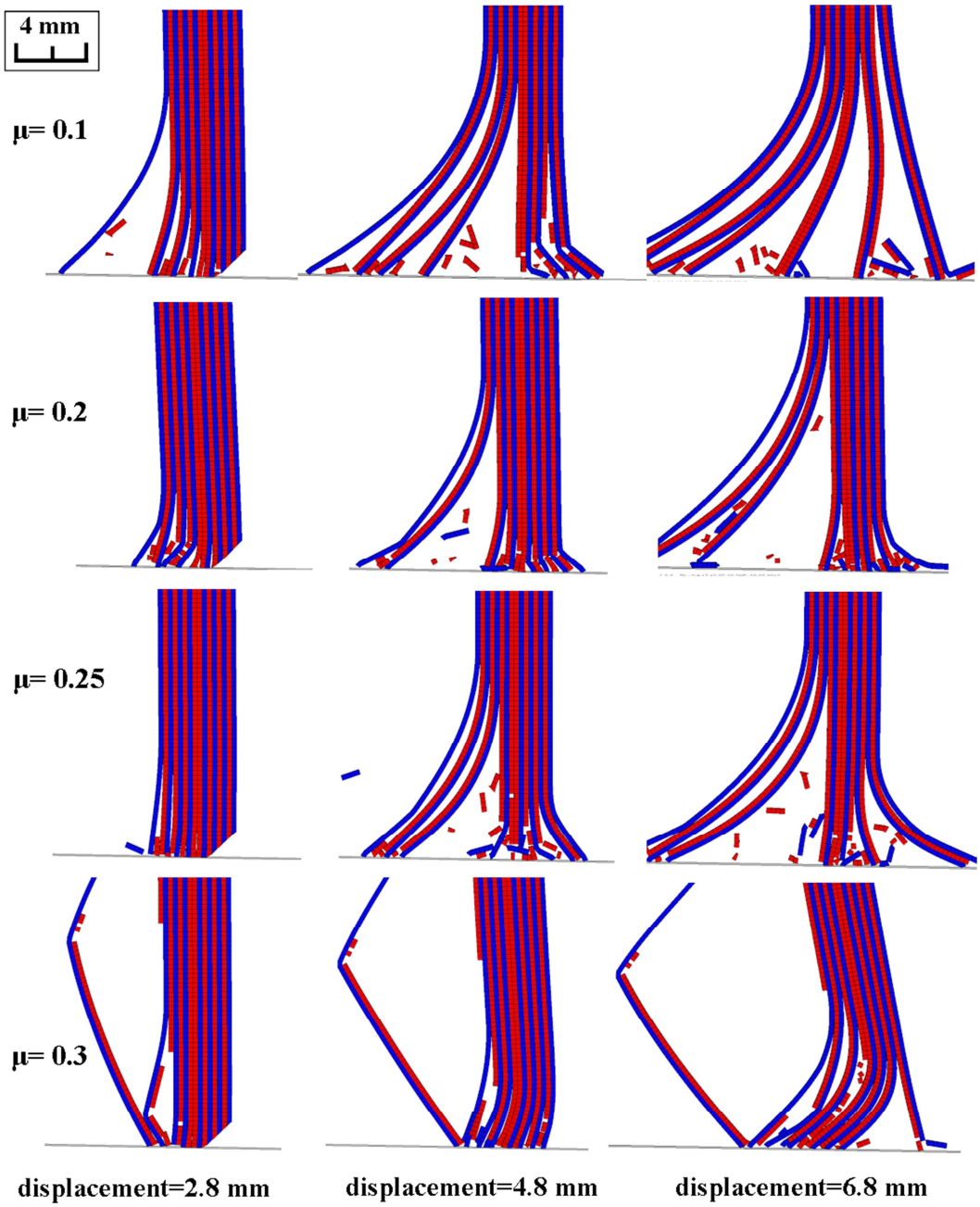

Figure 4-14: The crushing morphology of medium-scale static test simulations performed with different friction coefficients

Moreover, Figure 4-16 presents the evolution of the total energy absorbed in function of friction coefficient. As illustrated, simulation with μ=0.2 has delivered the highest energy absorbed as a result of more plies evolved in fragmentation mode as compared to the other simulations (see Figure 4-14). The drop in energy absorbed at higher friction coefficient (μ=0.25) is due to the observation mentioned above.

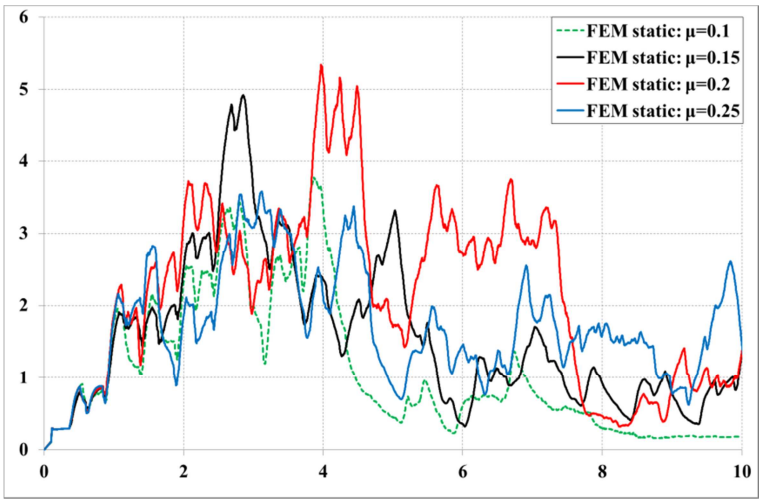

Figure 4-15: Force-displacement results with different friction coefficients

Besides that, Figure 4-16 also presents the comparison results of competing energy absorbing mechanisms for various friction coefficients. As expected, the energy absorbed through friction mechanism is augmented with the increase in friction coefficients. Apart from that, this figure also shows the dispersion in energy absorbing trend by other mechanisms which depend on the crushing morphologies. Nevertheless, the energy absorbed via 0° plies damages is always the main contributor towards the total energy absorbed.

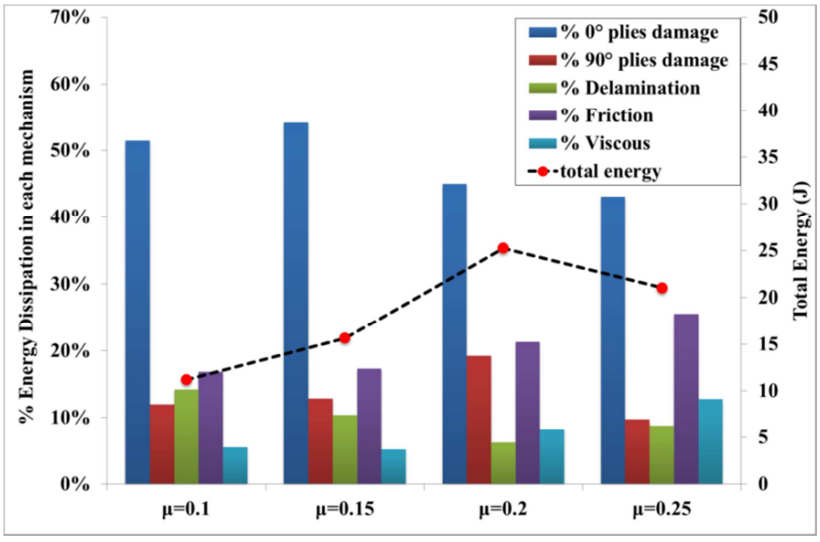

Figure 4-16: Comparison of total energy absorption and energy absorbing mechanisms with different friction coefficients

Based on the simulations results analysis, the friction coefficient is confirmed to have a great influence on the mixed-mode crushing response as demonstrated by Guillon [GUI08] for the plate crushing simulation under pure splaying mode. The same influence is also observed in the simulation of composite tube crushing carried out by Pinho et al [PIN04]. Due

to the absence of experimental data, it is not possible to qualify and quantify the performance of the current numerical model for different friction coefficients. In this study, the model is able to maintain the same mechanical phenomena for friction coefficients between μ=0.1 and μ=0.25. Nevertheless, it delivered a completely different crushing behavior for the crushing simulation with friction μ=0.3 that turn the laminate into global bending of the structure.

4.6 Conclusion

A pseudo 2D finite element model of CFRP laminated plates subjected to low velocity crushing has been presented that depends only on the elementary material characteristics of the ply. Based on the presented results, the current development of the numerical model shows the capability to represent mixed-mode crushing for 0°/90° laminates with all major damages as observed experimentally. In addition, a good correlation is observed on the force-displacement curves and energy absorption between numerical models and experimental tests.

Despite having differences in the numerical results, the use of a free-face-crushing concept has allowed the numerical models to simulate the localized crushing and inside ply failures at the same time. Furthermore, the implementation of the specific crushing criterion and the creation of a specific debris wedge in the 90° plies, free-face-crushing elements are capable to reproduce the complex localized damage mechanisms that occur at sub-ply scale and at all crushing modes (splaying and fragmentation) at the same time.

Besides that, the medium-scale static model has been used to study the influence of humid ageing on the CFRP laminates. Some of the mechanical properties of T700/M21 material have been changed according to the experimental tests to account for the influence of humid ageing. The simulation results have shown almost similar trend in crushing behaviors as experimentally observed. Moreover, the effect of the friction coefficient in the mixed-mode crushing is also studied in this chapter using the numerical model. Qualitatively, the model is able to maintain the main mechanical phenomena although it exhibits different crushing morphologies for simulations with friction coefficients below 0.25. At higher friction coefficient (μ=0.3), different crushing behaviors and mechanical phenomena are delivered by the model.

In term of energy absorbing mechanisms, in all cases, 0° plies damage mechanism via localized crushing absorbed the highest energy compared with the other mechanisms. Then, it is followed by the 90° plies damage and friction mechanisms which have quite close and similar level of energy absorbed. Besides that, one can notice although the presence of

delamination is significant and important to accurately capture the crushing morphology of mixed-mode crushing plate, it plays a minor role in energy absorption and shows no influence with the increased in crushing speeds. The energy absorbed via viscous on the other hand, is always less than 10% from the total energy absorbed.

In general, the laminate plate crushing is more complex compared with the composite tube crushing or any closed-profile and self-supporting specimens due to the dispersion in the tests. The difficulties come from the coupling behaviors between the splaying, crushing, bending and friction that can change the behavior at the crushing front which made it difficult to extract one to another coupling in plate crushing.

CONCLUSIONS & PERSPECTIVES

Nowadays, in aeronautics, it is necessary to design composite structures which are crash resistant. Except for some simple structures such as tube-like crash absorbers, it is difficult, both experimentally (cost of test campaigns, the number of input parameters) and numerically (limitation of existing models, lack of understanding of the crash mechanism) to make predictions about the energy absorption capacity of structures. Therefore, in this thesis, we propose a coupled approach testing and calculations to improve the understanding of the phenomena involved in the composites crash, and develop a model capable of representing these phenomena.

Initially, crushing tests of laminate $(0°)_n$, $(90°)_n$ and $[(0°/90°)_n]_{sym}$ at different scales, including tests under SEM were made for two materials (UD carbon-epoxy and carbon fabric-epoxy). The first observations have improved the usual classification of crushing modes; fragmentation and splaying mode. The fragmentation mode can be categorized into two sub-modes: localized crushing at the ply extremity, which means at the contact surface in contrast to the inside ply fragmentation. The latter is relatively conventional, as it is in fact a rupture of a ply or pack of plies under a combination of compression, bending and shearing. On the other hand, localized crushing is much more original, and tests have proven that the plies in 0° and 90° under localized crushing could only support a maximum compression stress of about 270 MPa. This observation has helped to define a new intrinsic parameter of the material which is the ply mean crushing stress, and the associated identification tests.

The SEM observations of the crushing zone also allowed identifying what mechanisms were taking place. For the 0° plies, the ply mean crushing stress is the result of micro-buckling of pre-delaminated pack of fibers at the contact surface. For the 90°, the ply mean crushing stress is due to the multiple shear-cracks of matrix. Within the $(0°/90°)_n$ laminate, it was also emphasized that the coexistence of both mechanisms had an influence on the evolution of the crash front: multiple cracks in the 90 °plies lead to the formation of debris

wedge which can drive the initiation of splaying of adjacent 0 ° plies, thus reducing the number of plies in fragmentation.

A series of tests was then performed on the same type of test specimens after submitting to humid ageing. It is difficult to conclude on the influence of humid ageing on the response of the specimens given the relatively small differences between sane and humid ageing specimens compared to the dispersion even within the tests for the sane specimens. However, it is clear that the ply mean crushing stress was influenced by humid ageing, with a significant decrease of approximately 10% for both directions (0 ° and 90 °), and 4% for woven fabrics.

From these observations, a damage modeling has been proposed for finite elements simulation. It is based on a concept called "free face crushing", which considers that the element at the ply extremity (crush front) undergoes localized crushing with less strength than the inside ply elements (far from the crush front). This element deforms under constant stress (pseudo-plastic law) which is equal to the ply mean crushing stress, and it is deleted when completely crushed. The next element is then assigned the same constitutive law, and so on during the crushing of the structure. To take into account the initiation of 0° plies splaying due to 90° debris wedge, the transverse pseudo-expansion of 90° element in "free crushing face" is imposed when it crushed. For other damage (breakage plies and delamination), conventional models are used.

This damage modeling is applied to the simulation of static and dynamic crushing tests presented before, and gives very satisfactory results since it allows to represent the main mechanisms discussed above which validating the modeling choices. The simulation also allows to make analyses of energy absorbed by each damage mechanism which not possible during the tests. The results has demonstrated that it is localized crushing dissipates the most, especially in the 0° plies.

The model is then applied to simulate the influence of humid ageing. Nevertheless, it does not give a clear tendency, but still seems to go in the direction of the test results.

Perspectives:

Of course, the work done during this thesis is only a step towards crash modeling of composite structures, and many still remain to be done.

In terms of experimental studies, it seems important to gradually increase the understanding of the crash by incorporating new mechanisms that have not yet been studied, such as the behavior of the 45 ° plies. Tests are currently under schedule to make observations in SEM to check whether there is also localized crushing of 45° ply in pure UD laminate and multi-plies orientation laminate.

An additional question raised during this thesis is the influence of speed on the crash response of composite structure. According to the "macroscopic" observations on plates crushing (force / displacement curve, overall morphology of crushing front), it seems that the influence is relatively small. However, some evidence suggests that there may be an influence on the ply mean crushing stress. But the transition from the existing static test to test at a speed of a few meters per second is complex (force acquisition problem in dynamic) and requires the development of a specific test.

Besides that, in a more complex plate structures tearing mode damage often appears. Therefore it would be interesting to introduce a test to study the mechanisms and to develop the law involved in this mode.

Regarding the numerical aspect, a model always faces some limitations. In the case of the model developed in this thesis, in particular it seems that the inside ply failure law for 0 ° and 90 ° plies requires some improvements. In particular, the shear accompanying the compression and bending is poorly taken into account, which could explain the significant peaks forces in the plateau phase compared to the tests.

Finally, the pseudo 2D model developed in this thesis is only a first step, and does not allow modeling a classical laminate with 45° ply. The model will be soon extended to a full 3D incorporating the concept of "free face crushing" in DPM (Discrete Ply Model) developed by Bouvet et al [BOU12, HON13], which has demonstrated its ability to simulate impact problems involving similar mechanisms as those observed during the crash except localized fragmentation.

REFERENCES

[AIR06]
Taking the lead: Airbus A350XWB presentation. December 2006

[ABD06]
Abdewi E.F, Sulaiman S, Hamouda A.M.S, Mahdi E. Effect of geometry on the crushing behaviour of laminated corrugated composite tubes. Journal of Mat Process Technol 2006; 172: 394–399

[ABQ09]
Abaqus 6.9 Analysis user's manual. Dassault Systèmes, 2009

[ALL97]
Allix O, Deü J.F. Delayed-damage modeling for fracture prediction of laminated composites under dynamic loading. Eng Transactions 1997; 45: 29-46

[BAM10]
Bambach M.R. Axial capacity and crushing of thin-walled metal, fibre–epoxy and composite metal–fibre tubes. Thin-walled Struct 2010; 48: 440-452

[BAR10]
Barnes G, Coles I, Roberts R, Adam D.O, Garner D.M. Crash safety assurance strategies future plastic and composite intensive vehicles (PCIVs). Volpe National Transportation Systems Center, Final Report, June 2010

[BAZ83]
Bazant Z.P, Oh B.H. Crack band theory for fracture of concrete. Mater Struct 1983; 16: 155-177

[BIS00]
Bisagni C., Numerical analysis and experimental correlation of composite shell buckling and post-buckling, Compos Part B 31 2000; 8: 655–667

[BIS05]
Bisagni C, Di Pietro G, Fraschini L, Terletti D. Progressive crushing of fiber-reinforced composite structural components of a Formula One racing car. Compos Struct 2005; 68(4): 491–503

[BOL95]
Bolukbasi A.O and Laananen D.H. Analytical and Experimental Studies of Crushing Behavior in Composite Laminates. Journal of Compos Mat 1995; 29: 1117-1139

[BOU09]
Bouvet C, Castanié B, Bizeul M, Barrau J-J. Low velocity impact modelling in laminate composite panels with discrete interface elements. Int Journal of Solids Structures 2009; 46(14–15): 2809–21

[BOU12]
Bouvet C, Rivallant S, Barrau J-J. Low velocity impact modeling in composite laminates capturing permanent indentation. Compos Sci Technol 2012; 72(16): 1977–88

[BRO77]
Browning C.E., Husman C.E, Whitney J.M.. Moisture effects in epoxy matrix composites. Nonmetallics material division, Air Force Materials Laboratory, Technical report AFML-TR-77-17 (1977)

[CAM03]
Camanho P.P, Davila C.G, de Moura M.F. Numerical simulation of mixed-mode progressive delamination in composite. Journal of Compos Mater 2003; 37(16): 1415-1438

[CAN02]
Cantelia A.F, Argüelles A., Viña J, Ramulub M, Kobayashib A.S. Dynamic fracture toughness measurements in composites by instrumented Charpy testing: influence of aging. Compos Sci Technol 2002; 62: 1315–1325

[CAP06]
Caporale A, Luciano R, Sacco E. Micromechanical analysis of interfacial debonding in unidirectional fiber-reinforced composites. Compos Struct 2006; 84(31-32): 2200–11

[CHA87]
Chang F.K, Chang K.Y. Post failure analysis of bolted composite joints in tension and shear-out mode failure. Journal of compos mat 1987; 21: 809-833

[CHI99]
Chiu C.H, Tsai K.H., Huang W.J. Crush-failure modes of 2D braided hybrid composite tubes. Compos Sci Technol 1999; 59: 1713-1723

[CUN08]
Cunha J.A.P, Costa M.L. and Rezende M.C. Study of the hygrothermal effects on the compression strength of carbon tape/epoxy composites, Latin American journal of solids and structures, 2008

[CZA91]
Czaplicki M.J, Robertson R.E. Comparison of bevel and tulip triggered pultruded tubes for energy absorption. Compos Sci Technol 1991; 40: 31-46

[DAN00]
Daniel L, Hogg P.J, Curtis P.T. The crush behaviour of carbon fibre angle-ply reinforcement and the effect of interlaminar shear strength on energy absorption capability. Compos Part B 2000; 31: 435–440

[DAV03]
Dàvila C.G, Camanho P.P. Failure criteria for FRP laminates in plane stress. NASA/TM-2003-212663

[DEL00]
Deletombe E, Delsart D, Kohlgrüber D, Johnson A.F. Improvement of numerical methods for crash analysis in future composite aircraft design. Aerospace Sci Technol 2000: 189-199

[DUO10]
Duong A.V, Rivallant S, Barrau JJ, Petiot C, Malherbe B. Influence of speed on the crushing behavior of composite plates. ACCM-7, Taipei, Taiwan, Nov. 2010

[DUB98]
Dubey D.D, Vizzini A.J. Energy Absorption of Composite Plates and Tubes. Journal of Compos Mat 1998; 32: 158-176

[FAR89]
Farley G.L, Jones R.M. Energy-absorption capability of composite tubes and beams. NASA TM-101634, 1989

[FAR92]
Farley G.L and Jones R. M. Analogy for the effect of material and geometrical variables on energy-absorption capability of composite tubes. Journal of Compos Mat 1992; 26: 78-89

[FEL11]
Feld N. Vers un pont micro-méso de la rupture en compression des composites stratifiés. PhD Thesis:ENS Cachan 2011

[FER08]
Feraboli P. Development of a corrugated test specimen for composite materials energy absorption. Journal of Compos Mat 2008; 42: 229-256

[FER09]
Feraboli P, Wade B, Deleo F, Rassaian M. Crush energy absorption of composite channel section specimens. Compos Part A 2009; 40: 1248-1256

[FER11]
Feraboli P, Wade B, Deleo F, Rassaian M, Higgins M, Byar A. LS-DYNA MAT54 modeling of the axial crushing of a composite tape sinusoidal specimen. Compos Part A 2011; 42(11): 1809-1825

[FLE06]
Fleming D.C. Finite element simulation of delamination with application to crashworthy design. In: proceedings of the American Helicopter Society 62nd annual forum, Phoenix, May, 2006

[FLE99]
Fleming D.C. Delamination modeling of composites for improved crash analysis. NASA CR-1999-209725

[FLEC97]
Fleck N. Compressive failure of fiber composites. Adv Appl Mech 1997; 33: 43–117

[FOU05]
Fouinneteau M. Damage and failure modelling of carbon and glass 2D braided composites. PhD Thesis: Cranfield Uni, 2005

[GHA09]
Ghasemnejad H., Blackman B.R.K, Hadavinia H., Sudall B. Experimental studies on fracture characterisation and energy absorption of GFRP composite box structures. Compos Struct 2009; 88: 253–261

[GOR10]
Gornet L, Ijaz H. Inelastic Interface Damage Modeling with Friction Effects: Application to Z-pinning reinforcement in carbon fiber epoxy matrix laminates. Journal of Compos Mat 2010; 44(17): 2067-2081

[GRE08]
Greve L, Pickett A.K, Payen F. Experimental testing and phenomenological modelling of the fragmentation process of braided carbon epoxy composite tubes under axial and oblique impact. Compos Part B 2008; 39: 1221-1232

[GUI08]
Guillon D. Etude des mécanismes d'absorption d'énergie lors de l'écrasement progressif de structures composites à base de fibre de carbone. Ph.D Thesis; ISAE; Université de Toulouse, 2008

[GUT10]
Gutkin R, Pinho S.T, Robinson P, Curtis P.T. On the transition from shear-driven fibre compressive failure to fibre kinking in notched CFRP laminates under longitudinal compression. Compos Sci Technol 2010; 70: 1223-1231

[HAD09]
Hadavinia H, Ghasemnejad H. Effects of Mode-I and Mode-II interlaminar fracture toughness on the energy absorption of CFRP twill/weave composite box sections. Compos Struct 2009; 89: 304-314

[HAL69]
Halpin J.C. Effects of environmental factors on composite materials. Nonmetallics material division, Air Force Materials Laboratory, Technical report AFML-TR-67-423 (1969)

[HAM95]
Hamada H, Ramakrishna S. Crushing mechanism of carbon fiber/PEEK composite tubes. Composites 1995; 26: 749-755

[HAN89]
Hanagud S, Craig J.I, Sriram P, Zhou W. Energy absorption behavior of graphite epoxy composite sine webs. Journal of Compos Mat 1989; 23: 448-459

[HAS80]
Hashin Z. Failure criteria for unidirectional fibre composites. Journal of Applied Mechanics 1980; 47: 329-334

[HEI10]
Heimbs S., Strobl F., Middendorf P., Guimard J. M. Composite crash absorber for aircraft fuselage applications. WIT Transactions on The Built Environment (*WIT Press*) 2010; 113

[HON13]
Hongkarnjanakul N, Bouvet C, Rivallant S. Validation of low velocity impact modelling on different stacking sequences of CFRP laminates and influence of fibre failure. Compos Struct 2013; 106: 549-559

[HUA09]
Huang J, Wang X. Numerical and experimental investigations on the axial crushing response of composite tubes. Compos Struct 2009; 91: 222–228

[HUL91]
Hull D. A unified approach to progressive crushing of fiber reinforced tubes. Compos Sci and Technol 1991; 40: 377-421

[HUT99]
Hutapea P, Yuan F.G. The effect of thermal aging on the Mode-I interlaminar fracture behavior of a high-temperature IM7/LaRC-RP46 composite. Compos Sci Technol 1999; 59: 1271-1286

[JAC11]
Jackson A, Dutton S, Gunnion A.J, Kelly D. Investigation into laminate design of open carbon–fibre/epoxy sections by quasi–static and dynamic crushing. Compos Struct 2011; 93: 2646-2654

[JIM00]
Jiménez M.A, Miravete A, Larrodé E, Revuelta D. Effect of trigger geometry on energy absorption in composite profiles. Compos Struct 2000; 48: 107-111

[JOO10]
Joosten M.W, Dutton S, Kelly D, Thomson R. Evaluation of a predictive stacked-shell analysis methodology for the analysis of energy absorbing composite crush elements. In: Proceeding of the 14th European Conference on Composite Materials (ECCM/14), Budapest, 7-10 June 2010

[JOO11]
Joosten M.W, Dutton S, Kelly D, Thomson R. Experimental and numerical investigation of the crushing response of an open section composite energy absorbing element. Compos Struct 2011; 93: 682–689

[JUM09]
Jumahat A, Soutis C, Jones F.R, Hodzic A. Fracture mechanisms and failure analysis of carbon fibre/toughened epoxy composites subjected to compressive loading. Compos Struct, 2009; 92(2): 295-305

[KIM11]
Kim J.S, Yoon H.J, Shin K.B. A study on crushing behaviors of composite circular tubes with different reinforcing fibers. Int J Impact Eng 2011; 38: 198-207

[KOM83]
Komorowski J.P. Hygrothermal effectsin continuous fiber reinforced composites. Part III: Mechanical properties 1 static tests. National Aeronautical Establishment, Aeronautical note NAE-AN-11 (1983)

[KUM08]
Kumar S.B, Sridhar I, Shivashanker S. Influence of humid environment on the performance of high strength structural carbon fiber composites. Mat Sci Eng A 2008; 498: 174-178

[LAD00]
Ladevéze P, Allix O, Deü J.F, Lévêque D. A mesomodel for localisation and damage computation in laminates. Computational. Methods Application Mech Eng 2000; 183: 105-122

[LAU07]
Laurea A.R.M. Finite element investigations on the microstructure of composite materials. Ph.D thesis; University of Nottingham, 2007

[LAU12]
Lau S.T.W, Said M.R, Yaakob M.Y. On the effect of geometrical designs and failure modes in composite axial crushing: A literature review. Compos Struct 2012; 94: 803–812

[LAV96]
Lavoie J.A, Kellas S. Dynamic crush tests of energy absorbing laminated composites plates. Compos Part A 1996; 27: 467-475.

[MAM05]
Mamalis A.G, Manolakos D.E, Ioannidis M.B, Papapostolou D.P. On the response of thin-walled CFRP composite tubular components subjected to static and dynamic axial compressive loading: experimental. Compos Struct 2005; 69; 407–420

[MAM06]
Mamalis A.G, Manolakos D.E, Ioannidis M.B, Papapostolou D.P. The static and dynamic axial collapse of CFRP square tubes: finite element modeling. Compos Struct 2006; 74(2): 213–35

[MAM96A]
Mamalis A.G, Manolakos D.E, Demosthenous G.A, Ioannidis M.B. Energy absorption capability of fibreglass composite square frusta subjected to static and dynamic axial collapse. Thin-Walled Struct 1996;25(4):269–295

[MAM96B]
Mamalis A, Robinson M, Manolakos D, Demosthenous G, Ioannidis M. The static and dynamic axial collapse of fiber glass composite automotive frame rails. Compos Struct 1996; 34: 77-96

[MAM97A]
Mamalis A, Robinson M, Manolakos D, Demosthenous G, Ioannidis M., Carruthers J. Crashworthy capability of composite material structures. Compos Struct 1997; 37: 109-134

[MAM97B]
Mamalis A.G, Manolakos D.E, Demosthenous G.A, Ioannidis M.B. The static and dynamic axial crumbling of thin-walled fibreglass composite square tubes. Compos Part B 1997; 28(4): 439–451

[MAR07]
Marguet S, Rozycki P. Gornet L. A rate dependent constitutive model for carbon-fiber reinforced plastic woven fabrics. Mechanics of Adv Mat and Struct 2007; 14(8): 619-631

[MATZ95]
Matzenmiller A, Lubliner J, Taylor R.L. A constitutive model for anisotropic damage in fiber-composites. Mechanics of Materials 1995; 20: 125-152

[MCG07]
McGregor C, Vaziri R, Xiao X. Simulation of progressive crushing development in braided composite tubes under axial compression. Compos Part A 2007; 38(11): 2247-2259

[MCG08]
McGregor C, Zobeiry N, Vaziri R, Poursartip A. A Constitutive Model for Progressive Compressive Failure of Composites. Journal of Compos Mat 2008

[MCG10]
McGregor C, Vaziri R, Xiao X. Finite element modelling of the progressive crushing of braided composite tubes under axial impact. Int J Impact Eng2010; 37: 662-672

[MEL08]
Melo J.D, Silva A.L, Villena J.E. The effect of processing conditions on the energy absorption capability of composite tubes. Compos Struct 2008; 82: 622-628

[MER06]
Mercier J. Prise En compte du vieillissement et de l'endommagement dans le dimensionnement de structures en materiaux composites. PhD Thesis, Ecole des Mines de Paris, 2006

[MOR95]
Moran P.M, Liu X. H, Shih C.F. Kink Band Formation and band broadening in fiber composites under compressive loading. Acta Metall Mater 1995; 43: 2943–58

[MOU10]
Moura M.F.S.F. Interlaminar and intralaminar fracture characterization of composites under mode I loading. Compos Struct 2010; 92: 144-149

[MUT10]
Muthirakkal S, Murthy H.N.R.N, Krishna M, Rai K.S, Karippal J.J. Hygrothermic behaviour of carbon/vinylester, glass/vinylester, carbon/epoxy and glass/epoxy composites. Iranian Polymer Journal 2010; 19(2): 89-103

[NIX09]
Nixon S, Barnes G. Effective crushing simulation for composite structures. ICCM-17, Edinburgh, UK, July 2009

[OBR12]
Obradovic J, Boria S, Belingardi G. Lightweight design and crash analysis of composite frontal impact energy absorbing structures. Compos Struct 2012; 94: 423-430

[OCH09]
Ochelski S, Gotowicki P. Experimental assessment of energy absorption capability of carbon-epoxy and glass-epoxy composites. Compos Struct 2009; 87: 215–224

[OSH13]
Oshkorv S.A, Taher S.T, Oshkour A.A, Ariffin A.K, Azhari C.H. Finite element modeling of axial crushed silk/epoxy composite square tubes. Compos Struct 2013; 95: 411-418

[PAL10A]
Palanivelu S, Paepegem M.V, Degrieck J, Kakogiannis D, Ackeren J.V, Hemelrijck D.V, Wastiels J, Vantomme J. Parametric study of crushing parameters and failure patterns of pultruded composite tubes using cohesive elements and seam, Part I: Central delamination and triggering modeling. Polymer Testing 2010; 29:729–741

[PAL10B]
Palanivelu S, Paepegem M.V, Degrieck J, Kakogiannis D, Ackeren J.V, Hemelrijck D.V, Wastiels J, Vantomme J. Parametric study of crushing parameters and failure patterns of pultruded composite tubes using cohesive elements and seam: Part II–Multiple delaminations and initial geometric imperfections. Polymer Testing 2010; 29: 803–814

[PAL10C]
Palanivelu S, Paepegem M.V, Degrieck J, Ackeren J.V, Kakogiannis D, Hemelrijck D.V, Wastiels J, Vantomme J. Experimental study on the axial crushing behavior of pultruded composite tubes. Polymer Testing 2010; 29: 224-234

[PAL10D]
Palanivelu S, Paepegem W, Degrieck J.V, Kakogiannis D, Ackeren J.V, Hemelrijck D.V, Wastiels J, Vantomme J. Comparative study of the quasi-static energy absorption of small-scale composite tubes with different geometrical shapes for use in sacrificial cladding structures. Polymer Testing 2010; 29: 381–96

[PAL11]
Palanivelu S, Paepegem M.V, Degrieck J, Vantomme J, Kakogiannis D, Ackeren J.V, Hemelrijck D.V, Wastiels J. Crushing and energy absorption performance of different geometrical shapes of small-scale glass/polyester composite tubes under quasi-static loading conditions. Compos Struct 2011; 93: 992-1007

[PIM09]
Pimenta S., Gutkin R., Pinho S.T., Robinson P. A micromechanical model for kink-band formation: Part I - Experimental study and numerical modeling. Compos Sci Technol 2009; 69: 948-955

[PIN04]
Pinho S.T, Camanho P.P, de Moura M.F. Numerical simulation of the crushing process of composite materials. Int J Crashworthiness 2004;9(3):263-276

[PIN05]
Pinho S.T. Modelling failure of laminated composites using physically-based failure models. Ph.D Thesis; Department of Aeronautics, Imperial College of London, 2005

[PIN12]
Pinho S.T, Darvizeh R, Robinson P, Schuecker C and Camanho P.P. Material and structural response of polymer-matrix fibre-reinforced composites. Journal Comp Materials 2012 46: 2313

[PIT96]
Pitkethly M.J. The use of interfacial test methods in composite materials development. Fiber, Matrix and Interface Properties, ASTM STP 1996; 1290: 34-45

[PRO07]
Prombut P. Chracterisation de la propagation de delaminage des stratifies composites multidirectionnels. PhD thesis, ENSICA, Toulouse, 2007

[RAM97]
Ramakrishna S. Microstructural design of composite materials for crashworthy structural applications. Mat Design, 1997; 18(3):167-173

[RAO07]
Rao G.V.G, Mahajan P, Bhatnagar N. Micro-mechanical modeling of machining of FRP composites – Cutting force analysis. Compos Sci Technol 2007; 67(3-4): 579–93

[RAY06]
Ray B.C. Temperature effect during humid ageing on interfaces of glass and carbon fibers reinforced epoxy composites. Journal of Colloid and Interface Science 2006; 298: 111–117

[RUS85]
Russell A.J, Street K.N. Moisture and temperature effects on the mixed-mode delamination fracture of unidirectional graphite/epoxy," Delamination and Debonding of Materials, ASTM STP 1985; 876: 349-368

[SAV06A]
Savona S.C, Hogg P.J. Investigation of plate geometry on the crushing of flat composite plates. Compos Sci Technol 2006; 66: 1639-1650

[SAV06B]
Savona S.C, Hogg P.J. Effect of fracture toughness properties on the crushing of flat composite plates. Compos Sci Technol 2006; 66: 2317-2328

[SCH96]
Schultheisz C.R, Waas A.M. Compressive failure of composites, part I: testing and micromechanical theories. Prog Aerosp Sci 1996; 32: 1-42

[SCH98]
Schultz M.R. Energy absorption capacity of graphite-epoxy composite tubes. Master thesis; Faculty of the Virginia Polytechnic Institute and State University, 1998

[SHE77A]
Shen C, Springer S.G. Effects of Moisture and Temperature on the tensile strength of composite materials. Journal of Compos Mat 1977; 11: 2-15

[SHE77B]
Shen C, Springer S.G. Environmental Effects on the Elastic Moduli of Composite Materials. Journal of Compos Mat 1997; 11: 250-264

[SHI10]
Shivakumar S, Shivarudraiah. Effect of temperature on the hygrothermal and mechanical behavior of glass-epoxy laminates. Int J Advanced Eng. Tech. 2010; 1: 225-231

[SIG91]
Sigalas I, Kumosa M, Hull D. Trigger mechanism in epoxy-absorbing glass cloth/epoxy tubes. Compos Sci Technol 1991; 40: 265-287

[SOK11]
Sokolinsky V.S, Indermuehle K.C, Hurtado J.A. Numerical simulation of the crushing process of a corrugated composite plate. Compos Part A 2011; 42(9): 1119-1126

[SUR06]
Surathi P, Karbhari V.M. Hygrothermal effects on durability and moisture kinetics of fiber-reinforced polymer composites. Interim Report, California Department of Transportation UCSD / SSRP-06/15 2006

[TAH09]
Taher S.T, Zahari R, Ataollahi S, Mustapha F., Basri S. A double-cell foam-filled composite block for efficient energy absorption under axial compression. Compos Struct 2009; 89: 399–407

[TSA71]
Tsai S.W, Wu E.M. A general theory of strength for anisotropic materials. Journal of Compos Mat 1971;5: 58-80

[VOG01]
Vogler T.J, Kyriakides S. On the initiation and growth of kink-bands in fiber composites: Part 1. Experiments. Int J solids and struct 2001; 38: 2639-2651

[WAR08]
Warrior N.A, Turner T.A, Cooper E, Ribeaux M. Effects of boundary conditions on the energy absorption of thin-walled polymer composite tubes under axial crushing. Thin Wall Struct 2008; 46: 905-913

[WIL01]
William K.V, Vaziri R. Application of a damage mechanics model for predicting the impact response of composite materials. Computers and Structures 2001; 79: 997-1011

[WIS10]
Wisnom M.R. Modelling discrete failures in composites with interface elements. Compos Part A 2010; 41(7): 795–805.

[XIA09]
Xiao X, McGregor C, Vaziri R., Poursartip A. Progress in braided composite tube crush simulation. Int J Impact Eng. 2009; 36(5): 711-719

[ZAR08]
Zarei H, Kröger M, Albertsen H. An experimental and numerical crashworthiness investigation of thermoplastic composite crash boxes. Compos Struct 2008; 85: 245–257